Ph.D. THESIS UNIVERSITY COLLEGE LONDON

APPLICATIONS OF NONLINEAR VISCOUS-INVISCID INTERACTIONS IN LIQUID LAYER FLOWS AND TRANSONIC BOUNDARY LAYER TRANSITION.

ROBERT IAN BOWLES.

ABSTRACT

The thesis is divided into two parts. The first is concerned with the fully developed, two-dimensional, free surface flow of a viscous, incompressible fluid over a horizontal surface and down a slope at high Reynolds number, Re. In both cases we concentrate on mechanisms for upstream influence through branching from the relevant basic flow. In the horizontal case it is found that branching can occur and, if the Froude number is sufficiently large, the solution resembles a hydraulic jump. The branching is studied computationally and analytically and the theory is used in a comparison with experiments. For the half-Poiseuille flow on a slope we consider free interactions for a range of gradients, identify when separation can occur and, in the limit of small gradient, find analytic solutions for the flow forced by simple geometries. The flow on larger slopes is addressed computationally.

The second part deals with some aspects of boundary layer transition beneath a transonic free stream (Mach number, M_∞, close to unity). Again the emphasis is on high Reynolds number theory and we concentrate on lower branch, Tollmien-Schlichting disturbances. Two unsteady interactions appropriate to transonic flow are studied. The first has $M_\infty^2-1 \sim O(Re^{-1/9})$ and is an extension of the triple deck structure when the free stream reacts unsteadily. This regime links previously studied subsonic and supersonic cases. Two-dimensional disturbances are little altered but there are new, weakly nonlinear, three-dimensional effects including enhanced growth for slightly oblique disturbances and novel triad interactions. The second has $M_\infty^2-1 \sim O(Re^{-1/5})$ and links an unsteady, nonlinear free stream, capable of containing shocks, and a quasi-steady boundary layer. The possibility of a resonance linkage between shock buffetting and boundary layer thickening is addressed, being a candidate for a bypass transition mechanism in transonic flows.

Table Of Contents.

ACKNOWLEDGEMENTS.

My grateful thanks go to Professor F.T. Smith for his help, encouragement and guidance throughout the work involved in this thesis. Thanks, too, go to my friends and colleagues at U.C.L. Mathematics Department, United Technologies Research Center and elsewhere. Special thanks go to my wife, Rowena Hurst, for her encouragement and help during the preparation of this manuscript.

Robert Bowles, February 1990.

This work was made possible by the financial support of the S.E.R.C. and United Technologies Research Center, Hartford, CT.

CHAPTER ONE

INTRODUCTION.

§1.1 Viscous-Inviscid Interactions At High Reynolds Numbers.

This thesis covers some aspects of liquid layer flow and transonic boundary layer transition through the application of the ideas of viscous-inviscid interaction. This interaction occurs when the flow is determined by an interplay of some effects caused by viscosity and others controlled by inviscid mechanics. The fact that the two areas considered in this thesis are so widely different is an indication of the widespread occurrence of these effects in fluid mechanics. The work on liquid layers is a study of the mechanism of upstream influence in a rapidly moving stream and the structure of the feature most commonly associated with it - the hydraulic jump. Upstream influence is made possible by an interaction between viscous retardation of the layer and the pressure gradient generated as the layer is caused to thicken. The sections on transition to turbulence in transonic boundary layers are centred on the study of the nonlinear development of Tollmien-Schlichting waves. These are the instability waves in an incompressible boundary layer with no external pressure gradient and they rely on an interaction between viscous effects close to the wall and pressure waves in the free stream for their growth.

A second idea running through this work is the asymptotic solution of the governing equations, making use of the large Reynolds numbers usually associated with these flows. A flow with a large Reynolds number is primarily governed by inviscid mechanics, but it is by no means possible to neglect viscous effects in such cases. In both of the physical areas studied, these governing equations are the Navier-Stokes equations of the flow of a Newtonian fluid. However, these equations, although simple in principle to derive, are very difficult to solve in practice, especially at large Reynolds numbers. This is due to their nonlinearity and problems associated with the wide variation of scales which arise due to the effects of viscosity at large Reynolds numbers. The assumption of an

infinitely large Reynolds number leads to the possibility of asymptotic solution of the equations. We offer no proof of the convergence of these asymptotic solutions to a solution of the Navier-Stokes equations but their history of success in describing fluid flows at high Reynolds numbers, from Prandtl's boundary layer theory onwards, enables us to have every confidence in the technique.

Hand in hand with the idea of a high Reynolds number expansion is the so-called structural approach to the solution. This enables the various scales of the motion to be identified. The flow domain is divided into regions and the governing equations capturing the dominant physics in each region are identified. The solution in each area is then found as an expansion in inverse powers of the Reynolds number and these solutions are matched across the boundaries of the regions. This is simply an example of the application of techniques for the solution of singular perturbation problems, of which high Reynolds number fluid flow is an exceedingly important example. See, for example, van Dyke (1964) and Stewartson (1974).

Prandtl's boundary layer theory is an example of a high Reynolds number expansion and of the use of matched asymptotic expansions. This theory is used, for example, to find the steady flow of a fluid past a body at high Reynolds numbers. In the main part of the flow the viscous terms in the Navier-Stokes equations are small and do not appear, to first order, in the expansion. Near to the body, in the boundary layer, the normal coordinate is scaled with the Reynolds number so that viscous effects do enter at first order. The solution proceeds as follows: first the exterior, inviscid, solution is found and then this is used to provide the boundary condition for the boundary layer flow. This solution then gives the forcing for the next term in the solution in the free stream. The solution proceeds in this hierarchical fashion. However this technique has its deficiencies in that the equations governing the boundary layer motion do not necessarily have a solution (Goldstein (1948), Stewartson (1970)). The method has failed in determining the flow around the body

due to its hierarchical structure - the solution is forced once the inviscid, exterior flow is known and this is calculated without regard for viscous effects. There is no mechanism by which viscous effects can act to alter this inviscid flow, i.e. no scope for a viscous-inviscid interaction.

The high Reynolds number structure which controls the viscous-inviscid interaction between the boundary layer and the external flow is the triple deck structure. See Stewartson and Williams (1969), Neiland (1969) and Messiter (1970). It first arose in the study of upstream influence and boundary layer separation in supersonic flow and most of the elements of the structure, including its scales, are given in Lighthill (1953). The basic idea is that quite a small pressure perturbation ($O(Re^{-1/4})$ as $Re \to \infty$ in supersonic flow) can act over a relatively small streamwise distance ($O(Re^{-3/8})$) to give a large ($O(Re^{1/8})$) pressure gradient. The short scales of the motion mean that the viscous effects are confined to a thin sublayer of the Prandtl boundary layer situated at the wall. The rest of the boundary layer reacts in an inviscid fashion. However the small displacement velocity, from the viscous sublayer response, forces, in the free stream, a significant adjustment due to the short scales involved. What is special about the these scalings with the Reynolds number is that this inviscid motion in the free stream produces a pressure of the same order as that driving the flow, namely $O(Re^{-1/4})$. There is therefore a mechanism for an interaction between the viscous motions within the boundary layer and the inviscid flow outside. The essence of the interaction is to be found in the pressure-displacement law, $P = \mathcal{F}(A)$, relating the pressure, P, to the (negative) displacement of the boundary layer, A. The equations governing the triple deck for steady two-dimensional disturbances are

$$UU_X + VU_Y = -P_X + U_{YY}, \qquad (1.1.1a)$$

$$U_X + V_Y = 0, \qquad (1.1.1b)$$

$$U = V = 0 \text{ at } Y = 0, \qquad (1.1.1c\text{-}d)$$

$$U \to Y + A \text{ as } Y \to \infty, \qquad (1.1.1e)$$

$$P = \mathcal{F}(A). \qquad (1.1.1f)$$

Here U and V are the streamwise and normal velocities respectively and X and Y the streamwise and normal coordinates. Equations (1.1.1a-e) govern the flow in the sublayer close to the wall where viscous effects are important. The pressure-displacement law (1.1.1f) is found by solving the inviscid free stream equations for the pressure response to the boundary layer displacement. The viscous-inviscid interaction captured by these equations can be clearly seen.

In the case of supersonic flow the pressure-displacement law is $P = -A_X$ and this allows a self-sustaining interaction to occur which ends in the separation of the boundary layer from the body surface. A small adverse pressure gradient causes the boundary layer to thicken and through the pressure-displacement law this reinforces the adverse pressure gradient and so the process continues. See Lighthill and Stewartson and Williams.

These ideas have been extended to channel flows, pipe flows, hypersonic flows, boundary layer jets and supercritical liquid layer flows. See, for example, the review by Smith (1982). In all these cases the governing equations seem to be parabolic at first sight allowing no mechanism for upstream influence. The possibility of a self-sustaining interaction between viscous and inviscid effects, however, allows branching and a non-uniqueness of the solution and so facilitates upstream influence.

In the field of boundary layer stability viscous-inviscid interaction plays an important rôle. This

is because, as we explain in §4.1, Tollmien-Schlichting waves, which are the stability waves in a flat plate boundary layer, are interactive phenomena. Viscous effects are essential for the instability as is the feedback from the inviscid reaction to these effects as the free stream adjusts. The governing equations of Tollmien-Schlichting waves at high Reynolds numbers are, in fact, the unsteady version of the triple deck equations (1.1.1). (Simply add a U_T term to the left hand side of (1.1.1a)). See Smith (1979a&b). The use of structural, high Reynolds number theory and the nonlinear triple deck in the study of boundary layer stability and transition in incompressible, supersonic and hypersonic flows has led to a great understanding of the mechanisms of transition, although the mechanism is by no means fully understood. See the work of Smith (1979a&b), Smith and Burgraff (1985), Smith (1986a&b), Smith and Stewart (1987), Smith (1989), Stewart (1990) and the many references therein.

§1.2 A Description Of The Work Of This Thesis.

This thesis starts with a study of the mechanisms for upstream influence in fully developed liquid layer flows. An introduction to liquid layer flows and to the hydraulic jump, and a description of the work of other authors in the application of high Reynolds number techniques and viscous-inviscid interaction in the area is given in §2.1. The governing equations contain within them the possibility of viscous-inviscid interaction and the structure of this interaction is identified in various limits in §2.6. There is a strong connection with the triple deck structure allied with the hypersonic pressure-displacement law, $P = -A$. This similarity was first identified in the work of Gajjar and Smith (1983). The work of chapter 2 is, in fact, an extension of the work of Gajjar (1983), Gajjar and Smith (1983), and Brotherton-Ratcliffe (1986) on liquid layer flows to cover motions over the long length scale $X \sim O(Re)$. On this scale viscous effects are important throughout the depth

of the layer and as a result the viscous-inviscid interaction is strongly influenced by the non-parallelism and simultaneous development of the basic flow. In some limits, for example that of large Froude number, the form of the interaction resembles the hydraulic jump. Section 2.7 is a comparison of the experiments of Craik, Latham, Fawkes and Gribbon (1981) on circular hydraulic jumps, formed when a vertical column of water falls onto a flat plate, with the theoretical results of the chapter. It is complementary to a similar comparison made by Brotherton-Ratcliffe.

Chapter three considers an extension of the work of chapter two to the half-Poiseuille flow of liquid layers down a favourable gradient. The free interaction is considered first, in §§3.2-3.5 and its structure on a range of gradients investigated. It is found to take different forms depending on the slope. For small slopes it is governed primarily by lubrication theory, but on larger slopes it takes on the structure of a hydraulic jump and separation occurs. The downstream asymptote in both cases has a horizontal free surface. Some of the effects of surface tension are also considered.

The limit of small gradient is paid special attention in §3.6. It is found that the relatively simple governing equation, derived using lubrication theory, yields solutions showing viscous-inviscid interaction and many of the features of interactions seen in more complicated flows. Numerical solution of the interactions forced by obstacles are presented in §3.7. On sufficiently large slopes and with severe obstacles the numerical solutions exhibit a hydraulic jump and separation upstream of the obstacle.

The second part of this thesis is concerned with extending the work on boundary layer transition, mentioned in §1.1, to the transonic regime. An introduction to the use of high Reynolds number theory in transition modelling is given in §4.1 and the introductions to Chapters 5 and 6 contain a summary of certain aspects of boundary layer transition. The major difference between the subsonic or

supersonic and the transonic regime lies in the closeness of the speed of the Tollmien-Schlichting waves to the speed at which the free stream is able to adjust to perturbations within the boundary layer at transonic speeds. This leads to two significant regimes. In the first, covered by chapters 4 to 6, the free stream equations, as well as the boundary layer equations, are unsteady. This occurs when the Mach number, M_∞ is such that $|M_\infty^2-1| \sim O(Re^{-1/9})$ as $Re \to \infty$. The second regime, discussed in Chapter 7, has $|M_\infty^2-1| \sim O(Re^{-1/5})$ and is of relevance to the unsteady interaction of a shock and a boundary layer.

Chapter 4 presents a derivation of the equations and scales governing Tollmien-Schlichting waves in the first regime. The properties of the linearised form of these equations are then considered in §4.3. This study is successful in illustrating the fate of the unstable Tollmien-Schlichting disturbances in a transonic flow as the Mach number increases and the flow becomes more supersonic - in supersonic flow it is known that all disturbances, unless sufficiently oblique, are stable (Ryzhov and Zhuk (1980)).

Chapter 5 considers a weakly nonlinear solution of these equations and effectively extends the work of Smith and Burgraff (1985) on some nonlinear aspects of incompressible boundary layer transition to transonic flows. The nonlinear growth of the disturbance is followed through a weakly nonlinear interaction to an essentially large-amplitude-inviscid stage (although with bursts of vorticity possible from a viscous sublayer at the wall). An important result in this section is that, in the weakly nonlinear stage, a two-dimensional wavepacket is susceptible to a rapidly growing sideband instability in the presence of a small degree of spanwise warping. Finally we consider the so-called Euler stage of transition in transonic flow.

The last two chapters, chapters 6 and 7, are shorter than the others and present results of work still in progress. In chapter 6 we consider the extension of the

work of Smith and Stewart (1987) on subharmonic resonance and triad interaction in boundary layer transition to transonic flows. Chapter 7 is concerned with flows in the second transonic regime. In it we consider the possibility of a self-sustained shock / boundary layer interaction, an essentially nonlinear process, being a mechanism for bypass transition in transonic flow.

Chapter Two

LIQUID LAYER FLOWS ON A HORIZONTAL PLATE.

§2.1 Introduction And The Governing Equations.

Liquid layer flows are commonly observed phenomena. They may be seen in nature, in rivers, weirs and spillways, for example. They are also widely used in industrial processes, where the liquid is less likely to be water. Common uses are in mixing processes in industrial chemistry or in the manufacture of films.

In chapters 2 and 3 of this thesis we consider, primarily, the steady two-dimensional flow of a fully developed liquid layer. The emphasis is on the study of the viscous forces at work in the layer and their interaction with the position of the free surface. We hope to develop a description of the mechanism for upstream influence in these flows based on these ideas. The steady hydraulic jump is the phenomenon commonly associated with upstream influence in liquid layer flows, and it can be seen in its many forms in situations ranging from rivers to the kitchen sink. The form of the jump varies with the Reynolds number and the Froude number of the oncoming layer. It is often turbulent or unsteady, with the energy loss required at the jump being effected by the scale reduction and viscous dissipation in the turbulence, or alternatively carried away in a wave train. See the theory of Benjamin and Lighthill (1954). A description of the possible forms of the jump can be found in Ishigai, Nakanishi, Mizumo and Imamura (1977). Although global considerations of mass and momentum can give useful results (for example Lamb (1932) or Lighthill (1978)), the internal structure of the jump remains largely unexplained. Progress has been made by the authors mentioned below, however, by considering the effects of viscosity which, through interaction with the free surface, can have a surprisingly large effect on the flow structure. The jump is assumed to be laminar and steady, with the viscous dissipation, therefore, being responsible for the required energy loss.

We concentrate here on fully developed flows on a horizontal surface (where they can be sensibly defined -

see later) in order to complement the work in this area of Gajjar and Smith (1983), Gajjar (1983) and Brotherton-Ratcliffe (1986). These authors study many aspects of steady liquid layer flow and of the stability of such flows. Their emphasis, however, is on a flow with a uniform velocity profile. Their results, as far as we are concerned, can be summarised as follows. If the velocity profile of the layer is uniform, allied with a Blasius boundary layer at the solid surface, then upstream influence is possible even if the Froude number is greater than unity. This supercritical upstream influence has its origin in the viscous-inviscid interaction between the boundary layer and the free surface, and is governed by the triple deck equations with the hypersonic pressure-displacement law, $P = -A$. These hold over a length scale L where $h^* << L << Reh^*$. Here h^* is the depth of the layer and Re the Reynolds number associated with the flow. The effects of surface tension are neglected. The equations have a solution with a downstream form in which the height of the free surface increases like X^m, where $m = 2(\sqrt{7} - 2)/3 \approx 0.43050$ as $X \to \infty$, and this blunt shape is reminiscent of the hydraulic jump studied in experiments performed by Craik, Latham, Fawkes and Gribbon (1981). Beneath this growing surface is a long separation bubble, with reattachment occurring far downstream, and the velocity profile above the bubble still uniform. The steady experimental jumps have Reynolds and Froude numbers both of the order of 100, and the jumps are typical of those one may view in an ordinary sink if the flow from the tap is not too strong. A comparison of the theory with these experiments is presented by Brotherton-Ratcliffe and gives good qualitative agreement, predicting both the change in length of the separation bubble and the jump strength with jump position, although the prediction of the strength itself is inaccurate, being too small. He points out, however, that a more suitable theory would be one in which the velocity profile could be taken as being fully developed, with the vorticity spread across the layer. Further evidence for the importance of fully

developed flow and the scale $L \sim h^*Re$, which would allow viscous effects to be important across the depth of the layer, comes from Gajjar who studies the adjustment of fully developed flow on a slope in preparation for a small increase in slope downstream. The length scale he considers ($O(Re^{1/7})$) is akin to that used in the studies of Smith (1976) on fully developed channel flow, in which the curvature of the streamlines as well as the free surface position interacts with viscous effects. Gajjar concludes that the return to Poiseuille flow downstream must take place on a longer scale. We therefore concentrate on interactions which take place on a length scale in which viscosity acts right across the layer and its direct effects are not confined to the wall region as in the cases described above.

On a downward sloping surface, considered in chapter 3, the fully developed layer consists of half-Poiseuille flow of a suitable thickness, but on a horizontal surface the lack of any gravitational force to counter viscous effects makes a fully developed flow difficult to define. Indeed it is clear that, for a finite Froude number, the equations derived and presented below have no solution as $x \to \infty$. The O(Re) scale is precisely that over which the development occurs, and we must therefore view the velocity profile and depth at a particular x-station to be in the process of developing due to this viscous retardation, whether or not it is also adjusting for any downstream boundary condition. This leads to important differences between the flow on the horizontal and that on a slope, however shallow. An exception is when the Froude number is large. As described in §2.2.2, the flow then develops into one described by Watson's (1964) solution with the depth increasing linearly and the velocity profile being governed by a balance between inertial and viscous forces. This may then be taken to be a fully developed flow and is, in fact, the basic flow assumed in the theory which is presented in §2.6 and describes the hydraulic jump.

The physical set-up of the problem is illustrated in

Figure 2.1.1. We consider two-dimensional motions. Let $X^* = 0$ be the station at which we are considering the flow, and let the depth and velocity profile here be h^* and $U^*(y^*/h^*)$ respectively. Here y^* is the vertical coordinate. The volume flux per unit width, Q, carried in the layer, is independent of X^*, and if the kinematic viscosity of the fluid is υ we can define a Reynolds number for the flow as Q/υ. A typical velocity at the particular X^*-station is $\tilde{U}^* = Q/h^*$ and a representative pressure is $\rho\tilde{U}^{*2}$, where ρ is the fluid density. We take h^* as a typical length scale. If we nondimensionalise the Navier-Stokes equations with respect to these values we find

$$UU_{\hat{X}} + \hat{V}U_y = -P_{\hat{X}} + Re^{-1}(U_{yy} + U_{\hat{X}\hat{X}}),$$

$$U\hat{V}_{\hat{X}} + \hat{V}\hat{V}_y = -P_y - s + Re^{-1}(\hat{V}_{yy} + \hat{V}_{\hat{X}\hat{X}}),$$

$$U_{\hat{X}} + \hat{V}_y = 0,$$

$$U = \hat{V} = 0 \text{ at } y = 0,$$

$$\int_0^{1+\eta(\hat{X})} U(y)dy = 1.$$

Here $y = 1 + \eta(\hat{X}) \equiv h(\hat{X})$ is the unknown position of the free surface. We define s to be the inverse Froude number of the problem, gh^{*3}/Q^2, where g is the acceleration due to gravity. If we neglect the stresses in the air above the layer and assume its density to be zero we can take the pressure at the free surface to be zero. The conditions at the free surface, including the effects of surface tension, are then

$$(U_{\hat{X}} - \hat{V}_y) \eta(\hat{X}) + 1/2 (U_y + \hat{V}_{\hat{X}}) (1 - \eta_{\hat{X}}^2) = 0,$$

$$P = \frac{2}{Re(1 + \eta(\hat{X})^2)} \left(U_{\hat{X}} \eta_{\hat{X}}^2 - (U_y + \hat{V}_{\hat{X}}) \eta_{\hat{X}} + \hat{V}_y \right) - \left(\frac{Ts}{\rho g h^{*2}} \right) \frac{\eta_{\hat{X}\hat{X}}}{(1 + \eta_{\hat{X}}^2)^{3/2}} .$$

Here T is the coefficient of surface tension of the fluid/air interface. We now assume that the length scale of the adjustment of the layer is long compared with its depth and make the boundary layer approximation. More specifically we scale $\hat{X}$ with Re ($\hat{X} = Rex$) and $\hat{V}$ with Re^{-1} ($\hat{V} = Re^{-1}V$) and let $Re \to \infty$ to get

$$UU_x + VU_y = -P_x + U_{yy},$$

$$P_y + s = 0,$$

$$U_x + V_y = 0,$$

$$\int_0^{1+\eta} U dy = 1,$$

$$U = V = 0 \text{ at } y = 0,$$

$$U_y = 0 \text{ at } y = 1+\eta,$$

$$P + \gamma \eta_{xx} = 0 \text{ at } y = 1+\eta.$$

See Figure (2.1.2). This assumes that surface tension effects are strong enough to ensure that $\gamma = Ts/\rho g h^{*2} Re^2$ is O(1) as $Re \to \infty$. If this is not the case, then the condition at the free surface is simply P = 0. If we now write

$$P = -s(y-1) + p,$$

and neglect surface tension, we are led to the system

$$UU_x + VU_y = -p_x + U_{yy}, \qquad (2.1.1a)$$

$$U_x + V_y = 0, \qquad (2.1.1b)$$

$$\int_0^{1+\eta} U dy = 1, \qquad (2.1.1c)$$

$$U = V = 0 \text{ at } y = 0, \qquad (2.1.1d)$$

$$U_y = 0 \text{ at } y = 1+\eta, \qquad (2.1.1e)$$

$$p = s\eta, \qquad (2.1.1f)$$

$$U = U_0(y), \ \eta = 0 \text{ at } x = 0. \qquad (2.2.1g)$$

These are the equations studied in chapter 2.

We can scale the Froude number out of the equations, leaving it to occur only in the initial conditions at $x = 0$. The scalings

$$[x,y,\eta,p,U,V] \sim [s^{-1/3}\tilde{x}, s^{-1/3}\tilde{y}, s^{-1/3}\tilde{\eta}, s^{2/3}\tilde{p}, s^{1/3}\tilde{U}, s^{1/3}\tilde{V}]$$

effectively replace s by unity in equation 2.1.1f, which becomes

$$\tilde{p} = \tilde{\eta}, \qquad (2.1.2a)$$

and the conditions at $x = 0$ become

$$\tilde{U} = s^{1/3}U(s^{-1/3}\tilde{y}) \quad \text{and } y \in (0,\tilde{h}) \quad \tilde{h} = s^{1/3}. \qquad (2.1.2b)$$

In addition, $1 + \eta$ in (2.1.1c&e) becomes $\tilde{h} + \tilde{\eta}$.

The next two sections of chapter 2 are initial analytic investigations of these equations, and study their behaviour as $s \to 0$, $s \to \infty$ and $x \to 0+$. This enables important scales to be identified. Section 2.4 details a numerical solution and reveals more information about the properties of the interaction. In §2.6 the numerical results are explained in terms of the interaction and a non-uniqueness in the solution of the system 2.1.1(a-g) which arises from it. This section also presents

asymptotic structures which govern the non-uniqueness in various limits. Finally a comparison, complementary to that of Brotherton-Ratcliffe, with the experiments of Craik et al. is made and the results support the proposal that, in the regime of their experiments, the hydraulic jump can be described in terms of a viscous-inviscid interaction in a steady, laminar and fully developed flow.

§2.2 Extremes Of The Froude Number, s^{-1}.

§2.2.1 Large s and the lubrication theory solution.

The limit $s \to \infty$ corresponds to a small Froude number and to gravity exerting a comparatively strong influence. It takes a relatively large pressure change to raise or lower the free surface and the effects associated with mass continuity are therefore of a higher order. The change in position of the free surface h is then small, $O(s^{-1})$, for some distance. We expect a half-Poiseuille flow , $U = -p_x(y^2/2-hy)$, to develop on an O(1) scale in x under what is, in effect, a locally rigid free surface. This flow requires a pressure $p = -3x/h^3$ to drive it. Over a long O(s) length scale, however, where $x = sX$ say, the change in depth becomes O(1) as the pressure drops. This slow change in depth provides the pressure to drive the Poiseuille flow. Hence lubrication theory is appropriate. Over the long length scale equations (2.1.1) become

$$s^{-1}(UU_X + VU_y) = -s^{-1}p_X + U_{yy},$$

$$U_X + V_y = 0,$$

$$\int_0^h U dy = 1,$$

$$U = V = 0 \text{ at } y = 0, \; U_y = 0 \text{ at } y = h,$$

$$p_X = sh_X.$$

Therefore for large s we find

$$U_{yy} = h_x. \tag{2.2.1}$$

Integrating this equation and applying the boundary conditions and the condition that the total mass flux is unity leads to

$$h_x = -3/h^3, \tag{2.2.2}$$

with the solution

$$h(X) = (1-12X)^{1/4}, \tag{2.2.3}$$

which becomes singular, or "chokes", as $X \to 1/12-$. This solution is therefore not valid where $x \sim s/12$. If we write $X = 1/12 - \hat{X}$, then the terms included in (2.2.1) are $O(h_x) \sim O(\hat{X}^{-3/4})$, whilst those neglected, the inertial terms, are $O(s^{-1}UU_x) \sim O(s^{-1}\hat{X}^{-3/2})$. So here, in a zone of x-extent $O(s^{-1/3})$, inertial effects enter to prevent the choking above and with the scalings $[U,y,p] \sim [s^{1/3},s^{-1/3},s^{2/3}]$ the full equations are reintroduced with s entering only through the scalings for this new problem, as in equations (2.1.1a-e, 2.1.2a-b). The upstream condition for this problem is that of half-Poiseuille flow as $\tilde{x} \to -\infty$, where $x = s/12 + s^{-1/3}\tilde{x}$. The depth varies as $(-12\tilde{x})^{1/4}$.

§2.2.2 Small s and Watson's solution.

At the other extreme, small values of s correspond to an inertia-viscosity balance with pressure effects secondary. Equations (2.1.1a-g) with $s = 0$ are those solved by Watson (1964) and they predict a linear thickening of the layer, $h \sim x$, with $U \sim 1/x$, as $x \to \infty$. Thus the inertial and viscous terms are $O(1/x^3)$ whereas the neglected pressure gradient is O(s). This solution fails therefore when $x \sim O(s^{-1/3})$. The rescaling $[U,y,p] \sim [s^{1/3},s^{-1/3},s^{2/3}]$ yields, again, the full set (2.1.1a-e, 2.1.2a-b), with the Froude number entering only

through the scalings.

So both the extremes of s described above lead to the full system eventually, downstream. This emphasises the need for tackling this full system, which is in general a numerical task. This is done is §2.4 below.

§2.3 Solution For Small x.

§2.3.1 The limit $x \to 0$.

Further features of interest are brought out by an expansion of the solution for a general starting velocity profile, U_0 say, as $x \to 0+$.

We assume that the profile at $x = 0$ has the form

$$U_0 \sim \alpha_1 y + \alpha_2 y^2 + \alpha_3 y^3 + \ldots \text{ as } y \to 0,$$

and that s and the constants α_i are O(1), with $\alpha_1 > 0$. The expansion has the following form

$$p \sim p_1 x + p_2 x^{4/3} \ln x + p_3 x^{4/3} + \ldots, \qquad (2.3.1a)$$

$$\psi \sim \psi_0 + \psi_1 x + \psi_2 x^{4/3} \ln x + \psi_3 x^{4/3} + \ldots, \qquad (2.3.1b)$$

across most of the flow, where $U = \psi_y$, $U_0 = \psi_{0y}$ and $\psi(0) = 0$, $\psi(1 + \eta) = 1$.

It is found that $\psi_{1y} \sim O(1)$ as $y \to 0$. As a result there is a boundary layer of thickness $x^{1/3}$ at the wall. This provides the balance between viscous effects, $O(U/y^2) \sim O(x/y^2)$, and inertial effects, $O(\psi_{0y}\psi_{1yX}) \sim O(y)$, required to reduce the slip velocity to zero at the wall. Here the solution expands as

$$\psi \sim \alpha_1 \xi^2 x^{2/3}/2 + x\, f_1(\xi) + x^{4/3} \ln x\, f_2(\xi) + x^{4/3} f_3(\xi) + \ldots, \qquad (2.3.2)$$

where $\xi = y/x^{1/3}$ is the appropriate similarity variable.

A viscous layer at the free surface, $y = 1 + \eta(x) =$

$1 + p(x)/s$, is also necessary but it is passive to our order of working. The boundary conditions to be applied there, namely $\psi = 1$ and $\psi'' = 0$, with $'$ denoting differentiation with respect to y, reduce, after linearisation about $\eta(x) = 0$, to

$$\psi_i(1) = -p_i U_0(1)/s, \quad i = 1,2,3, \tag{2.3.3a}$$

$$\psi_i''(1) = -p_i U_0''(1)/s, \quad i = 1,2,3. \tag{2.3.3b}$$

Substitution of the above expansion (2.3.1a-b) into equations (2.1.1a-f) gives, in the main part of the flow where $y \sim O(1)$, at successive orders 1, $x^{1/3}\ln x$, $x^{1/3}$,

$$\psi_0'\psi_1' - \psi_1\psi_0'' = -p_1 + \psi_0''',$$

$$\psi_0'\psi_2' - \psi_2\psi_0'' = -p_2,$$

$$\psi_0'\psi_3' - \psi_3\psi_0'' = -p_3.$$

These have solutions, using (2.3.3a-b),

$$\psi_1 = U_0\left[\int_1^y \frac{U_0'' - p_1}{U_0^2}\,dy - \frac{p_1}{s}\right], \tag{2.3.4a}$$

$$\psi_2 = U_0\left[\int_1^y \frac{-p_2}{U_0^2}\,dy - \frac{p_2}{s}\right], \tag{2.3.4b}$$

$$\psi_3 = U_0\left[\int_1^y \frac{-p_3}{U_0^2}\,dy - \frac{p_3}{s}\right]. \tag{2.3.4c}$$

In the wall layer the boundary conditions as $\xi \to \infty$ are such that a match with the solutions (2.3.4a-c) is achieved. We find, on substitution of (2.3.2) into (2.1.1a-g), that the governing equations and boundary conditions take the form

$$f_1''' + \alpha_1\xi^2/3\ f_1'' - \alpha_1\xi\ f_1' + \alpha_1\ f_1 - p_1 = 0,$$

$$f_1(0) = f_1'(0) = 0,$$

$$f_1 \sim \alpha_2\xi^3/3 + (p_1-2\alpha_2)/\alpha_1 \text{ as } \xi \to \infty,$$

(2.3.5a)

$$f_2''' + \alpha_1\xi^2/3\ f_2'' - 4\alpha_1\xi/3\ f_2' + 4\alpha_1/3\ f_2 - 4p_2/3 = 0,$$

$$f_2(0) = f_2'(0) = 0,$$

$$f_2 \sim 2\alpha_3\xi/\alpha_1 + p_2/\alpha_1 \text{ as } \xi \to \infty,$$

(2.3.5b)

$$f_3''' + \alpha_1\xi^2/3\ f_3'' - 4\alpha_1\xi/3\ f_3' + 4\alpha_1/3\ f_3 - 4p_3/3 = p_2 - \alpha_1(f_2-\xi\ f_2'),$$

$$f_3(0) = f_3'(0) = 0,$$

$$f_3 \sim \alpha_3/4\ \xi^4 + 6\alpha_3/\alpha_1\ \xi\ln\xi + \xi(\alpha_1K_2-\alpha_1p_1\{K_1-s^{-1}\}) + p_3/\alpha_1 \text{ as } \xi\to\infty,$$

(2.3.5c)

where $K_2 = \int_1^0 U_0''/\ U_0^2\ dy$, $K_1 = \int_1^0 1/\ U_0^2\ dy$ and $\int$ denotes the finite part of the integral.

The solution to the first of these equations is

$$f_1 = p_1\xi^3/6, \qquad p_1 = 2\alpha_2.$$

This solution corresponds simply to higher terms of the starting flow near the wall and to the pressure, p_1x, needed to drive this basic flow. The solutions at the next order are

$$f_2 = \frac{2\alpha_3\xi}{\alpha_1 I_1}\int_0^u\left\{\frac{e^{-v}U(v)}{v^{2/3}} - \frac{9\beta}{4v^{4/3}}\right\}dv, \quad p_2 = \frac{27\beta\alpha_3}{2I_1}\left(\frac{9}{\alpha_1}\right)^{1/3},$$

where $u = \alpha_1\xi^3/9$, $\beta = \Gamma(2/3)/\Gamma(1/3)$, $\mathcal{U}$ is the confluent hypergeometric function, U(7/3,5/3,u) (Abramowitz & Stegun, Chapter 13) and

$$I_1 = \int_0^\infty \left\{ \frac{e^{-v}\mathcal{U}(v)}{v^{2/3}} - \frac{9\beta}{4v^{4/3}} \right\} dv.$$

Further, f_3 is given by

$$f_3 = Au^{1/3}\int_1^u \frac{e^{-v}\mathcal{M}(v)}{v^{2/3}}dv + Bu^{1/3}\int_1^u \frac{e^{-v}\mathcal{U}(v)}{v^{2/3}}dv + Cu^{1/3} + p_3/\alpha_1$$
$$+ u^{1/3}\left[\frac{4\alpha_3}{\beta I_1}\left(\frac{\alpha_1}{9}\right)^{1/3}\right]\left\{ \int_1^u \frac{e^{-v}\mathcal{M}(v)}{v^{2/3}}\int_0^v e^{-w}\mathcal{U}^2 w^{5/3}dwdv \right.$$
$$\left. - \int_1^u \frac{e^{-v}\mathcal{U}(v)}{v^{2/3}}\int_0^v e^{-w}\mathcal{U}\,\mathcal{M}\,w^{5/3}dwdv \right\},$$

and

$$p_3 = \alpha_1 27\beta B/4,$$

where A, B, C are constants to be found and $\mathcal{M}$ is M(7/3,5/3,u), a confluent hypergeometric function (Abramowitz and Stegun, Chapter 13).

§2.3.2 The case of half-Poiseuille flow and discussion.

We can calculate the coefficients A, B, C in particular cases from the boundary conditions imposed on f_3, (2.3.5c), but the results are of relatively little interest. Instead we concentrate on the case of a flow with $\alpha_3 = 0$, e.g. Poiseuille flow. In this case we lose the logarithmic terms proportional to $x^{4/3}\ln x$ and find

$$p_3 = \frac{27\beta}{4}\,\alpha_1^{5/3}\,\frac{9^{1/3}}{I_1}\left[\, K_2 - 2\alpha_2(\, K_1 - 1/s)\,\right],$$

$$f_3 = \frac{4p_3}{27\beta\alpha_1}\,u^{1/3}\int_0^u \left(\frac{e^{-v}\mathcal{U}}{v^{2/3}} - \frac{9\beta}{4v^{4/3}} \right) dv.$$

In the case of Poiseuille flow, which has $\alpha_1 = 3$,

$\alpha_2 = -3/2$ and $K_2 = 2\alpha_2 K_1$, this reduces to

$$p \sim -3x - \frac{243\,\beta\,3^{1/3}}{4\,I_1\,s}\,x^{4/3}, \qquad (2.3.6a)$$

$$\eta \sim p/s. \qquad (2.3.6b)$$

We note that as $s \to \infty$ this behaviour mirrors the solution (2.2.3) for large s with the pressure predominantly being that needed to drive the starting flow, but that, as $s \to 0$, the solution (2.3.6a) becomes invalid when $x \sim O(s^3)$. Also as $\alpha_1 \to \infty$, $p_3 \sim O(\alpha_1^{5/3})$, and so for large skin friction the expansion fails when $x \sim O(\alpha_1^{-5})$. We return to this later, in §2.6, when we consider possible branching of the solution to equations (2.1.1a-g), and matters of upstream influence in these, seemingly parabolic, equations.

It seems clear that there are two processes in the solution. Firstly there is the pressure needed to drive the starting flow. This must come from an alteration in the depth of the layer, since the wall is horizontal. Secondly there is the response of the flow to this change in depth. More precisely, there is a pressure term, $p_1 x$, driving the basic flow, overcoming viscous resistance and this causes a change in the position of the free surface $p_1 x/s$. The inertial response in the main part of the stream interacts with this change in depth but also provokes a viscous boundary layer giving rise to a pressure $p_3 x^{4/3}$. The failure of the expansion occurs when $p_3 x^{4/3}$ alters the position of the free surface to the same order as does $p_1 x$ and we lose the sequential form of the expansion, originally dominated by the pressure change needed to provide the flow.

To investigate the downstream development of these initial stages of the flow a numerical solution of the full equations is required. This is performed in the next section.

§2.4 Numerical Solution Of The Free Interaction Problem.

§2.4.1 The numerical method.

We have seen in §2.2 that the full system emerges, eventually, downstream in the limits of both large and small s and in §2.3 that the nature of the interaction between the change in position of the free surface and the response of the flow changes as s decreases. This section aims to shed more light on these effects with a numerical solution of the interaction governed by (2.1.1a-g).

Initially we treat the system as parabolic in x, although part of the overall purpose of this investigation and of the calculations is to reveal the nature of the mechanisms for upstream influence in the equations. Here, then, we consider the general so-called "free interaction" problem, rather than one forced by a particular downstream boundary condition which must, instead, be accommodated by an elliptic method (see §3.7). Given this assumption the solution is simply obtained by a marching scheme in x. The solution is marched downstream from an initial profile using a second order accurate Crank-Nicholson scheme.

In order to deal with the problem that the position of the free surface, $y = 1 + \eta(x)$, is an unknown, the equations are rewritten by introducing

$$\xi = (y - f)/(1 + E),$$

where $E = \eta - f$ and $y = f(x)$ is the position of the plate, obstacle or slope over which the stream is flowing. Here ξ takes values only in the range [0,1], with the free surface identified with $\xi = 1$. We also use a modified stream function, $\hat{\psi}(\xi)$, such that

$$U = \frac{\hat{\psi}_\xi}{1 + E}, \qquad \hat{V} = -\hat{\psi}_x = V - U\,[\xi\, E_x + f_x],$$

giving

$$UU_x - \frac{\hat{\psi}_x U_\xi}{1+E} = -p_x + \frac{U_{\xi\xi}}{(1+E)^2}, \qquad (2.4.1a)$$

$$U = \frac{\hat{\psi}_\xi}{1+E}, \qquad (2.4.1b)$$

$$\hat{\psi} = U = 0 \text{ at } \xi = 0, \quad U_\xi = 0, \ \hat{\psi} = 1 \text{ at } \xi = 1, \qquad (2.4.1c\text{-}f)$$

$$p = s\eta. \qquad (2.4.1g)$$

Although the integrations in this section are all on a horizontal surface (f = 0), f is introduced here since the same numerical scheme is used in §3.2 to solve for the flow down a slope ($f = -\alpha x$). Also, the equations in the two cases are identical when we acknowledge the ellipticity of the problem, as we do in §3.7, and investigate the forced interaction problem of the flow over an obstacle on an inclined plate. It is noted that in the above rewriting we have made use of a Prandtl shift in y. In chapter 3 we change notation slightly and a further Prandtl shift is made allowing us to define the case f = 0 to be flow down a uniform slope.

System (2.4.1a-g) constitutes a third order system for $\psi(x,\xi)$ in ξ. The fourth boundary condition in ξ enables us to determine the unknown E and so the depth of the layer, which, of course, provides the pressure gradient driving the flow. These equations are written in finite difference form as

$$\left(\frac{U_{i,j} + U_{i-1,j}}{2}\right)\left(\frac{U_{i,j} - U_{i-1,j}}{\Delta x}\right) -$$

$$\left(\frac{\hat{\psi}_{i,j} - \hat{\psi}_{i-1,j}}{\Delta x}\right)\left(\frac{U_{i,j+1} - U_{i,j-1} + U_{i-1,j} - U_{i-1,j-1}}{4\Delta z}\right) + \frac{p_i - p_{i-1}}{\Delta x}$$

$$- \left(\frac{U_{i,j+1} - 2U_{i,j} + U_{i,j-1} + U_{i-1,j+1} - 2U_{i-1,j} + U_{i-1,j-1}}{2\Delta z^2}\right)$$

$$= 0, \quad j=2,J-1, \qquad (2.4.2a)$$

$$\left(\frac{U_{i,j}+ U_{i,j-1}}{2}\right) - \left(\frac{\hat{\psi}_{i,j}- \hat{\psi}_{i,j-1}}{\Delta z}\right) = 0, j=2,J, \qquad (2.4.2b)$$

$$\hat{\psi}_{i,J} = 1, \quad \hat{\psi}_{i,1} = 0, \quad U_{i,1} = 0, \qquad (2.4.2c\text{-}e)$$

$$3U_{i,J}- 4U_{i,J-1}+ U_{i,J-2} = 0, \qquad (2.4.2f)$$

$$\Delta z = \Delta\xi(1 + (p_i+ p_{i-1})/s - (f_i+ f_{i-1})/2).$$

Here $\Delta\xi = 1/(J-1)$, where J is the number of points used in y. The method of solution and of finding the unknown E, which appears in the above as p/s - f, is as follows. If the solution is known at *x*-station i-1, the above 2J equations are solved for the 2J unknowns, $\hat{\psi}_{i,j}$, $U_{i,j}$, j = 1,J. The nonlinearity is dealt with by using Newton iteration until successive iterates differ by less than a specified amount, typically 10^{-6}. This takes only 5 or 6 iterations using as an initial guess the solution at *x*-station i-1. For each iteration a single (2J-1)x(2J-1) matrix, $\underline{\underline{a}}$, is derived from the above system without equation (2.4.2f). This is inverted for the iterates $\delta\hat{\psi}_{i,j}$, $\delta U_{i,j}$, j=1, J. The matrix $\underline{\underline{a}}$ has a single band about the diagonal and so this is easily performed by Gaussian elimination. The term in the equations arising through the unknown pressure iterate, δp_i, is considered as part of the inhomogenous term. Thus if $\underline{g}$ is the vector made up of $\delta\hat{\psi}_{i,j}$, $\delta U_{i,j}$, we have

$$\underline{\underline{a}}\ \underline{g} = \underline{b}+\delta p\ \underline{c},$$

where $\underline{b}$, $\underline{c}$ are vectors. The solution is written in the form

$$\underline{g} = \underline{\alpha}+\delta p\ \underline{\beta}.$$

The inversion of $\underline{\underline{a}}$ recursively defines α_j, β_j, given that equations (2.4.2d-e) imply $\alpha_1 = \beta_1 = \alpha_2 = \beta_2 = 0$. Finally, knowing α_J, β_J, α_{J-1}, β_{J-1}, α_{J-2}, β_{J-2}, we impose the neglected boundary condition (2.4.2f) and fix δp_i. Hence all the iterates can be calculated. This method is

commonly used in computing interactive boundary layers where the pressure is unknown and is constant throughout the boundary layer depth. See Smith (1974).

§2.4.2 Results and discussion.

For the case of liquid layer flow along a horizontal surface we use f = 0. Usually the initial condition used is half-Poiseuille flow, with depth 1 at $x = 0$. A typical numerical solution in this case is shown in Figure 2.4.1. This has s = 2, $\Delta x = 10^{-6}$, $\Delta\xi = 10^{-2}$, and the solution remains quantitatively similar when finer grids are used. The most notable feature is that it ends, at some finite x, in a singularity in which the skin friction, $U_y(0)$, and pressure gradient become infinite although the pressure itself remains finite. The structure of the solution in the neighbourhood of the singularity is investigated in §2.5. The singularity is attained remarkably soon ($x = 0.0373$), although it is postponed for larger s and hastened for smaller s. Figure 2.4.2 shows solutions for a variety of values of s. The singularity itself seems to have the same qualitative form for all s.

For values of s numerically of the order of 0.01 a very small value of Δx (10^{-8}) is needed to advance the solution, which still attains the singular form described above. If larger values of Δx are used (10^{-4}) the solution develops into one similar to Watson's solution with the depth growing linearly. See Figure 2.4.3. Watson's solution is equivalent to setting s = 0, and suppressing the interaction. However as the depth reaches a certain value, further downstream, the method fails. We can presume that, as explained in §2.2, at this downstream station the depth has increased sufficiently to reinstate the pressure term into the equations and allow the interaction. An explanation of this small s behaviour is offered below in §2.6.5 in terms, suggested by §2.3, of the interactive development becoming rapid as s decreases and the interaction being suppressed if we choose a sufficiently coarse discretisation in x.

In addition to half-Poiseuille starting flow, smooth

initial profiles with the vorticity confined to near the wall and with a large skin friction were followed in their downstream development. If the skin friction is not too large these develop initially with the vorticity diffusing from the wall, the skin friction dropping, and the depth decreasing. Then, however, they attain the same singular form as do the half-Poiseuille profiles. For a larger initial skin friction similar behaviour to that for small s is observed, with the method unable to advance the solution by a single x-station. This is true whatever the value of s. Again we offer an explanation of this below.

§2.5 The Structure Of The Expansive Singularity.

The singularity revealed by the free interaction calculations of §2.4 is found to have the structure described below, which is essentially that of the expansive singularity in hypersonic flow; see Brown, Stewartson and Williams (1975), Gajjar and Smith (1983). This similarity is due to the relationship between the pressure-displacement law in hypersonic interactions ($P = -A$), and the corresponding law in liquid layer flow ($p = s\eta$). We follow the analysis of Brown, Stewartson and Williams (BSW) who consider the singularity in the hypersonic case and expand the solution as $x \to 0-$, where we have assumed the singularity to occur at $x = 0$ after a shift of origin.

For $y \sim O(1)$, viscous effects are small and the solution for the stream function here is

$$\psi(y) \sim \psi_0(y) + A(x)\, U_0(y) + p(x)\, U_0 \int_y^a \frac{1}{U_0^2}\, dy, \qquad (2.5.1)$$

where ψ_0 is the stream function at $x = 0$. This develops from the initial profile and contains information about the history of the flow, so we expect it to depend on s. Here a is the depth of the liquid layer at $x = 0$ and

$U_0 = \psi_{0y}$. The unknowns A and p are O(1) functions of x, with p corresponding to the pressure, and A the negative displacement suffered by the main part of the flow relative to its position at $x = 0$. The free surface in the vicinity of $x = 0$ is given by $y = a + p/s$.

As $y \to 0$ (2.5.1) predicts a non-zero vertical velocity at the wall unless $U_0 \sim 3\lambda y^{1/2}/2$ as $y \to 0$, where λ is to be determined. We therefore deduce that the velocity must develop into a profile with this form. In this case

$$\psi \sim \lambda y^{3/2} + A(x)\ 3\lambda y^{1/2}/2 + p(x) \left[-\frac{2}{3\lambda} y^{1/2} \ln y + K\, y^{1/2} \right], \quad \text{as } y \to 0, \qquad (2.5.2)$$

$$K = \left[\frac{2\ln a}{3\lambda} + \frac{3\lambda}{2} \int_0^a \left(\frac{1}{U_0^2(t)} - \frac{4}{9\lambda^2 t} \right) dt \right] = \frac{3\lambda}{2} \int_0^a \frac{1}{U_0^2} dt.$$

To smooth out this non-analytic behaviour as $y \to 0$ the solution requires a boundary layer near $y = 0$. Inertial effects here will be of order $U^2/x \sim y/x$ and the viscous terms of order $y^{1/2}/y^2 = y^{-3/2}$. A balance is possible, therefore, which brings in inertial, viscous and pressure effects near the wall if $y \sim |x|^{2/5}$, $\psi \sim |x|^{3/5}$ and $p_x \sim |x|^{-3/5}$. Accordingly we substitute a form

$$\psi \sim \alpha |x|^{3/5} f(\alpha y/|x|^{2/5}), \quad p_x \sim 2\alpha^4 |x|^{3/5}/5,$$

as $x \to 0-$, into equations (2.1.1a-f). The constant α is to be determined but is related to λ. This gives the following for the function f, written in terms of the similarity variable $\zeta = \alpha y/|x|^{2/5}$,

$$f_{\zeta\zeta\zeta} - 3/5\ f\ f_{\zeta\zeta} + 1/5\ (\ f_\zeta^2 + 2\ ) = 0,$$

$$f(0) = 0, \quad f_\zeta(0) = 0, \quad f \sim G_0 \zeta^{3/2}, \quad \zeta \to \infty$$

for some G_0. A solution to this equation exists, (BSW),

with $f_{\zeta\zeta}(0) = 1.398$ and an asymptote as $\zeta \to \infty$ of

$$f \to G_0(\zeta^{3/2} - 2/3\zeta^{1/2}\ln(\zeta)) + C_0\zeta^{1/2},$$

$$G_0 = 1.380, \qquad C_0 = -1.703.$$

This allows us to fix α in terms of λ, by matching the term proportional to $\zeta^{3/2}$ to the solution (2.5.2). We find $\alpha = (\lambda/G_0)^{2/7}$. Matching the rest of the two solutions gives

$$\frac{A(x)}{p(x)} \sim \frac{2}{3\alpha^6}\left[C_0 - \frac{2}{3}\ln\alpha - \frac{3\alpha^6}{2}\int_0^a \frac{1}{U_0^2}dt - \frac{4}{15}\ln\left(\frac{1}{|x|}\right)\right]. \quad (2.5.3)$$

However the boundary condition at the free surface, $\psi(a+p/s) = 1$, applied by linearising (2.5.1) about $y = a$, leads to

$$\frac{A(x)}{p(x)} = -\frac{1}{s}.$$

The matching is complete and λ and α found, but for the slow dependence on $\ln(1/|x|)$ in (2.5.3). This mismatch stems from the large-ζ behaviour of the boundary layer equation, in which the second biggest term at infinity is not the "displacement" term $C_0\zeta^{1/2}$, but the logarithmically larger term forced by the dominant $\zeta^{3/2}$-like behaviour of the solution. As in BSW this mismatch can be reduced by further refinement of the singularity structure, including an inviscid buffer region between the boundary layer and the free stream. Its thickness is $O(|x|^{2/5}/\{\ln(1/|x|)\}^{1/5})$, and it adjusts the size of the pressure gradient to be $O(|x|^{-3/5}\ln(1/|x|)^{4/5})$. However this still does not determine λ for similar reasons to those above, there being a mismatch now of $O(\ln(\ln(1/|x|))$, and further buffer regions are implied. This mismatch continues as these further buffer regions are included and so, as discussed by BSW, it becomes impossible to determine the

actual coefficients of the expansion, α and λ, although the structure of the singularity is clear. We have the predictions

$$p_x \sim P|x|^{-3/5}\ln(1/|x|)^{4/5}L_1(|x|),$$

$$\tau \sim T|x|^{-1/5}\ln(1/|x|)^{3/5}L_2(|x|).$$

Here τ is the skin friction at the wall, and L_1 and L_2 are functions which vary more slowly than any power of $\ln x$. The values of P and T remain unknown constants.

Figure 2.5.1 shows a comparison of this singularity structure with the numerical solutions of §2.4. Figure 2.5.1a shows the velocity profiles (in terms of the ξ of §2.4), and clearly shows the development of a boundary layer near the wall. Figures 2.5.1b and 2.5.1c show τ^{-5}, $\tau^{-5}(\ln\tau)^3$ and $(-p_x)^{-5/3}$, $(-p_x)^{-5/3}(\ln(-p_x))^{4/3}$ against $|x|$ in the neighbourhood of the singularity which occurs at $x = 0.0373$ in this case in which $s = 2$. As can be seen the curves are approximately straight lines, as they should be, but for the slow logarithmic behaviour, and this behaviour is improved in the cases where some of the effects of the buffer zone are included. Therefore we have some degree of confidence that the structure outlined above is a correct description of the singularity experienced by the numerical computations.

§2.6 The Branching Solutions.

§2.6.1 Introduction.

This section aims to explain the results of the computations of §2.4 in terms of solutions which can branch from the basic flow. These are initially small but grow in x and when nonlinear effects begin to enter they can alter the basic flow. The solutions found in §2.2 do not take this branching into account, and therefore the solutions which we calculate are not those predicted in §2.2.

Solutions branching from a parallel oncoming flow are commonly used to explain the mechanism for upstream influence in many flows, such as supercritical liquid layers (Gajjar and Smith (1983)), supersonic boundary layer flow (Stewartson and Williams (1969), Lighthill (1953)), and pipe and channel flows (Smith (1976)), where the governing equations at first seem parabolic. The branching solutions render them elliptic enabling the flow to adjust for any downstream boundary conditions. The non-uniqueness in flows of this type has its origin in the possibility of a viscous-inviscid interaction in the flow. In the case of liquid layers the inviscid mechanism is that of pressure changes due to the hydrostatic effects of raising or lowering the free surface. Viscous effects enter as they affect the flow beneath the surface as it adjusts to these alterations. This, in turn, causes a change in the position of the free surface and so the interaction continues. In the case of flow over a horizontal surface the flow is not parallel, since the layer thins due to viscous retardation. This non-parallelism has an effect on the form of the branching solutions.

In the case of small s or large skin friction the failure of our numerical method, which assumes the equations are parabolic, and can thus march downstream in a simple fashion, may well be due to the growth rate of these departures being rapid in these limiting cases. The method is unable to pick out one of the many rapidly growing solutions and this non-uniqueness of possible solutions causes it to fail. Increasing the size of the x-step in the marching suppresses the branching, which occurs on a short length scale, in the finite difference form of the equations and the solution can proceed to that predicted in §2.2 for small s i.e. a linear increase in depth. The large skin friction case is associated with a uniform flow and allied Blasius boundary layer profile. This is known (Gajjar and Smith (1983)) to admit branching solutions.

The singularity that the numerical results exhibit

has been shown in §2.5 to be akin to that occurring in the hypersonic boundary layer interaction studied by Brown Stewartson and Williams (1975). There the flow upon which the initially small perturbations grow is the parallel shear near the wall in a boundary layer. In this case, of hypersonic flow, there are two qualitatively different departures possible. In the first the boundary layer thickens and there is no singularity. Instead a downstream form is attained which is described in Gajjar and Smith (1983). This is known as a compressive free interaction because of its relevance to upstream influence in compressive corner flows. The second type is known as the expansive interaction for similar reasons. Here the boundary layer thins and continues to do so until attaining the singular form we have described. We see only this expansive singularity in our computations of liquid layer flows because the departure is forced by the thinning of the layer which is needed to provide the pressure gradient driving the original flow over the horizontal surface. This is an effect which has its basis in the non-parallel nature of the basic flow and it is represented by the first term in the expansion for small x presented in §2.3. For O(1) s the development of the departure is slow and we can follow it with our numerical method. It is a development which occurs through essentially the same mechanism as described for small s below, but which is affected by the non-parallel nature of the starting flow.

From the small x expansion of §2.3 we can pick out that the x-scale of the rapid growth of the departures for small values of s is $O(s^3)$. Below we present the structure of these rapidly growing solutions together with several other structures relevant to departures in other related limits, such as small depth or large skin friction, or to alternative starting flows, such as those shown in §2.2 to be relevant to the full set of equations in the limits of small and large s. These are two-dimensional Watson's flow as $x \to 0+$ and half-Poiseuille flow with a depth of $(-12x)^{1/4}$ as $x \to -\infty$ respectively.

§2.6.2 Small s.

We seek a perturbation to the oncoming flow of the form

$$\psi \sim \psi_0 + s\,\psi_1,$$

$$\eta \sim \eta_0 + s\,\eta_1,$$

$$p \sim sp_0 + s^2 p_1,$$

where ψ_0, η_0, p_0 represent the oncoming flow and are functions of x satisfying equations (2.1.1a-g). See Figure 2.6.1. Without loss of generality we can let η_0 be zero so that the depth of the layer is initially unity. In addition, therefore, $p_0 = \eta_0 = 0$. The perturbation quantities, ψ_1, η_1, p_1 are functions of the fast variable $\hat{x} = x/s^3$ and $p_1 = \eta_1$. In the main part of the flow where $y \sim O(1)$ (region I in Figure 2.6.1) the rapid growth of the perturbation dominates and the solution is governed by inertial effects, with the pressure term reduced in importance by the smallness of s. Therefore equations (2.1.1a-g) reduce here to

$$\psi_0'\psi_{1_{\hat{x}}}' - \psi_0''\psi_{1_{\hat{x}}} = 0,$$

where $'$ indicates differentiation with respect to y. This has solution $\psi_1 = A_1(\hat{x})\psi_0'$. Application of the boundary conditions at the free surface which reduce to $\psi_1(1) = -\eta_1\psi_0'(1)$ and $\psi_1''(1) = -\eta_1\psi_0(1)$, yields

$$A_1 = -\eta_1 = -p_1. \qquad (2.6.1)$$

As $y \to 0$ we obtain, if $\psi_0 \sim \lambda y^2/2$,

$$\psi \sim \lambda y^2/2 + s\,A\,\lambda\,y,$$

so a sublayer (region II in Figure 2.6.1) of thickness $y \sim O(s)$ is produced at the wall to reduce the resulting slip velocity, $sA\lambda$ to zero. Here we write $y = sz$ and $\psi = s^2\hat{\psi}(z)$, $U \sim s\hat{U}(z)$ where $\hat{U} = \hat{\psi}_z$ and so we obtain a

nonlinear inertia-viscosity-pressure balance in this sublayer,

$$\hat{U}\hat{U}_{\hat{x}} - \hat{\psi}_{\hat{x}}\hat{U}_z = -p_{1_{\hat{x}}} + \hat{U}_{zz}, \tag{2.6.2a}$$

$$\hat{U} = \hat{\psi}_z, \tag{2.6.2b}$$

$$\hat{U}(0) = \hat{\psi}(0) = 0, \tag{2.6.2c}$$

$$\hat{U} \sim \lambda(z + A), \quad z \to \infty, \tag{2.6.2d}$$

$$\hat{U} \sim \lambda z, \quad \hat{x} \to -\infty, \tag{2.6.2e}$$

and, from (2.6.1),

$$p_1 = -A. \tag{2.6.2f}$$

The system (2.6.2a-f) consists of the equations governing the hypersonic free interaction. Gajjar and Smith show them to be relevant to supercritical (in the sense Fr > 1) liquid layer flow if there is no vorticity in the main body of the flow (unlike here). These equations hold on a length scale L, where $1 \ll L \ll Re$. The above analysis shows that we can expect branching from profiles with vorticity in the same fashion as from those without, provided that the Froude number is sufficiently large. The free interaction problem for these equations leads either to the hypersonic expansive singularity or, in the compressive case, to a downstream form with separated reversed flow and the pressure (proportional to the depth) growing like $0.94796\hat{x}^m$ where $m \approx 0.43050$. Here, therefore, as $\hat{x} \to \infty$ we have a depth increasing like $s\hat{x}^m$. Brotherton-Ratcliffe (1986) makes a comparison of this blunt form of the free surface with the experiments of Craik et al. (1981) who take measurements of an axisymmetric hydraulic jump, which, qualitatively at least, has the same shape of free surface. Brotherton-Ratcliffe assumes the oncoming profile to be

essentially uniform and inviscid in his comparison. There is good qualitative agreement, although the depth is somewhat under-predicted. In §2.7 we take up this idea and, believing the flow to be fully developed at the position of the jump, we make a comparison of the above result with the experiments.

§2.6.3 Small depth, h.

Related to the above is a similar structure leading to the same set of equations (2.6.2a-f) governing the branching for small depth, h, at some position x_0. This is of relevance to the problem mentioned in §2.1, in which s is scaled out of the equation but remains in the boundary conditions. In this normalisation a small initial depth corresponds to a large value of the Froude number from (2.1.2b). We can expand on a small length scale, $L \ll 1$, about x_0 and derive the scalings as follows. Since $\psi_0 \sim O(1)$ the oncoming velocity, $U_0 \sim O(1/h)$. A velocity perturbation of size $\delta \ll 1/h$ carries a small mass flux and so the position of the free surface is altered only by $O(h\delta)$. As a result, although the relative change in the free surface position is $O(\delta)$, the pressure generated is only $O(h\delta)$ (since $s \sim O(1)$, or is scaled out of the equations). The main body of the flow reacts therefore as in §2.6.2 above, leading to a slip velocity of size δ at the wall. In a sublayer similar to that in §2.6.2, but of thickness $h\delta$ and where the velocity is $O(\delta)$, this is brought to zero. Again the response here is of the interactive inertia-pressure-viscosity kind, of equation (2.6.2a-f). This requires $\delta^2/L \sim \delta h/l \sim \delta/h^2\delta^2$, leading to $\delta \sim h$ and $L \sim h^5$. This result also ties in with the result that the small x expansion in §2.3 fails when $x \sim O(\lambda^{-5}) \sim O(h^5)$ here.

§2.6.4 Large skin friction, λ.

We now consider the case wherein the depth and Froude number are both order unity, but the starting flow has a large skin friction λ. The analysis is valid for any profile U_0 for $y \sim O(1)$, provided that $U_0 \sim O(1)$ as $y \to 0$,

and that it is reduced to zero at the wall. The thickness of the sublayer which effects this reduction is $O(\lambda^{-1})$. A simple modification of the analysis in Gajjar and Smith shows that branching is possible on a length scale $O(\lambda^{-5})$. We put their small parameter, ε, equal to λ^{-1} and follow their analysis through. In effect the analysis is similar to that in §2.6.2. We find that, after a factoring out of various O(1) constants, equations (2.6.2a-f) hold in a sublayer at the wall of thickness $O(\lambda^{-2})$, for a perturbation of size $O(\lambda^{-1})$. The criterion for supercritical flow and the pressure-displacement law being $p = -A$, rather than $p = A$, which is appropriate to subcritical flow but does not give rise to branching, is

$$\frac{1}{s} - \int_0^1 \frac{1}{U_0^2}\, dy > 0.$$

This reduces to $s < 1$ if $U_0 = 1$, the case studied by Gajjar and Smith.

§2.6.5 Branching from Watson's solution.

An alternative form of branching solution, related to the case covered in §2.6.3 above, can be used to explain the sudden failure of the numerical solutions in §2.4 which develop into Watson's form. These have s small but a step size large enough so that, initially at least, the interaction responsible for the branching is suppressed. The flow develops into Watson's form with a linear increase in depth and this solution remains valid until the increasing depth reinstates the pressure term in the equations. A rescaling, see §2.2, gives equations (2.1.1a-e, 2.1.2a), with a condition as $x \to 0+$ given from Watson's solution which may be written, on further factoring of the variables,

$$\psi \sim f(\xi), \quad \xi = y/xq, \quad h = qx,$$

where

$$qf''' + f'^2 = 0,$$

$$f(0) = f'(0) = f''(1) = 0, \quad f(1) = 1.$$

Here $'$ indicates $\partial/\partial\xi$. This fixes q and $f''(0) \equiv \lambda$, both of which are positive. See Figure 2.6.2.

We perturb this starting profile as follows:

$$\psi = f + E\,\hat{\psi}(\xi),$$

$$h = xq(1 + E\,\hat{\eta}),$$

where $E = \exp(-\gamma/x^9)$ and γ, presumed positive, is to be found. We substitute this form into the governing equations and expand as $x \to 0+$. As in §2.6.2, the main part of the flow (region I of Figure 2.6.2) reacts in a fashion dominated by inertia and gives the solution

$$\hat{\psi} = -\hat{\eta}\, f'.$$

The pressure governing the perturbation is $xE\hat{\eta}q$, and there is a slip velocity at the wall of size $E\lambda(-\hat{\eta})/xq$. A sublayer in y with thickness $O(x^4)$ in which the velocities are $O(x^2)$, is generated in order to reduce this slip velocity to zero. This is region II of Figure 2.6.2. As $y \to 0$, we write $z = y/x^4$, and

$$U \sim x^2(\lambda q^{-2}z - \lambda^2 q^{-6}x^9 z^4/12 + \ldots - E\hat{\eta}\lambda q^{-1}x^{-3}\hat{u}(z)).$$

On substitution of this form into the governing equations we find that at $O(Ex^{-9})$ a linearised form of system (2.6.2) results,

$$z\hat{u} - \hat{v} = \lambda^{-2}q^4 + q^2\hat{u}''/(9\lambda\gamma),$$

$$\hat{v}' = \hat{u}, \quad \hat{u}(0) = 0, \quad \hat{u} \to 1 \text{ as } z \to \infty,$$

where ′ now represents differentiation with respect to z.

We can solve this eigenvalue problem for γ to give $\gamma = \lambda^5(3|Ai'(0)|)^3/(9q^8)$, with Ai representing Airy's function. This value is positive as required. The coefficient of the growing exponential, $\hat{\eta}$, can have any value, and so we have the possibility of the flow developing onward from the origin in a non-unique fashion.

We note that the perturbation has a very rapid growth rate as $x \to 0$. Also, the departure does not necessarily develop and become nonlinear in the same fashion as in cases considered in §§2.6.2-4, all of which end with the depth increasing as $x^{0.4305}$, or falling into a singularity, as predicted by the hypersonic free interaction equations.

An axisymmetric version of this theory can be derived along similar lines. The base flow here has a quadratic increase in depth and the perturbation initially grows like $\exp(-\hat{\gamma}/x^{18})$. The size of the slip velocity at the wall is $O(E/x^3)$ and the viscous sublayer has thickness $y \sim O(x^7)$.

These results are of relevance to the problem of a fully developed liquid layer at high Froude number originating at $x = 0$, initially on a horizontal surface but adjusting, via the above non-uniqueness, for some obstacle and then eventually flowing down a slope. This slope provides the pressure gradient to drive the flow as $x \to \infty$.

§2.6.6 Branching from half-Poiseuille flow.

From §2.2 we know that in the limit of large s the profile at $x = 0$ develops according to lubrication theory, with the pressure needed to drive the flow coming from a slow decrease in the depth of the layer. Eventually, however, inertial effects enter and the flow, after rescalings detailed in §2.2, is governed by (2.1.1a-e,

2.1.2a), i.e.

$$UU_x + VU_y = -p_x + U_{yy}, \tag{2.6.3a}$$

$$U_x + V_y = 0, \tag{2.6.3b}$$

$$p_x = h_x, \tag{2.6.3c}$$

$$U = V = 0 \text{ at } y = 0,\ U_y = 0 \text{ at } y = h, \text{ and } \int_0^h U dy = 1. \tag{2.6.3d-g}$$

The boundary conditions as $x \to -\infty$ are

$$h \sim h_0 = (-12x)^{1/4}, \quad U \sim (3/h_0^3)(yh_0 - y^2/2). \tag{2.6.3h-i}$$

To search for the possibility of upstream influence in these equations we first make the change of variable, $z = y/h_0$, and introduce a stream function ψ. We have, using the result $h_{0x} = -3/h_0^3$, that $\partial/\partial y \to h_0^{-1}\partial/\partial z$ and $\partial/\partial x \to \partial/\partial x + 3h_0^{-4}z\partial/\partial z$. This leads to

$$h_0(\psi_z\psi_{zx} - \psi_x\psi_{zz}) = -h_0^3 p_x + \psi_{zzz}, \tag{2.6.4a}$$

$$z \in [0,1], \tag{2.6.4b}$$

$$p_x = h_x, \tag{2.6.4c}$$

$$\psi \sim 3(z^2/2 - z^3/6), \quad h \sim h_0(x) \text{ as } x \to -\infty. \tag{2.6.4d}$$

We consider a perturbation to this flow at $-\infty$ of the form $a\hat{E}$ in depth and $a\hat{E}f$ in stream function. Here $\hat{E} = \exp(-\gamma h_0)$ for some positive γ to be found. Substitution into equations (2.6.4) gives

$$(3\gamma h_0^{-2})(F'f' - F''f) = -3\gamma + f''',$$

where $F' = 3(z-z^2/2)$. However h_0 is large and so

$$f''' \sim 3\gamma \text{ as } x \to -\infty.$$

The boundary conditions satisfied by f at z = 1 are obtained by linearising the position of the free surface about z = 1, and are f(1) = -3/2 and f''(1) = 3. Therefore

$$f = -3z(z-z^2/2),$$

$$\gamma = 3.$$

The size of the perturbation, a, can take any value and so, again, the development forward in x, from $x = -\infty$, is not unique.

The perturbation itself is governed by lubrication theory, at least initially, and so too is the flow from which it branches. It also grows in the region of large negative x and so we can expect similar departures from the large s flow examined in §2.1. We see therefore that branching is possible on an O(1) lengthscale in x in the large s limit and is governed by equation (2.2.1), although the branching is ignored in the analysis of §2.2.1. This behaviour has strong similarities with the branching of liquid layer flow on a small slope as discussed in §3.6.

§2.6.7 Discussion.

Most of the above structures have one thing in common - they represent eigensolutions growing on a flow that is parallel on the length scale over which the eigensolutions develop. There is an exception of sorts in §2.6.5, but here the base flow has a similarity form, which is in effect a parallel flow solution depending on only one variable, ξ. For example, in the case of small s the development length of the perturbation is relatively short, on an O(Re) scale in $\hat{X}$ ($\hat{X}$ is defined in §2.1.1), whilst in the case of large s the development length of the basic flow is relatively long. The search for similar structures for finite values of s is hampered by the non-parallelism involved.

It is tempting to suggest that branching is still possible in these non-parallel cases, not in the form of eigensolutions, but in the development of a perturbation which, as it grows on an O(1) scale, must interact with the base flow right from the start. It is thus no longer clear what is base flow and what is perturbation. The numerical computations of §2.4 seem to suggest that such branching is possible, but it has not been possible to find analytic descriptions for the process, and so we can only put this forward as a tentative suggestion.

This is in contrast to the case of half-Poiseuille flow down a gradient. Here the pressure differences povided by gravity as the flow descends drive the flow and overcomes viscous retardation. Therefore the flow is parallel for all slopes. We show in §3.5 that branching in the form of eigensolutions can be found for all slopes, corresponding to all Froude numbers on a horizontal surface. In support of the above suggestions the subsequent development of the perturbations in the case of an expansive interaction, the only type seen in the numerical computations on a flat surface , is very similar to that which occurs on the flat. The compressive interaction on a flat plate, leading to a hydraulic jump and separation, seems to be possible only if it occurs on a short length scale, i.e. if the Froude number, s^{-1}, is large. It may be possible for smaller s^{-1} but its form will certainly be altered by non-parallel effects which may stop it occurring altogether.

§2.7 Comparison With Experiment.

§2.7.1 Introduction; axisymmetric hydraulic jumps.

Experiments performed by Craik, Latham, Fawkes and Gribbon (1981) on an axisymmetric hydraulic jump are close to the parameter range covered by the high Reynolds number theory described in the preceding sections. The experiments study the jump formed when a column of liquid falls onto a flat plate and spreads, just as from a tap

into a sink. Here we make a comparison between these experiments and the proposal that the jump is described by the large Froude number structure in §2.6.2. We suggest that the jump is the final form of a solution which branched from the upstream flow, which we presume to be laminar and fully developed, and with a Froude number sufficiently large that the theory applies.

Brotherton-Ratcliffe (1986) makes a comparison of the theory of Gajjar and Smith (1983) with the same experiments. Essentially, of course, our comparison and his are for the same proposal, that the jump is described by the equations of the hypersonic interaction. Even the scalings with respect to the Froude number and skin friction are the same. The difference lies in the result of §2.6.2 that the same equations describe the jump even for fully developed flow if the Froude number is large. Brotherton-Ratcliffe presumes that the flow upstream of the jump is essentially inviscid, but with a Blasius sublayer at the wall. This is used to give predictions for the depth and skin friction of the flow at the radius of the jump. It implies that the depth varies inversely as the radius, due to mass continuity effects, and that the skin friction varies as the inverse square root of the radius. Overall the prediction for the height of the jump is approximately 40% too small. The comparison is most accurate in the case where the depth used in the prediction is not that calculated as above but that measured from Figure 6 of Craik et al., reproduced here as Figure 2.7.1. The inviscid theory predicts the upstream depth to be approximately a fifth of its actual value. However there are many encouraging qualitative agreements between the behaviour and structure of the experimental jumps and the predictions of the high Reynolds number, interactive theory. For example, in the experiments the main body of the layer does not slow suddenly, as presumed by traditional inviscid models of the hydraulic jump (Watson (1964), Lamb (1932), Lighthill (1978)), but instead seems to ride over a separated region below it, of great length compared with the depth of the layer. The

theoretical prediction is that the flow should react in two regions with separation possible in the viscous sublayer but the main part of the flow merely being displaced. In addition, in the experiments, as the position of the jump moves towards the source of the water the length of the separated region decreases. This can be explained as being due to an increase in the skin friction or the Froude number in the thinner, faster-moving layer here, and so from the scalings involved, presented below, a decrease in the length scale of the interaction.

§2.7.2 The theoretical prediction.

Our suggestion is that the circular hydraulic jumps described above are self-induced, free, viscous-inviscid interactions, of the type described in §2.6.2, on fully developed flow.

We believe that the flow is fully developed at the position of the jump for two reasons. Firstly the Froude numbers of the layers in the experiments are large, typically 120. The development is therefore likely to be governed by Watson's solution which assumes an infinite Froude number and predicts, in this axisymmetric case, a quadratic growth in the depth of the layer. This growth agrees qualitatively with that seen in Figure 2.7.1. The depth just upstream of the jump position, predicted with this assumption, is much closer to the measured values than those predicted by inviscid theory. Secondly consider the equations

$$UU_x - \psi_x U_z = x^2 U_{zz}, \qquad (2.7.1a)$$

$$U = \psi_z, \qquad (2.7.1b)$$

$$U(0) = \psi(0) = 0, \; U_z(T) = 0, \; \psi(T) = 1, \qquad (2.7.1c\text{-}f)$$

$$z \in [0,T], \quad T \text{ unknown}. \qquad (2.7.1g\text{-}h)$$

This system is related to that governing the high Froude number ($s = 0$), axisymmetric flow of a liquid layer via

the transformation $y = z/x$. In deriving this dimensionless form we nondimensionalise the "depth", z, with $\sigma^2/2$, where σ is the radius of the jet of water falling on the plate, the radial coordinate, x, with $L_\infty = (Q\sigma^2/4\pi\nu)^{1/3}$, and the stream function, ψ, with $(Q/2\pi\sigma)$. Here Q is the volume flux in the jet and ν the kinematic viscosity of the fluid. The radius of the jet, σ, appears in the nondimensionalisation since we desire to match the solution with the inviscid behaviour of the jet near $x = 0$, where we can take the flow as uniform and governed only by the continuity condition, $Q = U_0\pi\sigma^2 = U_0 2\pi x h$, where U_0 is the velocity in the jet (assumed uniform) and h is the depth of the layer. This predicts $T \sim \sigma^2/2$ as $x \to 0$. The equations do not exhibit branching since we suppress the interaction by neglecting the pressure term, $(sT/x)_x$, due to the small value of s. We integrate these equations forward in x from an initial condition using a suitable adjustment of the Crank-Nicholson scheme used in §2.4. This initial condition consists of uniform velocity for $z > 0.05$ which is reduced to zero at $z = 0$ with a cubic in z, ensuring continuity of velocity and shear at $z = 0.05$. The flow becomes fully developed with $T \sim (\pi/3\sqrt{3})(x^3+d^3)$, as predicted by Watson's theory for $x >> 1$. The value of d^3 is estimated to be 0.69 and this is used later. See Figure 2.7.2. The nondimensional values of the jump radius in the experiments are in the range 1.5 to 3 and are therefore well above the value, of about $x = 1$, where these integrations indicate the flow has become fully developed.

Using this theory to give the flow upstream of the jump, we can now go ahead and use the results of §2.6.2 to predict the free surface shape, h(x), downstream. The result is

$$\frac{(h - h_J)}{h_J} = (0.9167)\frac{s}{\lambda^2}\left(\frac{(x - x_J)\,\lambda^5}{Re\; s^3\; h_J} \right)^{0.4305},$$

where λ is the O(1) skin friction parameter and is

calculated, under the assumption of Watson's flow upstream of the jump, to be 2.279. Here h_J is the depth of the fluid just upstream of the jump at radius x_J and Re is the Reynolds number which, from mass conservation, is $Q/2\pi x_J \nu$. The inverse Froude number, s, is $gh_J^3/(Q/2\pi x_J)^2$. The above assumes that the jump occurs on a length scale short compared with its radius, allowing us to neglect its axisymmetric form and approximate it as two-dimensional.

If we use Watson's theory to give a value for h_J, Re, and s, given x_J, Q, and σ, we get the following prediction. We use $\nu = .01$ and $g = 981$ in c.g.s. units.

$$L_\infty = 1.996(Q\sigma^2)^{1/3}, \tag{2.7.2a}$$

$$\lambda = 2.279, \tag{2.7.2b}$$

$$h_J = 0.0380(x_J^3 + 5.49Q\sigma^2)/(Qx_J), \tag{2.7.2c}$$

$$Re = 15.91Q/x_J, \tag{2.7.2d}$$

$$s = 2.123(x_J^3 + 5.49Q\sigma^2)^3/(Q^5 x_J), \tag{2.7.2e}$$

$$\frac{\delta h}{h_J} = \frac{1.1306(\delta x)^{0.4305} Q^{1.4574} x_J^{1.7525}}{(x_J^3 + 5.49Q\sigma^2)^{1.305}}. \tag{2.7.2f}$$

Here we have used $d^3 = 0.69$ and δh and δx represent $h-h_J$ and $x-x_J$ respectively.

§2.7.3 A discussion of the approximations made in the prediction.

We now reconsider the approximations implicit in deriving and using the result of §2.6.2. Firstly since s is small, the small perturbation, of amplitude $O(s/\lambda^2)$, develops in the main part of the layer in a way dominated by inertial effects, i.e. $UU_x >> -p_x$. This is true however short the scale of the interaction if s is small. Streamline curvature, generating a normal pressure gradient p_y, becomes increasingly important as the length

scale shortens, however, adding a curvature term to the pressure-displacement law which then becomes $p = -A - c_1 A_{xx}$, where $c_1 = (\lambda^{10}\int_0^1 U_0^2 dy/s^7 Re^2)$ and U_0 is the nondimensionalised oncoming velocity profile. This term is similar to that responsible for upstream influence in channel flows (Smith 1976). It reappears too in §3.5.3 where it is shown to be the cause of branching on slopes of O(1) gradient as $Re \to \infty$. Surface tension is also important, as can be seen from Figure 2.7.1, and the experimental photographs of Craik et al. which clearly show a capillary wave upstream of the jump. Surface tension (see §2.1) adds a term $+c_2 A_{xx}$ where $c_2 = s(T/\rho g h_j^2)(\lambda^{10}/Re^2 s^7)$, and ρ and T are the density and coefficient of surface tension of the fluid (1.0 g/cm^3 and 73 dyn/cm^2 in c.g.s. units for water). The numerical values of c_1 and c_2 are very large, a point we take up later. Including these extra effects therefore we have the effective pressure-displacement law

$$P = -A - c_2(1 - \mu)A_{xx}, \qquad (2.7.3a)$$

$$\mu = sT/(\rho g h^{*2} I), \quad I = \int_0^1 U_0^2 dt, \quad c_2 >> 1. \qquad (2.7.2b)$$

A pressure-displacement law of the form $p = A_{xx}$, is, like the law $p = -A$, capable of giving rise to branching and upstream influence, but in this case the behaviour far upstream is wavy with a departure initially growing like $\exp(3Gx\pi i/7)$ $(x \to -\infty)$, where $G = (3|Ai'(0)|)^{3/7}$. This behaviour is not unlike the experimental capillary wave. Recent calculations of the solution of the interactive boundary layer equations allied to the pressure-displacement law $p = cA_{xx}$ (Professor F.T. Smith, private communication) indicate that, initially, the branching solution has the form of oscillations in A and p but with no separation occurring. Downstream, however, the amplitude of these oscillations increases rapidly and separation occurs. After separation there are no further oscillations and, instead, the downstream asymptote $p \sim P_\infty$, $A \sim P_\infty X^2 c^{-5/7}/2$ is attained. P_∞ is negative. In

the present context this implies that far downstream on the interaction length scale, as the displacement grows, the -A term on the right hand side of the pressure-displacement law dominates and the structure here is just that described by Gajjar and Smith with the blunt, $A \sim -x^{0.4305}$, surface shape, independent of the surface tension. This behaviour is also seen, and made explicit, in the analysis of surface tension effects on the corresponding interaction on a small slope, in §3.6.6.

In contrast the pressure law $p = -cA_{xx}$ does not give a wave-like departure, although the downstream asymptote is similar with $p \sim P_0 \approx 0.675$ and $A \sim -P_0X^2c^{-5/7}/2$ (Smith and Duck (1977)). So, although the downstream form of the hydraulic jump is likely to be similar to the case above, the upstream form will not be wave-like.

If we use the assumption of Watson's flow upstream of the jump we can estimate the value of μ. We find

$$\int_0^1 U_0^2 dt = (L_\infty^2 \int_0^1 f'^2 dt)/(4\pi^2 x_J^2) \approx (0.012)L_\infty^2/x_J^2, \qquad (2.7.4a)$$

where f′ is the similarity function defining the velocity profile. Thus we find

$$\mu = [2400/(\sigma^{2/3}Q^{11/3})]\, x_J^3\, (x_J^3 + 5.49Q\sigma^2), \qquad (2.7.4b)$$

using the results (2.7.2). For the experimental cases covered by Craik et al., μ is in the range 300 to 500 approximately. Thus the shape of the jump is dominated initially by surface tension effects and by hydrostatic effects far downstream. If μ is less than unity the result (2.7.3a) predicts no waves just upstream of the jump.

Due to the smallness of s and the relative smallness of the Reynolds number in the experiments, the length scale of the interaction, namely $Re\lambda^{-5}s^3h_J$, is very short and c_1 and c_2 very large. For the case Q = 29 in Figure 2.7.1 we find s = .0097, Re = 111.2, $L = 2.2\times10^{-5}h_J$, $c_2 \approx 6\times10^{13}$. L is the length scale of the interaction. So the experimentally small Reynolds number and large Froude

number is stretching the applicability of the large Reynolds number theory quite a bit: the relative error in neglecting streamwise derivatives in the viscous terms, and making the boundary layer approximation itself is $O(s^{-2}Re^{-2})$ and is of order unity here. Strictly we should expand in suitable powers of the inverse Reynolds number, and scale s, c_1 and c_2 suitably with Re in order to describe the structure of the jump at these high Froude numbers. However the discussion above indicates that the downstream form is still dominated by the hydrostatically produced pressure term and these extra effects serve only to delay the development of the jump profile and to add a constant to the downstream asymptote $A \propto -x^{0.4305}$. It is encouraging to note that in the above case we need $(x-x_J) >> 170h_J$, approximately, for the -A to dominate the c_2A_{xx} in the P/A law and, although long, this is much closer to the observed scale of the interaction than is L above, especially given the possibility of errors being introduced by the sensitive dependence of c_2 on s combined with the sensitivity of s to errors in x_J.

§2.7.4 The comparison with experiment and discussion.

The discussion above gives rise to the question of where we take the jump position to be and how we measure the increase in depth from Figure 2.7.1 in order to make the comparison. The present theory takes no account of surface tension which we have shown to be primarily responsible for increasing the length of the interaction region and for the dip in the surface near the jump. This however only adds a constant to the downstream depth (although, of course, this could be quite large numerically). Therefore we feel it is most suitable to measure the actual change in depth, δh, from the dip just before the rapid rise in depth, but consider it to have taken place at the point where the upstream depth is a maximum, before which the flow is well-approximated by Watson's solution. We consider therefore that the interaction starts near this point of maximum depth, and we use the flow here to nondimensionalise our equations.

The interaction continues, through a region where surface tension dominates and then, after the rapid rise in depth, the final form is governed by the hydrostatic part of the pressure-displacement law.

We make a comparison with Figure 2.7.1 from which we make the measurements of the jumps as detailed in Table 1. The values of the radius of the falling jet are estimated from similar cases, both in the height of the falling water column and its flux, mentioned in Table 1 of Craik et al.. The depths predicted using the formulae (2.7.2a-f) are displayed in Table 2. Table 3 shows the results of calculating the same quantities using the measured value of the depth upstream of the jump, i.e. the depth at the crest of the capillary wave. This uses the prediction

$$\frac{\delta h}{(\delta x)^m} = (0.0150)\,\frac{Q^{0.1525}}{h_J^{0.305}\,x_J^{0.1525}}\,. \qquad (2.7.5)$$

The results are seen to be encouraging in that the predicted depths are close to those measured from Figure 2.7.1. This measurement is of course itself a source of error in the comparison. The approximate error is similar to that in Brotherton-Ratcliffe's comparison, with the better agreement being near to the start of the jump where the displacement is smallest. The theory used is for relative changes in surface position of $O(s/\lambda^2)$ and this is small in these experiments. Therefore, further downstream where the layer has thickened we cannot expect the theory to be as accurate. Effects associated with the longer length scale over which the displacement ceases to grow and becomes constant will need to be incorporated. The comparison seems most succesful for the jump with the largest Reynolds number.

§2.8 SUMMARY.

Below we list the main results of this chapter.

1) Upstream influence eigensolutions in liquid layer flows on a flat plate over the long, O(Re), length scale are strongly affected by the non-parallelism and simultaneous development of the basic flow.

2) Analytic progress can be made when either (i) the Froude number is large so that the branching solutions are rapidly established on an $O(s^3Re)$ length scale where s is the inverse Froude number, or (ii) the Froude number is small so that the basic flow develops slowly.

3) The expansive free interaction terminates in a singularity with a structure in common with the corresponding interaction in hypersonic flow.

4) The compressive free interaction, which is perhaps possible only for relatively large Froude numbers, is similar in form to the corresponding interaction in hypersonic flow.

5) A proposition is made, that the experimental results of Craik et al. (1981) on hydraulic jumps can be explained in terms of a viscous-inviscid interaction on a fully developed flow at high Froude number. The comparison with the experiments is encouraging if the very important effects of surface tension are also incorporated.

Table 1 This table gives measurements of the experimental hydraulic jumps of Craik et al. (1981). The volume flux contained within the jump is Q. The position of the jump, x_J, and the depth of the layer at this point, h_J, for jumps with various values of Q are taken from Figure 6 of Craik et al., reproduced here as Figure 2.7.1. The value of σ, the radius of the water column falling onto the plate, is estimated from Table 1 of Craik et al.. The position of the jump is taken to be at the crest of the capillary wave which occurs just upstream of the jump. The values of δh, the change in the depth of the layer, at a point δx further downstream are measured, using as a reference point the point of minimum depth, which occurs just upstream of the jump. We use c.g.s. units.

Table 1(a)

Q	σ	x_J	h_J
11	0.15	2.55	0.034
18	0.17	2.95	0.026
29	0.22	4.15	0.028

Table 1(b)

Q	δh			$\delta h/h_J$		
δx	0.25	0.5	1.0	0.25	0.5	1.0
11	0.0375	0.0625	0.1	1.103	1.84	2.94
18	0.0375	0.075	0.119	1.44	2.88	4.56
29	0.0313	0.0625	0.103	1.11	2.32	3.67

Table 2 This table presents a comparison of the measurements of Table 1 with the predictions of equation (2.7.2). Table 2(a) gives the calculated values of the layer depth, h_J, the inverse Froude number, s, and the Reynolds number, Re, at the jump position. The length scale, L_∞, is that associated with the development of Watson's solution upstream of the jump. The flow can be taken to be fully developed at the jump if $L_\infty < x_J$. Tables 2(b) and 2(c) present the calculated change in the depth at a distance δx downstream of the minimum in the depth. The figures in brackets are a comparison of these calculated values with the measured values in Table 1(b).

Table 2(a)

Q	x_J	h_J	s	L_∞	Re
11	2.55	0.024	0.030	1.25	68.67
18	2.95	0.020	0.0088	1.60	97.13
29	4.15	0.023	0.0097	2.23	111.2

Table 2(b)

Q	$\delta h/(\delta x)$	$\delta h\|_{\delta x=0.25}$	$\delta h\|_{\delta x=0.5}$	$\delta h\|_{\delta x=1.0}$
11	0.0615	0.0339 (90%)	0.0465 (73%)	0.0615 (62%)
18	0.0684	0.0337 (90%)	0.0507 (68%)	0.0684 (58%)
29	0.0673	0.0371 (118%)	0.0499 (79%)	0.0673 (65%)

Table 2(c)

Q	$\delta h/(h_J\delta x)$	$\delta h/h_J\|_{\delta x=0.25}$	$\delta h/h_J\|_{\delta x=0.5}$	$\delta h/h_J\|_{\delta x=1.0}$
11	2.53	1.39 (126%)	1.88 (102%)	2.53 (86%)
18	3.35	1.84 (128%)	2.49 (86%)	3.35 (73%)
29	2.93	1.61 (145%)	2.17 (94%)	2.93 (80%)

Table 3 This presents a comparison similar to that in Table 2, but using the measured values of the depth at the crest of the capillary wave rather than the predictions from Watson's theory, in the calculation of the depth further downstream. The predictions are made using equation (2.7.5).

Table 3(a)

Q	$\delta h\|_{\delta x=0.25}$	$\delta h\|_{\delta x=0.5}$	$\delta h\|_{\delta x=1.0}$
11	0.0289 (77%)	0.0389 (62%)	0.0525 (53%)
18	0.0331 (88%)	0.0446 (59%)	0.0601 (51%)
29	0.0330 (105%)	0.0445 (71%)	0.0600 (58%)

Table 3(b)

Q	$\delta h / h_J\|_{\delta x=0.25}$	$\delta h / h_J\|_{\delta x=0.5}$	$\delta h / h_J\|_{\delta x=1.0}$
11	0.85 (77%)	1.14 (62%)	1.54 (52%)
18	1.27 (88%)	1.72 (60%)	2.31 (51%)
29	1.18 (106%)	1.59 (68%)	2.14 (58%)

FIGURE CAPTIONS FOR CHAPTER TWO.

Figure 2.1.1 A definition sketch for fully developed flow on a horizontal surface, defining the dimensional coordinate system (X^*, Y^*), velocity profile (U^*), free surface height (η^*) and mass flux per unit width (Q).

Figure 2.2.2 Figure 2.1.1 in normalised, dimensionless coordinates for motions over a length scale of the order of the Reynolds number, Re.

Figure 2.4.1 A typical solution of (2.1.1a-g) with half-Poiseuille flow as an initial condition, s = 2, $\Delta x = 10^{-6}$ and $\Delta\xi = 10^{-2}$. Figures (a) and (b) illustrate the pressure and skin friction of the solution respectively. The solution ends in a singularity at $x = 0.0373$.

Figure 2.4.2 Integrations of (2.1.1a-g) for values of s of 1, 2, 4, 8. All solutions have half-Poiseuille flow at $x = 0$ and end in a singularity, with the singularity occurring at larger values of x for larger values of s.

Figure 2.4.3 An integration of (2.1.1a-g) for s = 0.001 and with $\Delta x = 10^{-4}$. The x-grid is too coarse to capture the interaction and the solution develops into Watson's (1964) form. The initial condition is half-Poiseuille flow at $x = 0$. Figures (a), (b), and (c) illustrate the development of the pressure (proportional to the position of the free surface), the velocity profile at $x = 0.1$ and the development of the skin friction respectively.

Figure 2.5.1 A comparison of the singularity calculated numerically, and illustrated in Figure 2.4.1, with the theoretical structure of §2.5. Figure (a) illustrates the velocity profiles at $x = 0$, 0.01,

0.02, 0.03, 0.35, and 0.0373, and clearly shows the development of a boundary layer near y = 0. Figure (b) shows τ^{-5} (curve (a)) and $\tau^{-5}(\ln\tau)^3$ (curve (b)) against $x_s - x$, where x_s is the position of the singularity and τ is the skin friction of the solution. Figure (c) similarly shows $(-p_x)^{-5/3}$ (curve (a)) and $(-p_x)^{-5/3}(\ln(-p_x))^{4/3}$ (curve (b)), where $-p_x$ is the pressure gradient in the direction of the flow. The near-linear character of these plots illustrates that the theoretical structure is likely to be correct.

Figure 2.6.1 A sketch illustrating the scales and asymptotic structure of the large Froude number interaction described in §2.6.2. The inverse Froude number, s, is small and the free surface suffers an O(s) perturbation over a short $O(s^3)$ length scale. The nonlinear boundary layer at the wall (II) has thickness O(s).

Figure 2.6.2 This illustrates the structure of the interaction leading to a non-uniqueness in the development of Watson's (1964) similarity solution as the depth becomes large enough to reinstate the pressure term. Region (I) reacts in an inviscid fashion to a departure of size $\exp(-\gamma/x^9)$, for some positive γ, as $x \to 0$. There is a viscous layer near to the wall of thickness $O(x^4)$.

Figure 2.7.1 Figure 6 of Craik et al. (1981) illustrating the experimental hydraulic jumps used in the experimental comparison of §2.7.

Figure 2.7.2 The solution of (2.7.1a-h) illustrating (T-1) and $3\sqrt{3}(T-1)/\pi - X^3$ which asymptotes to the value 0.69 as $X \to \infty$. This value is taken to be the value of d^3 in the comparisons of §2.7.2.

Figure 2.1.1.

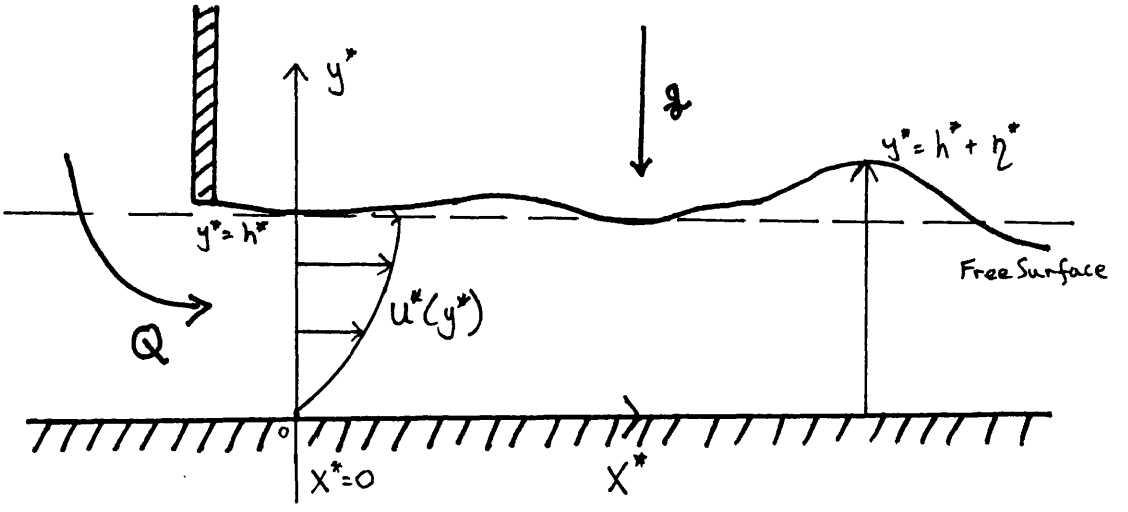

Figure 2.1.2.

$$Re = Q/\nu \quad , \quad S = g h^{*3}/Q^2$$

$$x^* = Re\, x\, h^*$$
$$y^* = y\, h^*$$
$$\eta^* = \eta\, h^*$$
$$u^* = Q\, u_0/h^*$$

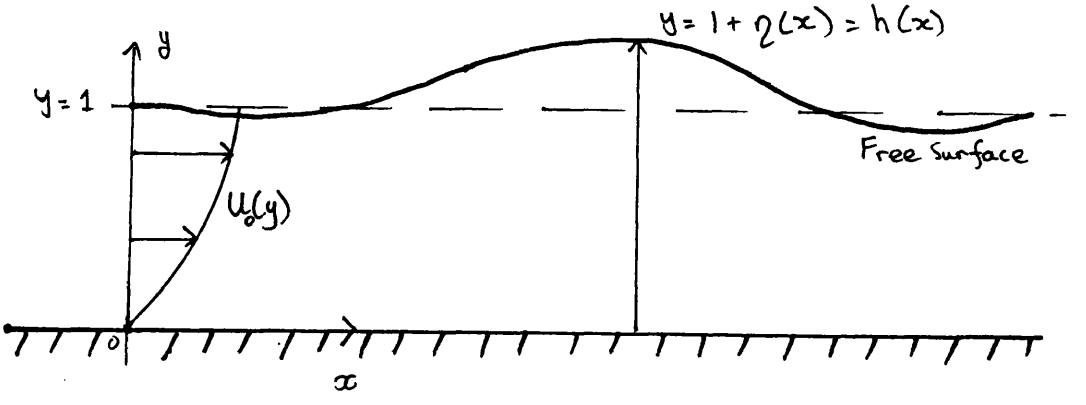

Figure 2.4.1

(a)

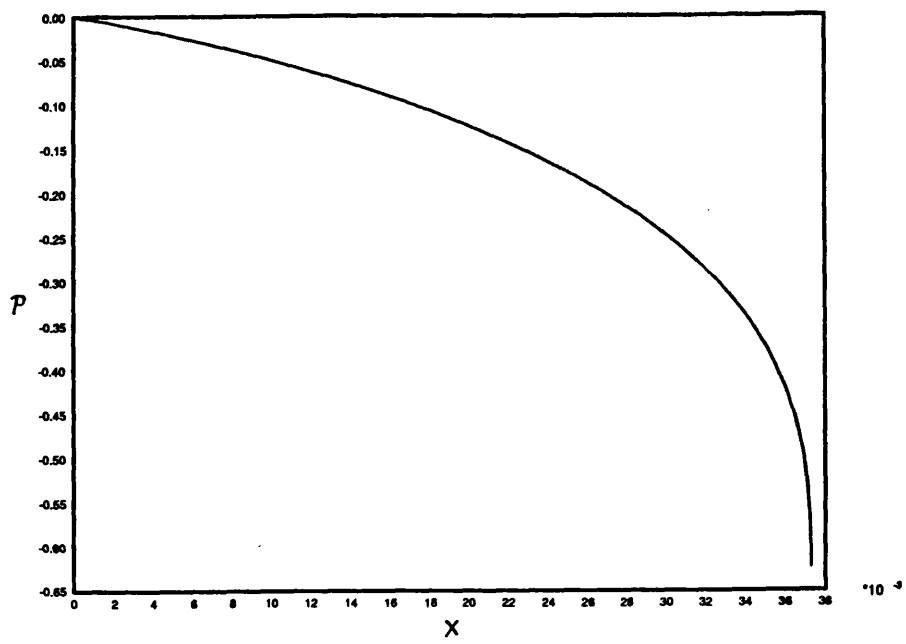

(b)

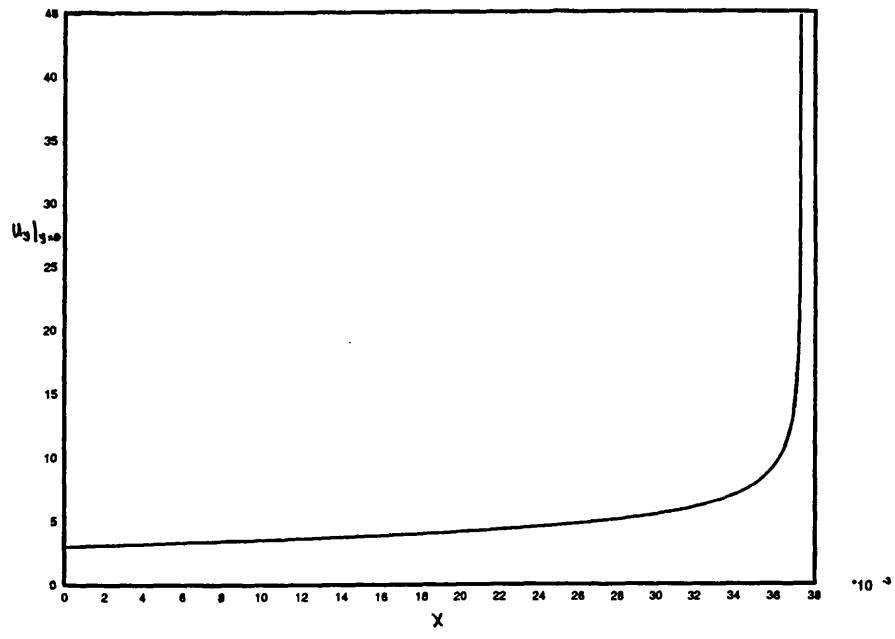

Figure 2.4.2

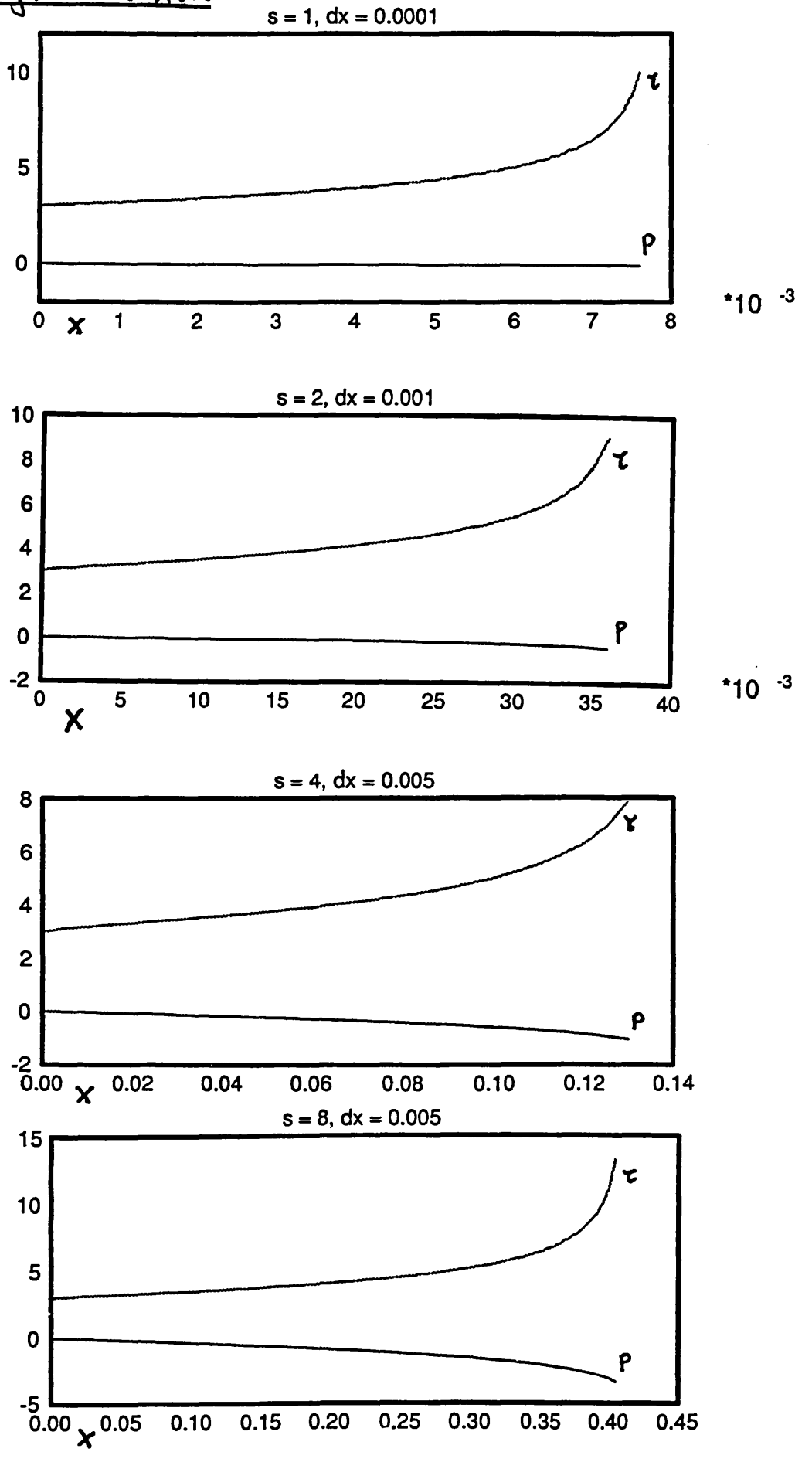
s = 1, dx = 0.0001
10
5
0
τ
P
0 X 1 2 3 4 5 6 7 8
*10 -3
s = 2, dx = 0.001
10
8
6
4
2
0
-2
τ
P
0 5 10 15 20 25 30 35 40
X
*10 -3
s = 4, dx = 0.005
8
6
4
2
0
-2
τ
P
0.00 X 0.02 0.04 0.06 0.08 0.10 0.12 0.14
s = 8, dx = 0.005
15
10
5
0
-5
τ
P
0.00 X 0.05 0.10 0.15 0.20 0.25 0.30 0.35 0.40 0.45

Figure 2.4.3.

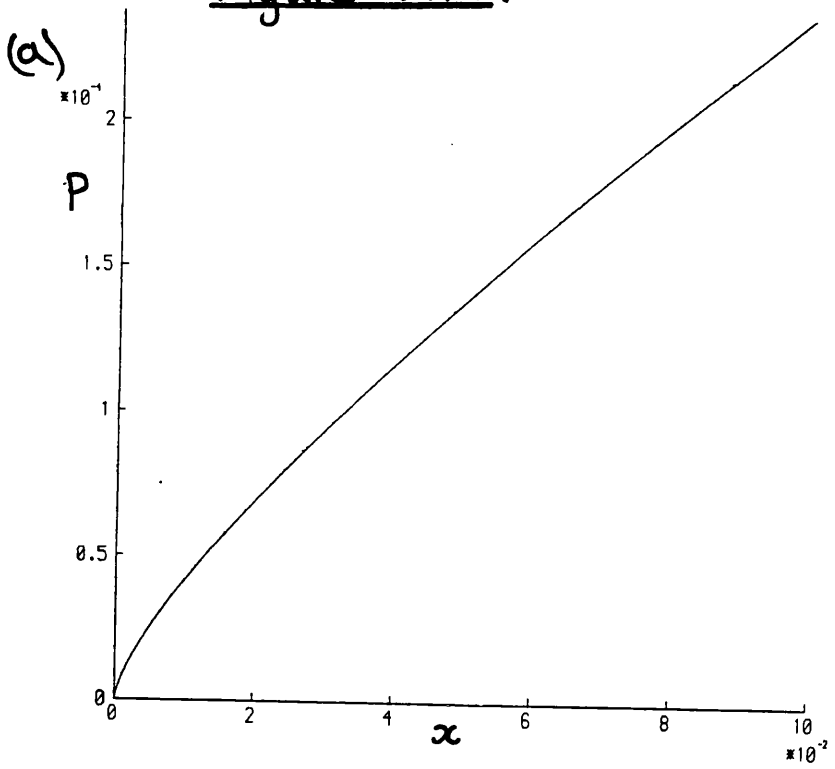
(a)
*10⁻¹
2
P
1.5
1
0.5
0
0
2
4
6
8
10
x
*10⁻²

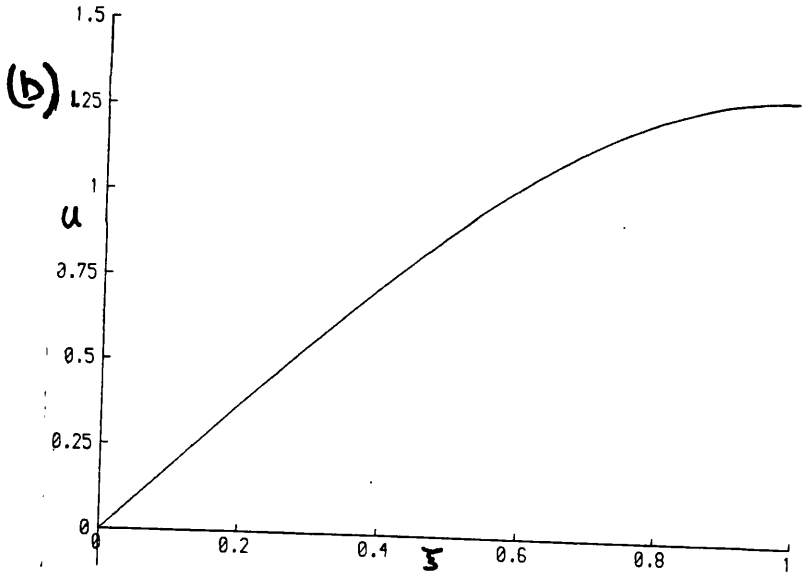
(b)
1.5
1.25
1
u
0.75
0.5
0.25
0
0
0.2
0.4
ȳ
0.6
0.8
1

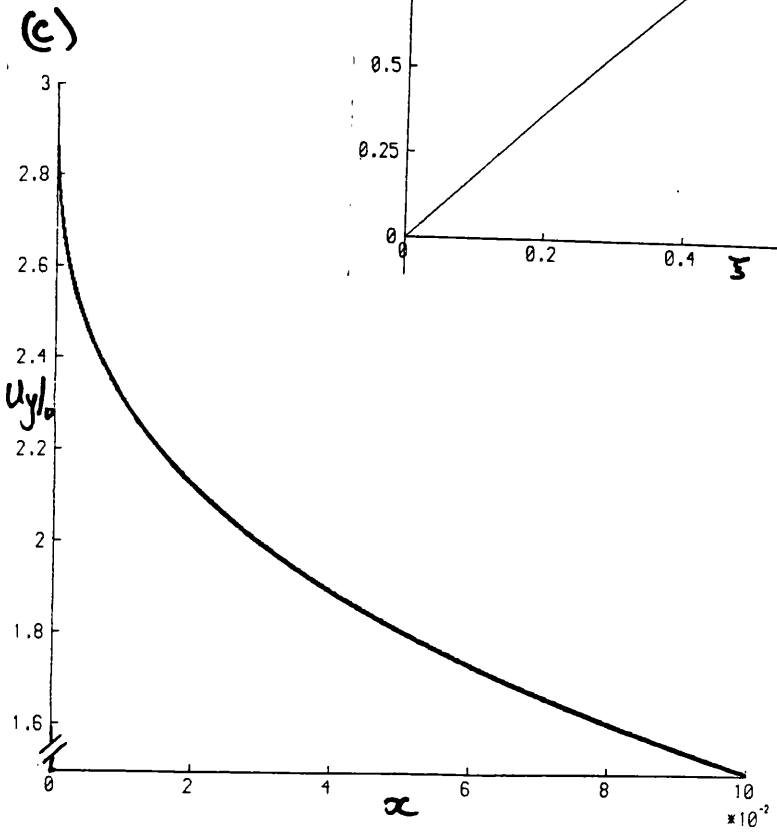
(c)
3
2.8
2.6
2.4
uy/u
2.2
2
1.8
1.6
0
2
4
6
8
10
x
*10⁻²

(a)

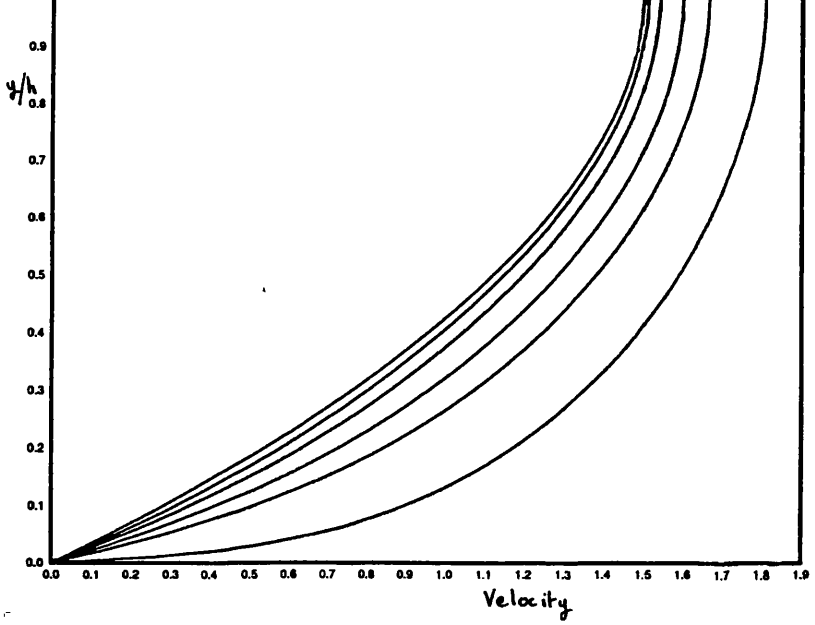
y/h
0.0 0.1 0.2 0.3 0.4 0.5 0.6 0.7 0.8 0.9 1.0 1.1 1.2 1.3 1.4 1.5 1.6 1.7 1.8 1.9
Velocity

(b)

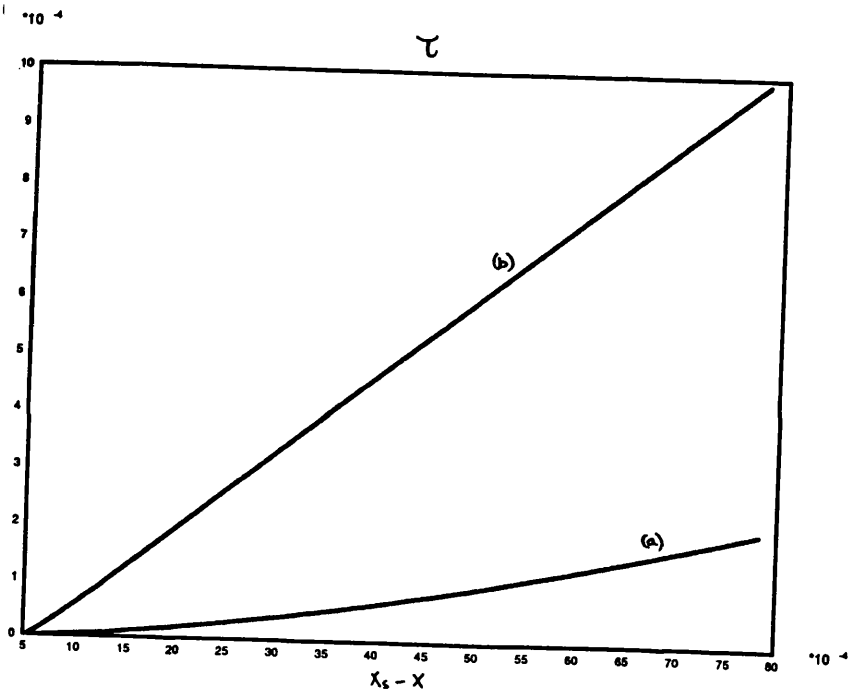
*10 -4
τ
(b)
(a)
5 10 15 20 25 30 35 40 45 50 55 60 65 70 75 80
*10 -4
Xs - X

(c)

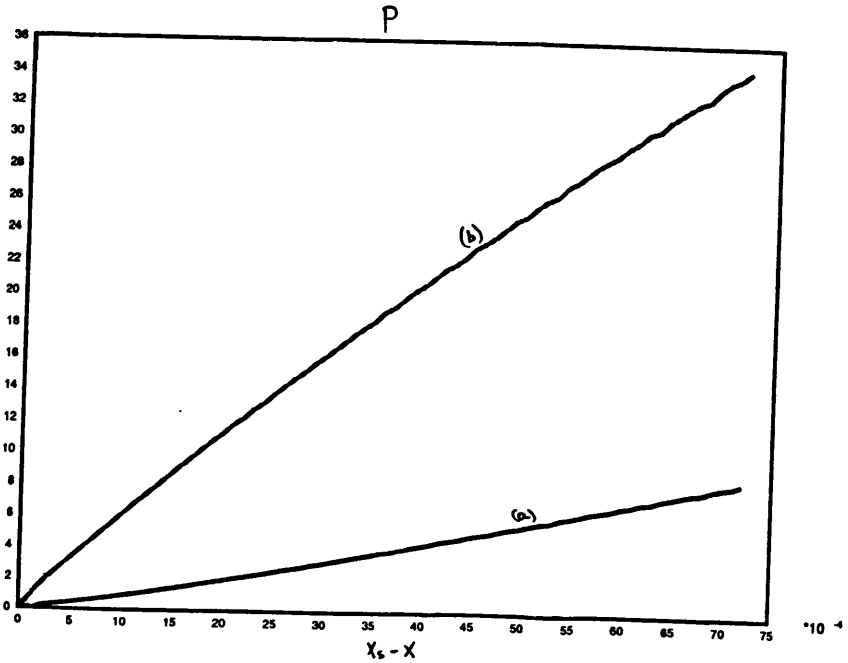
*10 -3
P
(b)
(a)
0 5 10 15 20 25 30 35 40 45 50 55 60 65 70 75
*10 -4
Xs - X

Figure 2.6.1

$s \ll 1 \qquad \eta = s\eta_1 \;, \qquad x = s^3 \hat{x}$

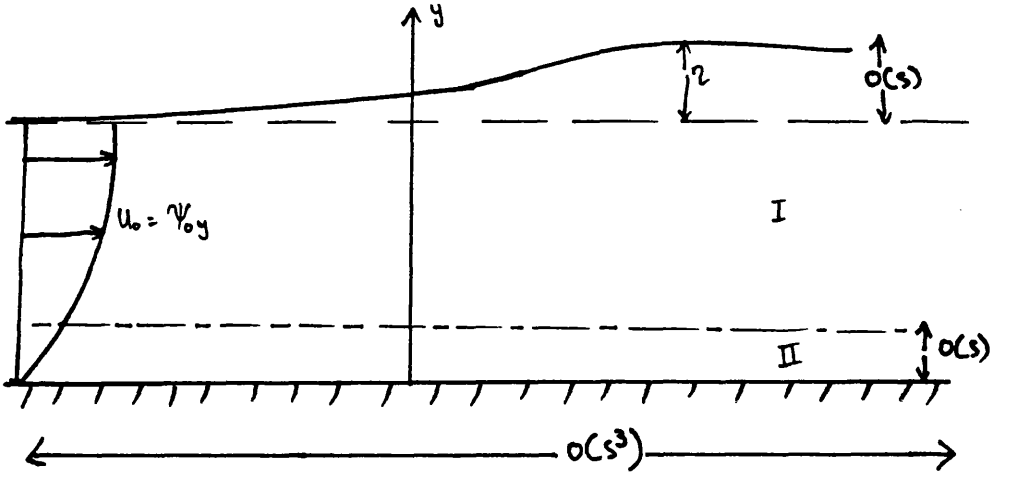

Figure 2.6.2

$E = \exp(-\gamma/x^q) \;, \quad x \to 0+$

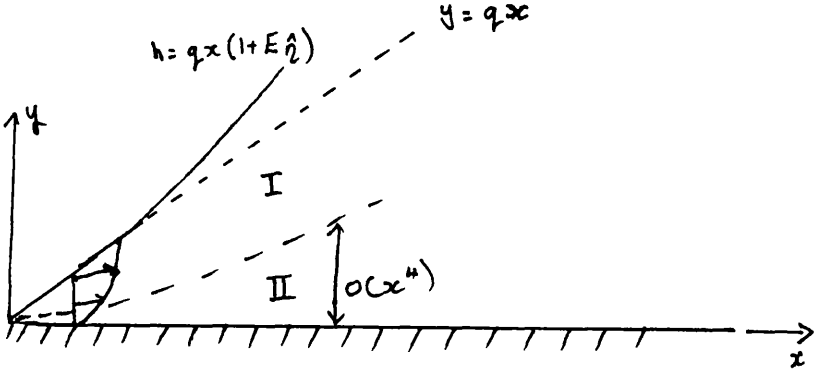

Figure 2.7.1.

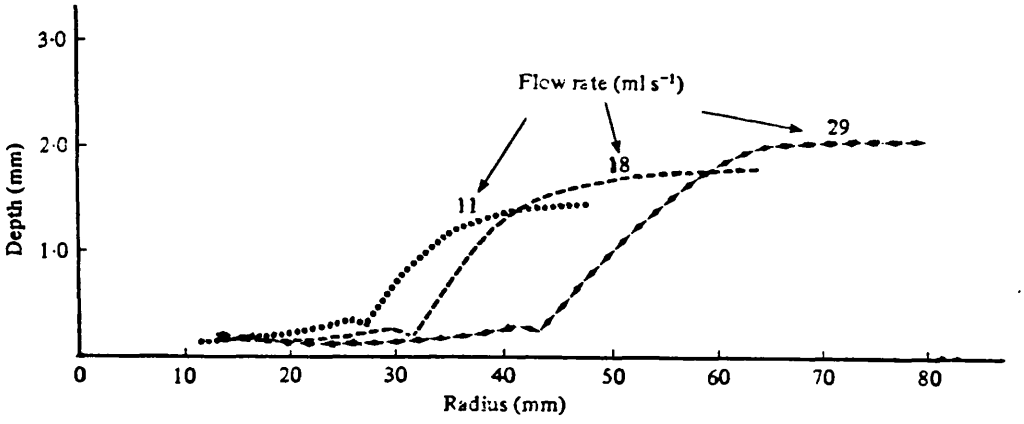

Figure 2.7.2

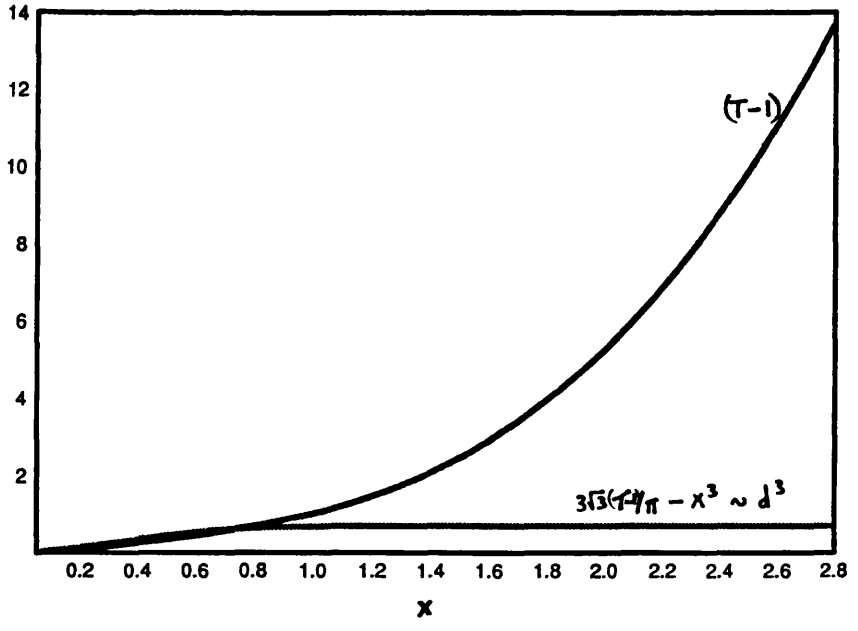

Chapter Three

UPSTREAM INFLUENCE IN LIQUID LAYER FLOWS ON A FAVOURABLE SLOPE.

§3.1 Introduction And The Governing Equations.

Chapter two concentrates on the problem of liquid layer flow on a horizontal surface. Complementary to this study, the present chapter investigates two-dimensional liquid layer flow upstream of, and over, obstacles mounted on a slope. Typical physical problems are illustrated in Figure 3.1.1. Questions such as whether or not separation occurs will affect the stability of the flow and a determination of its depth is important in calculating the efficiency at which gas can be expected to dissolve into the liquid film - a question with important industrial implications. Also of interest is the effect that surface tension may have on these flows.

The study of flow on a slope is perhaps of more physical relevance than the problems tackled in chapter 2. An assumption, shared by these two sections, is that the development is over a scale sufficiently long that viscous effects are important throughout the layer's depth. This severely restricts the relevance of the solutions found in chapter 2, but here an obvious fully developed flow exists, namely half-Poisueille flow. This chapter, therefore, concentrates on mechanisms for upstream influence in half-Poiseuille flow on a downward slope. Again the emphasis is on the effects of the interaction between viscous and inviscid effects and in order that the pressure gradient generated by the interactive process is not swamped by the gravitational force which also drives the layer the slope must be shallow. In fact if we are looking at the problem on a length scale proportional to the Reynolds number then the slope, $\tan(\alpha^*)$ say, must be $O(Re^{-1})$ i.e. $\tan \alpha^* = \alpha/Re$ as $Re \to \infty$. If the slope is greater than this and we still insist on studying interactions on an $O(Re)$ length scale the problem becomes one of a classical boundary layer type with the pressure gradient given by the slope or obstacle shape and not determined by the flow itself in an interactive fashion. Problems of liquid layer flow described by the classical boundary layer formulation have been studied by many

authors, e.g. Eagles and Daniels (1986) and Eagles (1988).

With a slope of this magnitude it is a simple matter to extend the equations derived in §2.1 to cover flow over a slope by means of a Prandtl shift in y so that y now becomes, in effect, a coordinate normal to the slope. The resulting equations are similar,

$$UU_x + VU_y = -p_x + U_{yy}, \qquad (3.1.1a)$$

$$U_x + V_y = 0, \qquad (3.1.1b)$$

$$U = V = 0 \text{ at } y = 0, \qquad (3.1.1c\text{-}d)$$

$$U_y = 0 \text{ at } y = 1 + \eta + \alpha x, \qquad (3.1.1e)$$

$$p = s\eta, \qquad (3.1.1f)$$

but the initial condition at $x = 0$ is replaced with the condition

$$\eta \sim -\alpha x, \text{ as } x \to -\infty. \qquad (3.1.1g)$$

Alternatively we can view the system as an initial value problem in which the conditions are given at some finite x ($x = 0$ say), rather than as $x \to -\infty$. This is the approach taken in §3.2. The length used to nondimensionalise the problem is h_0^*, the depth far upstream (or at $x = 0$). The depth of the liquid layer, h, is then $1 + \eta + \alpha x$, and so the equation arising from the conservation of mass flux is

$$\int_0^{1+\eta+\alpha x} U(y)dy = 1. \qquad (3.1.1h)$$

If we represent an obstacle on the slope by writing the surface over which the layer flows as $y = f(x)$ then the lower limit of this integral (only) is altered to $f(x)$. Again the slopes which make up this obstacle must be $O(Re^{-1})$. See Figure 3.1.2.

If we consider half-Poiseuille flow on a uniform slope then equation (3.1.1) reduces to

$$p_x = U_{yy},$$

$$p = s\eta,$$

$$U = 0 \text{ at } y = 0 \text{ and } U_y = 0 \text{ at } y = 1 + \eta(x) + \alpha x,$$

$$\int_0^{1+\eta+\alpha x} U(y)dy = 1.$$

However in parallel flow $\eta = -\alpha x + (h-1)$, with h, the fluid depth, defined above. So, given half-Poiseuille flow,

$$h = (3/s\alpha)^{1/3}.$$

Now, since the equations are normalised such that the upstream depth is 1, this means that

$$s\alpha = 3, \qquad (3.1.2)$$

and so for the case of flow on a slope the requirement that the profile be fully developed, i.e. be half-Poiseuille, implies that s and α are not independent. Thus fixing the slope determines the depth of the layer for a given mass flux and thus determines the Froude number.

This chapter investigates equations (3.1.1) in a similar fashion to the approach taken in chapter 2. There are, in fact, many similarities, stemming mainly from the relationship (3.1.2), which implies a similarity between large/small Froude numbers on a horizontal surface and steep/shallow slopes. The main difference arises in that the compressive interaction, which leads to a self-induced thickening of the layer and possibly to separation, is able to occur for all slopes whereas in chapter 2 it is positively identified as being possible on a horizontal surface only if the Froude number is large. This leads to a class of solutions distinct from those found in chapter 2. These solutions are studied first in a numerical solution of the flow on a uniform slope in §3.2. The

chapter goes on to study the downstream asymptotes of these solutions and finds that there are two possible asymptotes, depending on the steepness of the slope and the severity of the separation (if any) which occurs on it. This variation has implications for the type and shape of hydraulic jump to be expected on different sizes of slope. Again the numerical solutions are interpreted in terms of a non-uniqueness in the solutions of the system. The limit of small α is discussed in §3.6 and it is found that the flow is governed by a particularly simple equation which allows numerical and analytic solutions for the whole flow field over an obstacle. These solutions exhibit many of the characteristics commonly associated with the upstream influence of an obstacle and allow a prediction of the flows which are to be expected in the case of larger values of α. Finally in §3.7 a numerical solution of the equations for finite α is attempted and confirms many of the features of this prediction. Of particular interest is the apparent emergence of two scales for the interaction, as the severity of the slope and obstacle are increased. One, the short scale, governs separation upstream of the obstacle and the second, longer, scale governs the flow over the obstacle and the return to half-Poiseuille flow downstream.

§3.2 Numerical Solution Of The Free Interaction Problem In Flow On A Slope.

Solutions of equations (3.1.1), describing the liquid layer flow down a uniform gradient of magnitude $O(Re^{-1})$, can be obtained using the method developed for the similar problem on a horizontal surface in §2.4. Here, as in §2.4, we consider the free interaction problem. We go on later to investigate forced interactions numerically in §3.7.

We therefore march the solution of equations (3.1.1) downstream from an initial condition at $x = 0$. The equations are first rewritten in a similar fashion to that detailed in §2.4 taking into account the Prandtl shift

already introduced in deriving (3.1.1). First we introduce

$$\xi = (y - f)/(1 + E),$$

where $E = \eta + \alpha x - f$ and, in this instance, $f = 0$, since the slope is uniform. Then, if $\hat{\psi}$ is an appropriate stream function,

$$UU_x - \frac{\hat{\psi}_x U_\xi}{1+ E} = -p_x + \frac{U_{\xi\xi}}{(1+ E)^2}, \qquad (3.2.1a)$$

$$U = \frac{\hat{\psi}_\xi}{1 + E}, \qquad (3.2.1b)$$

$$\hat{\psi} = U = 0 \text{ at } \xi = 0, \quad U_\xi = 0, \ \hat{\psi} = 1 \text{ at } \xi = 1. \qquad (3.2.1c\text{-}f)$$

The conditions imposed at $x = 0$, the start of the slope, are $\eta = 0$, which corresponds to an oncoming flow of depth 1 in dimensionless variables, and $U = 3\xi(1-\xi/2)$, $V = 0$, i.e. a velocity profile given by half-Poiseuille flow in a direction parallel to the slope. (Note that we used a Prandtl shift in deriving equations (3.2.1)). The Froude number and scaled slope, α, are varied. As explained in §3.1, for a given s and α, the depth of a half-Poiseuille flow should be $(3/s\alpha)^{1/3}$, so unless $s\alpha = 3$, the initial conditions do not constitute a flow which can continue unaltered. Instead we expect to see it develop downstream. The actual development for various s and α is described below.

Firstly, if $s\alpha < 3$ the depth decreases monotonically from 1, and the skin friction similarly increases. The solution eventually falls into the singularity described in §2.5, in just the same fashion as on a horizontal surface. See Figure 3.2.1, which presents solutions for various values of s on the slope $\alpha = 0.25$.

In contrast, if $s\alpha > 3$ the layer thickens, the skin friction decreases, and the solution far downstream seems to depend only on α, the slope, and not on the Froude number of the oncoming flow. This solution consists of an

approach to a horizontal free surface, which would provide only a weak pressure gradient, and a slowing flow beneath. For small values of α the flow does not separate and remains forward throughout its depth. The approach of the free surface to the horizontal is from above. For larger α, in contrast, there is a region of reversed flow and on increasing the gradient further the separated region becomes larger and most of the forward flow is confined near to the free surface. The decay towards the horizontal is from below. The asymptotic structure of these various regimes is described in §3.2 and §3.3. Numerically the separated regions, with reversed flow, are handled simply using the so-called Flare approximation (Reyner and Flügge-Lotz (1968)) in which the term UU_x is set equal to zero if $U < 0$. This is an effective and, since the speed of any reversed flow is usually much less than that of forward flow, quite accurate device for obtaining solutions. It does alter the equations however making them parabolic in regions where reversed flow is present. Figure 3.2.2 shows solutions for $s = 10$ and $\alpha = 4$ and 6. We note here that the solution with $\alpha = 6$ shows a separation whilst that for $\alpha = 4$ does not. Also, the approach of the free surface to the horizontal ($p \rightarrow$ constant) is from below whilst the approach on the smaller slope illustrated in Figure 3.2.1 is from above.

If $s\alpha$ is equal to 3 the flow seems to continue as half-Poiseuille flow, but perhaps with a small departure.

It is worth considering why $s\alpha = 3$ is the dividing line between the two types of behaviour, especially as if $s\alpha < 3$ the half-Poiseuille flow on such a slope has a depth greater than 1 and so we might expect the depth to increase towards this depth rather than decrease towards the singularity as described above. The explanation can be found by considering the sign of the perturbation the flow receives at the start of the interaction. The profile $U = 3(\xi - \xi^2/2)$ needs a pressure varying as $-3x$ to drive it and on the horizontal plate this is provided by an initial fall in the free surface and so this initial perturbation will drive the flow into the singularity. This will always

be the case on a horizontal plate. However on a favourable gradient gravity provides the energy to drive the profile. The pressure provided by the slope is $-s\alpha x$, and so if this is too small, i.e. $s\alpha < 3$, the layer will thin to provide the extra pressure gradient needed. Similarly if $s\alpha > 3$ the layer will thicken to reduce the pressure gradient to the correct value. These cause the initial perturbations which determine the subsequent behaviour of the solution. In the case $s\alpha = 3$, there is no initial perturbation, and the flow is parallel. The slow departure seen in the calculations in this case comes from numerical errors which act as a source of small perturbations.

It seems clear that the singularity experienced in these computations is identical to that which the equations suffer on a horizontal surface. Indeed if we repeat the analysis of this singularity of §2.5, we see that, due to the increased pressure gradient caused by the rapid change in the free surface position, the contribution from the slope is negligible and the same analysis is succesful in describing this singularity. The other type of behaviour seen, corresponding to a compressive interaction, is not experienced on a flat surface, except in various limits described in §2.6, where the interaction develops relatively rapidly. The next two sections investigate the downstream asymptotes of this solution.

§3.3 Large X Asymptotes for the Smaller Gradients.

§3.3.1 The expansion leading to the Jeffrey-Hamel equations.

For the smaller values of α the asymptotic form, for large x, of the solution calculated in §3.2 is similar to that for a flow through diverging plates. This can be seen from a consideration of the possible symmetry of these flows about the centre of the channel, where necessarily $U_y = 0$. Replacing this symmetry line with the horizontal asymptote of the free surface gives us our liquid layer

flow. These channel flows are of course Jeffrey-Hamel flows and have been studied by many authors (Jeffrey (1915), Hamel (1916), Rosenhead (1940), Fraenkel (1962)). Here we need consider only the high Reynolds number limit of these flows, with the angle between the plates $O(Re^{-1})$ as $Re \to \infty$, and concentrate on those which are symmetric and with net outflow.

To derive the governing equations at large x we write the position of the free surface as

$$y = 1 + 1/s\ (p_0 + p_1/x^2 + \ldots), \quad x \to \infty$$

and the stream function, ψ, as

$$\psi = \psi_0 + \psi_1/x^3 + \ldots, \quad x \to \infty$$

where ψ_0 and ψ_1 are functions of

$$\xi = y/(\ 1 + p_0/s + \alpha x\ ).$$

The value of p_0 will not be found in this large x analysis since it is related to the total drop or rise in the free surface during the interaction and therefore contains information about the history of the flow. Substitution of the above expansion into equations (3.1.1) yields, at $O(x^{-3})$, as $x \to \infty$,

$$\psi_0''' + \alpha\ \psi_0'^2 + 2p_1\alpha^3 = 0,$$

$$\psi_0(1) = 1,\ \psi_0''(1) = 0, \quad \psi_0(0) = \psi_0'(0) = 0,$$

$$p_1 \text{ is to be found.}$$

Here $'$ indicates $\partial/\partial\xi$.

To simplify this equation we make the substitution $V = \alpha\psi_0'$, $P = 2\alpha^4 p_1$, and find

$$V'' + V^2 + P = 0, \qquad (3.3.1a)$$

$$V'(1) = V(0) = 0, \quad \int_0^1 V \, d\xi = \alpha. \qquad (3.3.1b\text{-}d)$$

This system can be solved in terms of elliptic functions and we do so by following the work of Fraenkel (1962). We first integrate once and put W=-V/6, to give

$$W'^2 = 4(W^3 + P/12\ W + 1/4\ (\tau/6)^2), \qquad (3.3.2)$$

where $\tau = V'(0)$. This is now in a standard form for integration to give elliptic functions. The type of solution depends on the number of real roots of the cubic on the right hand side of (3.3.2). If it has only one, r_2 say, with the other roots, r_1 and r_3, making up a conjugate pair we write

$$a^4 = (r_2-r_3)(r_2-r_1) = 2r_2^2 + r_1r_3,$$

$$r_2 = -\ 2/3\ a^2\ (2m-1),$$

defining a and m. This means that the pressure and skin friction can be written as,

$$1/4(\tau/6)^2 = -r_1r_2r_3 = a^6(2/3)(2m-1)(1 - (8/9)(2m-1)^2),$$

$$P/12 = r_1r_2 + r_2r_3 + r_1r_3 = a^4(1 - (4/3)\ (2m-1)^2).$$

(3.3.3a-b)

The solution for V can be written as

$$V = 6a^2(sn^2a\ dc^2a - sn^2a(\xi-1)\ dc^2a(\xi-1)),$$

where sn and dc are Jacobian elliptic functions with modulus m. See, for example, Abramowitz and Stegun (1964). The boundary conditions on V give

$$m = 1/2\ (1 + 3/2\ sn^2(a\backslash m)\ dc^2(a\backslash m)), \qquad (3.3.4a)$$

$$\alpha = 6a^2(sn^2a\ dc^2a + 2E(a)/a - 1 - sn(a)dc(a)/a). \qquad (3.3.4b)$$

Here E(a) is the incomplete elliptic integral of the second kind with modulus m.

These two equations together define α and m in terms of a. In our problem, however, we are given α, the slope of the plate, and not a. We therefore hope to invert (3.3.4) to give a and m in terms of α. Fraenkel (1962) shows that in this case the inversion is possible, with unique values of a and m corresponding to a given α. We are therefore able to calculate the velocity profile and pressure P. The profile is monotonically increasing from zero at the wall. The derivative of the velocity, V′, is monotonically decreasing. See Figure 3.3.1. This type of solution is representative of those with smaller values of α.

The second type of solution occurs if r_1 and r_3 are real, say $r_3 \geq r_1 \geq r_2$. In this case there is more than one zero of W′ possible. If one occurs within the range $\xi \in (0,1)$ there is a minimum in V within the flow field as well as the maximum at $\xi = 1$. Therefore the flow in this case can be separated. We define b and m in this case by

$$r_3 - r_2 = b^2, \quad r_1 - r_2 = b^2m.$$

Just as for the smaller slopes we can find expressions for P and τ,

$$P = -\ 4/3\ b^4\ (m^2 - m + 1) < 0,$$

$$1/4\ (\tau/6)^2 = 2b^6/27\ (m + 1)(m - 1/2)(2 - m).$$

Solving (3.3.1) we find, in terms of elliptic functions,

$$m = 1/(3\ sn^2b\ -1), \quad \alpha = b^2\ (E(b)/b - dn^2b), \qquad (3.3.5a\text{-}c)$$

$$V = 6mb^2(sn^2b - sn^2b(\xi-1)).$$

In contrast to the solutions of the first type, given m we have a large choice of b satisfying (3.3.5). Any b such that

$$b = n\,K(m) \pm \beta, \quad sn^2\beta = sn^2 b, \quad 0 \le \beta \le K(m), \qquad (3.3.6)$$

with n an integer, is suitable. This freedom of choice is responsible for the solutions for Jeffrey-Hamel flow with multiple regions of inflow and outflow. Here, however, we have two choices. If we choose $n = 0$, $b = \beta$ we get unseparated profiles with V increasing but a zero in V''. On the other hand if $n=0$, $b=-\beta$, we get separated profiles with one region of backflow near the wall. The condition separating the two types of profile and the two choices of b is $b = K(m)$, corresponding to just-separating flow. Again, given α, we can attempt to invert (3.3.5), and find the complete solution. However, Fraenkel shows that $d\alpha/db$ is zero at $\alpha = \alpha_c = 5.461$, and so the equation has no unique inverse at this point.

§3.3.2 Some special cases of interest.

Some special cases of the above analysis are presented below.

1) Poiseuille Flow, $\alpha \to 0$.

Consider equation (3.3.4a) for small a. It yields the asymptote

$$m \sim 1/2 + 3/4\ a^2,$$

and so

$$sn(a) \sim a(1-a^2/4), \quad dc(a) \sim (1+a^2/4), \quad E(a) \sim a(1-a^2/6).$$

From equations (3.3.3a-b), therefore, we now find that

$$\alpha \sim 4a^4,$$

$$V \sim 12a^4(\xi-\xi^2/2) \sim 3\alpha(\xi-\xi^2/2), \quad P \sim 3\alpha,$$

$$\psi_0' \sim 3(\xi-\xi^2/2), \quad p_2 \sim 3 \,/\, 2\alpha^3.$$

Therefore the downstream form is one of half-Poiseuille flow, of linearly increasing depth. Since the error in fixing the position of the free surface at $\xi = 1$ is $O(p_2/s\alpha x)$ and p_2 is large the above is only valid when $x\alpha >> (s\alpha)^{-1/3}$.

2) Transition between the two types of solution.

This occurs at $m = 1$, i.e. $sn^2(a\backslash 1)dc^2(a\backslash 1) = \tanh^2(a) = 2/3$, from equation (3.3.4a). Thus $E(a)=\tanh(a)=\sqrt{2/3}$ and from (3.3.5b) we get $\alpha = 2.988$. The profile is

$$V = 4a^2 \, (1 - 3/2 \, \tanh^2 a(1-\xi)).$$

This equation is valid if $x >> (s\alpha)^{-1}$.

3) Just-separating flow.

Here $b = K(1/2)$ and from equations (3.3.5a-c), we find

$$\alpha = 4.712,$$

$$V = 3K^2 \, cn^2 K(\xi-1).$$

This profile has $\partial V/\partial \xi = 0$ at $\xi = 0$.

4) P = 0.

This corresponds to the approximate dividing line between the approach towards the asymptote $\eta \sim \alpha x$ being from above and it being from below. If $P = 0$ equations (3.3.1a&c) imply

$$\xi = \sqrt{3U/2} \int_0^{V/U} \frac{d\hat{v}}{(1 - \hat{v}^3)^{1/2}},$$

where $V = U$ at the point where $V' = 0$. Thus from equation (3.3.1b)

$$U^{1/2} = \sqrt{3/2} \int_0^1 \frac{d\hat{v}}{(1 - \hat{v}^3)^{1/2}} = 1.717.$$

Therefore

$$\alpha = \int_0^1 V\, d\xi = \sqrt{3U/2}\int_0^1 \frac{\hat{v}\, d\hat{v}}{(1 - \hat{v}^3)^{1/2}} = \frac{\pi}{\sqrt{3}} = 1.814.$$

Thus $\alpha = 1.814$ is the critical slope, delineating the alternative shapes for the hydraulic jump. If α is less than 1.814 the approach is from above and there is no obvious "jump". If α is bigger a rise in the level of the free surface, or "jump", is possible.

§3.3.3 Discussion.

In summary, consider increasing α from zero. The modulus, m, of the elliptic functions appearing in (3.3.4) increases from 1/2 to 1, at which point all the roots, r_i, become real, and the solution changes to being of the second type (3.3.5). This occurs at $\alpha = 2.988$. Increasing α still further causes m to decrease again to 1/2 at which point the flow is just separating (b = K(1/2), $\alpha = 4.712$). Larger α still causes m to increase from 1/2 again. However Fraenkel shows that at m = 0.5725, b = 2.364, $\alpha = 5.461$ there is no unique solution. Above this value of α there is the possibility of more than one solution, or perhaps none, for a given α, corresponding to different choices of b and n in (3.3.6) and with multiple regions of backflow. As $\alpha \to \alpha_c-$, $dV/d\alpha = (dV/db)(db/d\alpha)$ becomes infinite. Figure 3.3.1 illustrates this change in the profile as α increases. In addition Figure 3.3.2 presents a numerical solution of the free interaction with $\alpha = 4.712$, the critical angle for separation.

In the numerical work of §3.2 there is no evidence of large x solutions with more than one region of reversed flow, even for $\alpha > \alpha_c$. The different types of profiles, described above, are appropriate in the cases where $\alpha < \alpha_c$, and the critical values of α dividing the types are reflected in the numerical solution. We propose, as an explanation, that the form of the large x asymptote for $\alpha > \alpha_c$ is that described in §3.4, in which the vorticity of the oncoming flow breaks away from the wall, leaving

beneath it a slowly moving, reversed and irrotational flow with a viscous sublayer at the wall. Thus for larger α the separation is of the breakaway type, whereas for smaller slopes the development is slow enough for viscosity to diffuse the vorticity across the whole depth of the liquid layer. The profiles have to develop from the initial half-Poiseuille flow at the start of the interaction, and the vorticity must diffuse through an increasingly thick layer with, of course, the rate of thickening increasing with α. In addition it is shown in §3.5.2 that the scale over which the actual separation occurs decreases as α increases, and so viscosity has an even shorter distance over which to act.

§3.4 Large X Asymptote for Breakaway Separation.

§3.4.1 The flow structure and expansion for large x.

As suggested in §3.3.3, it seems likely that breakaway separation occurs for scaled slopes, α, greater than 5.461. Below we study the downstream form of this separation on the long, O(Re), length scale by obtaining an alternative asymptotic solution to equation (3.1.1) to that described in §3.3. This form has the vorticity concentrated near the free surface, rather than distributed throughout the layer's depth.

The thickness of the layer is given by αx + p/s say, where p is the pressure. Without loss of generality we can ignore the O(1) contribution to the pressure and free surface position since this expansion is for large x and so its origin in x is uncertain. For the purposes of this analysis, therefore, we can use this freedom to write the thickness of the layer in a form with no O(1) component as $x \to \infty$.

The flow divides into three regions. Region I, near to the free surface, is of thickness $O(x^{2/3})$ and here we use the variable $\chi = (\alpha x + p/s - y)/x^{2/3}$, so $\chi = 0$ at the free surface and approaches infinity towards the interior. The stream function ψ is $O(-x^{1/3})$, and the velocity profile

here turns out to be that of a $\mathrm{sech}^2\chi$-like jet. In the main part of the flow, region II, which is of thickness $O(x)$, there is a slow backflow with $\psi \sim O(x^{1/3})$ and $U \sim O(x^{-2/3})$. Accompanying this is region III, a reversed flow boundary layer at the lower wall of thickness $O(x^{5/6})$, and in which $\psi \sim O(x^{1/6})$. We combine regions II and III into region II in the analysis below and use the variable $\zeta = y/x^{5/6}$ to describe it. See Figure 3.4.1. The variables ζ and χ are related by

$$\zeta = \alpha x^{1/6} - x^{-1/6}\chi + p/s\ x^{-5/6}, \qquad (3.4.1a)$$

$$\chi = -\zeta x^{1/6} + \alpha x^{1/3} + p/s\ x^{-2/3}. \qquad (3.4.1b)$$

With this structure, then, we expand as follows. In region I,

$$\psi \sim -\{x^{1/3}f_1(\chi)+x^{1/6}f_2(\chi)+f_3(\chi)+x^{-1/6}f_4(\chi)+x^{-1/3}f_5(\chi) + \ldots\}.$$

In region II,

$$\psi \sim x^{1/6}g_1(\zeta) + g_2(\zeta) + x^{-1/6}g_3(\zeta) + x^{-1/3}g_4(\zeta) + \ldots ,$$

and

$$p \sim -(p_1x^{-4/3} + p_2x^{-3/2} + p_3x^{-5/3} + p_4x^{-11/6} + \ldots).$$

The relevant boundary conditions are $f_i''(0) = f_i(0) = 0$, for $i = 1\text{-}5$ at least, before the change in position of the free surface has an effect, with the exception that $f_3(0) = -1$ for the net mass flux to be unity. The value of $f_1'(\infty)$ should be zero to match with the slow reversed flow in region II. The other $f_i(\infty)$ should match with the higher-order solutions in region II. Here, $g_i(0) = g_i'(0) = 0$ and $g_i'(\infty) < 0$ to give reversed flow in the main body of the layer.

Substituting the above asymptotes into equations (3.3.1) and using the result that f_2 turns out to be zero

in the equations for f_3, f_4 and f_5, gives the following.

$$f_1''' + 1/3\ (f_1 f_1'' + f_1'^2) = 0,$$

$$f_2''' + 1/3\ f_1 f_2'' + 5/6\ f_1' f_2' + 1/6\ f_1'' f_2 = 0,$$

$$f_3''' + 1/3\ f_1 f_3'' + f_1' f_3' = 0,$$

$$f_4''' + 1/3\ f_1 f_4'' + 7/6\ f_1' f_4' - 1/6\ f_1'' f_4 = 0,$$

$$f_5''' + 1/3\ f_1 f_5'' + 4/3\ f_1' f_5' - 1/3\ f_1'' f_5 = -4/3\ p_1 + 2/3\ f_3'^2,$$

where $'$ indicates $\partial/\partial\chi$. Also,

$$g_1''' + 1/6\ g_1 g_1'' + 2/3\ (g_1'^2 - 2p_1) = 0,$$

$$g_2''' + 1/6\ g_1 g_2'' + 3/2\ (g_1' g_2' - p_2) = 0,$$

$$g_3''' + 1/6\ g_1 g_3'' - 1/6\ g_1'' g_3 + 5/3\ (g_1' g_3' - p_3 + 1/2\ g_2'^2) = 0,$$

$$g_4''' + 1/6\ g_1 g_4'' - 1/3\ g_1'' g_4 + 11/6\ (g_1' g_4' - p_4) = 1/6 g_2'' g_3,$$

where $'$ indicates $\partial/\partial\zeta$.

We note that in the main part of the flow, region II, where the vorticity is zero, these equations give p_1 to p_4 in terms of the backflow velocities $g_1'(\infty)$.

We can now go ahead and solve for these unknown functions. In region I, f_1 is found to be

$$f_1(\chi) = a \tanh (a\chi/6) \qquad (3.4.2)$$

giving a jet with a velocity $\propto \mathrm{sech}^2(a\chi/6)$ near the free surface. This jet is a balance of inertial and viscous effects, the viscosity being important due to the long, O(Re), length scale. The value of a is undetermined and will remain so throughout this work (see, however, the

discussion at the end of this section). The momentum flux contained within the jet is $a^3/9$, and is $O(1)$ as $x \to \infty$. In addition the pressure is asymptotically zero as the free surface is horizontal and the shear stresses at the free surface and at the wall are zero and $O(x^{-3/2})$ respectively. An application of the momentum integral theorem, therefore, suggests that this momentum flux is the same as that emerging from the interaction at $x \sim O(1)$, and so is equal to that of the original profile except for some possible losses in the process of separation. These losses are due to either viscous stresses at the wall or work done by the initial flow in countering any rise in depth and so adverse pressure gradient, near to the start of the interaction. It seems unlikely, therefore, that the value of a will be determined by this large x theory.

We now turn to completing the expansion. Noticing that $f_i = f_1'$ is a complementary function to all the equations for f_i allows us to write the full complementary function for f_i, $i \geq 2$, in the form

$$f_i = C_i \operatorname{sech}^2 z - \frac{1}{2} \operatorname{sech}^2 z \int_1^{\operatorname{sech}^2 z} \frac{H_i(u)}{u^2(1-u)^{1/2}}\, du, \qquad (3.4.3)$$

where $z = a\chi/6$ and

$$H_i(u) = A_i F(r,s;1;u) + B_i F(r,s;1/2;1-u) = A_i \phi_1 + B_i \phi_2, \text{ say.}$$

Here F is the hypergeometric function (Abramowitz and Stegun, Chapter 15), with $r+s = 1/2$ and $rs = (1-i)/4$. If $i = 3$ there is a relation between F and Legendre polynomials so that f_3 can be found explicitly in terms of hyperbolic functions. The function ϕ_2 has a logarithmic singularity as $u \to 0$, corresponding to $z \to \infty$. This implies that the growth of this part of $f_i(z)$, as $z \to \infty$, is at most linear and is derived from a combination of this singularity and the exponential decay towards zero of

$\mathrm{sech}^2 z$. At the free surface, $u \to 1$, ϕ_2 behaves like $(1-u)^{1/2}$, but the parabolic behaviour of $\mathrm{sech}^2 z$ near to $z = 0$ ensures that the behaviour in z is analytic. Using the asymptotic forms of ϕ_1 and ϕ_2 leads to the following relationships between the unknown constants,

$$f_i \sim \frac{B_i \Gamma(1/2)}{\Gamma(r)\Gamma(s)} z + \frac{1}{2}\left\{ A_i + B_i \frac{\Gamma(1/2)\,(K_0 - 1 - \ln 4)}{\Gamma(r)\Gamma(s)} \right\}, \quad z \to \infty \tag{3.4.4a}$$

$$f_i(0) = C_i, \tag{3.4.4b}$$

$$f_{iz}(0) = A_i \Gamma(1/2)/(\Gamma(1-r)\Gamma(1-s)) + B_i, \tag{3.4.4c}$$

$$f_{izz}(0) = -2C_i + A_i \Gamma(-1/2)/(\Gamma(r)\Gamma(s)), \tag{3.4.4d}$$

where $K_0 = 2\psi(1) - \psi(r) - \psi(s)$, with ψ the Di-Gamma function, Γ'/Γ. Hence, using the boundary conditions, we find $C_i = A_i = 0$, $i = 2,4$, $C_3 = -1$, and $A_3 = -2$, since then $r = 1$, and $s = -1/2$. We do not consider f_5 here, other than to note that, since the forcing for it is later shown to be zero at infinity, the solution for large χ is given by (3.4.3) and it too is at most linearly increasing.

The equations in region II, for the reversed flow, must be solved numerically. The transformations

$$\hat{\zeta} = \zeta (2p_1)^{1/4} \sqrt{6}, \quad \sigma = p_3 - p_2^2/4p_1, \quad \mu = p_2^2/(4p_1\sigma),$$

$$\gamma_1 = \sqrt{6}\,(2p_1)^{1/4}, \quad \gamma_2 = \sqrt{6}\, p_2/(2p_1)^{3/4}, \quad \gamma_3 = \sigma\sqrt{6}/(2p_1)^{3/4},$$

$$g_i = \gamma_i \hat{g}_i(\hat{\zeta}),$$

lead to the normalised equations

$$\hat{g}_1''' + \hat{g}_1 \hat{g}_1'' + 4\,(\hat{g}_1'^2 - 1) = 0,$$

$$\hat{g}_2''' + \hat{g}_2'' \hat{g}_1 + 9\,(\hat{g}_1' \hat{g}_2' - 1) = 0,$$

$$\hat{g}_3''' + \hat{g}_3'' \hat{g}_1 - \hat{g}_3 \hat{g}_1'' + 10\,(\hat{g}_1' \hat{g}_3' - 1 + \mu(\hat{g}_2'^2 - 1)) = 0,$$

with boundary conditions

$$\hat{g}_1(0) = \hat{g}_1'(0) = 0, \quad \hat{g}_1 \sim -\hat{\zeta} + \hat{c}_1 \quad \text{at } \infty.$$

These are solved using finite difference methods and the results checked using a variety of grid sizes and values of $\hat{\zeta}_\infty$. It is found that

$$\hat{g}_1''(0) = -2.273, \quad \hat{c}_1 = 0.414,$$

$$\hat{g}_2''(0) = -3.715, \quad \hat{c}_2 = -0.140.$$

The constant $\hat{c}_3$ depends on μ, which turns out to be independent of a but not of α, and therefore no unique value can be given to it. The decay towards the reversed flow solutions at infinity is like $\hat{\zeta}^{-7}$, i.e. algebraic.

We are now in a position to match the solutions in regions I and II, and find the unknown coefficients and the pressure. Writing $c_i = \gamma_i \hat{c}_i$ and using (3.4.1a) to write the solution in region II as $\zeta \to \infty$ in terms of χ, we find

$$\psi \sim x^{1/3}(-\alpha\sqrt{2p_1}) + x^{1/6}(c_1 - \alpha p_2/\sqrt{2p_1}) + (\sqrt{2p_1}\chi + c_2 - \sigma/\sqrt{2p_1}) \quad \text{as } \zeta \to \infty. \tag{3.4.5}$$

So, matching, we find, from the $O(x^{1/3})$ term,

$$p_1 = \frac{1}{2}\left(\frac{a}{\alpha}\right)^2,$$

since $f_1(\infty) = a$. At $O(x^{1/6})$ there are no terms proportional to χ in (3.4.5) and therefore $B_2 = 0$. Since A_2 and C_2 are also zero we find $f_2 = 0$ and

$$p_2 = c_1\frac{\sqrt{2p_1}}{\alpha} = 1.014\frac{a^{3/2}}{\alpha^{5/2}}.$$

At O(1) we get, using (3.4.4a) and r = 1, s = -1/2,

$$B_3 = -12/\alpha,$$

$$f_3(\chi) = -1 + a\chi/\alpha - 9/\alpha\ (a\chi/6\ \mathrm{sech}^2 a\chi/6 + \tanh a\chi/6),$$

$$\sigma = -\frac{a}{\alpha^2}\left(1 + \frac{9.348}{\alpha}\right).$$

In principle higher order terms in this expansion can be found. For example A_4, B_4 and C_4 are found easily from (3.4.4) and (3.4.5), and further terms follow in a clear fashion. There is new physics entering at $O(x^{-2/3})$, due to the change in the position of the free surface, and at $O(x^{-1})$ due to the algebraic decay of the solutions in region II. Uncertainties over the O(1) position of the free surface, i.e. the pressure rise in separation, and the origin of the expansion in x, would bring in eigensolutions to the problem but these have been suppressed by the use made of this freedom of choice of the origin at the beginning of the analysis. None of these extra effects, however, serve to fix the value of a, which as explained above will depend on the momentum flux emerging from the region $x = O(1)$. In summary, therefore, given both a and α,

$$p \sim -\{\ (a^2/2\alpha^2)x^{-4/3} + 1.014a^{3/2}/\alpha^{5/2}x^{-3/2} -$$

$$(\ a/\alpha^2 + 8.834a/\alpha^3)x^{-5/3} + \ldots\},$$

$$U_y|_{wall} \sim -0.928a^{3/2}/\alpha^{3/2}x^{-3/2}(1 + 1.657x^{-1/6}/a).$$

§3.4.2 Discussion.

We have shown that the momentum flux of the oncoming flow, except for any losses at separation, is concentrated in a jet (f_1) of thickness $O(x^{1/3})$ near to the free surface. The speed of this jet is $O(x^{-1/3})$, which is faster than the $O(x^{-1})$ velocities in the Jeffrey-Hamel flow of §3.3. The large, $O(x^{1/3})$, volume flux in the jet is balanced by a slower backflow in the wider main part of the thickening layer. This backflow is brought to zero by

a boundary layer at the wall. The flux of the original oncoming flow is carried in f_3 and g_2 and the velocity associated with f_3 in the jet is of the same order as that dominating the backflow. The pressures are simply those required to drive the backflow and so make up the required corrections to the mass flux due to the effects of the boundary layer or of the jet. It seems possible to accommodate any momentum flux and therefore any oncoming flow/separation pair with a structure of this kind.

It is worth noting that this structure, at least to these lower orders, before the position of the free surface enters into the expansion, can describe the asymptotic form of breakaway separation in a diverging channel. The differences appearing at higher orders will not result in the general form of the expansion becoming unsuitable.

The question of whether this asymptotic form is attained for all slopes greater than $\alpha_c = 5.461$, or indeed whether it is appropriate for slopes smaller than α_c in some circumstances, has yet to be answered. There is no hard evidence to suggest that α_c is the lower limit for breakaway separation, although there is clearly no need for the separation to be of the breakaway type for slopes less than α_c. The numerical calculations of §3.2, however, show that for α of the order of 15 to 60, the largest value studied, profiles qualitatively similar to those described in this section develop. For example, see Figure 3.4.2, which details the downstream development of such a profile. There is much qualitatively similar with the theory above, although the comparison is hindered by the relatively thick boundary layer on the lower wall, which is predicted theoretically.

However, there remains the possibility that these types of asymptote are only seen in the numerical calculations due to the large perturbation received by the starting flow at the start of the interaction. These are due to the large values of $s\alpha$ used. As explained in §3.2, these will cause the slope to provide relatively large pressure gradients which are countered by a rapid initial

thickening of the layer. On the other hand, and this seems more likely, it is shown in §3.5.2 that the length scale over which separation can occur for large α is small, $O(\alpha^{-3})$. In this case the main part of the initial flow reacts inviscidly and is lifted off the lower wall by a separated region of backflow. As the solution emerges from these shortened length scales, viscosity acts on this, now-free shear layer and forces it to take a jet-like profile. This implies that the momentum flux in the jet is precisely that in the initial profile and enables us to determine a in equation (3.4.2).

§3.5 Branching Solutions On A Favourable Slope.

§3.5.1 The initial stages of the branching.

We now turn to a consideration of the initial stages of the branching, i.e. the structure and growth rates of the linear, small perturbations which can develop to give the large x asymptotes described in the previous two sections. Here, however, we change the set-up of our problem a little and consider a half-Poiseuille flow at $x = -\infty$ as our basic flow. This is in contrast to the numerical solutions of §3.2 which have a similar profile at $x = 0$, and values of the Froude number and slope unsuitable for a layer of depth unity. The form used here is ultimately more sensible in considering the problem of free interactions than the form used in §3.2. However we can expect the downstream asymptotes of the two systems to be identical. In this section, too, we do not initially presume that the slope is $O(Re^{-1})$, nor the length scale of the interaction to be $O(Re)$, since we go on after considering these scalings to consider the interaction on steeper slopes, which occurs on a shorter length scale. We neglect surface tension effects, apart from a short discussion of the differences they are likely to make to the results.

Let the slope have gradient α, here $O(1)$, and write $\sin\alpha$, $\cos\alpha$ and $\tan\alpha$ as s_α, c_α and t_α respectively. The

governing equations are

$$UU_x + VU_y = -p_x + s_\alpha Fr^{-1} + Re^{-1}(U_{yy} + U_{xx}),$$

$$UV_x + VV_y = -p_y + Re^{-1}(V_{yy} + V_{xx}),$$

$$U_x + V_y = 0,$$

$$p|_{y=h} = hc_\alpha Fr^{-1},$$

$$U = V = 0 \text{ at } y = 0, \quad \int_0^h U dy = 1, \quad U_y = 0 \text{ at } y = h.$$

Here h is the depth of the layer, Fr the Froude number of the flow and x and y are coordinates in directions parallel to and perpendicular to the slope respectively. Also, p is the pressure with the variation perpendicular to the slope due to hydrostatic effects subtracted out. The basic flow is half-Poiseuille with depth 1. This has

$$V = 0 \qquad \text{and} \qquad U = 3(y-y^2/2),$$

and therefore

$$Res_\alpha = 3Fr. \tag{3.5.1}$$

We introduce a stream function ψ, such that $U = \psi_y$ and $V = -\psi_x$. Then the basic flow is

$$\psi = \psi_0 = F(y) = 3(y^2/2 - y^3/6).$$

Consider a perturbation to this basic flow of a size which is initially exponentially small. This is similar to the method suggested by Lighthill (1953), who extends the work of earlier authors to include the important viscous effects, in considering departures from the shear flow near the wall in a supersonic boundary layer. So

$$\psi = F(y) + a\ E\ f(y),$$

$$h = 1 + a\ E,$$

where $E = \exp(xq)$, and a is an O(1) constant. If we substitute these forms into the Navier-Stokes equations we find

$$(qa)[F'f' - fF''] = -p_x + aRe^{-1}(f''' + q^2f'), \tag{3.5.2a}$$

$$-q^2aF'f = -p_y - qaRe^{-1}(f'' + q^2f), \tag{3.5.2b}$$

where $'$ represents $\partial/\partial y$. If we write

$$p = c_\alpha\, Fr^{-1} + a\, E\, c_\alpha\, Fr^{-1}\, \Pi,$$

so that $\Pi(1) = 1$, then using (3.5.1), we find

$$(F'f' - fF'' + 3\Pi/(Ret_\alpha)) = Re^{-1}(f''' + q^2f'), \tag{3.5.3a}$$

$$\Pi' = (t_\alpha Req^2/3)F'f - (t_\alpha q/3)\,(f'' + q^2f), \tag{3.5.3b}$$

These, then, are the equations which govern the perturbation profile and the variation in the pressure across the depth of the layer. The boundary conditions appropriate to these equations are $f(0) = f'(0) = 0$, and, at the free surface, linearising about $y = 1$, we find

$$\psi(h) \sim F(1+aE) + aEf(1+aE) + \ldots = 1,$$

$$\psi''(h) \sim F''(1+aE) + aEf''(1+aE) + \ldots = 0,$$

giving

$$f(1) = -3/2, \quad f''(1) = 3. \tag{3.5.3c-d}$$

The final condition is

$$\Pi(1) = 1. \tag{3.5.3e}$$

We now go on to consider (3.5.3) as $Re \to \infty$ for progressively steeper slopes.

§3.5.2 Slopes of $O(Re^{-1})$: relatively small slopes; larger slopes. The shape of hydraulic jumps.

If the slope is $O(Re^{-1})$ we write $t_\alpha = \hat{t}_\alpha/Re$, $q = \hat{q}/Re$, and find that (3.5.3a-b) reduce to,

$$\Pi' = 0, \tag{3.5.4a}$$

$$\hat{q}(F'f' - fF'' + 3/\hat{t}_\alpha) = f'''. \tag{3.5.4b}$$

This is an eigenvalue problem for the growth rate $\hat{q}$. We hope that there will be at least one positive value of $\hat{q}$ satisfying (3.5.4) so that our assumption that the perturbation is small as $x \to -\infty$ is valid. The problem is solved using finite differences, and the positive values of $\hat{q}$ against $\hat{t}_\alpha$ are plotted in Figure 3.5.1. There are many negative values of $\hat{q}$ satisfying (3.5.4), but only one positive growth rate is found for a given $\hat{t}_\alpha$.

The two limits $\hat{t}_\alpha \to 0$ and $\hat{t}_\alpha \to \infty$ are easily examined. For small $\hat{t}_\alpha$ the predominant balance is one between viscosity and pressure and we find that the perturbation is governed by lubrication theory,

$$\hat{q} \sim 3\hat{t}_\alpha,$$

$$f \sim 3(y^3/2 - y^2) = -yF'.$$

The stream function can thus be written as,

$$\psi = F - aEyF',$$

so that,

$$\psi(\zeta(1+aE)) = \psi_0(\zeta) + O(E^2).$$

Thus the flow is still of a half-Poiseuille type but is thickening. The adjustment occurs on a sufficiently long length scale, $O(Re\hat{t}_\alpha^{-1})$, that viscosity can smear out any changes across the whole depth and the profile remains of a viscous character throughout this depth. Note the

similarity here with the large s behaviour of the flow on a horizontal surface in §2.6.6. The connection is through the relation (3.5.1), which implies that a small value of α, i.e. a nearly horizontal surface, corresponds to a large value of s.

In the limit of large $\hat{t}_\alpha$, moving towards gradients larger than $O(Re^{-1})$, we find that the solution splits into two regions. The growth rate of the disturbance becomes large and we write $\hat{q} \sim \hat{t}_\alpha{}^3 q^*$, where q^* is $O(1)$ as $\hat{t}_\alpha \to \infty$. In the main part of the flow, where $y = O(1)$, inertia dominates and $f = -F'$. Thus there is a slip velocity at the wall of magnitude -3. This is reduced to zero in a boundary layer of thickness $\hat{t}_\alpha{}^{-1}$ where a linearised form of equations (2.6.2) hold,

$$zu - v = -1 + u''/(3q^*),$$

$$v' = u,$$

$$u = v = 0 \text{ at } z = 0, \quad u \to -3 \text{ as } z \to \infty.$$

Here $'$ represents $\partial/\partial z$, where $z = y\hat{t}_\alpha$. We can calculate that

$$\hat{q} \sim 9(3|Ai'(0)|)^3 \hat{t}_\alpha{}^3 = 4.213\ \hat{t}_\alpha{}^3.$$

The structure here is just the same as is relevant to the case of small s studied in §2.6.2. This is to be expected since, again, equation (3.5.1) implies $s \propto 1/\alpha$ and the length scale of the interaction in this limit decreases so that the flow does not experience the slope. A nonlinear structure for the interaction which, in the limit of large $\hat{t}_\alpha$, shows that in a region near the wall the flow reacts according to equation (2.6.2), can be constructed along lines similar to those in §2.6.2. The disturbance amplitude for such a nonlinear reaction is $O(\hat{t}_\alpha{}^{-1})$. So we can expect the hydraulic jump on slopes of this magnitude to have the same form as those on a horizontal surface. Separation occurs rapidly on this

short length scale and, although the stages in the subsequent development have yet to be fully investigated, it seems likely that the linear increase in depth due to the slope soon dominates the $X^{0.4305}$-like growth as a result of the separation. Here X measures the short $O(\hat{t}_\alpha^{-3})$ scales of the interaction. The new term enters into the equation governing the lower deck, and causes the growth to flatten off, as follows. The pressure-displacement law, including the prescribed pressure gradient due to the slope, is

$$P = -A + d_1 X \hat{t}_\alpha^{-1}, \quad d_1 = O(1), \quad \hat{t}_\alpha >> 1.$$

Now, far downstream $A \sim X^{0.4305}$ so that the two terms in this law become comparable if $X \sim O(\hat{t}_\alpha^{1.7559})$ or $x \sim O(\hat{t}_\alpha^{-1.244})$. Further downstream it seems likely that the prescribed term in the law dominates and A attains a constant value so the free surface flattens off, although the depth increases due to the effects of the slope. A similar effect, due to this given component in the pressure-displacement law, is seen in the work on asymptotically small slopes in §3.6.3. Eventually, on an O(1) scale in x, the solution asymptotes the form described in §3.4. See also the numerical solutions of the forced interaction presented in §3.7.

§3.5.3 Slopes of $O(Re^{-5/7})$ and greater. Some effects of surface tension.

We now consider larger slopes. If we substitute this large $\hat{t}_\alpha$ asymptote into equations (3.5.3), we find that the relative error in neglecting the transverse pressure gradient generated by the streamline curvature as the branching commences is $O(\hat{t}_\alpha^{7}/Re^2)$. This becomes O(1) if $\hat{t}_\alpha = O(Re^{2/7})$, or $t_\alpha = \tilde{t}_\alpha Re^{-5/7}$, say. With this scaling for t_α we find that $q = \tilde{q} Re^{-1/7}$ with $\tilde{t}_\alpha$ and $\tilde{q}$ both O(1). In this case we find, where y = O(1),

$$\Pi' = (\tilde{t}\, \tilde{q}^2/3)\, F'f,$$

$$F'f - fF'' = 0.$$

These can be integrated, and the boundary conditions used to give f = -F′ and therefore

$$\Pi(1) - \Pi(0) = -(\tilde{t}_\alpha \tilde{q}^2/3)\int_0^1 F'^2 dy,$$

and so

$$\Pi(0) = 1 + (2/5)\ \tilde{t}_\alpha \tilde{q}^2.$$

We see, therefore, that on these scales the pressure is made up of both gravitational and curvature terms.

In a boundary layer of thickness $O(Re^{-2/7})$ we find again that the equation reduces to a linearised interactive boundary layer equation, and $\Pi' = 0$. The equation satisfied by the eigenvalue is

$$\tilde{q}(1 + 2/5\ \tilde{t}_\alpha \tilde{q}^2)^3 = \tilde{t}_\alpha{}^3 9(3|Ai'(0)|)^3.$$

This has a real positive root for all $\tilde{t}_\alpha$. As $\tilde{t}_\alpha$ increases we find $\tilde{q} \sim 9^{1/7}(15|Ai'(0)|/2)^{3/7}$, so the growth rate levels off at $O(Re^{-1/7})$ as the slope increases. Examining equation (3.5.3), we see that this asymptote will hold even for O(1) slopes. So the branching on anything other than shallow slopes is dominated by the effects of streamline curvature. The nonlinear version of this structure for slopes large on the $O(Re^{-5/7})$ scale, so that the gravitational term diminishes in size, is governed by the interactive boundary layer equations with the pressure given by $P = -cA_{xx}$, with X measuring these $O(Re^{-1/7})$ scales and c of $O(\tilde{t}_\alpha)$ as $\tilde{t}_\alpha \to \infty$. These are the equations governing upstream influence in channel flow (Smith (1976)) and in boundary layer jet-like flows (Smith and Duck (1977)). They predict a downstream form with separated flow and $A \sim -P_0 c^{-5/7} X^2/2$, $P_0 \approx 0.675$ as $X \to \infty$. However, using a argument similar to that used in §2.7.3, with regard to a large surface tension coefficient, the neglected gravitational term is reinstated at large values of X, as A becomes large but A_{xx} remains finite. It is possible, therefore, that a jump is possible with a free

surface shape of the blunt form predicted by the law $P = -A$. This possibility, however, neglects the effects of the slope which may enter as the solution develops downstream and swamp this jump. If we consider, then, the prescribed gravitational component to the pressure-displacement law (as in the arguments of the previous sub-section) we find that it now reads

$$P = -A - d_2 \hat{t}_\alpha A_{xx} - d_3 Re^{-2/7} \hat{t}_\alpha X,$$

$$d_2,\ d_3 \text{ both } O(1). \qquad (3.5.5)$$

If we consider this equation, as $\hat{t}_\alpha$ and X become large, together with the result that downstream $A = O(\hat{t}_\alpha^{-5/7} X^2)$, we see that the first term will only enter and give the blunt shape of the free surface (and an obvious "jump"), if the distance required for it to become important, $O(\hat{t}_\alpha^{1/2})$, is sufficiently short. The last term will enter and stop this occurring when $X \sim O(Re^{2/7} \hat{t}_\alpha^{-12/7})$. So, for a "jump" to be seen, we require $\hat{t}_\alpha << Re^{4/31}$. If this is not the case, as is true for slopes of O(1) as $Re \to \infty$, the flow will not be affected at all by the hydrostatic term, -A, in the pressure law. As a result, it seems that the flow will proceed to attain the downstream form of §3.4 with the free surface remaining concave throughout the interaction.

Surface tension effects, as described in §2.1 and §2.7.3, will result in the addition of a term $+ A_{xx}$ to the pressure-displacement law. If the coefficient of surface tension is large enough, then the growth rate, q, will have an imaginary part and the initial departure will be wave-like. See also §3.6.6. It is interesting to note also that the effects of surface tension can reduce the magnitude of the coefficient of the A_{xx} term in (3.5.5) and allow the first, "jump-producing", term to enter before the growth of the last, prescribed, term destroys the interaction. Thus a large (although not too large) surface tension coefficient will mean that "jumps" will be more likely to be seen as the slope increases.

§3.5.4 Further comments and discussion.

The Froude number of the flow and so the magnitude of the slope has a further effect on the length scale of these interactions via its influence on h, the depth of the layer far upstream which is used in the above analysis as a scaling for the distances parallel to the slope.

The results of this section, allied with the large-x asymptotes of §3.3 and §3.4, seem to provide a complete description of the compressive free interaction problem for half-Poiseuille flow on a slope. The range of slopes covers any up to those large on an $O(Re^{-5/7})$ scale as $Re \to \infty$, but it seems reasonable that the mechanisms due to streamline curvature or surface tension can account for upstream influence on slope of O(1) or near-vertical slopes. In this latter case the hydrostatic effects necessarily become less important.

All the interactions develop into a form in which the free surface becomes horizontal. For the smallest slopes, $O(t_\alpha Re^{-1})$ where $Re \to \infty$, $t_\alpha \to 0$, the whole flow remains half-Poiseuille in character throughout its development, which occurs only slowly. Separation is not possible. This limit is considered further in §3.6, where its simplicity allows the easy analytical and numerical solution of certain forced interaction problems. This also has strong similarities with the branching from low Froude number flows on a horizontal plate.

As the slope increases, the flow departs from the Poiseuille form, but viscosity still manages to spread vorticity throughout the depth of the flow. For larger slopes separation occurs within this viscosity-affected structure. The profiles emerging in these cases as $x \to \infty$ are all Jeffrey-Hamel flows. There is a complicated interplay between viscosity, pressure and inertia in this regime and it is not possible to clarify the structure of the interaction in any asymptotic sense. The development on an O(Re) length scale.

For larger slopes the length scale over which the branching occurs shortens and the asymptotic structure becomes clear. It is similar to that in the large Froude

number limit on a horizontal surface and so is governed by the hypersonic free interaction equations which hold in a sublayer near the wall. The main body of the flow is merely displaced. Downstream it seems that the free surface flattens out and the displaced initial profile develops into a spreading jet at the free surface. Beneath this there is a strong recirculation, in the sense that it carries a great deal of fluid, although the actual velocities are small.

At still larger slopes, up to O(1) as $Re \to \infty$, it is the pressure increase through the depth of the fluid and its relation to the curvature of the streamlines as the branching commences which governs the branching process. In this regime, if the effects of surface tension are weak, the blunt shape of the hydraulic jump is lost as the slope becomes more severe.

§3.6 The Limit Of Small Gradient.

§3.6.1 Introduction and the governing equations.

We have seen in §3.3.2 and §3.5.2 that if the scaled slope, α, is small the flow remains of half-Poiseuille type throughout the compressive free interaction. Both the initial stages and the final large x asymptote, with a horizontal free surface, are governed by lubrication theory; the development in x is slow and viscosity acts to redistribute the vorticity and keep the flow half-Poiseuille in character. This means that separation is not possible.

We can use these simplifying features to develop a simple first order equation for the depth of the layer which includes the effects of the viscous-inviscid interaction. This equation can be solved analytically for simple geometries and numerically for more complicated cases. The effects of surface tension, which raise the order of the equation to third, and of a moving wall can easily be incorporated.

We therefore start with the Navier-Stokes equations

appropriate to the flow down a slope

$$UU_x + VU_y = -P_x + \sin(\alpha)\ s + Re^{-1}(U_{yy} + U_{xx}), \qquad (3.6.1a)$$

$$UV_x + VV_y = -P_y - \cos(\alpha)\ s + Re^{-1}(U_{yy} + V_{xx}), \qquad (3.6.1b)$$

$$U_x + V_y = 0, \qquad (3.6.1c)$$

$$U = V = 0,\ y = 0, \quad U_y = 0,\ y = H, \qquad (3.6.1d\text{-}f)$$

$$\int_0^H U\ dy = 1. \qquad (3.6.1g)$$

Here $y = H$ corresponds to the unknown position of the free surface and x and y are measured parallel and perpendicular to the slope.

We scale the length on $Re/\sin(\alpha)$ so that $x = Re\ X\ /\ \sin(\alpha)$, and rewrite the pressure as $P = p - s\cos(\alpha)\ y$, so that p is the reduced pressure. Then if we write α for $\sin(\alpha)$ we find that (3.6.1a-b) become

$$\alpha(UU_x + VU_y) = -\alpha\ p_x + \alpha\ s + (U_{yy} + \alpha^2/Re^2\ U_{xx}),$$

$$\alpha^2/Re^2\ (UV_x + VV_y) = -p_y + \alpha/Re^2(V_{yy} + \alpha^2/Re^2\ V_{xx}).$$

If we consider flow over the obstacle given by $y = f(X)$ then the equation obtained from considering the balance of forces across the free surface, given by $y = h + f(X)$ say, including the effects of surface tension becomes

$$p - s\ (h + f) + (T/\rho g h_0^{\,2})s(\alpha^2/Re^2)\ \left(\frac{h_{xx} + f_{xx}}{(1+\alpha^2/Re^2(h_x+f_x)^2)^{3/2}}\right)$$

$$= 0. \qquad (3.6.2)$$

Here h_0 is the depth used in the nondimensionalisation of the equations as a representative length. It is the depth of the layer upstream and so is $(3\nu Q/g\alpha)^{1/3}$ where ν is the kinematic viscosity of the fluid and Q the volume flux per unit width carried by the layer. In addition, T is the

coefficient of surface tension of the air/liquid interface, ρ is the density of the liquid and g the acceleration due to gravity. We now use the assumption that $\alpha << 1$ to simplify the equations. Note that for half-Poiseuille flow on a small slope the Froude number, s^{-1}, must be small and so we presume that $s\alpha$ remains O(1) as $\alpha \to 0$. The equations reduce to

$$\alpha p_x = \alpha s + U_{yy}, \tag{3.6.3a}$$

$$p_y = 0, \tag{3.6.3b}$$

$$\alpha p_x = (\alpha s)\left(h_x + f_x - \gamma \left(h_{xxx} + f_{xxx}\right)\right), \tag{3.6.3c}$$

where

$$\gamma = (T/\rho g h_0^2)\ (\alpha^2/Re^2) \text{ is assumed } 0(1), \text{as } \alpha \to 0. \tag{3.6.3d}$$

We can write γ as $(T\mu^{4/3}/(3^{2/3}\rho^{7/3}g^{1/3}))\ (\alpha/Q)^{8/3}$, where μ is the viscosity of the fluid. Using physical constants typical of film-coating processes, namely $\rho = 1$ gm/cm^3, T = 50 dyn/cm, $\mu = 50$ gm/cm sec (taken from Christodoulou and Scriven (1989)), gives $\gamma \approx (10\alpha/Q)^{8/3}$ if Q is measured in c.g.s. units. Thus the large γ approximation, used later in this chapter, requires a small volume flux.

The flow is governed by lubrication theory. Integrating equation (3.6.3) in y, and applying the boundary conditions at y = 0 and y = f + h we find

$$1 = (-h^3)(\alpha s/3)\left(h_x + f_x - \gamma \left(h_{xxx} + f_{xxx}\right) - 1\right). \tag{3.6.3e}$$

Far upstream h_x and f_x are zero and h = 1 so we must have $\alpha s = 3$, and therefore

$$h_x - \gamma\, h_{xxx} = 1 - 1/h^3 - f_x + \gamma\, f_{xxx}. \tag{3.6.3f}$$

This, then, is the equation governing the depth of

the half-Poiseuille flow. The assumptions used in deriving it are as follows. Firstly $\alpha UU_x << U_{yy}$, which reduces to $\alpha << h^3$, or to f_x being O(1) or less. Secondly, we require $Re >> \alpha$, and since α is small the theory is therefore valid for Re = O(1).

Similar equations have been derived and solved by Wilson and Jones (1983) in the study of the fall of a thin liquid film down a vertical wall into a pool. In this case, since the wall is vertical, the hydrostatic contributions to the pressure are negligible and surface tension dominates. See also Christodoulou and Scriven (1989) and Higgins and Scriven (1979). There is also a strong connection with the work of Chester (1966), who uses lubrication theory to give a description of a viscosity-dominated bore, or moving hydraulic jump travelling downstream. As a first step in the study of these equations we re-derive and extend some of the results of Chester. We go on to investigate the solutions of (3.6.3f), first with $\gamma = 0$, in both forced and free interactions, using both analytical solutions and a numerical scheme. We then investigate the free interaction in the limit of large γ. Finally we make some deductions about the form of the forced interaction on slopes larger than these. Computations to check these predictions are carried out in §3.7.

§3.6.2 Travelling bores.

If the speed of a bore on the liquid layer is constant, W say, then moving in a frame with the bore gives an upstream moving wall of speed W. See Figure 3.6.1. If the wall is smooth and there is no surface tension then we can derive, in a similar fashion to the derivation of (3.6.3f) from (3.6.3a-d), the following equation

$$h_x = 1 - 1/h^3 + W\,(1/h^3 - 1/h^2). \qquad (3.6.4)$$

As Chester shows, there is the possibility of a smooth transition from an upstream depth of 1 to a depth D

< 1 downstream, if

$$W = D^2 + D + 1.$$

If $D = 1 - \varepsilon$ ($\varepsilon << 1$) we get the weak bore examined by Chester, namely

$$W \sim 3 - 3\varepsilon + \varepsilon^2,$$

$$h \sim 1/2\ (1 - \tanh\ (3\varepsilon X/2)).$$

See Figure 3.6.2(a). On the other hand for small D, say $D = \hat{\varepsilon}$ with $\alpha << \hat{\varepsilon}^3$, we get a relatively strong bore moving with speed

$$W \sim 1 + \hat{\varepsilon} + \hat{\varepsilon}^2.$$

This is illustrated in Figure 3.6.2(b). Upstream of the bore position, $X = X_0$, the depth is O(1) and equation (3.6.4) becomes

$$h_X = 1 - 1/h^2,$$

and so the solution here is simply

$$X - X_0 = h + 1/2\ \ln\ |(1-h)/(1+h)|.$$

However as $X \to X_0-$, $h \sim (3(X - X_0))^{1/3}$ and so in a small region of X-extent $O(\hat{\varepsilon}^3)$ the governing equation is

$$\tilde{h}_{\tilde{X}} = 1/\tilde{h}^3 - 1/\tilde{h}^2,$$

where $h = \hat{\varepsilon}\tilde{h}$ and $(X - X_0) = \hat{\varepsilon}^3\tilde{X}$. Thus here

$$(-\tilde{X}) = \tilde{h}^3/3 + \tilde{h}^2/2 + \tilde{h} + \ln|\tilde{h} - 1|.$$

As $\tilde{X} \to \infty$, $\tilde{h} \to 1$ and so

$$h = \hat{\varepsilon} \text{ for } X > X_0.$$

Of course inertial effects will enter as the depth becomes small, rendering our approximation invalid when $\hat{\varepsilon} \sim \alpha^{1/3}$.

§3.6.3 Stationary hydraulic jumps; free and forced interactions.

In this section we concentrate on the case $W = 0$, $\gamma = 0$, so that

$$h_x = 1 - 1/h^3 - f_x, \tag{3.6.5a}$$

$$h \to 1, \; X \to \pm\infty. \tag{3.6.5b}$$

This equation contains within it the possibility of viscous-inviscid interaction. It is first order in X but we wish to impose two boundary conditions. That is we wish to consider a forced interaction. However we first consider the case $f_x = 0$ and look at free interactions and neglect the boundary condition as $X \to \infty$. A possible solution is $h = 1$, but this is not unique and an initially small disturbance of the form $h = 1 + \varepsilon g(X)$, $\varepsilon << 1$, will grow according to $g_x = 3g$ which implies $g = a \exp(3X)$ with a arbitrary, as in §3.5.2. Further downstream we have the three possible asymptotes $h \sim X$, $h \sim 1$ or $h \sim (4(X_0 - X))^{1/4}$ for some finite X_0. The first of these corresponds to the compressive free interaction studied in §3.5.2 ($a > 0$). The second is undisturbed flow ($a = 0$) and the last will lead to the expansive interaction ($a < 0$). As the layer thins inertial effects will become important and, as in §2.2.1, prevent choking. In the case of a large Reynolds number, the final form of this interaction will be governed by the full boundary layer equations with the singularity described in §2.5 being attained.

We now turn to the forced interaction. We first note that if the position of the free surface is $H = f+h$ then, from equation (3.6.5), the gradient of this is always less than unity, since h is positive. Since the gradient of the slope is exactly unity it is impossible for the free surface level to rise. We later present a numerical scheme for solving a general forced interaction but first we consider a case which can be solved analytically and which exhibits many of the features common to forced interactions. The case considered is that of a simple

change in slope at $X = 0$,

$$f_x = 0, \quad X < 0,$$

$$f_x = \beta, \quad X \geq 0.$$

A numerical solution of this problem, with $\beta = 4/5$, using the numerical scheme developed in the next subsection is presented in Figure 3.6.3.

In the limit $\beta \to 1-$ the slope downstream of $X = 0$ becomes nearly horizontal and the depth of the layer becomes large. In contrast, the gradient here increases as $\beta \to -\infty$ and inertial effects must enter as the layer thins. For $X > 0$ the equation (3.6.5a) reduces to

$$h_x = (1 - \beta) - 1/h^3.$$

The appropriate downstream boundary condition is $h_x \to 0$ as $X \to \infty$, corresponding to uniform flow downstream. It is clear from the arguments presented above for the free interaction that the only possible solution has $h_x = 0$ for all positive X i.e.

$$h = (1 - \beta)^{-1/3} \text{ for } X > 0.$$

This implies that $h(0) = (1 - \beta)^{-1/3}$ and so for $X < 0$ we have

$$h_x = 1 - 1/h^3,$$

$$h(0) = (1 - \beta)^{-1/3},$$

$$h \to 1 \text{ as } X \to -\infty.$$

We write $(1 - \beta)^{-1/3} = \delta$ and then this equation has a solution given implicitly by

$$X = (h - \delta) + 1/3 \ln \left| \frac{h - 1}{\delta - 1} \sqrt{\frac{\delta^2 + \delta + 1}{h^2 + h + 1}} \right| -$$

$$1/\sqrt{3} \tan^{-1} \left\{ \frac{2/\sqrt{3}\ (h - \delta)}{1 + 4/3\ (h + 1/2)(\delta + 1/2)} \right\}.$$

If we examine this as $\delta \to \infty$ $(\beta \to 1-)$, corresponding to the downstream slope nearing the horizontal and so the depth there becoming infinite, we find, writing $h = \delta\hat{h}$ and $X = \delta\hat{X}$ where $\hat{h}$ and $\hat{X}$ remain O(1) as $\delta \to \infty$, that

$$\hat{h} \sim 1 + \hat{X}.$$

This implies that upstream of $X = 0$ the free surface is horizontal and the depth alters due to the slope beneath this free surface, which is scaled to be unity. In the vicinity of $\hat{X} = -1$, ie $X = -\delta$, the depth becomes O(1) and the solution here is

$$X + \delta = h + 1/3 \ln \left| \frac{h - 1}{\sqrt{(h^2 + h + 1)}} \right| + 1/\sqrt{3} \tan^{-1} \left\{ \frac{\sqrt{3}}{2h + 1} \right\}.$$

This is the solution of (3.6.5a) for a free interaction. As $X + \delta \to -\infty$ the solution is

$$h = 1 + \sqrt{3} \exp\ (3(X + \delta)), \qquad (3.6.6)$$

corresponding to the form of the solution predicted for the free interaction.

For finite δ the solution is more complicated, but as $X \to -\infty$ it always has the form

$$h = 1 + a \exp\ (3X),$$

where

$$a = (\delta-1)\frac{\sqrt{3}}{\sqrt{(\delta^2+\delta+1)}} \exp\left\{3(\delta-1) + \sqrt{3} \tan^{-1}\left(\frac{1}{\sqrt{3}}\left(\frac{1-\delta}{1+\delta}\right)\right)\right\}.$$

If now $\delta >> 1$ this reduces to

$$a \sim \sqrt{3} \exp(3\delta),$$

and this agrees with the result (3.6.6), corresponding to the position of the free interaction moving a distance $O(\delta)$ upstream. On the other hand, if we consider the case of a large increase in slope so that $\delta \to 0+$, then

$$a \sim -\sqrt{3}/\delta \exp(-3 + \sqrt{3} \tan^{-1}(1/\sqrt{3})),$$

and this indicates that the adjustment towards a large increase in slope starts at a position $O(\ln(\delta))$ upstream. Of course the limit $\delta \to 0$ is not strictly valid as inertial effects will enter as the depth of the liquid layer decreases. It is possible, however, that the initial stages of the interaction will be governed by lubrication theory as they are for small Froude number, high Reynolds number flow on a horizontal surface (§2.6.6) and this result will hold upstream of $X = 0$ as $\delta \to 0$. Near $X = 0$ the flow will be affected by inertial effects.

This simple example, for which a complete analytic solution is available, illustrates features common to many forced interaction problems especially the movement of the start of the interaction upstream as the size of the departure from uniform flow increases. See Smith (1982). Also clear is the development, in the limit $\delta \to \infty$, of a flow containing a free interaction far upstream of $X = 0$.

§3.6.4 The numerical solution of some forced interaction problems.

To study more complicated interactions, for example the flow over the obstacle given by $f(X) = d\exp(-bX^2)$, the following numerical scheme is used. It is based on an adjustment of Carter's (1979) method which is successfully used by Brotherton-Ratcliffe (1986) (BR) in his study of the forced interaction problem with the hypersonic pressure-displacement law ($P = -A$). This is appropriate to liquid layers that are not fully developed, unlike the cases we consider here. It is, like Carter's method, an iterative process. A guess is made at the displacement for

the whole flow field and the boundary layer equations used to solve for the pressure field associated with this displacement. In this case the boundary layer equations reduce to lubrication theory and so a guess at the depth, $h^n(X)$ say, gives a pressure gradient P_X^a, from lubrication theory, of

$$P_X^a = -3/(h^n(X))^3.$$

A pressure field, P_X^b, is also calculated from the appropriate pressure-displacement law, the two pressures are compared and the difference used to update the guess for the displacement. As the iteration continues the displacement will, if the updating is done correctly, converge to a solution of the elliptic interactive problem. In this case the equivalent of the pressure-displacement law predicts that

$$P_X^b = 3(h_X^n + f_X - 1).$$

The update of the depth is achieved as follows. If we introduce the artificial time τ and imagine the convergence of h^n to h to occur as τ increases with τ increasing by a discrete amount on each iterative cycle we can write the formula used in the updating as

$$h_\tau = P_X^a - P_X^b. \qquad (3.6.7)$$

This is the method of updating used in BR. In contrast to Carter's method it compares the pressure gradients rather than the pressures themselves. The former approach was also tried by BR but was found to give divergence. Whether convergence is obtained or not depends on the size of the artificial timestep $\Delta\tau$ between iterates and the value giving the most rapid convergence must be found by trial and error due to the nonlinearity of the problem. Equation (3.6.7) is written in finite difference form and yields the formula

$$h_i^{n+1} = \{\Delta X/(1+\phi)\}\ \{g_{i+1} + 1/(h_{i+1}^n)^3 + g_i + 1/(h_i^n)^3\}$$

$$+ h_{i+1}^n + (1-\phi)/(1+\phi)\ \{h_{i+1}^{n+1} - h_i^n\}. \qquad (3.6.8)$$

Here ΔX is the grid size in X, ϕ is $\Delta X/\Delta\tau$ and $g(X) = f_X - 1$. The subscripts refer to the station in X and the superscripts the iteration number. The boundary condition as $X \to \infty$ is $h \to 1$, for obstacles that decay as $|x| \to \infty$, and this fixes the value of h^{n+1} far downstream. Equation (3.6.8) then allows the update of the depth at the other X stations. As an initial guess the depth is taken to be uniformly equal to 1 and the iterations are continued until $|P_X^a - P_X^b|$ is less than some specified amount, usually 10^{-4}. Typical solutions are shown in Figures 3.6.3&4. These use $\Delta X = 10^{-1}$, $\Delta\tau = 10^{-2}$ and typically require 800 iterations for convergence. If the method fails the use of a smaller value of $\Delta\tau$ is usually successful in achieving convergence.

The main characteristic of the solutions presented in Figures 3.6.3&4 is that the height of the free surface does not increase as the flow thickens. The liquid layer adjusts upstream of the obstacle and flows over it satisfying this constraint. The mechanism for this upstream influence is the viscous-inviscid interaction, and the nonlocal behaviour which is included in equation (3.6.5) by considering the possibility of this interaction. This is in contrast with the work and results of Eagles (1988) who does not use lubrication theory but instead considers non-interactive flow over beds varying in such a way that the flow is always of a Jeffrey-Hamel type which is determined locally. Jeffrey-Hamel flows develop for reasons explained in §3.3. The results given by this approach which, although valid for steeper slopes upon which separation can occur, does not allow for the possibility of viscous-inviscid interaction, suggest that the position of the free surface can rise smoothly as the liquid layer passes over the upstream face of the obstacle. This does not occur in the results presented

here and in the next section, §3.7, where the interaction on steeper slopes is addressed numerically. It is possible, as discussed later in this chapter, to make estimates of the flow field in the case of interactive flow on these larger slopes from the results of this lubrication theory, and it is suggested there that the possibility of a rise in the position of the free surface exists in these cases, but this rise is shown to occur far upstream of a large obstacle and to be very short in extent. In other words it occurs as part of a hydraulic jump. See §3.6.7.

§3.6.5 The asymptotic structure of flow over a large obstacle.

We now turn to the asymptotic structure of the solutions of equation (3.6.5) in the limit of a tall obstacle of O(1) width. Here equation (3.6.5) becomes

$$h_x = 1 - 1/h^3 - df_x, \tag{3.6.9a}$$

$$f = O(1) \text{ as } d \to \infty, \tag{3.6.9b}$$

$$h \to 1 \text{ as } X \to \pm\infty, \tag{3.6.9c}$$

$$f \sim 1 - f_o X^2/2 \text{ as } X \to 0, \text{ f decays exponentially as } X \to \pm\infty. \tag{3.6.9d}$$

The obstacle shape, f, is typically of the type used in the numerical solutions in Figure 3.6.4. We presume, too, that it is symmetric about X = 0. We look for a solution of the type suggested by the numerical solutions and consider the equation in the following three regions. See Figure 3.6.5.

I) The lee side and the slope downstream of the obstacle.

Here the primary balance is local in character and h_x is relatively small. The solution is

$$h \sim (1 - df_x)^{-1/3}, \quad d \to \infty.$$

Thus as $X \to \infty$ and f decays exponentially to zero, $h \to 1$. In addition, on the lee slope of the obstacle the depth is determined solely by the local slope. Thus, for this asymptotic structure to be valid, $d << 1/\alpha$. As $X \to 0+$, i.e. approaching the crest of the obstacle, we find, for large d, that

$$h \sim (df_0)^{-1/3}X^{-1/3} - (1/3)(df_0)^{-4/3}X^{-4/3}(1+O(X)). \tag{3.6.10}$$

since f is symmetric.

II) The crest of the obstacle (i.e. near X = 0).

At the crest of the obstacle the slope nears zero and so a locally defined depth would be infinite. To counter this the non-local term h_x enters and a balance including this effect is possible if $h \sim O(d^{-1/7})$ and $X \sim O(d^{-4/7})$. Therefore we write

$$h = \hat{h}/d^{1/7}, \quad X = \xi/d^{4/7}, \ \hat{h} \text{ and } \xi \text{ both } O(1) \text{ as } d \to \infty,$$

and find

$$\hat{h}_\xi = -1/\hat{h}^3 + \xi f_0 + 1/d^{3/7} + O(d^{-4/7}), \text{ as } d \to \infty.$$

We now write

$$\hat{h} = \hat{h}_0 + d^{-3/7}\hat{h}_1,$$

and substitute into (3.6.9) to get, with boundary conditions from equation (3.6.10),

$$\hat{h}_{0\xi} = -1/\hat{h}_0^{\,3} + \xi f_0, \quad \hat{h}_0 \sim (f_0\xi)^{-1/3} \text{ as } \xi \to \infty, \tag{3.6.11a-b}$$

$$\hat{h}_{1\xi} = 3\hat{h}_1/\hat{h}_0^{\,4} + 1, \quad \hat{h}_1 \sim -1/3\ (f_0\xi)^{-4/3} \text{ as } \xi \to \infty. \tag{3.6.11c-d}$$

Equation (3.6.11a-b) can be solved numerically using a method similar to that described above for the full

problem. This has not been done since it seems clear that a solution can be found. The asymptotes as $\xi \to -\infty$ are

$$\hat{h}_0 \sim \xi^2 f_0/2 + E_0 + (8/5)\, f_0^{-3}\xi^{-5} - (48E_0/7)\, f_0^{-4}\xi^{-7} + \ldots \qquad (3.6.12a)$$

and

$$\hat{h}_1 \sim \xi + E_1 + \ldots \quad . \qquad (3.6.12b)$$

The value of E_0 is fixed by equations (3.6.11a&b) and is given by $E_0 = \tilde{e} f_0^{-1/7}$ where

$$D_z = -1/D^3 + z,$$

$$D \to 1/z^{1/3} \text{ as } z \to \infty \quad \text{and} \quad (D - z^2/2) \to \tilde{e} \text{ as } z \to -\infty.$$

E_1 is also fixed and can be calculated from the relation

$$\hat{h}_1 = \hat{h}_0^{-3}\exp\left(3\int_0^{\xi}(f_0 t/\hat{h}_0)dt\right)\left[\int_{\infty}^{\xi}\hat{h}_0^{\,3}\exp\left(-3\int_0^{s}(f_0 t/\hat{h}_0)\, dt\right)ds\right].$$

III) Upstream of the obstacle.

From (3.6.12) we see that, as $X \to 0-$,

$$h \sim d\,(X^2/2) + X + d^{-1/7}\, E_0 + d^{-4/7}\, E_1 + \ldots \qquad (3.6.13)$$

and so we write, for $X < 0$,

$$h = d\, H_0 + H_1 + d^{-1/7}\, H_2 + d^{-4/7}\, H_3 + \ldots \quad .$$

Substitution of a solution of this form into equation (3.6.9) gives, on matching with (3.6.13),

$$H_0 = 1-f, \quad H_1 = X, \quad H_2 = E_0, \quad H_3 = E_1,$$

and as $X \to -\infty$ we find that

$$h \sim d + X + d^{-1/7}E_0 + d^{-4/7}E_1 + \ldots \quad .$$

We now consider the region in the vicinity of $X = -d$. Here h becomes O(1) once more and we expect a free interaction to occur here. To first order the position of this interaction is $X = -d$, as found earlier in the section for the case of an adjustment of the flow to that on a nearly horizontal slope. However in this case we have shown that the next term in the position of the interaction is $\tilde{e}_0(f_0 d)^{-1/7}$ and so depends on the curvature of the obstacle at its crest, with a sharper crest having a smaller effect on the upstream behaviour of the solution. If $X = -d - E_0/d^{1/7} - E_1/d^{4/7} + \zeta$ then in the vicinity of $\zeta = O(1)$, as $d \to \infty$, the flow is governed by the equation of the free interaction and this ensures that $h \to 1$ as $X \to -\infty$.

§3.6.6 The effects of surface tension on the free interaction.

We now consider the effect that surface tension has upon the compressive free interaction. As shown earlier the governing equation, including capillary effects, is

$$h_X - \gamma\, h_{XXX} = 1 - 1/h^3, \qquad h \to 1 \text{ as } X \to -\infty,$$

where γ (> 0) measures the relative importance of surface tension and $\gamma >> 1$ if surface tension dominates. The large X asymptote which we expect to emerge from the interaction is still $h \sim X$ since there we expect gravitational effects to dominate over capillary effects which typically have an influence over relatively short length scales.

First we note that the mechanism for upstream influence involves surface tension as well as hydrostatic effects however small the value of γ. An initally small exponential departure from $h = 1$ grows like $\exp(qX)$ where

$$\gamma q^3 - q + 3 = 0, \qquad (3.6.14)$$

and as $\gamma \to 0$ this gives

$$q \sim \gamma^{-1/2} + 3\gamma^{1/2}/2.$$

In contrast if $\gamma = 0$ then $q = 3$. So we see that the addition of a small amount, $O(\gamma)$, of surface tension effects leads to a singular perturbation problem giving rise to two possible length scales over which upstream influence can occur. First there is the O(1) scale associated with the viscosity-hydrostatic pressure interactiopn and second the shorter, $O(\gamma^{1/2})$, scale over which the inviscid hydrostatic and capillary effects interact to effect the upstream influence. This second type of interaction is the most rapidly growing and therefore the most likely to be seen in practice for small values of γ. As γ is increased these two modes of upstream influence coalesce as the positive real roots of (3.6.14) become closer. For larger γ the roots with positive real part become imaginary and the upstream influence wave-like. As $\gamma \to \infty$ we have

$$q = \pm i(3/\gamma)^{1/3},$$

and so the length scale of the interaction becomes long, $O(\gamma^{1/3})$. The mechanism is now a viscosity-capillary interaction.

We confine our attention to the limit of large γ and consider the structure of the whole of the free interaction. We first choose a length scale appropriate to this limit and write $X = \gamma^{1/3}z$, where $z = O(1)$ as $\gamma \to \infty$, to get

$$h_{zzz} - \gamma^{-1/3}h_z = 1/h^3 - 1,$$

$$h \to 1 \text{ as } z \to -\infty,$$

and study this equation in the limit $\gamma \to \infty$. Similar equations are discussed by Wilson and Jones (1983) (WJ) in the case of a vertical plate where hydrostatic effects are identically zero but there is a small parameter entering in the denominator of the curvature term in equation (3.6.2), which they retain. We follow much of their analysis. As a first step we consider the equation with $\gamma = \infty$. The solution in this case consists of a nonlinear

wave train of increasing amplitude. In regions where h is relatively large the equation becomes

$$h_{zzz} = -1, \tag{3.6.15}$$

with solution

$$h = 1/6\ (z_0-z)^3 + a(z_0-z)^2 + b(z_0-z), \tag{3.6.16}$$

for arbitrary values of a, b and z_0. Thus h will always return to a small value as z approaches z_0. In these regions of relatively small h the equation is dominated by the balance

$$h_{zzz} = 1/h^3. \tag{3.6.17}$$

This has solutions (WJ) in which

$$h \sim -z \text{ as } z \to -\infty, \tag{3.6.18a}$$

$$h \sim z^2 \text{ as } z \to +\infty, \tag{3.6.18b}$$

and so another region with large h is entered where the solution has the form (3.6.16) with the coefficients a and b found by matching to these regions of small depth. As explained in WJ, and below, it is possible to fit these regions together in such a way that the amplitude of these nonlinear leaps decreases as -z increases. Thus if $\gamma = \infty$ the solution is one of an infinite series of increasingly large leaps in the depth. We expect, however, that even for large γ the downstream form will be dominated by gravitational effects with the free surface horizontal and the depth increasing linearly. To effect the match between these two types of solution let us start at this downstream end and look for scales such that h is large and the hitherto neglected gravitational effects and the capillary effects balance. See Figure 3.6.7. This is possible if $h \sim O(\gamma^{1/2})$ and $z \sim O(\gamma^{1/6})$ as $\gamma \to \infty$. So, with $h = \hat{h}\gamma^{1/2}$ and $z = \hat{z}\gamma^{1/6}$ with $\hat{h}$ and $\hat{z}$ both O(1) as $\gamma \to \infty$,

we have

$$\hat{h}_{\hat{z}\hat{z}\hat{z}} - \hat{h}_{\hat{z}} = -1,$$

with solution

$$\hat{h} = \hat{z} + \hat{B} + \hat{C}e^{-\hat{z}}.$$

Therefore as $\hat{z} \to \infty$ gravitational effects dominate and the first order viscous-inviscid interaction is lost, whilst as $\hat{z} \to 0+$ we wish to match to a region of small depth and important capillary effects. The point $\hat{z} = 0$ is therefore the position of the last dip in the level of the free surface as we move downstream, after which point gravitational effects balance surface tension and the free surface flattens off. In order to match with the solution (3.6.18b) of the equation governing the flow in these thin regions (3.6.17) we must have $\hat{h} \sim O(\hat{z}^2)$ as $\hat{z} \to 0+$ and so $\hat{B} = -1$ and $\hat{C} = 1$, i.e.

$$\hat{h} = \hat{z} + e^{-\hat{z}} - 1.$$

As $\hat{z} \to 0+$ we find that $h \sim \gamma^{1/6}z^2/2$. We now search for a balance with h small over a short length scale so that surface tension is important. If $h = \beta_1 h_1$ and $z = \alpha_1 z_1$ where α_1 and β_1 are powers of γ to be found and h_1 and z_1 are O(1) as $\gamma \to \infty$, then we find the balance,

$$h_{1z_1z_1z_1} = 1/h_1^3,$$

emerges if $\beta_1^4 = \alpha_1^3$. However, in order to match as $z_1 \to \infty$, we also require $\beta_1/\alpha_1^2 = \gamma^{1/6}$ so $\beta_1 = \gamma^{-1/10}$ and $\alpha_1 = \gamma^{-2/15}$. We now consider the solution as $z_1 \to -\infty$. From WJ the asymptote here is

$$h_1 \sim (-z_1)\lambda,$$

where λ is found numerically to be $1.03\sqrt{2}$ (WJ) and so the depth increases once more as we move just upstream of $z = 0$ with $h \sim \gamma^{1/30}z$. We now search for scalings that will give us the balance appropriate for a large depth of

fluid and including surface tension (3.6.15). Again we write $h = \beta_a h_a$ and $z = \alpha_a z_a$ and find the balance

$$h_{aZ_a z_a z_a} = -1,$$

if $\beta_a = \alpha_a^3$. However to match with the solution about $z = 0$ we must have $\beta_a/\alpha_a = \gamma^{1/30}$. Hence $\beta_a = \gamma^{1/20}$ and $\alpha_a = \gamma^{1/60}$. Thus, in this region, the depth is relatively great for a long z-extent. The solution here is

$$h_a = 1/6\ (-z_a)^3 + a/2\ (-z_a)^2 + b\ (-z_a),$$

where a and b are to be found. Matching as $z_a \to 0-$ yields $b = \lambda$ and further upstream h_a must return to small values. Let h_a be zero at $z_a = z_a^* < 0$ as well as at $z_a = 0$, then if the zero is a double root the solution in the vicinity of $z_a = z_a^*$ is similar to that near $z_a = 0$ with the flow governed by equation (3.6.17) with a quadratic growth in the depth downstream and linear growth upstream. Since the root is a double root this fixes z_a^* and a in terms of b, and so

$$h_a = -z_a(z_a - z_a^*)^2/6, \qquad z_a^{*\,2} = 6b = 6\lambda.$$

The solution just downstream of this last but one dip in the depth of the layer is

$$h \sim |z_a^*|(z - z_0)^2\gamma^{1/60}/6 \quad \text{as } X \to X_0+, \qquad (z_0 = z_a^*\gamma^{1/60}).$$

It is now easy to see how this structure consisting of a pair of regions, one where h is relatively small and a second where h is large can be repeated indefinitely upstream as $X \to -\infty$. However the size and extent of the leaps decreases as we follow the solution further upstream. For example if the narrow region about $z = z_0$ is of z-extent $O(\alpha_2)$ and the depth there is $O(\beta_2)$ then we have, just as before, $\beta_2^4 = \alpha_2^3$ and $\beta_2/\alpha_2^2 = \gamma^{1/60}$ and therefore $\beta_2 = \gamma^{-1/10.1/10}$ and $\alpha_2 = \gamma^{-1/10.2/15}$. Indeed it can be shown that in the nth trough (moving upstream) the

depth of the liquid layer is $O(\gamma^{-(1/10)^n.1/10})$ whilst under the nth crest the depth is $O(\gamma^{(1/10)^n.1/20})$. Thus the decay in the size of the jumps is very rapid and, although asymptotically an infinite number of waves are needed to reduce the depth to O(1) as required upstream, in practice only a few waves will be seen.

In summary we see that the interaction for large values of γ has the form illustrated in Figure 3.6.6. There are a few nonlinear waves upstream dominated by surface tension, whilst the decay towards the downstream asymptote, $h \sim X$, in which the interaction is lost and gravitational effects dominate, is from below, causing there to be a final dip in the position of the free surface before it becomes horizontal.

§3.6.7 Implications for the forced interaction on larger gradients.

We now turn to the possibility of speculation on the flow field for large obstacles of the type discussed above but on slopes steeper than those required for lubrication theory to be appropriate, although still small in the sense that $\alpha Re = O(1)$ as $Re \to \infty$. The gradients generated by the addition of the obstacle to this basic slope must also be $O(Re^{-1})$. Since the obstacle is high the upstream influence is of large extent and a free interaction occurs far upstream. From the numerical solutions of the free interactions on these slopes in §3.2 we know that a downstream form of this interaction is a flow with a horizontal surface which develops over a scale which is at least O(Re) in length but which can be reduced to $O(Re\alpha^{-3})$ for the larger slopes. We would therefore expect that the horizontal surface would develop upstream of the obstacle just as in the case of small slopes. On the lee of the obstacle, where the slope is large and negative, a possible solution is one similar to that shown above to be appropriate to small slopes. This has the depth essentially determined by the local slope and a half-Poiseuille velocity profile. Beneath the horizontal

surface on the upstream side of the obstacle there would not be separated flow unless the slope is greater than 4.712 (see §3.3.2). If the slope is larger still the flow here will take the form of a jet just below the free surface with a slower moving reversed flow region beneath. Together with this basic structure we must consider the effect of the result (Smith 1988) that reversed flow within an interacting boundary layer is subject to a singularity. This, or an appropriate adjustment of this theory to the long length scale acting here, implies that the interacting boundary layer equations are not necessarily sufficient to describe the process of separation and reattachment upstream of an obstacle which is larger than some finite limit. The effect of this in this context is unclear but it could indicate that several separation bubbles occur upstream of the obstacle.

The final question to address is whether the free surface can ever rise. We know, from the numerical solutions above and from a consideration of (3.6.5), that in the limit of small slopes it cannot, but the numerical solutions of §3.2 indicate that for the larger slopes the approach of the free surface to the horizontal is from below and we know that in the limit of large slope the interaction has a form similar to that on a horizontal surface at large Froude number, with the free surface initially moving upwards before the effect of the slope is felt and it flattens off. The dividing line seems to be in the regime where the downstream asymptote is still a Jeffrey-Hamel flow and is given by the condition $P = 0$ in equation (3.3.1). This implies that the slope is $\alpha = 1.814$, which is less than the slope required for separation to occur. Thus it seems that for slopes smaller than this the free surface gradient is likely to remain negative, but larger slopes will, in contrast, give rise to a region of positive gradient in the vicinity of the free interaction. This, of course, is similar to the form of a hydraulic jump. If the slope becomes larger than $O(Re^{-1})$, however, then this jump shape may be lost, as explained in §3.5.3.

§3.7 The Numerical Solution of Forced Interaction Problems On Steeper Slopes.

§3.7.1 An introduction to the solution of interactive boundary layer problems.

Section 3.6 considers the flow of a liquid layer over an obstacle on a very shallow slope. This simplifying feature allows an easy numerical solution and, in simple geometries, an explicit solution for the depth. The main constraint in flows of this type seems to be the inability for the position of the free surface to rise and this subsequently dictates the qualitative nature of the flow field. This feature was also conjectured to be likely on larger slopes. Exceptions stem from the form of the free interactions studied in §§3.2&5 and the fact that the approach of the surface to the downstream asymptote (i.e. the horizontal) is from below in some of the solutions. This leads to an increase in the surface height in the vicinity of the free interaction which is far upstream in the case of large obstacle, where a free interaction can be expected to make up a distinct part of the flow field. Separation from the solid surface is also possible on these larger slopes. This section considers the numerical solution of forced interactions on slopes where the inertia of the fluid is an important feature and must be included in the solution. This turns out to be quite a difficult problem and although several methods were tried only one proved successful and the results presented here are those found using this so-called lubrication method (Smith (1986c)). We do however describe all three methods used, the other two being variations of Carter's (1979) method and of Davis' (1984) method. Despite the success of the first method it still proved impossible to find solutions in cases where the slope was sufficiently steep and the obstacle sufficiently large to provoke separation obviously of the breakaway type discussed in §3.4, although features similar to those which could be expected in this case are observed. Flows with separation of the less severe type which occurs on smaller slopes are found

successfully, however.

Two types of problem are addressed, corresponding to the two types of geometry studied in §3.6. The first consists of a slope connected smoothly and over a relatively short distance to a shallower slope downstream thus causing the liquid layer to thicken. The second is of an obstacle, with a height proportional to $\exp(-bx^2)$, mounted on a slope.

There are many examples in the literature of computations of forced interactions in the case where the interactive equations are based on the triple deck formulation. In these cases the equations reduce to the steady boundary layer equations in the domain $(x,y) \in ((-\infty,\infty)x(-\infty,\infty))$, with $U \sim y + A(x)$ as $y \to \infty$, and with a pressure displacement (P-A) law linking A and the pressure driving the boundary layer. For example Smith and Merkin (1982) give solutions for subsonic flow past corners and wedged trailing edges and also mention many techniques for improving the accuracy and the ease of calculation of the solutions. Brotherton-Ratcliffe (1986) presents solutions with the hypersonic P-A law, $P = -A$, shown to be of relevance to liquid layer flows. See also Carter (1979), Davis (1984) and Veldman (1983). Three-dimensional problems can also be solved, see Edwards and Carter (1985). The particular problem of interest here differs from these in that the range in y is finite due to the finite depth of the layer and in the fact that viscosity is important throughout the depth of the fluid. This difference could be the cause of the failure of the schemes used successfully by the authors above. The equations to be solved here are, from §3.2,

$$UU_x - \frac{\hat{\psi}_x U_\xi}{1+E} = -p_x + \frac{U_{\xi\xi}}{(1+E)^2}, \qquad (3.7.1a)$$

$$U = \frac{\hat{\psi}_\xi}{1+E}, \qquad (3.7.1b)$$

$$\hat{\psi} = U = 0 \text{ at } \xi = 0, \qquad U_\xi = 0, \ \hat{\psi} = 1 \text{ at } \xi = 1, \quad (3.7.1c\text{-}f)$$

$$\xi = (y - f)/(1 + E), \quad (3.7.1g)$$

$$p = s\eta, \quad (3.7.1h)$$

where $E = \eta + \alpha x - f$ and $f = d\exp(-bx^2)$ in the case of an obstacle on a slope. The inverse Froude number is s, and since there is half-Poiseuille flow far upstream $s\alpha = 3$. The boundary conditions are $E \to 0$ as $x \to \pm\infty$. See Figure 3.1.2. We know that upstream influence is possible in these equations and first starts as an initially exponentially small departure from half-Poiseuille flow upstream of the obstacle. We can find the form of an initial perturbation to equations (3.7.1) in a fashion similar to that used in §3.5.1. The results are

$$\hat{\psi} \sim \psi_P + 3c(\hat{g} + \xi U_P/3), \quad (3.7.2a)$$

$$U \sim U_P + 3c(\hat{g}' + \xi U_P'/3), \quad (3.7.2b)$$

$$\eta - \alpha x = c << 1. \quad (3.7.2c)$$

Here the subscript P refers to the basic Poiseuille flow and $\hat{g}$ satisfies equation (3.5.4) for a given slope α. Also $'$ indicates differentiation with respect to ξ and c is an unknown constant which determines the size of the perturbation and depends on the downstream conditions.

Davis' and Carter's methods were chosen in an initial approach to the problem due to their successful use by Brotherton-Ratcliffe in dealing with the interactive boundary layer equations and the hypersonic P-A law which we know governs the solution of (3.7.1) on relatively short scales. He finds that Davis' scheme works if there is no significant separation present and Carter's can be used to take the solution further into the separated regime. Reversed flow in the boundary layer is simply dealt with using the Flare approximation (Reyner & Flügge-Lotz (1968)). Both of these schemes rely on introducing an artificial time dependence into the P-A

law. In our context we write $p = s\eta$, or equivalently $p_x = s\eta_x$, as

$$s\eta_t = -p_x + s\eta_x. \qquad (3.7.3)$$

This unsteady relation is used in the hope that as $\partial t \to 0$ convergence to the steady solution is achieved. The adjustment towards this solution is via the waves admitted by the unsteadiness. Other methods of introducing time will lead to waves with different dispersion relations and stability characteristics. These features determine the efficiency or suitability of the particular method. For a successful scheme waves must travel upstream, providing for upstream influence, as well as downstream, and these waves must decay in time and space. In the case of the triple deck equations the dispersion relation for linear waves can be derived to check these properties. However in the case of equation (3.7.1) this is a more difficult task and the form used, (3.7.3), is chosen because of its similarity to that used by Brotherton-Ratcliffe in the hope that the dispersion relations are similar (a fact which we know will be true for short waves where the interaction is governed by the triple deck structure).

Davis' method is iterative and we start from an initial guess for the position of the free surface, $\eta^1(x)$ - the initial value in terms of t. Equations (3.7.1a-g and 3.7.3) are then integrated forward, from $x = -\infty$, using a scheme similar to that used for the free interaction problems studied in §2.4 and §3.2. The initial conditions on ψ and U are given by (3.7.2) and the value of c appropriate to η^n, the displacement as $x \to \infty$, from the previous timestep. The P-A law is written in finite difference form as

$$-s/\Delta t\{\ (\hat{\eta}_{i+1} + \hat{\eta}_i) - (\eta^n_{i+1} + \eta^n_i)\ \} =$$

$$(1/\Delta x)(\hat{p}_{i+1} - \hat{p}_i) - (s/\Delta x)(\eta^n_{i+1} - \eta^n_i).$$

Here η^n_i is the position of the free surface at x-station i

from the previous timestep and we solve for $\hat{\eta}(x)$ and $\hat{p}(x)$, the values at time $t+\Delta t/2$. With this form of discretisation there is a balance between $\hat{p}_{i+1}$ and $-\hat{\eta}_{i+1}$ on this forward sweep. As a result the possibility of upstream influence is suppressed, the equations are rendered truly parabolic and hence the marching scheme is stable. The nonlinearity in the equations is dealt with using Newton iteration but only a single iteration cycle is completed at each x-station since this saves on computation time and the accuracy increases to second order (as would be achieved by completing the iteration) as the method converges (Smith and Merkin).

On the reverse sweep the P-A law is written as

$$(-s/\Delta t)\{ (\eta_{i+1}^{n+1} + \eta_i^{n+1}) - (\hat{\eta}_{i+1} + \hat{\eta}_i) \} =$$

$$(1/\Delta x)(\hat{p}_{i+1} - \hat{p}_i) - (s/\Delta x)(\eta_{i+1}^{n+1} - \eta_i^{n+1}).$$

This, given the downstream boundary condition and $\hat{p}$ and $\hat{\eta}$ which are known from the forward sweep, can be integrated upstream to give $\eta^{n+1}(x)$, the free surface at the next timestep and the basis for the next forward sweep.

Carter's method differs from Davis' method in that on the forward sweep the pressure and displacement are not allowed to interact. Instead the value of $\hat{\eta}_i$ is fixed at η_i^n and the equations (3.7.1a-g) are solved for the pressure alone. The reverse sweep is identical however. Carter's method is generally slower to converge than Davis' because of the suppression of the interaction in the forward sweep.

§3.7.2 A numerical scheme based on lubrication theory.

As mentioned earlier, neither of these methods proves successful in obtaining solutions for any but the most shallow of slopes and obstacles. As an alternative, a scheme based on the successful combination of Carter's method and lubrication theory in the limit of small slope (§3.6.4) and a suggestion by Smith (1986c) is developed. The method is basically that used in §3.6.4 but includes

the inertial terms by lagging them at the previous timestep. Thus we write equation (3.7.1a) as

$$R^n = -p_x^{n+1} + U_{\xi\xi}^{n+1}(1+E^{n+1})^{-2},$$

where

$$R^n = U^n U_x^n - \psi_x^n U_\xi^n (1+E^{n+1})^{-1}.$$

Just as in the case of lubrication theory we can integrate this in ξ to give

$$p_x^{n+1} = 3(I_3(1) - I_1(1)/2 - 1/(1+E^{n+1})^3), \qquad (3.7.4a)$$

$$U_\xi^{n+1} = (1+E^{n+1})^2\{ p_x^{n+1}(\xi-1) + I_1(\xi) - I_1(1) \}, \qquad (3.7.4b)$$

$$U^{n+1} = (1+E^{n+1})^2\{ p_x^{n+1}(\xi^2/2-\xi) + I_2(\xi) - I_1(1)\xi \}, \qquad (3.7.4c)$$

$$\psi^{n+1} = (1+E^{n+1})^3\{ p_x^{n+1}(\xi^3/6-\xi^2/2) + I_3(\xi) - I_1(1)\xi^2/2 \}, \qquad (3.7.4d)$$

$$I_1(\xi) = \int_0^\xi R^n(\xi_1)d\xi_1, \qquad (3.7.4e)$$

$$I_2(\xi) = \int_0^\xi\int_0^{\xi_2} R^n(\xi_1)d\xi_1 d\xi_2, \qquad (3.7.4f)$$

$$I_3(\xi) = \int_0^\xi\int_0^{\xi_3}\int_0^{\xi_2} R^n(\xi_1)d\xi_1 d\xi_2 d\xi_3. \qquad (3.7.4g)$$

If we replace E^{n+1} by E^n we fix the displacement on the forward sweep to be that calculated at the previous time level and so do not need to use a P-A law on the forward sweep. The method used is then effectively that of Carter. That is to say, given the displacement we use equation (3.7.4a-g) to calculate p_x^{n+1} by marching forward from $x = -\infty$. The value of c at $-\infty$ in equations (3.7.2) is calculated from E_1^n and allows $U_{\xi\,1}^{n+1}$, U_1^{n+1} and ψ_1^{n+1} to be found. This initiates the x-sweep. To evaluate R at a particular x-station we write it as

$$U_i^{n+1}(\xi)\{\ U_{i+1}^{n+1}(\xi)-U_{i-1}^{n}(\xi)\ \}/(2\Delta x)\ -$$

$$U_{i\xi}^{n+1}(\xi)\{\ \psi_{i+1}^{n+1}(\xi)-\psi_{i-1}^{n}(\xi)\ \}/(2\Delta x(1+E_i^n)),$$

i.e. we use values calculated at previous sweeps for the x-stations at i and i+1 but use values already calculated on the present sweep for the station at i-1. This differencing means the method is second order accurate in Δx and, if the integrations in equations (3.7.4) are done using the trapezium rule, the scheme is also second order accurate in $\Delta\xi$. Once p_x is calculated it can be integrated to give p and the position of the free surface is simply p/s. To try to speed up the convergence, and also to affect the stability of the method, R^n is updated to R^{n+1} using relaxation so that

$$R_i^{n+1} = \omega(UU_x - \psi_x U_\xi(1+E)^{-1})\Big|_i^{n+1} + (1-\omega)R_i^n,$$

where ω is a chosen relaxation parameter.

The upstream sweeps to update E^n given P^{n+1} are performed just as in Carter's method above, and the whole process is then repeated. Convergence is tested using the error norm

$$\max_i|\ p_i - s\eta_i\ |, \qquad (3.7.5)$$

and is said to be achieved when this is less than some small value typically 10^{-1} or 10^{-2}. In the solutions presented this represents an error of about 1% or 0.1%. This is not particularly small but is necessitated by the slow convergence of the method.

The technique described above has two advantages. Firstly, reversed flow is dealt with automatically as convergence is obtained and secondly it reduces the amount of differentiation used, replacing it with integration, thus increasing the accuracy and the stability of the method.

§3.7.3 Results and Discussion.

Although more successful than either Carter's or Davis' methods, the above technique is still very slow to converge and this limits the geometries which can be studied. For example Figure 3.7.2(d) uses a timestep of 10^{-3}, a relaxation parameter of 10^{-1} and has $\Delta x = 0.038$ and it requires just over 10000 time steps. These sweeps are quick compared with the calculation involved in other methods, allowing many more sweeps to be used but still a great deal of computation time is required. The solutions presented here are similar to those obtained when slightly finer or coarser grids are used, although grid size checks are hampered by the fact that a smaller Δx requires a smaller Δt in order that the backward sweep remains stable, and so the convergence is much slower. Generally 21 points were used in the ξ integrations, giving a $\Delta\xi$ of 0.0476.

Figures 3.7.1(a&b) show solutions illustrating the flow adjustment over a change in slope, i.e. $f = (\alpha_u - \alpha_d)x\tanh x$ for $x > 0$, where α_u and α_d are the upstream and downstream slopes respectively. In both cases the upstream slope is 5 and the downstream slopes are 3 and 1 respectively. It can be seen that in the second, more extreme, geometry the adjustment is rapid and separation occurs. The extent of the upstream influence is very short in both cases since, from §3.5.2, the growth rate of the exponential departure, $\exp(qx)$, is large ($q = 358$ when α is 5). Also evident is an increase in the height of the free surface over a very short distance. The profile here is reminiscent of a hydraulic jump and indicates that perhaps, as suggested by the large value of q, the adjustment has a structure similar to that of the hypersonic free interaction. The separation and upstream influence occur on a short scale, $O(Re\alpha^{-3})$, but reattachment and a return to half-Poiseuille flow occurs over a much longer scale, O(Re). Gajjar (1983) studies interactions in fully developed flow but on a shorter length scale $O(Re^{1/7})$ and suggests that a return to Poiseuille flow occurs over a much longer scale.

We now turn to some examples of flow over obstacles, as shown in Figures 3.7.2 where the obstacle is $f = d\exp(-x^2/9)$. Here we have shown solutions with slope 5 and the height, d, of the obstacle increasing from 16 to 20. In these solutions Δx is .044, although the two solutions shown for the height of 18 are for $\Delta x = 0.038$ and 0.068 and illustrate the independence of the solution to grid alterations. A characteristic of the solutions for the larger obstacles is the slight kink just before separation occurs. This is similar to the wobbles in the solutions shown in Figures 3.7.1. This kink persists as the convergence error under the norm (3.7.5) is varied but alters form as Δx is changed. We therefore believe that it is a numerical feature due to the grid being too coarse in a region of very rapid change. The case $d = 20$ clearly shows a hydraulic jump, associated with flow separation, quite far upstream of the obstacle.

The solutions are indeed of the general form predicted in §3.6.7, with the free surface tending to become horizontal upstream of the obstacle. The lengthscale of the upstream influence grows as the obstacle height is increased although the scale of the more active adjustment, i.e. the hydraulic jump itself, is very short due to the steep slope. On the lee of the obstacle the flow seems to be close to half-Poiseuille with a depth and skin friction determined locally by the slope there. There are therefore two scales for the adjustment, one rapid - the jump itself - and one long over which the flow reattaches and negotiates the obstacle and eventually returns to being half-Poiseuille.

§3.8 SUMMARY.

Below we list the main results of this chapter.

1) Half-Poiseuille flow is not a unique solution for a liquid layer flow down a slope. Branching solutions caused by a viscous-inviscid interaction render the solution non-unique and allow upstream influence.

2) The form of the interaction alters as the slope increases. For small slopes it is slow to develop and is governed by lubrication theory. As the slope increases, inertial effects become important. For larger slopes the interaction takes place on a short length scale.

3) The downstream asymptote for the compressive free interaction has a horizontal free surface, and the viscous-inviscid interaction is a weak effect here. The flow is governed by the Jeffrey-Hamel equations for the smaller slopes. Separation does not necessarily occur. For larger slopes breakaway separation occurs over a short distance and the vorticity of the original half-Poiseuille flow develops into a jet at the free surface.

4) The steady hydraulic jump takes different forms as the slope varies. On slopes small on an $O(Re^{-1})$ scale the height of the free surface cannot increase. For larger slopes a jump is possible, leading to an increase in the free surface height. For slopes steep on the $O(Re^{-1})$ scale this jump has the same blunt shape as is seen in jumps on a flat plate. On slopes steeper than $O(Re^{-1})$, for flows with little surface tension, this blunt shape can be lost. Surface tension can have the effect of reinstating the blunt shape, as well as causing capillary waves upstream of the jump.

5) In the limit of vanishing slope the flow is governed by lubrication theory. Again, viscous-inviscid interaction is possible and analytic solutions to some forced interaction problems are given.

6) Some numerical solutions for forced interaction problems of flow over an obstacle on a steeper slope are calculated. For large obstacles a hydraulic jump and separation are seen upstream of the obstacle. This jump occurs over a very short length scale.

FIGURE CAPTIONS FOR CHAPTER THREE.

Figure 3.1.1 Typical problems involving upstream influence in fully developed liquid layer flow on a slope.

(i) How does the flow adjust on approaching a decrease in gradient ?

(ii) What is the form of a hydraulic jump and separation upstream of a decrease in slope.

(iii) How does the flow adjust on approaching an increase in slope ?

(iv) & (v) In flow over a large obstacle, does an obvious "jump" in the level of the free surface occur and how does the layer return to half-Poiseuille flow downstream ?

(vi) The viscous flow over a less severe obstacle.

Figure 3.1.2 A sketch defining the variables used in §3.1-§3.4 and §3.7, illustrating the horizontal and the vertical (after a Prandtl shift) coordinates (x, y), the definition of η, the height of the free surface above its height at $x = 0$, and the function f describing an obstacle on an otherwise uniform slope.

Figure 3.2.1 A numerical solution of (3.1.1) with half-Poiseuille flow at $x = 0$. The slope, α, is 0.25 whilst s takes values of 2, 3, 5, 10, 12, 20, 50. The cases such that $s\alpha < 3$ have a solution which ends in a singularity. If $s\alpha > 3$ the solution continues with the pressure approaching a constant value from above. If $s\alpha = 3$ the pressure gradient is approximately constant at -3. Figure (a) illustrates the pressure and Figure (b) the skin friction of the solutions. In these integrations $\Delta\xi = 10^{-2}$ and $\Delta x = 10^{-2}$.

Figure 3.2.2 Solutions of (3.1.1) for larger values of α than those illustrated in Figure 3.2.1. Here $\alpha = 4$ and 6 and s is fixed at 10. Figure (a) shows the pressure, which asymptotes a constant value from

below. Figures (b) and (c) show the development of the skin friction and the velocity profiles at $x = 5$. Separation occurs for $\alpha = 6$ but not for $\alpha = 4$. $\Delta\xi = 10^{-2}$, $\Delta x = 0.05$.

Figure 3.3.1 Velocity profiles predicted by Jeffrey-Hamel flow for the large x asymptotes of equation (3.1.1). The last figure is the profile which is assumed to develop if $\alpha > 5.461$, in which case the Jeffrey-Hamel flows are no longer appropriate to describe the asymptote.

Figure 3.3.2 Numerical solutions of (3.3.1) for $\alpha = 4.712$, the value at which, according to Jeffrey-Hamel theory, separation just occurs. The inverse Froude number, s, is 10. There are two curves in each figure, one with $\Delta x = 0.05$ and one with $\Delta x = 0.01$. They are almost indistinguishable. Figure (a) shows the pressure, (b) the skin friction and (c) the velocity profile at $x = 10$.

Figure 3.4.1 A sketch defining the asymptotic structure, for large x, that is appropriate to breakaway separation. Region (I) contains the jet. Region (II) has slow irrotational backflow and region (III) is the boundary layer at the wall associated with this backflow.

Figure 3.4.2 A solution of (3.1.1) for $\alpha = 60$, s = 10, $\Delta x = 0.00035$. Figures (a) and (b) show the development of the pressure and of the skin friction respectively. Figures (c) and (d) show the velocity and stream function profiles at numerous values of x throughout the development of the solution. It is possible to see the emergence of the similarity structure described in §3.4 and illustrated in Figure 3.4.1.

Figure 3.5.1 The solution of (3.5.4) for the eigenvalue, $\hat{q}$, governing the spatial growth rate of upstream influence in liquid layers on a slope of $Re^{-1}\hat{t}_\alpha$. Figure (a) shows smaller slopes and Figure (b) larger ones. Also shown are asymptotic solutions of the equation for small and large $\hat{t}_\alpha$.

Figure 3.6.1 A sketch of a travelling bore (speed W) on a shallow slope. The depth alters from unity upstream to D < 1 downstream. The figure shows the motion in both the laboratory frame and the frame of the bore.

Figure 3.6.2 (a) A sketch of a weak bore on a shallow slope ($D \approx 1$).

(b) A relatively strong bore on a shallow slope ($D = \hat{\epsilon} << 1$).

Figure 3.6.3 A numerical solution of (3.6.5) for liquid layer flow on a shallow slope encountering a decrease in the gradient. This problem is solved analytically in §3.6.

Figure 3.6.4 Numerical solutions, using the scheme described in §3.6.4, of equation (3.6.5), governing the flow over an obstacle on a shallow slope. The obstacles are of the form $dexp(-(X/b)^2)$. In Figure (a) d = 1 and b = 1/4. In (b) d = 3, b = 1 and in (c) d = 11, b = 2. The position of the free interaction can be seen to move upstream as the severity of the obstacle increases. Figure (d) shows the flow over an obstacle with d = -7, b = 3 and shows both a compressive and an expansive interaction.

Figure 3.6.5 The asymptotic structure of the solution for the depth, h, of liquid layer flow over a tall ($O(d) >> 1$) obstacle of O(1) width.

Figure 3.6.6 The asymptotic structure of the free interaction governed by equation (3.6.3f) in the limit of a relatively large surface tension coefficient ($\gamma >> 1$). A nonlinear wave train is followed by an approach of the free surface towards a horizontal asymptote.

Figure 3.7.1 The solution of equation (3.1.1) governing the flow on a slope, $\alpha = 5$, on encountering a decrease in slope to $\alpha = 3$ (Figure (a)) and $\alpha = 1$ (in Figure (b)). The change in slope is gradual and the solution uses the lubrication scheme described in §3.7.2. Figure (b) clearly shows a hydraulic jump, separation and reattachment of the flow (illustrated by the crosses). The extent of the upstream influence is short due to the relatively large upstream slope. In both solutions $\Delta t = 10^{-4}$, $\Delta x = 0.44$, $\Delta\xi = 0.0476$ and the relaxation parameter, ω, is 0.1.

Figure 3.7.2 The numerical solution of (3.1.1) for flow over humps, $f(x) = d\exp(-(x/3)^2)$ on an otherwise uniform slope, $\alpha = 5$. The Figures show both the position of the free surface and the skin friction as the flow encounters the obstacle and then returns to half-Poiseuille flow downstream. In Figures (a) and (b) d is 16 and 17 respectively. Figures (c) and (d) have d = 18 and show solutions with $\Delta x = 0.068$ and 0.038 respectively indicating, to some extent, the grid-independence of these solutions. The case d = 18 is also the stage at which the obstacle gives rise to a reasonable extent of near horizontal wall. Lastly, Figure (e) has d = 20 and clearly has a hydraulic jump and separation upstream of the obstacle. The positions of separation and reattachment are indicated by crosses. In all these calculations $\Delta t = 10^{-3}$, except the last, which has $\Delta t = 10^{-4}$. The relaxation parameter, ω, is 0.1 and $\Delta\xi = 0.0476$. Except in cases (c) and (d), $\Delta x = 0.044$.

Figure 3.1.1.

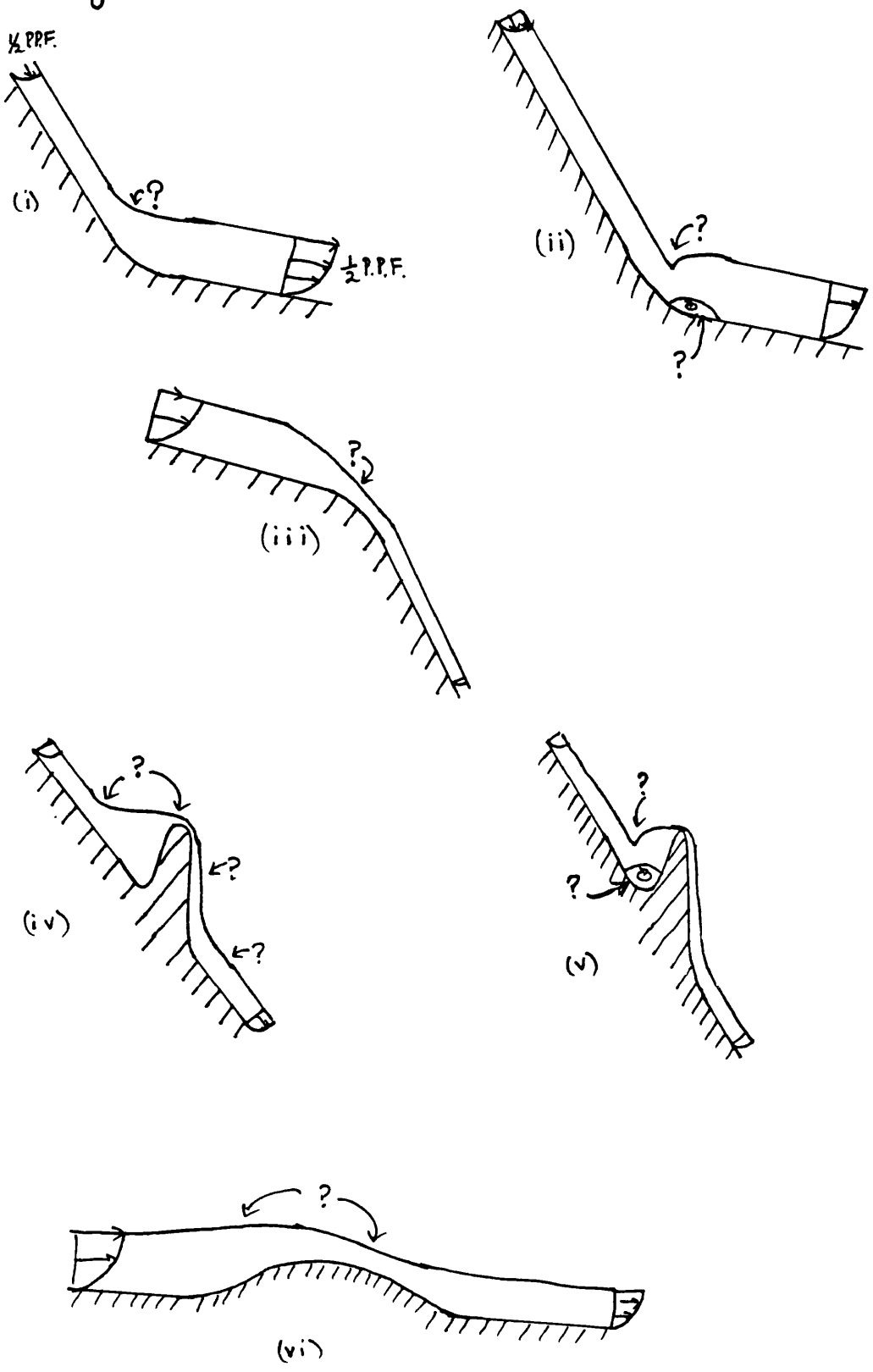

Figure 3.1.2

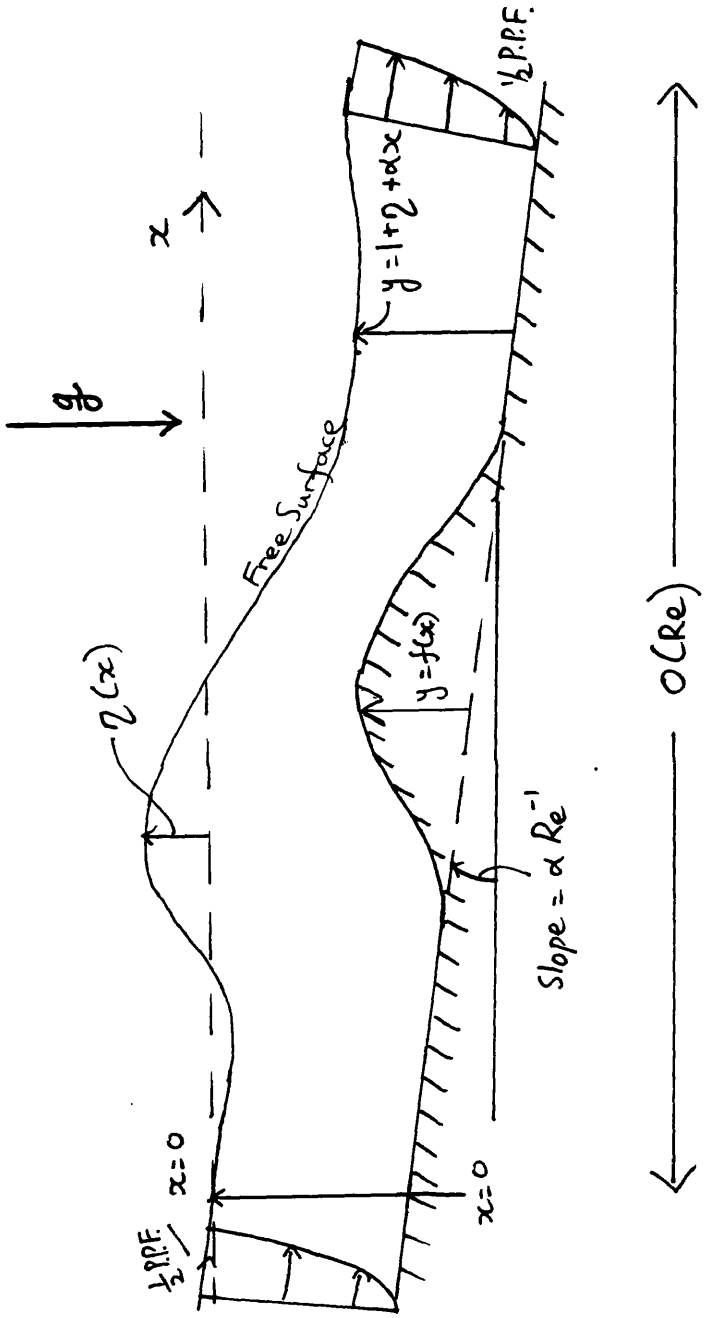

Figure 3.2.1

(a)

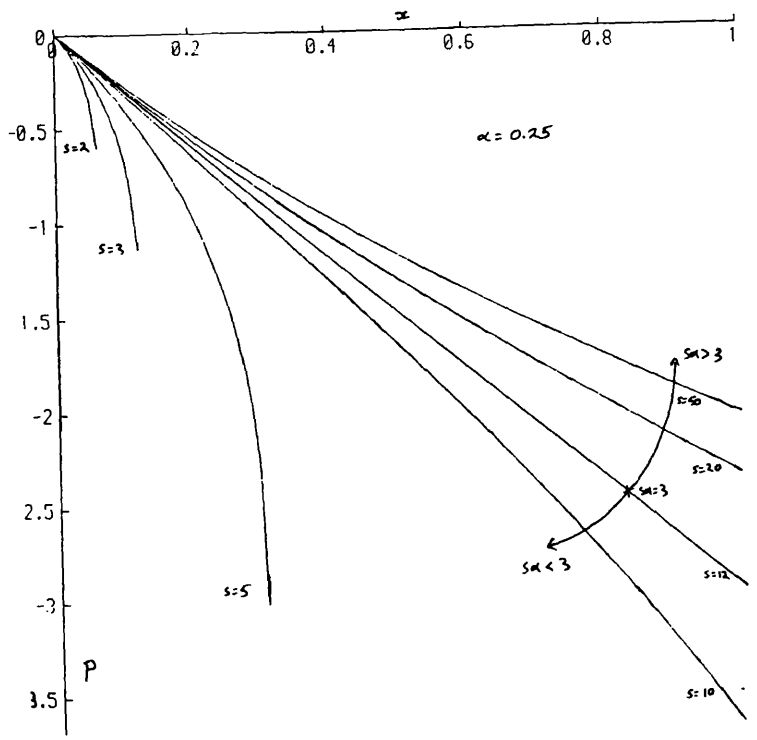

(b)

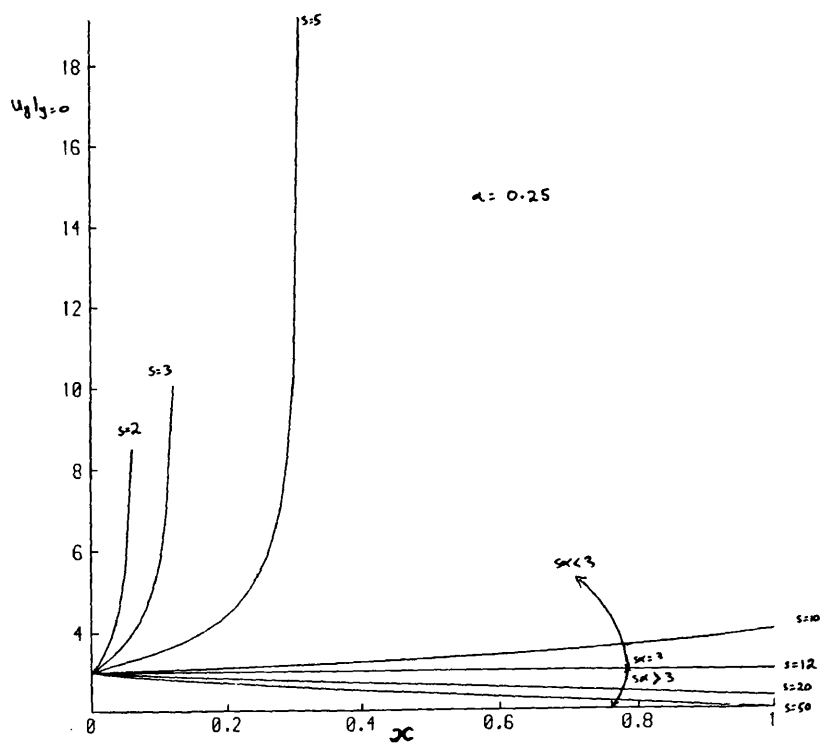

Figure 3.2.2

(a)

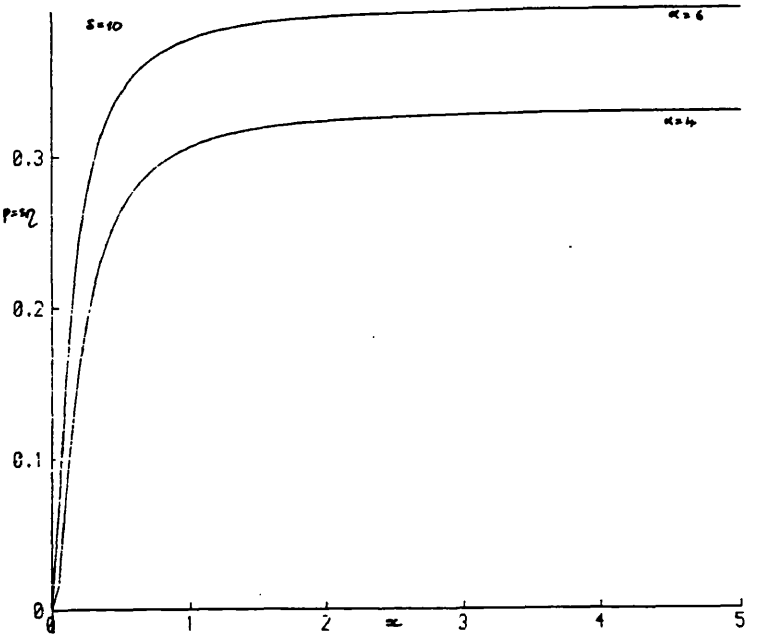

(b)

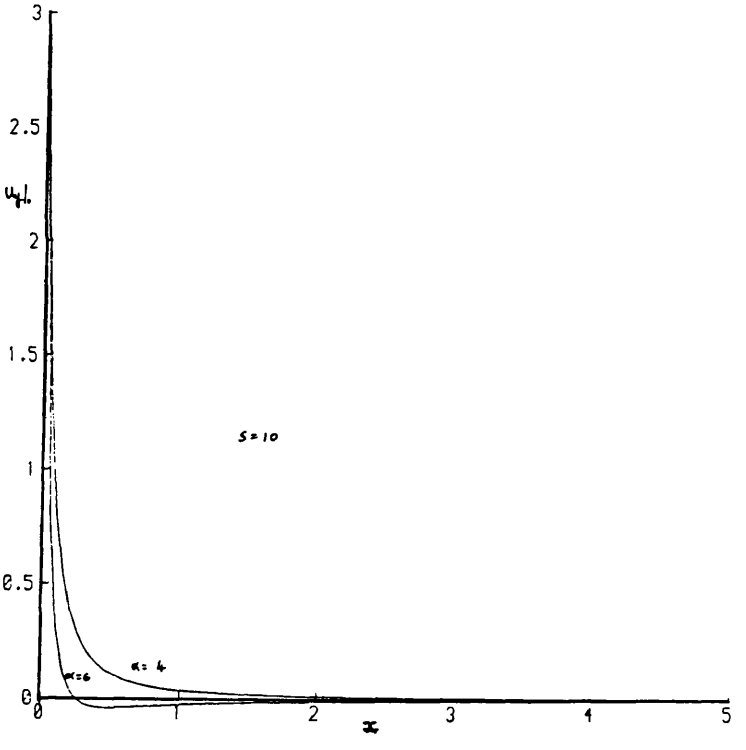

(c)

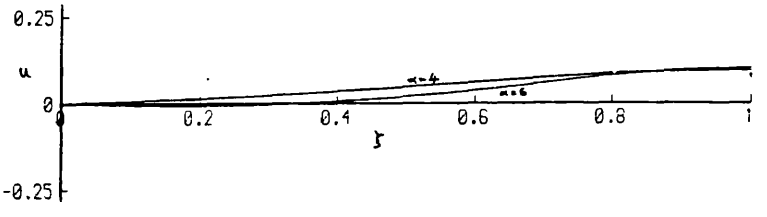

Figure 3.3.1.

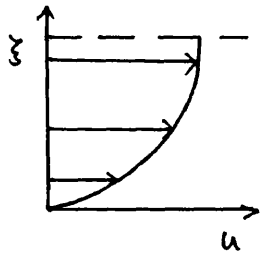

$\alpha \ll 1$: Half Poiseuille Flow

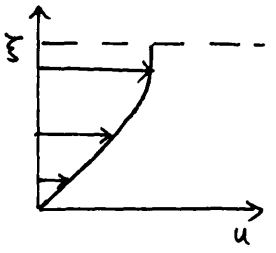

$\alpha < 2.988$: No point of inflexion

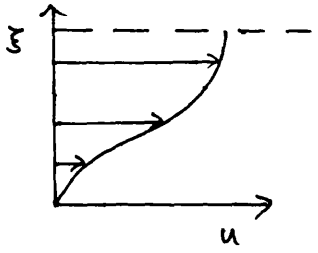

$2.988 < \alpha < 4.712$: One point of inflexion

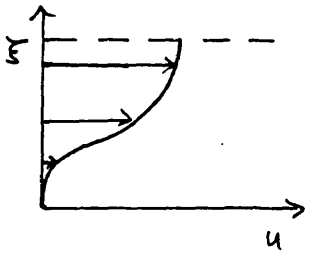

$\alpha = 4.712$: Just Separating

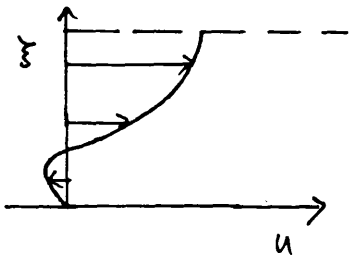

$4.712 < \alpha < 5.461$: Separated flow

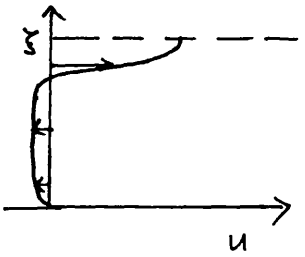

$\alpha > 5.461$: Breakaway Separation

Figure 3.3.2.

(a)

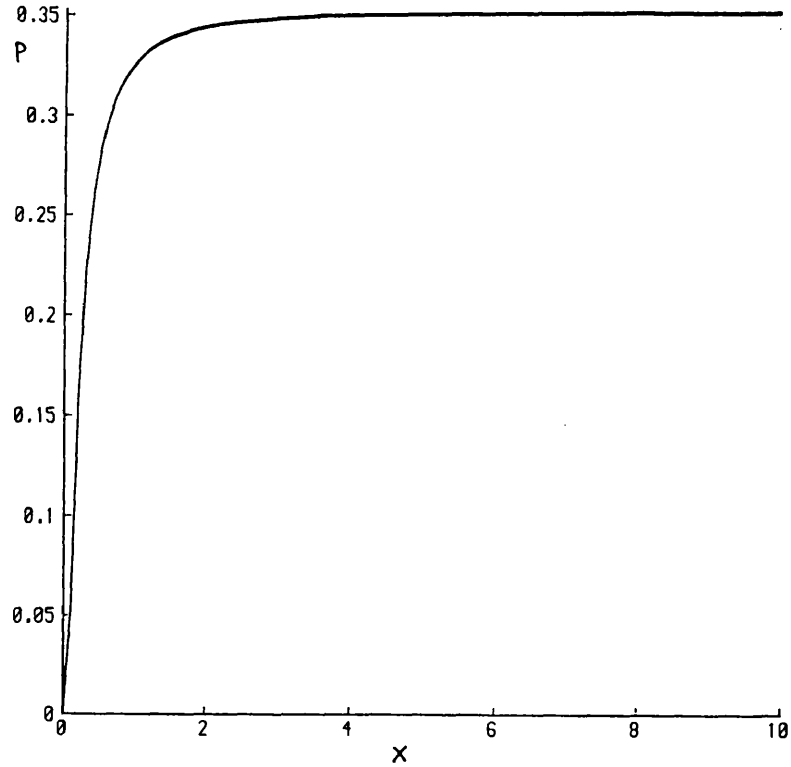

(b)

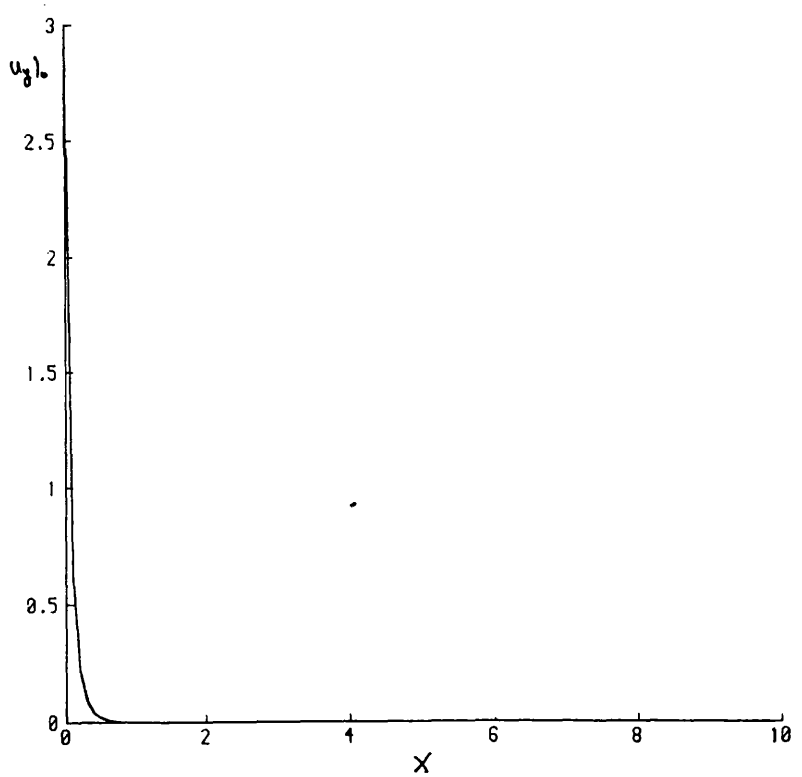

(c)

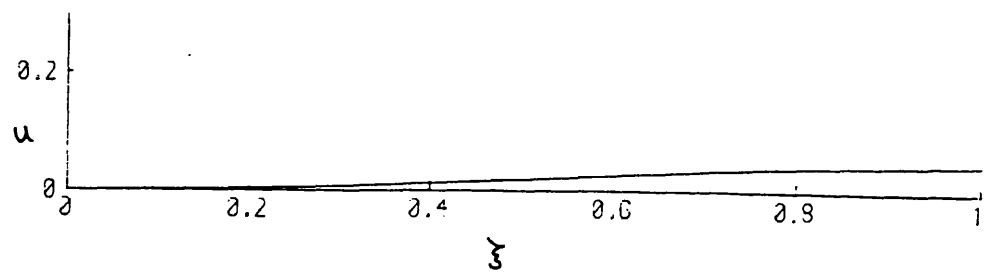

Figure 3.4.1

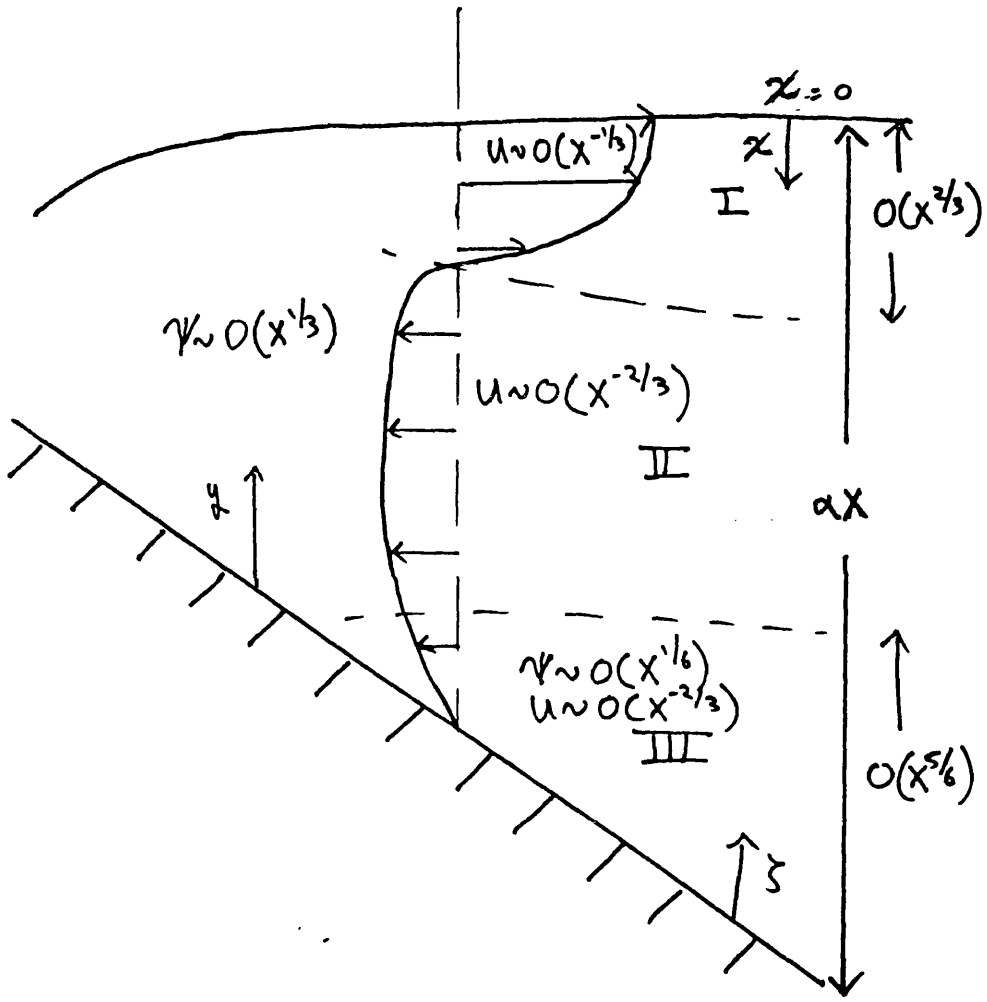

Figure 3.4.2

(a)

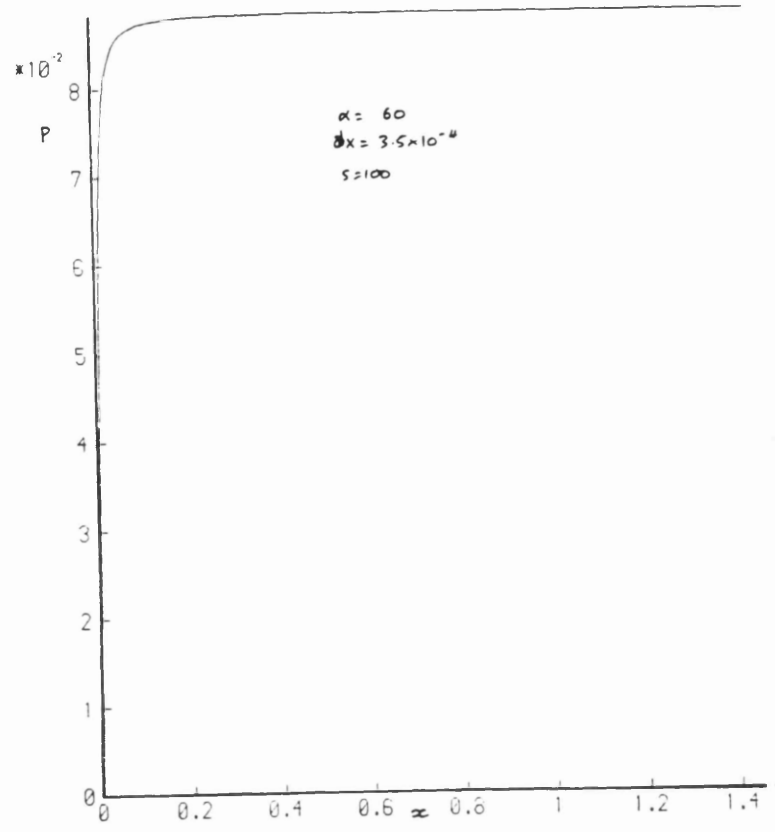

(b)

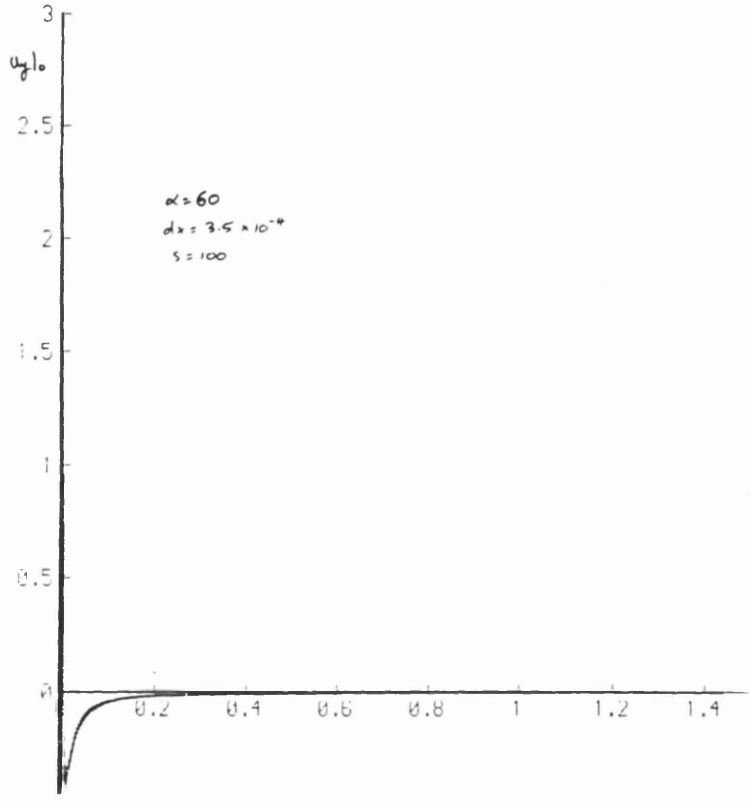

Figure 5.4.2

(c)

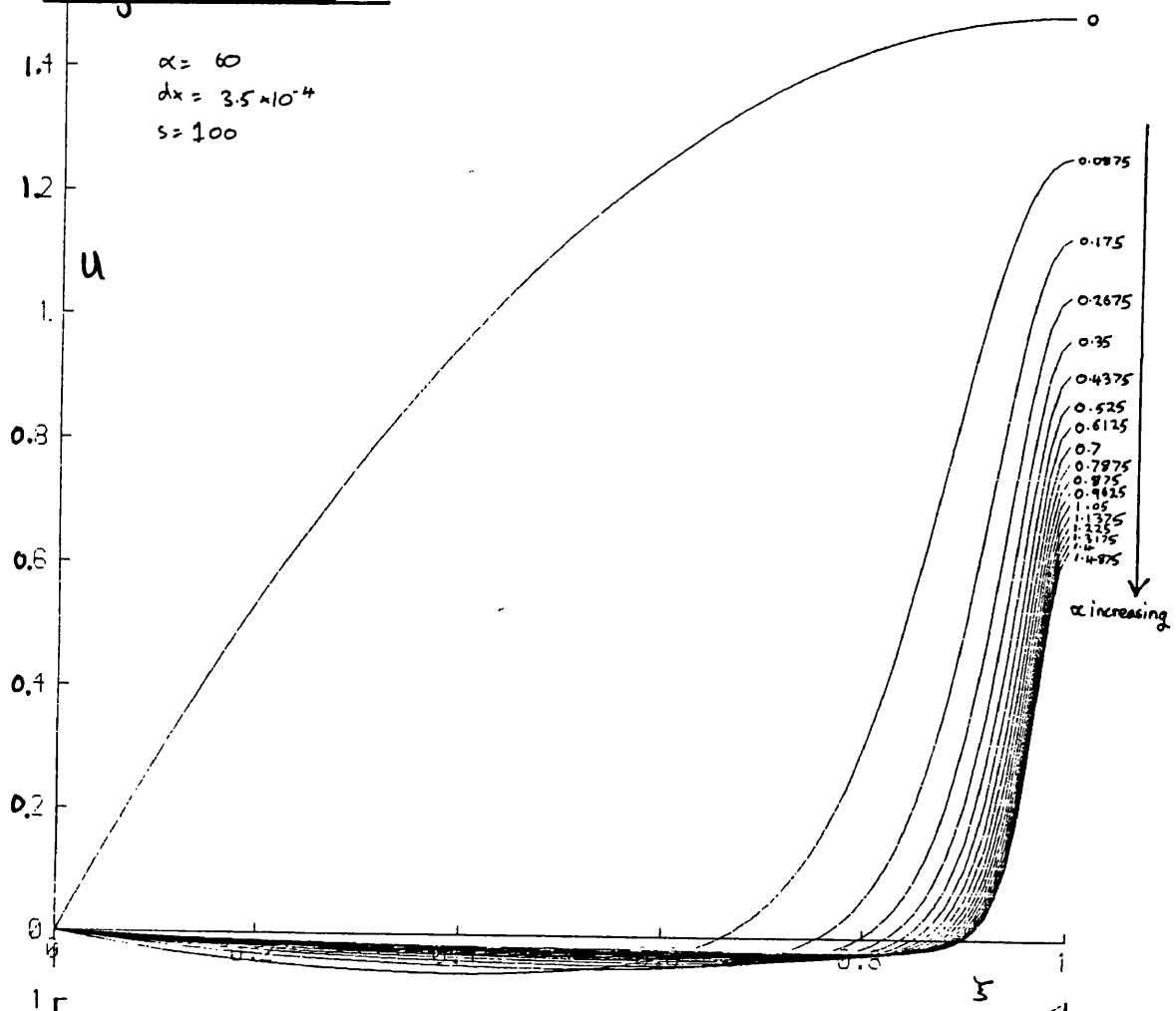

(d)

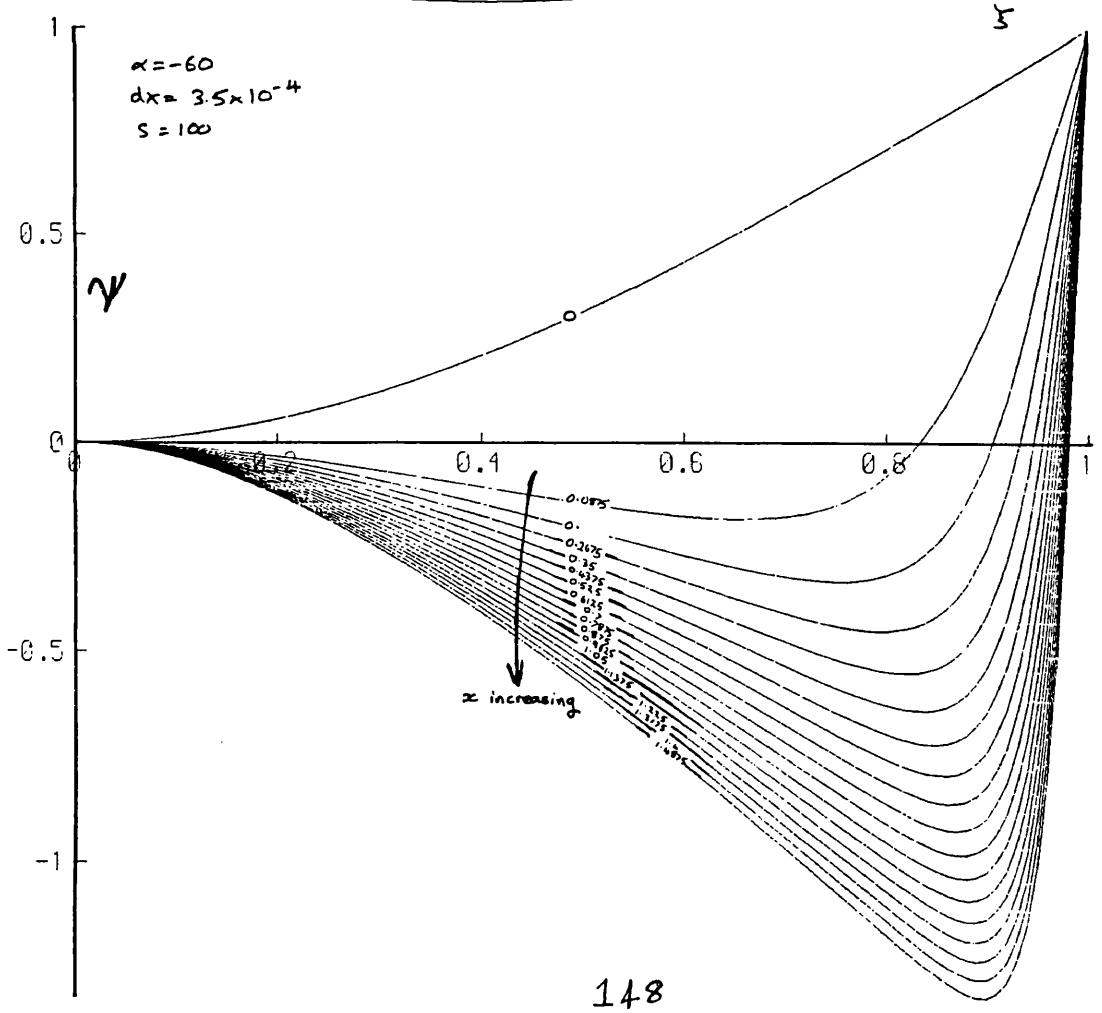

Figure 3.5.1.

(a)

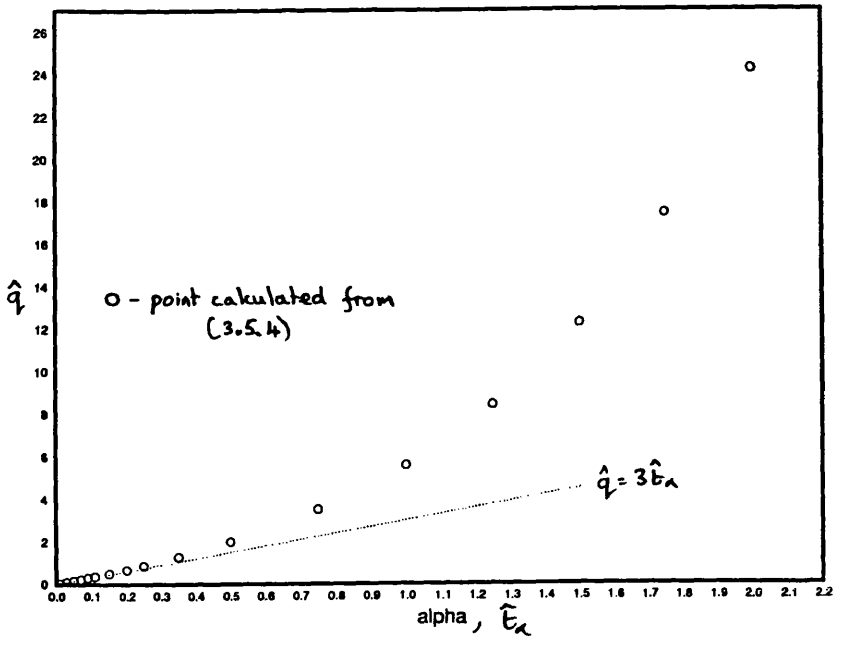

(b)

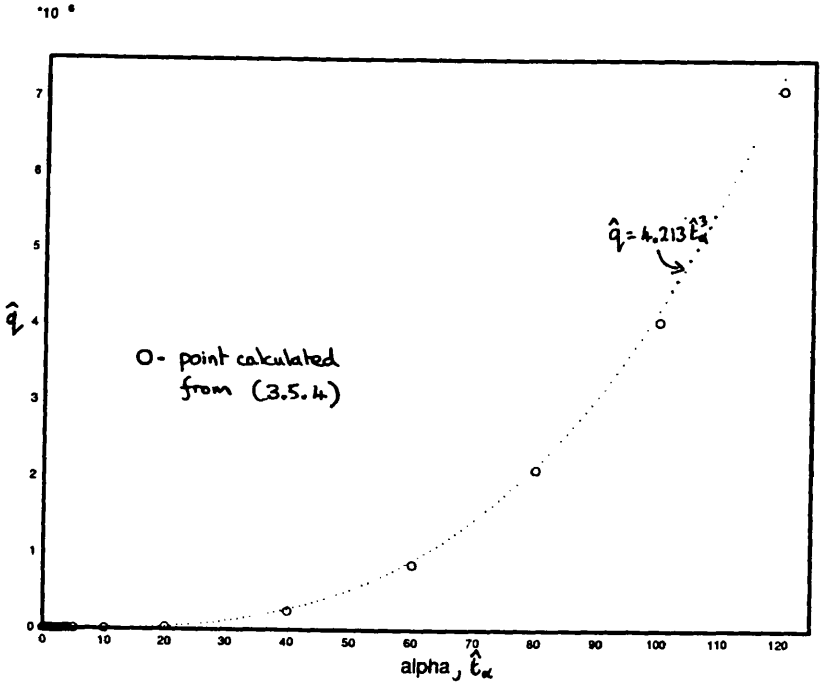

Figure 3.6.1

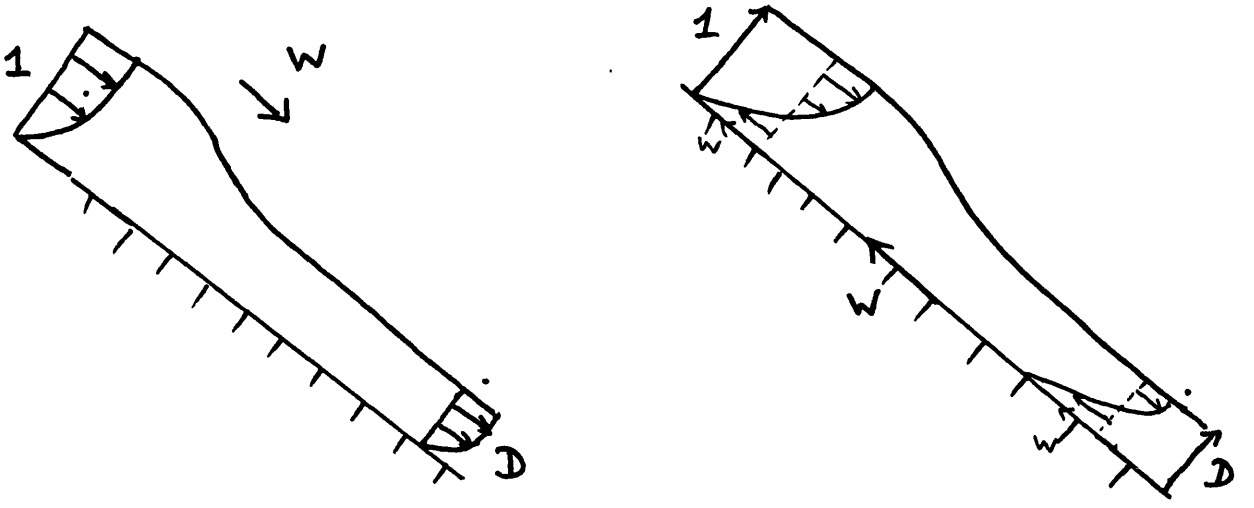

Figure 3.6.2(a)

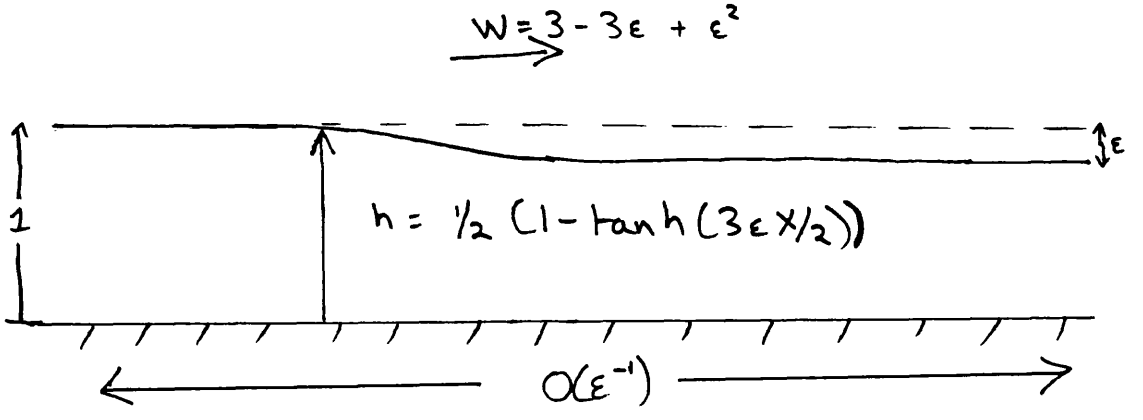

Figure 3.6.2(b)

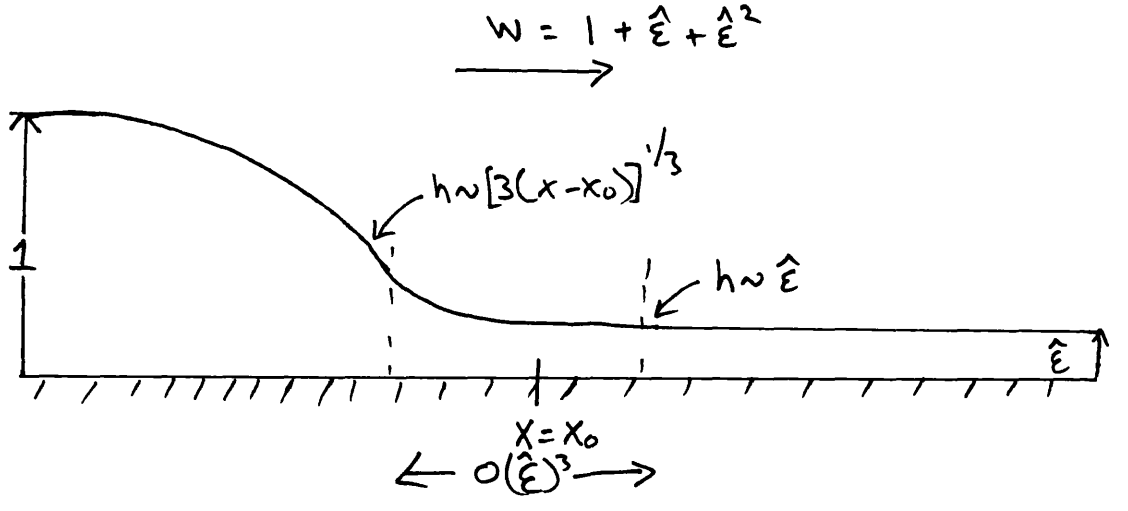

Figure 3.6.3

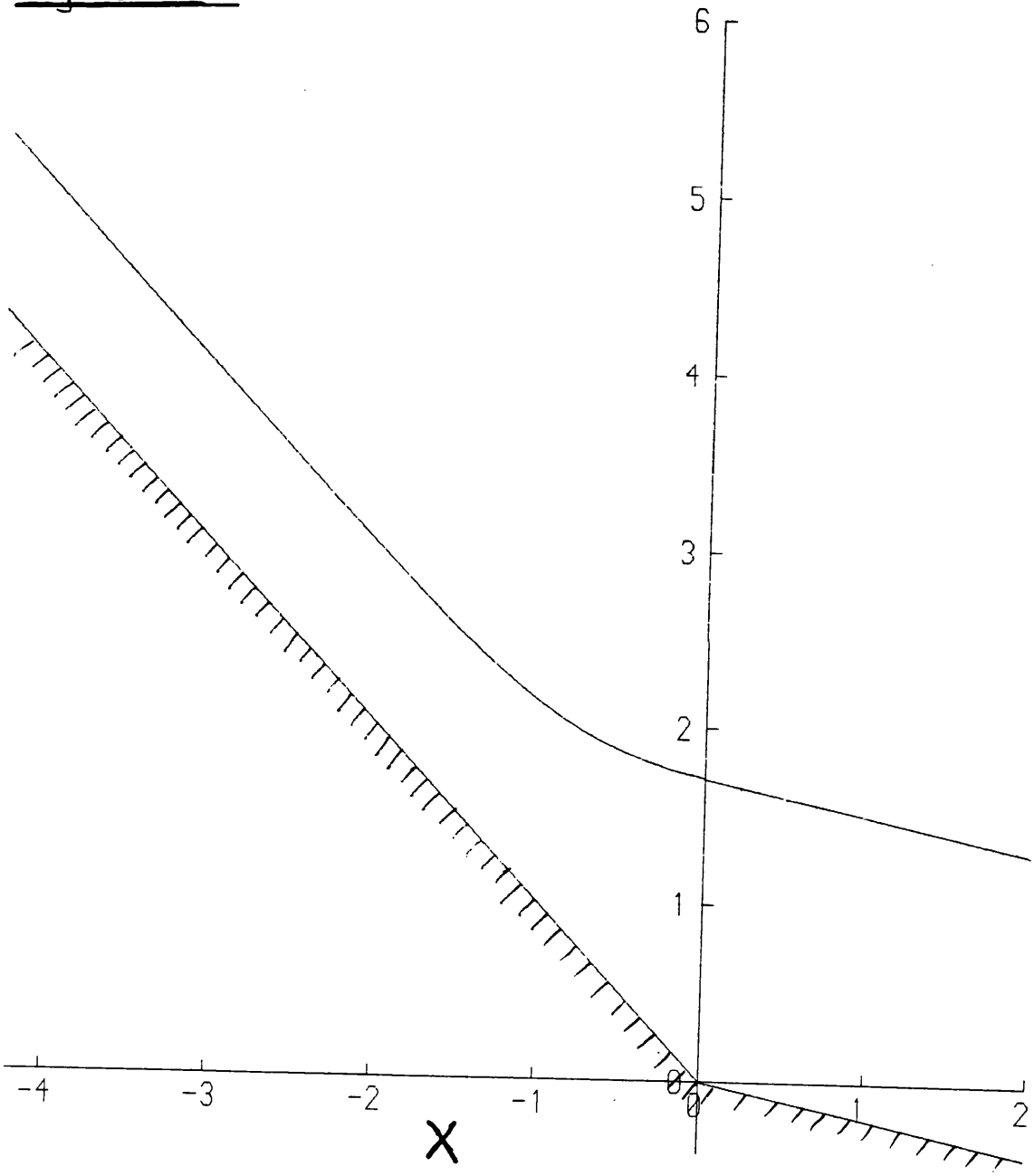

Figure 3.6.4(a)

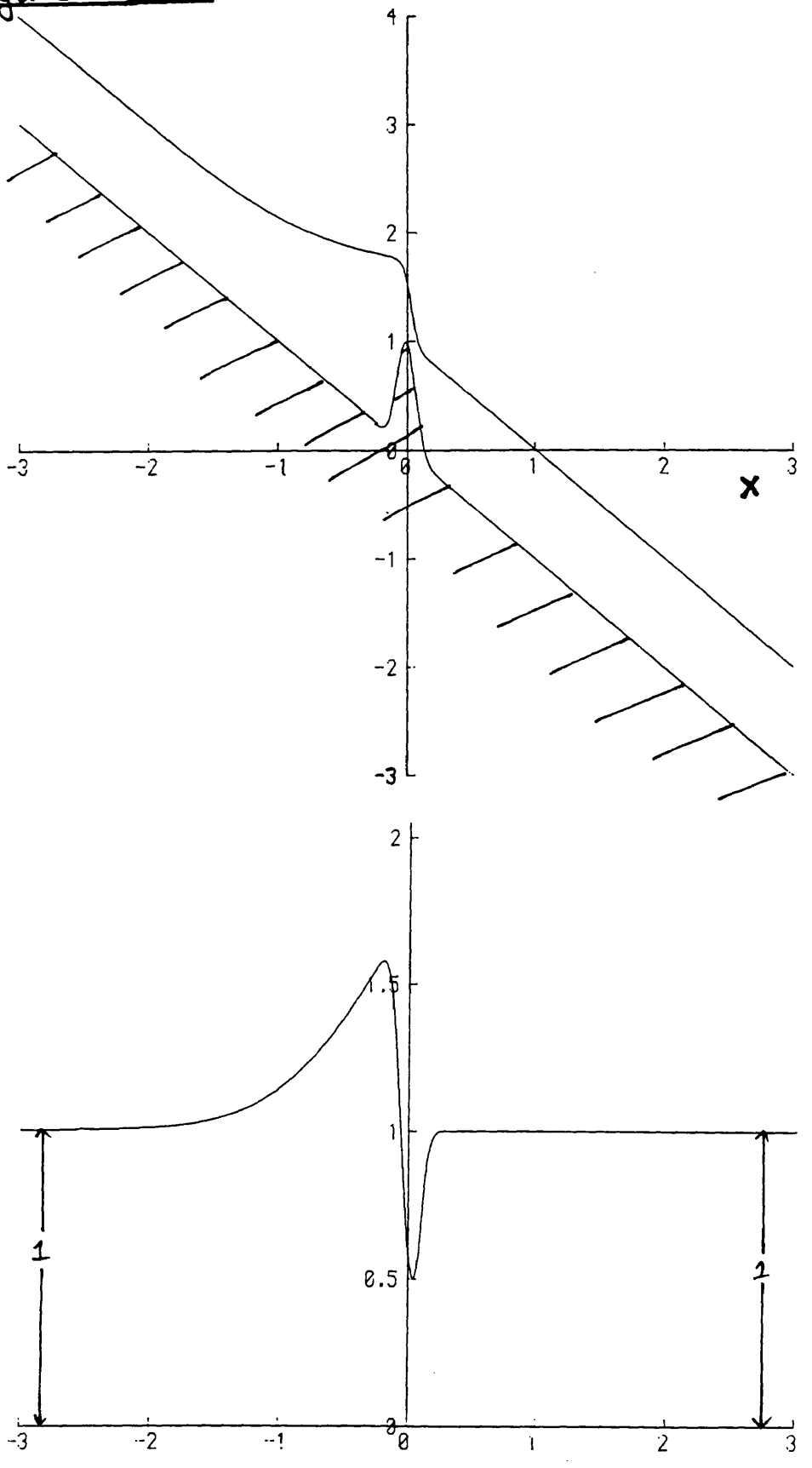

Figure 3.6.4(b)

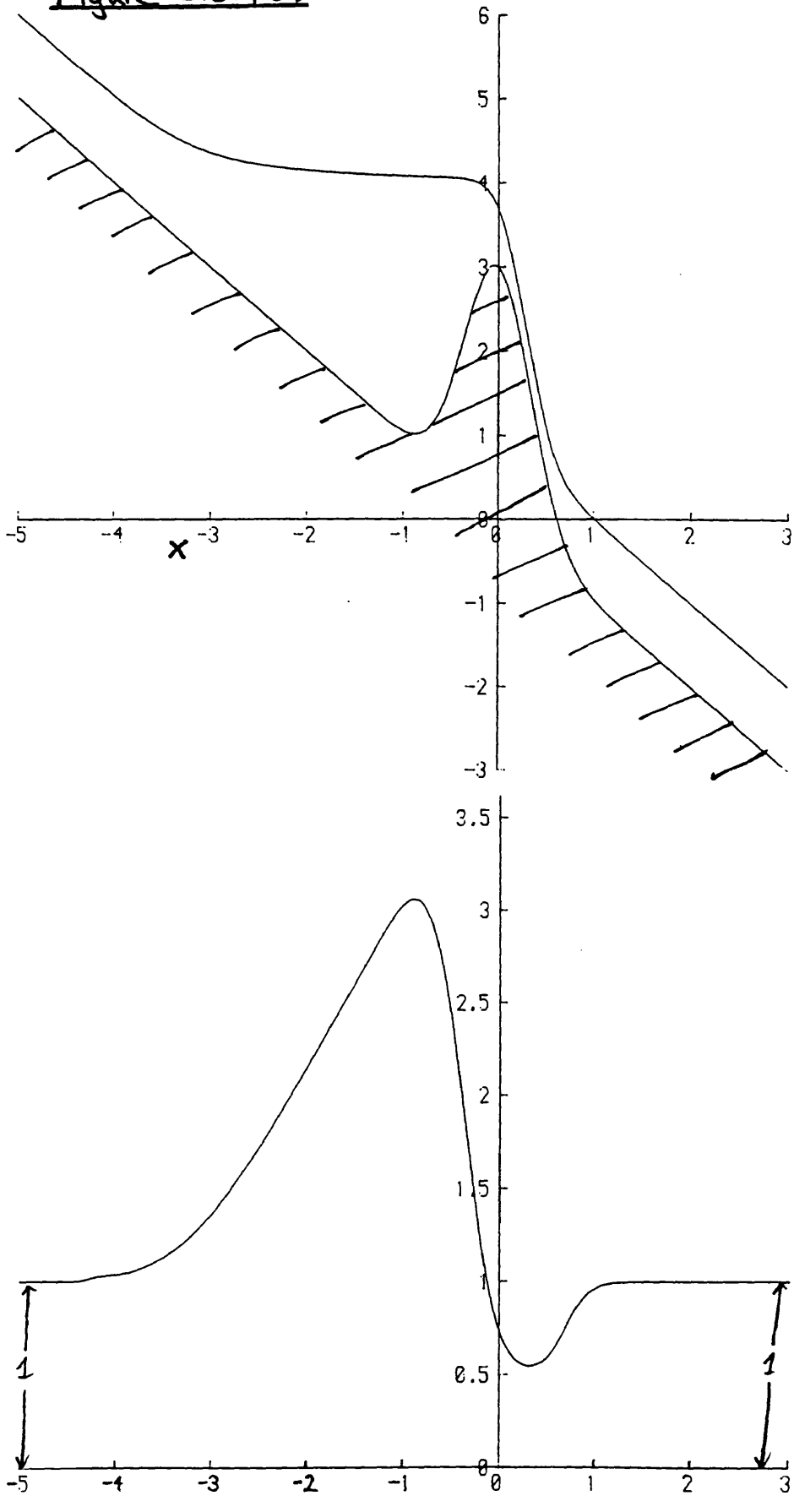

Figure 3.6.4 (c)

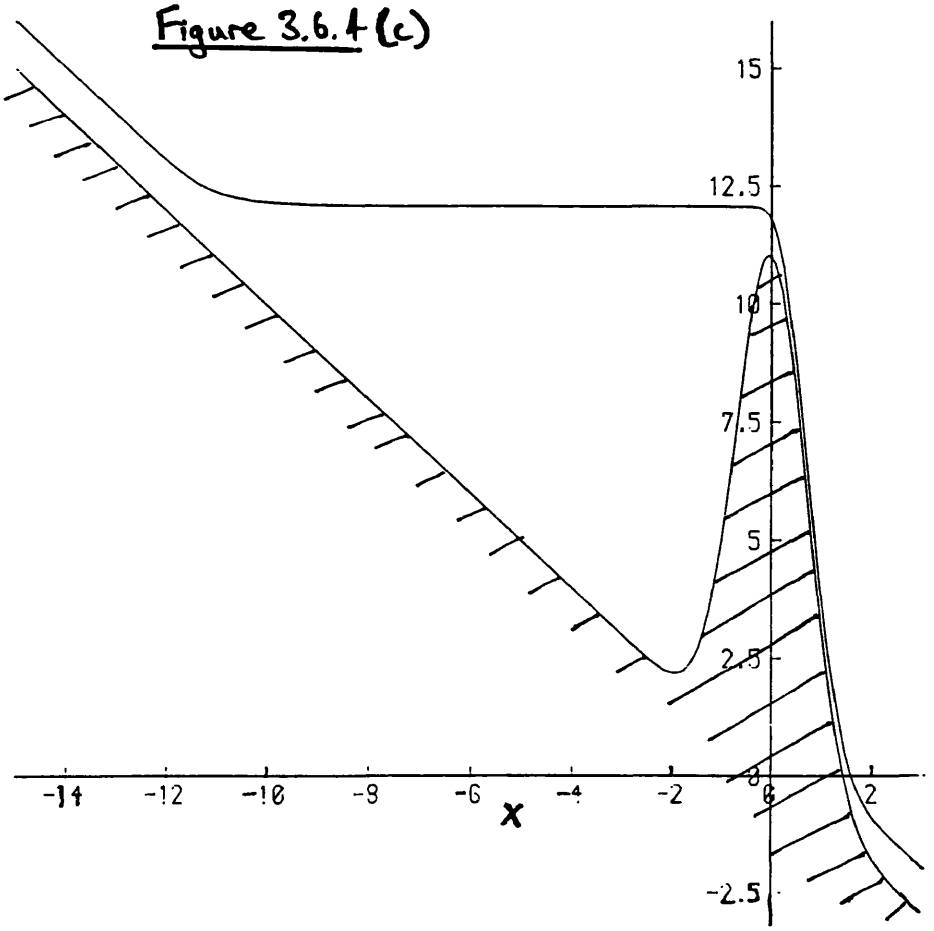
15
12.5
10
7.5
5
2.5
0
-2.5
-14
-12
-10
-8
-6
-4
-2
0
2
x

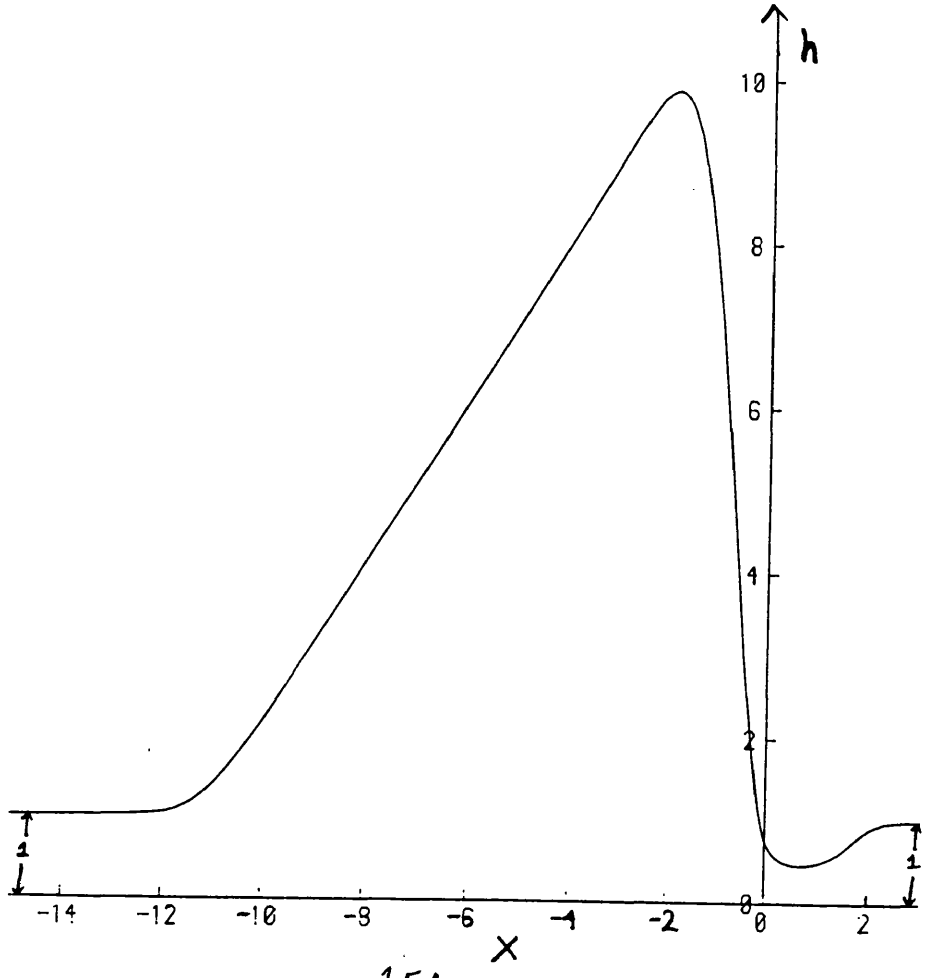
h
10
8
6
4
2
0
1
1
-14
-12
-10
-8
-6
-4
-2
0
2
x

Figure 3.6.4 (d)

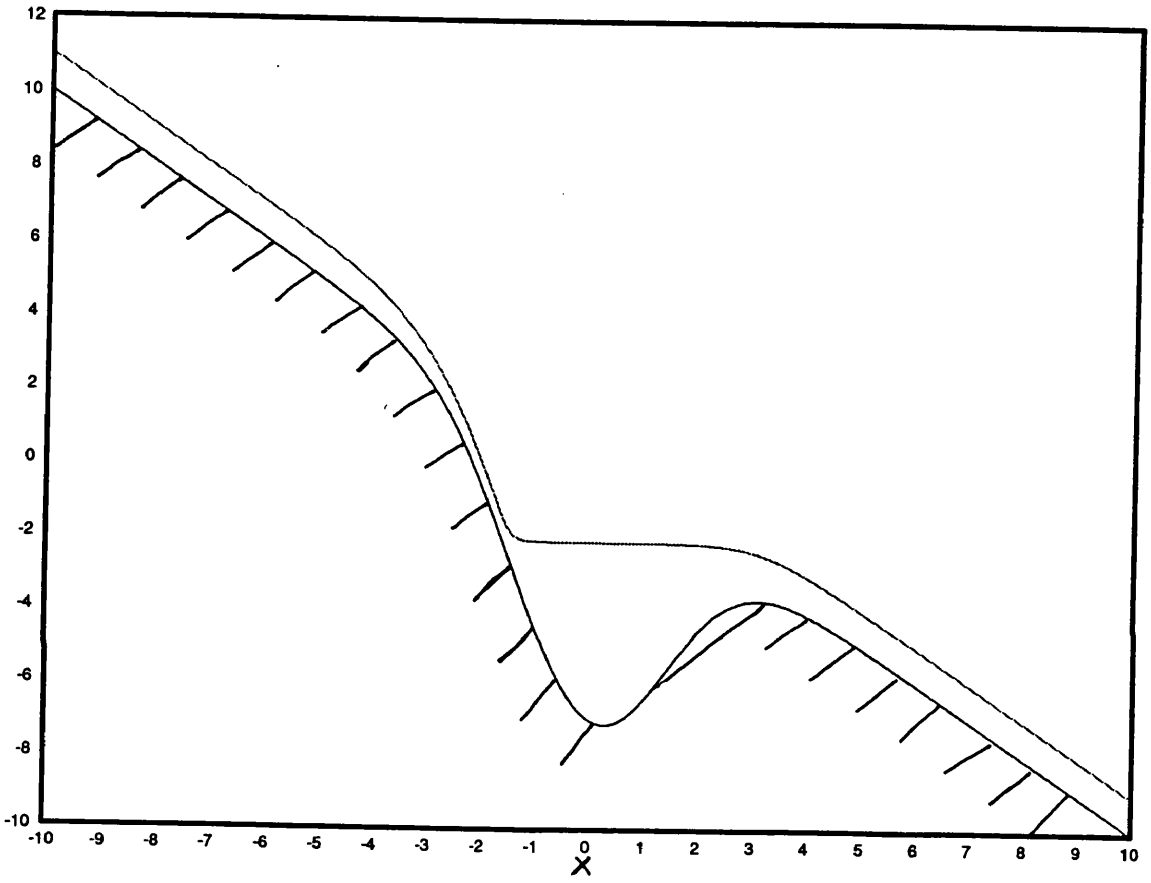

Figure 3.6.5.

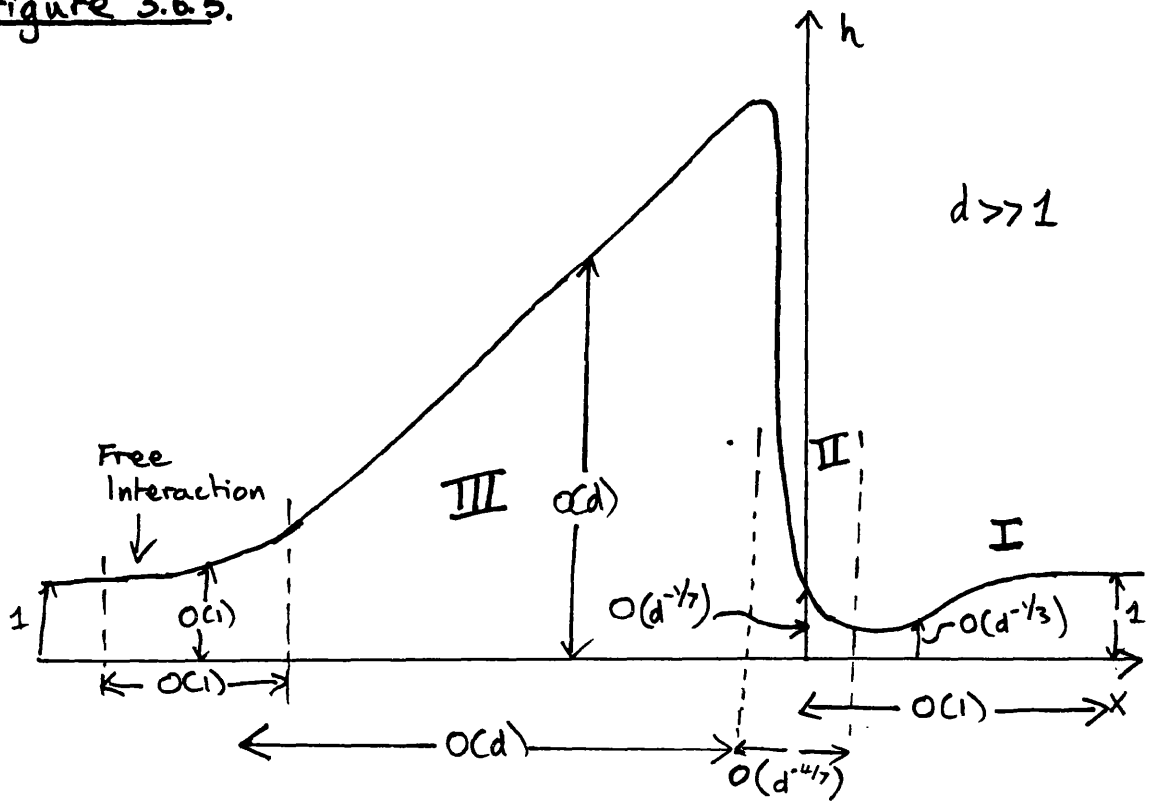

Figure 3.6.6.

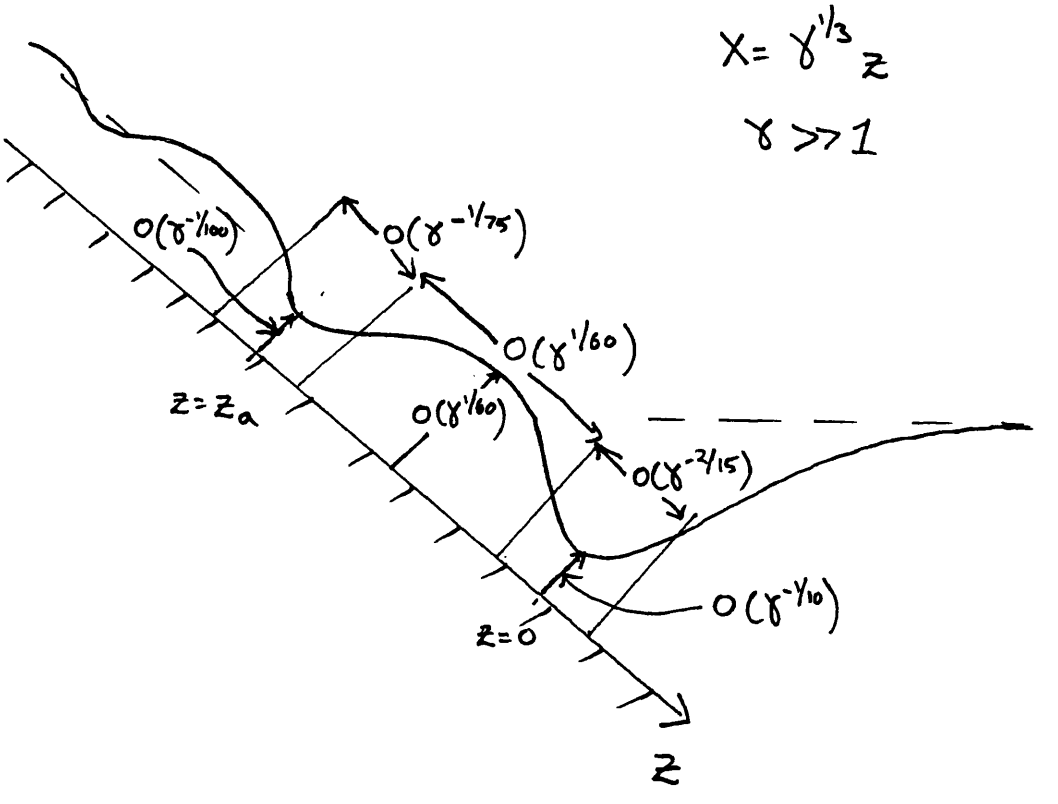

Figure 3.7.1(a)

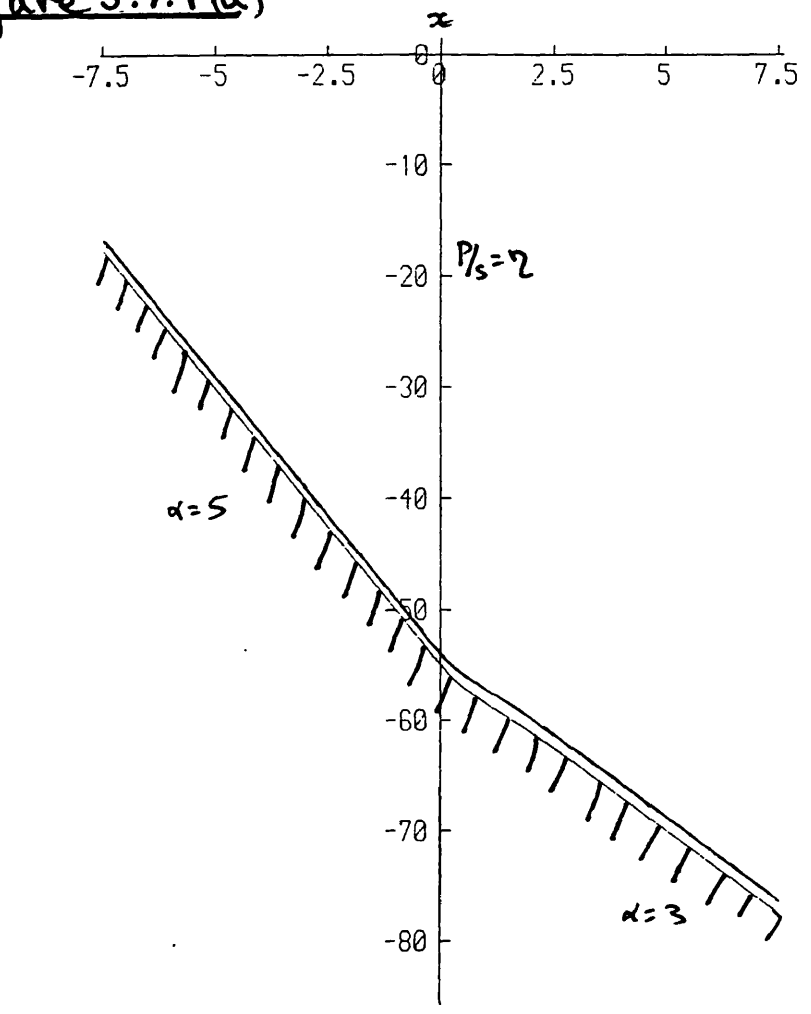
x
0
-7.5
-5
-2.5
0
2.5
5
7.5
-10
-20
-30
-40
-50
-60
-70
-80
P/s=2
α=5
α=3

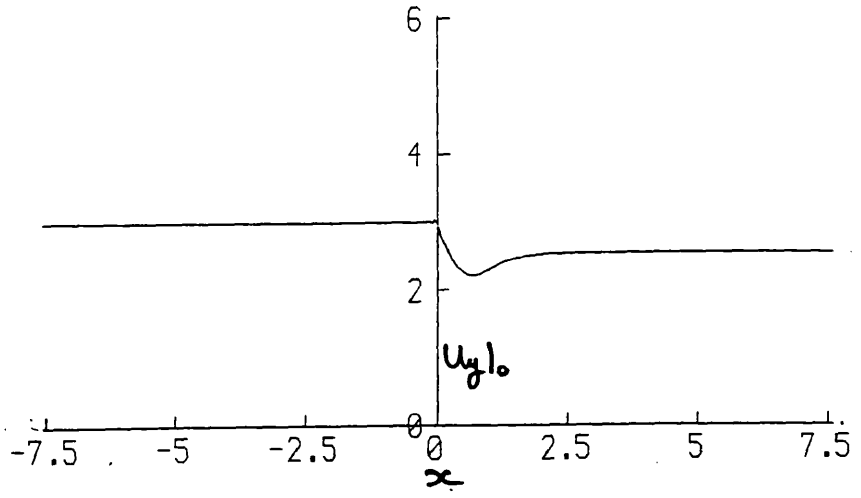
6
4
2
0
-7.5
-5
-2.5
0
2.5
5
7.5
x
Uy/Uo

Figure 3.7.1.(b)

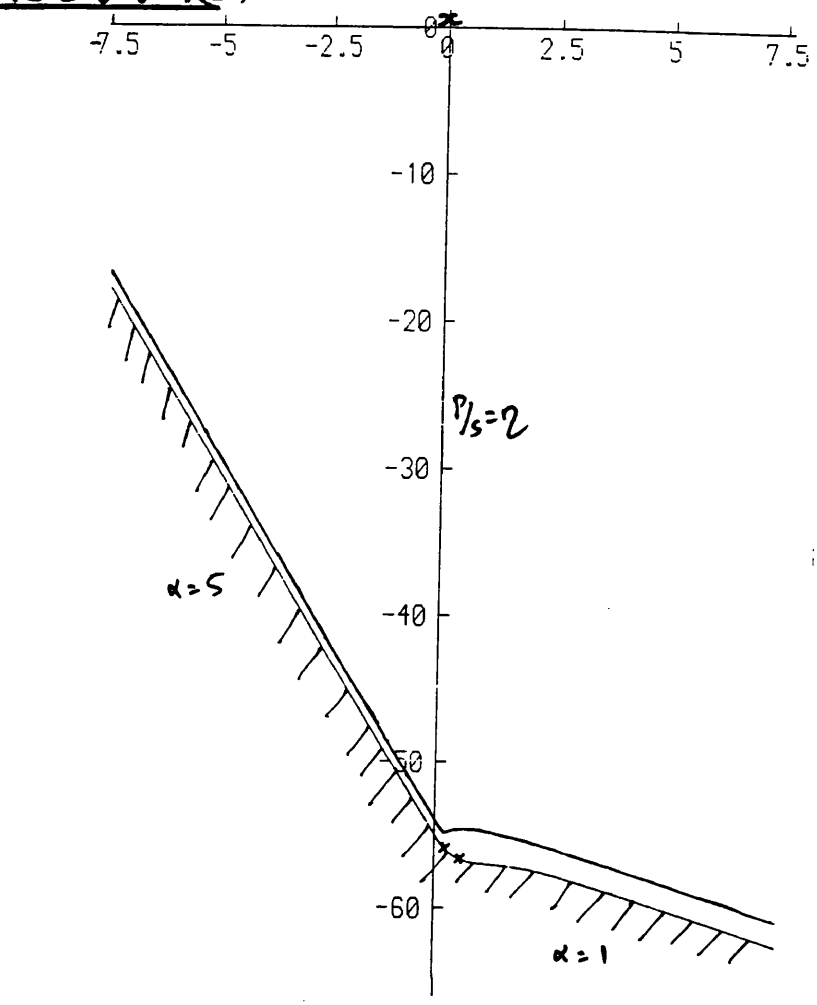
-7.5
-5
-2.5
0
2.5
5
7.5
-10
-20
-30
-40
-50
-60
x
$p/s=2$
$\alpha=5$
$\alpha=1$

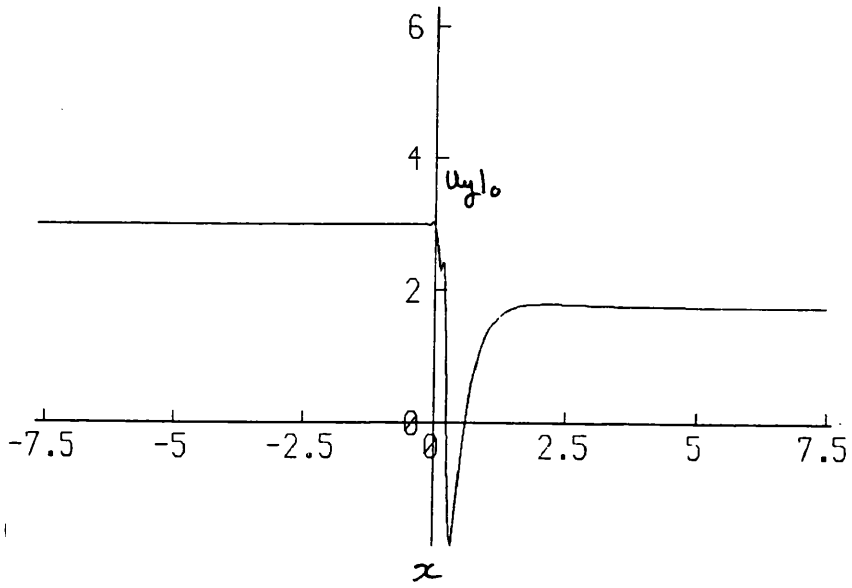
6
4
2
0
$u_y|_0$
-7.5
-5
-2.5
0
2.5
5
7.5
x

Figure 3.7.2(a)

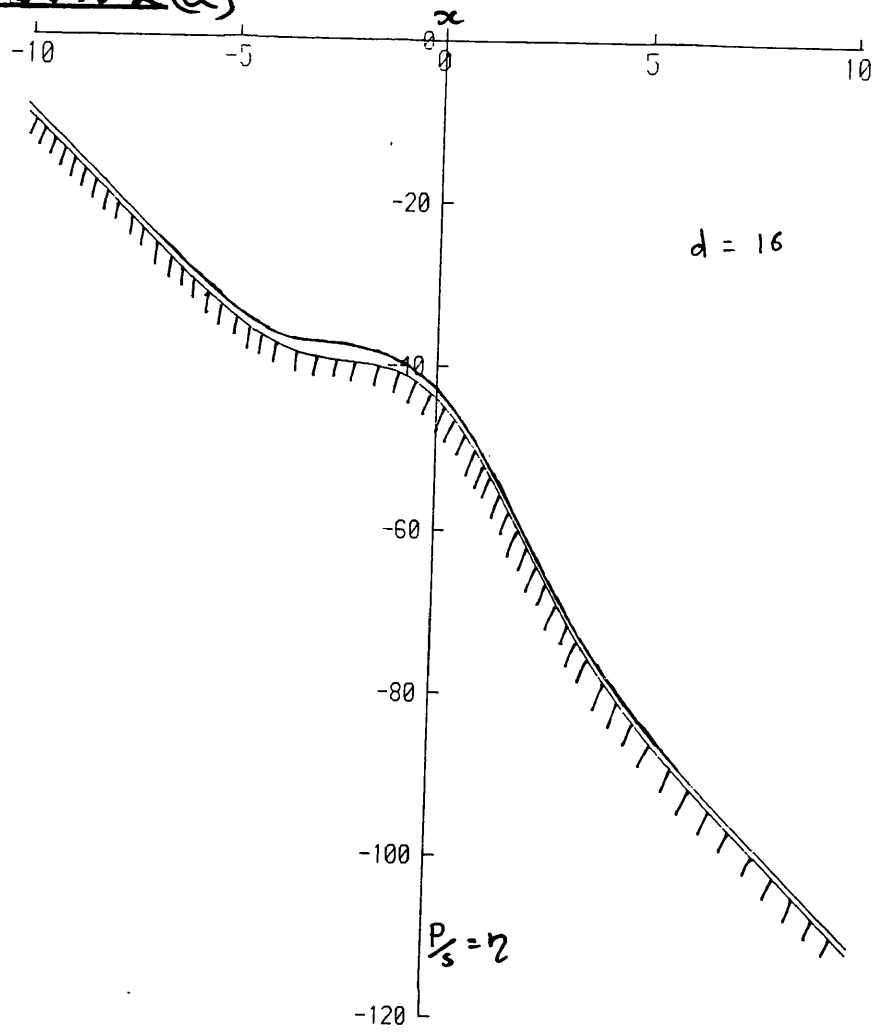

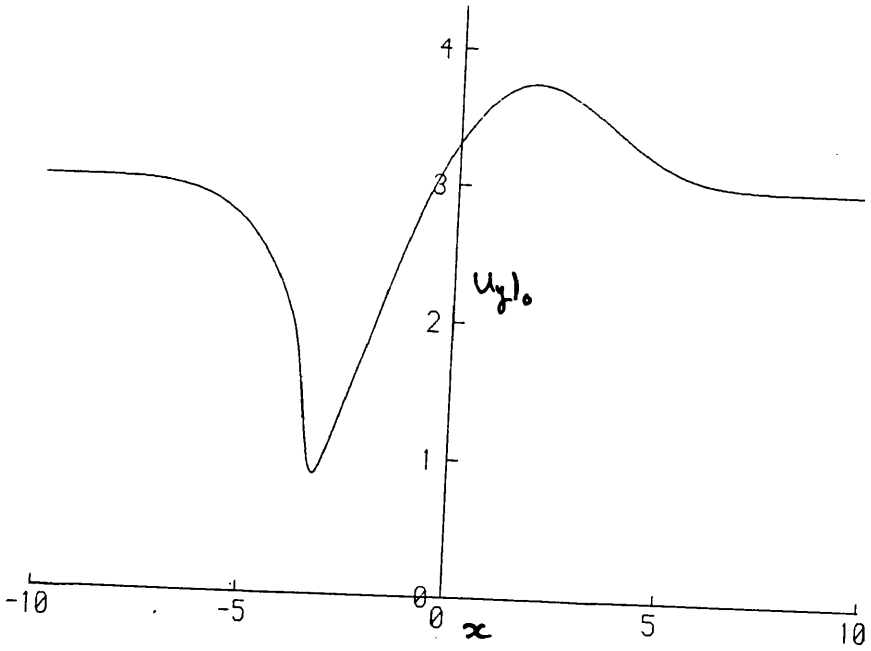

Figure 3.7.2 (b)

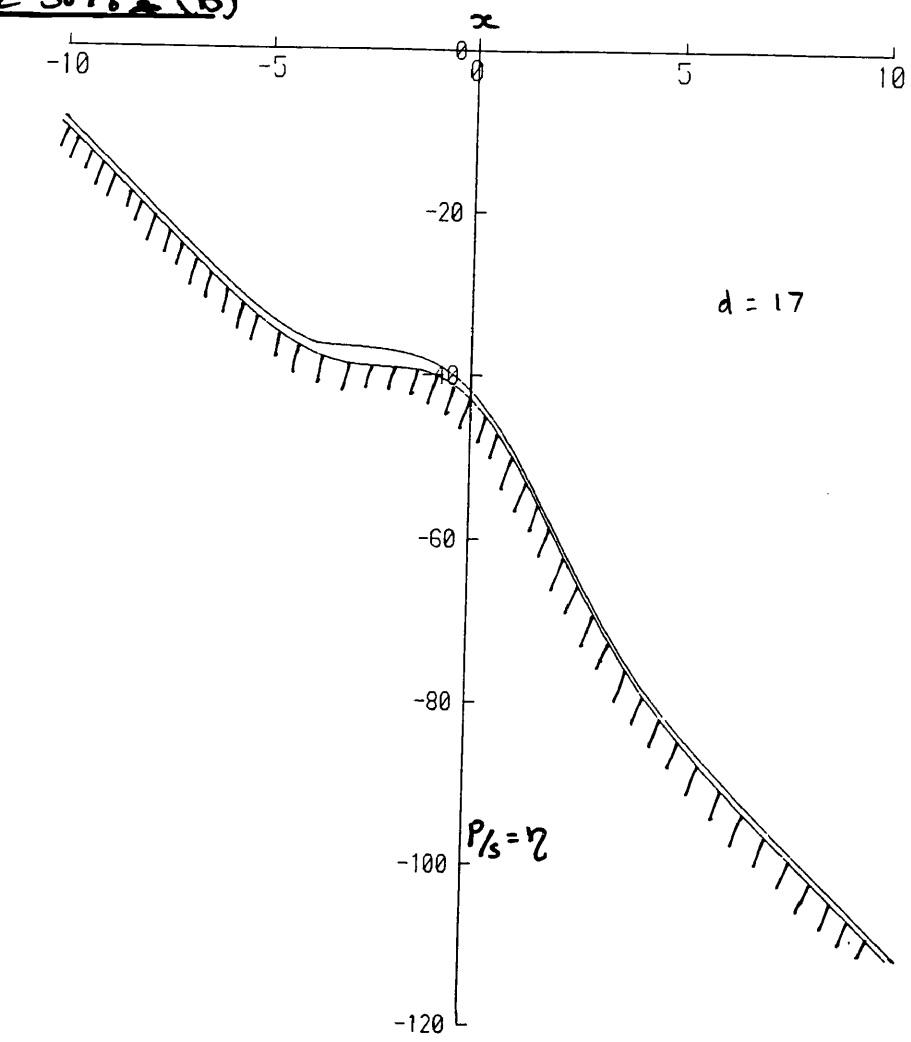

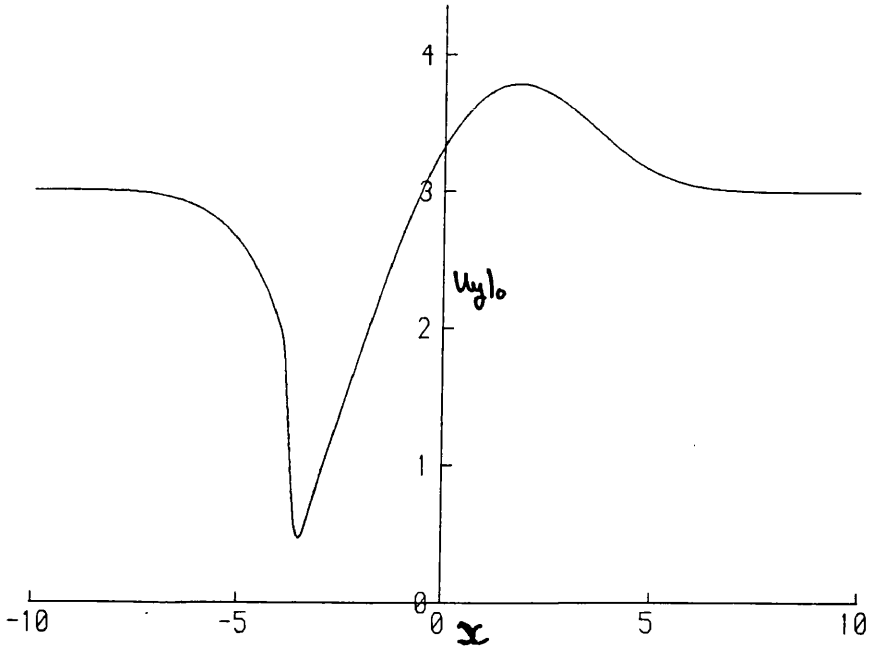

Figure 3.7.2 (c)

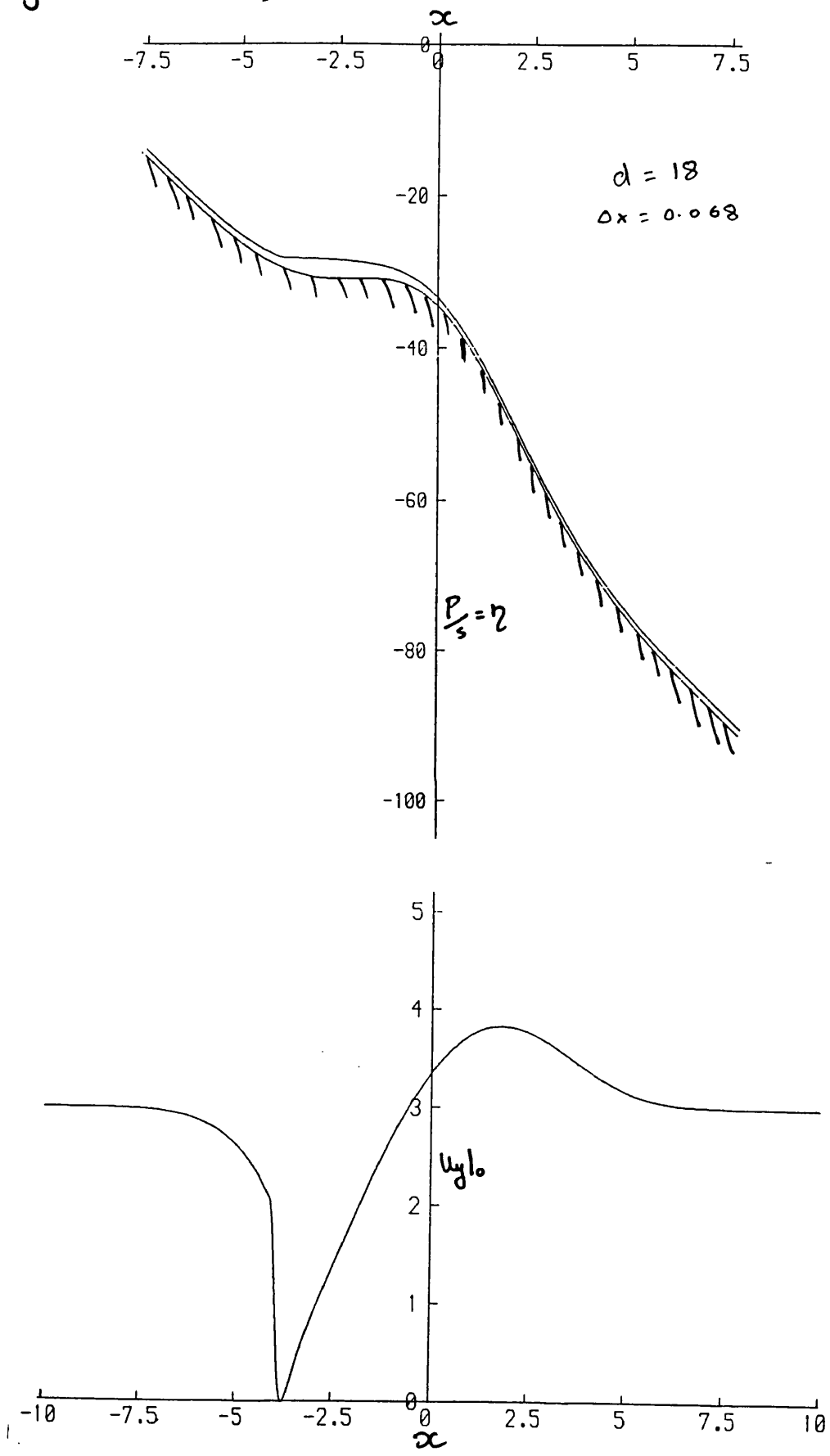
x
-7.5
-5
-2.5
0
2.5
5
7.5
d = 18
Δx = 0.068
-20
-40
-60
-80
-100
P/s = 2
5
4
3
2
1
0
u_y/u_0
-10
-7.5
-5
-2.5
0
2.5
5
7.5
10
x

Figure 3.7.2.(d)

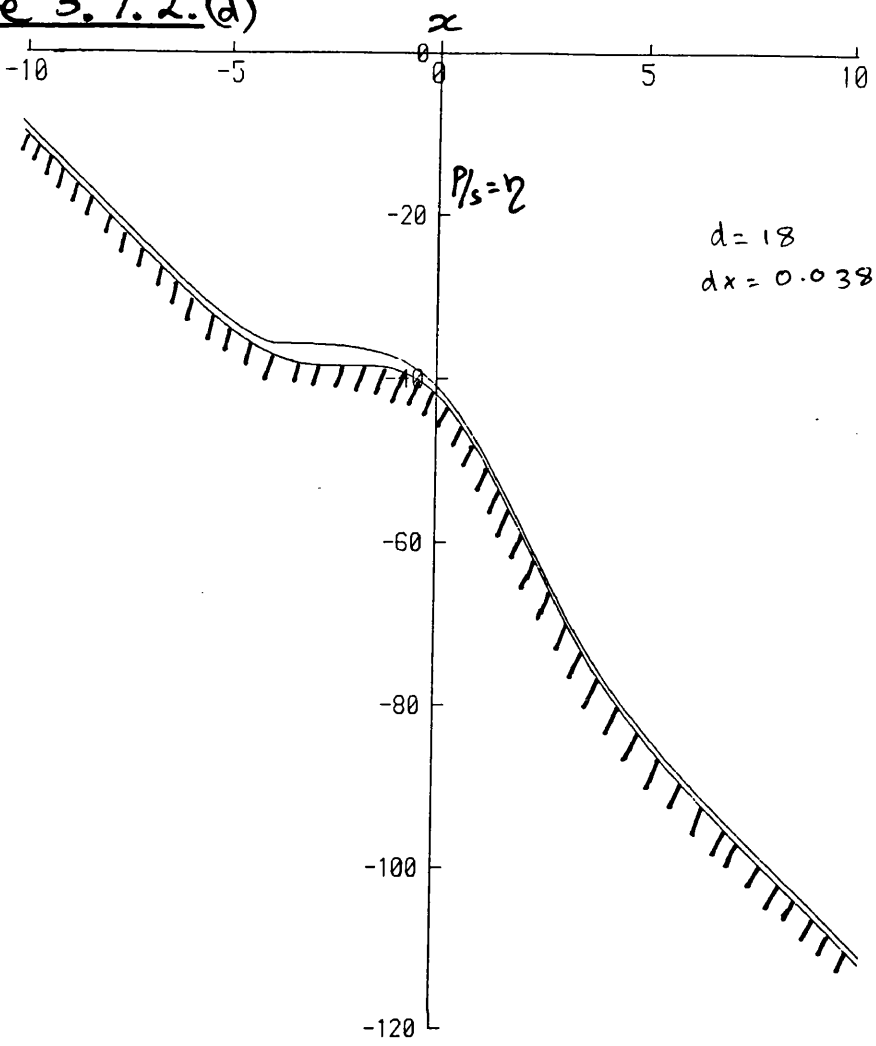

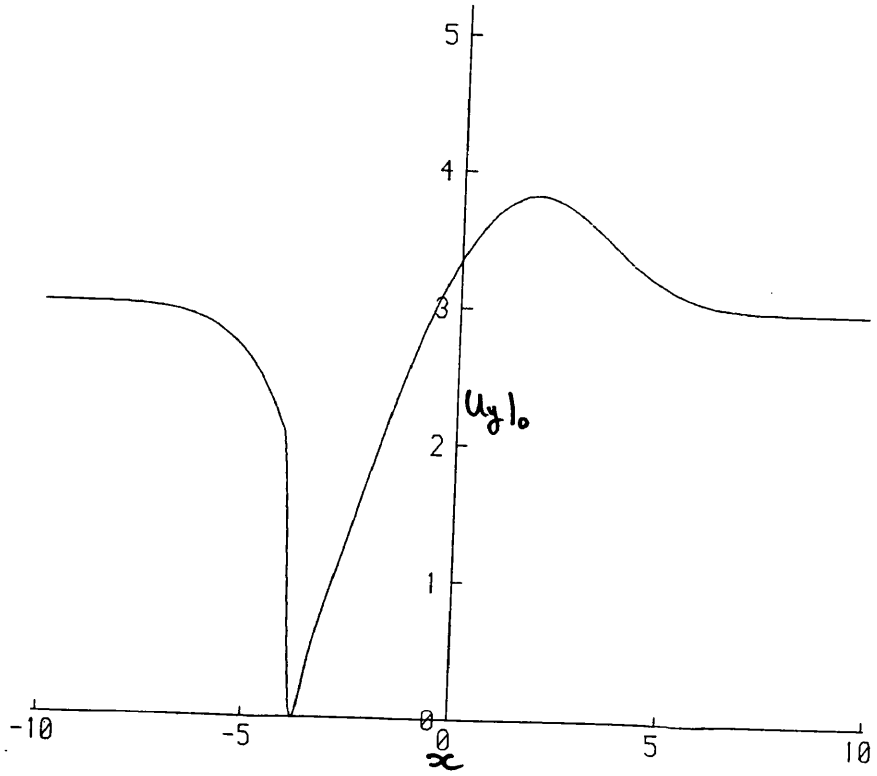

Figure 3.7.2.(e)

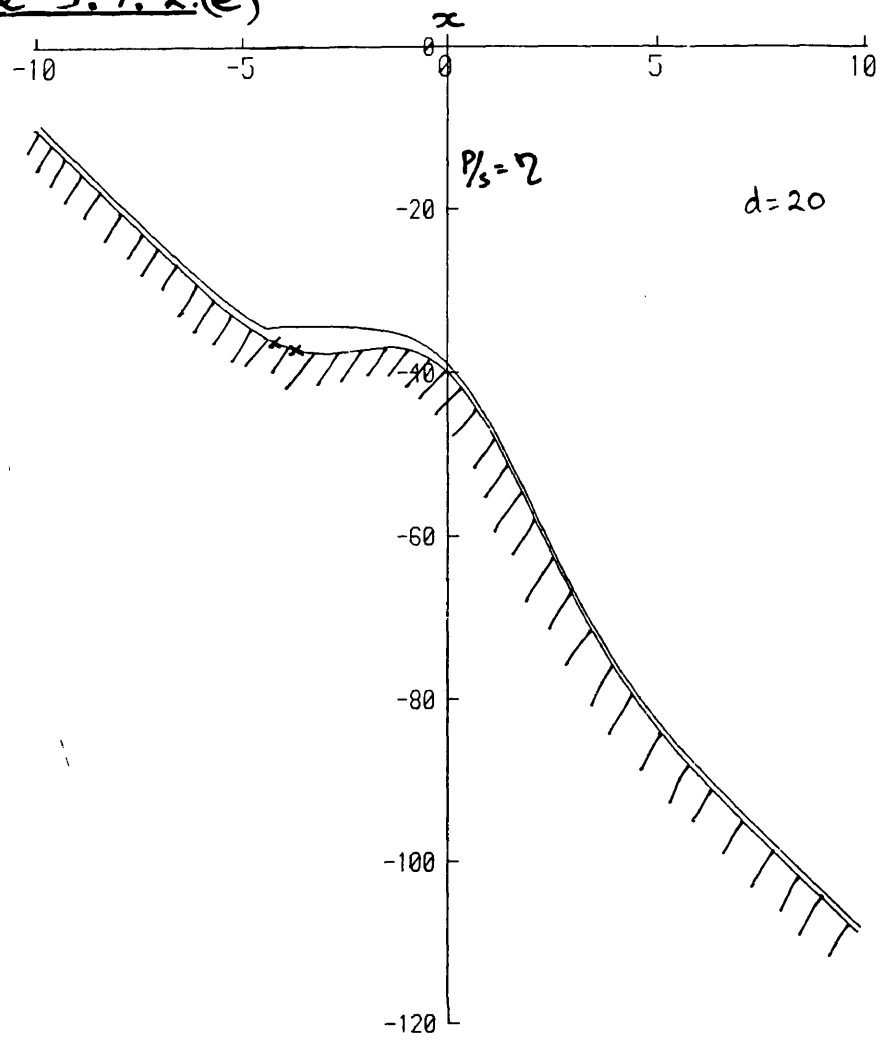

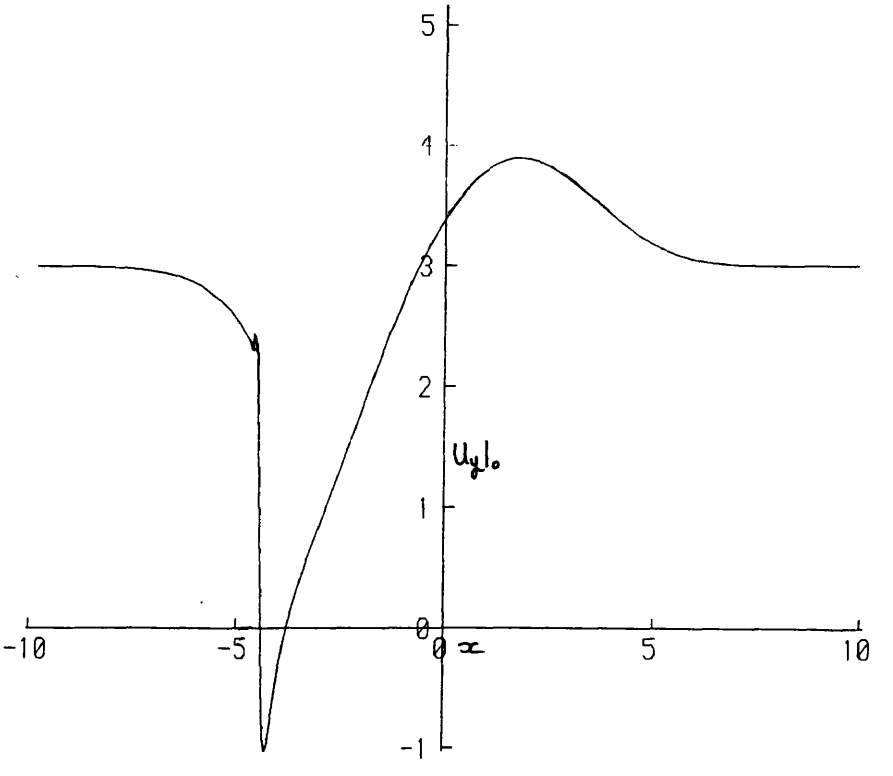

Chapter Four

TOLLMIEN-SCHLICHTING DISTURBANCES IN TRANSONIC FLOW.

§4.1 Introduction; The Problem Of Boundary Layer Transition.

The question of the stability of a laminar boundary layer and the associated problem of transition from laminar to turbulent flow are of great technological importance and theoretical interest. The history of their study goes back to Reynolds (1883) experiments on Poiseuille flow in a pipe, and even the work of Leonardo da Vinci contains illustrations of turbulent flow. The differences between laminar and turbulent boundary layers are obvious and striking. Laminar boundary layers consist of orderly unidirectional flow; turbulent flow is unsteady, with a mean profile defined only in a statistical sense, and containing a wide spectrum of eddy motions and scales. Turbulent boundary layers are, in a time-averaged sense, thicker and much more efficient in mixing momentum thoughout their thicknesses than are laminar boundary layers. This implies a greater skin friction at the wall and an increase in the drag. In the passenger aircraft and automobile industries the recent increases in the cost of fuel and in the level of environmental awareness have focussed the attention of designers on the need for the development of effective techniques for the control of the type of flow in a boundary layer. Such techniques aim at keeping the boundary layer laminar in flow regimes and at external pressure gradients where it would otherwise be turbulent. In addition the possibility of a sudden transition of the boundary layer flow can affect the handling of high performance aircraft.

There are also many occasions where it is desirable to provoke such a transition. In areas where efficient mixing is important, such as in the chemical industry or in the air intakes of high performance jet engines, where mixing of fuel with air takes place, the increased mixing efficiency of turbulent motion makes it useful. This increased ability to diffuse quantities extends to the

momentum content of the boundary layer. This means that a turbulent boundary layer is able to withstand more extreme adverse pressure gradients without separating than can a laminar boundary layer. This can be used to advantage in the design of high lift aerofoils where it is important to keep the pressure over the upper surface as low as possible. Here the presence of a separation bubble containing a region of slowly recirculating flow would reduce the efficiency of the design. This feature can also be used to reduce the likelihood of dynamic stall.

An understanding of the most efficient means of controlling transition phenomena must be underpinned by an understanding of the mechanisms by which transition occurs and by which turbulent motion is maintained. Consider the structure of the vorticity field both in two-dimensional laminar flow and in turbulent flow, which is strongly three-dimensional in nature. The laminar boundary layer flow consists of a balance between the convection downstream of vorticity and its production at the wall and diffusion away from it (both viscous phenomena). This balance occurs over a vertical scale of the order of the boundary layer thickness, $O(Re^{-1/2})$ as $Re \to \infty$. The only effective mechanism acting in the streamwise direction is the convection of the vorticity downstream. Free turbulent flows, on the other hand, consist of a wide variety of scales of unsteady motion with a constant cascade of energy and vorticity to the smaller scales, where they are dissipated by viscous effects. In an incompressible boundary layer the velocity fluctuations are, on average, about 10% of the free stream speed, and the motions have the same scale in both the vertical and spanwise or streamwise directions, except close to the wall. In addition the motions are strongly three-dimensional with vortex line stretching close to the wall being the dominant mechanism of vorticity production. The physics seem to be those of the three-dimensional, inviscid Euler equations with viscous dissipation occurring in a sublayer at the wall. There is a net transport of vorticity towards the wall where it is dissipated. The production of

vorticity by three-dimensional effects is vital in maintaining this transport which takes place against the mean vorticity gradient in the layer. This description of the structure of a turbulent boundary layer is primarily taken from Lighthill (1963), but see also Townsend (1956).

The mechanisms by which transition proceeds, therefore, must give rise to a redistribution of the vorticity of the oncoming flow, an increase in the three-dimensional nature of the motion, a decrease in the physical scales of the motion and a broadening of the spectrum of the disturbances. It must also be inherently nonlinear. There are many types of transitional behaviour, some of which we describe later in this thesis. Here, however, we make the distinction between "bypass" and "natural" transition. Bypass transition is a catch-all phrase describing the multitude of mechanisms involved in the response of a boundary layer to a large amplitude disturbance. It is often important in internal flows such as engines where the amplitude of a disturbance may be large and its spectrum dominated by relatively high frequency components. Natural transition, which can also be of several types, is associated with smaller disturbance amplitudes and so with external flows, especially with the performance of aircraft flying at high altitudes where the level of free stream turbulence is generally low. It is characterised by the presence of several well-defined stages in the development of an initially small disturbance. These include the onset of three-dimensionality in an initially two-dimensional flow and the nonlinear excitation and interaction of instability modes present in the initial disturbance spectrum at only small amplitudes. The process ends, as the disturbance proceeds downstream, in vorticity production due to the induced three-dimensional motions, an alteration of the original boundary layer profile, including an increase in the stress at the wall, and finally in the dominance of inviscid mechanics away from the wall with bursts of vorticity from a sublayer. We concentrate on natural transition although many of the

equations which we show to govern the latter stages of transition will also be of relevance in describing the response of the boundary layer in bypass transition. The work of chapter 7 investigates a possible bypass mechanism unique to transonic flow.

The process of natural transition starts with the generation of low amplitude waves in the boundary layer in response to some forcing such as free stream turbulence, acoustic waves or, as is often used in experiments, a vibrating ribbon. This was first established in the experiments of Schubauer and Skramstad (1947) in the case of a Blasius boundary layer. The waves are long with respect to the boundary layer thickness and, as it transpired, exactly those predicted by the theoretical, linear work of Tollmien (1929) and Schlichting (1933). The experiments of Schubauer and Skamstrad were the first to positively identify these so-called Tollmien-Schlichting (TS) waves with the process of transition on a flat plate. Previous experiments suffered from too high a level of background disturbance to be able to pick out the stages in transition.

The linear theory of these waves, which presumes a parallel basic flow profile, predicts that, as it moves downstream and the local Reynolds number increases, a relatively low frequency disturbance will pass through a region where it decays and then through a neutral point and into a region of growth. This is the lower branch neutral point. Further downstream a second neutral point is encountered, the upper branch neutral point, and finally the waves become stable once more. See, for example, Lin (1955), Stuart (1963), Drazin and Reid (1981). Depending on the local Reynolds number at the point at which the disturbance is introduced a wave can join this process at any stage. The height above the plate at which the speed of the boundary layer profile is equal to the phase speed of the wave is associated with the critical layer of the disturbance. It is at this point that the energy is extracted from the mean flow. TS waves are a viscous instability. This means that the instability

does not survive as the Reynolds number of the flow tends to infinity. Unlike the Rayleigh instability, which is important in boundary layers with a profile with a vorticity maximum (unlike the Blasius profile) or in an extended sense in compressible boundary layers (see §4.3.6), the TS instability relies on viscous effects for its amplification. Viscous effects within the critical layer result in a phase change in the vorticity profile across it and, in addition, vorticity diffuses out from the Stokes layer near the wall. If the position of the critical layer is such that this vorticity, when it reaches the critical layer, is in phase with the vorticity fluctuations there it will reinforce the disturbance thus causing it to grow. See Lighthill (1963).

The lower branch of disturbances correspond to the critical layer being within the Stokes layer itself and in upper branch disturbances it is situated further away from the wall. Lower branch disturbances are therefore longer and slower than upper branch ones. Asymptotic results for the wavelength of the lower branch neutral wave as the Reynolds number becomes large (Lin (1955)), yield the result that the length scale of the disturbances are of $O(Re^{-3/8})$ where length scales are now normalised with respect to the the plate-length. This scaling is exactly that which governs the steady interactive boundary layer in external flow. See Stewartson and Williams (1969), Messiter (1970) and Smith (1982). In fact the asymptotic structure of TS waves at large Reynolds number is exactly the triple deck structure. Therefore Tollmien-Schlichting waves are essentially an viscous-inviscid interaction phenomenon, with the inviscid mechanism being pressure waves in the free stream. Smith (1979a&b) notes that the only valid way of studying these TS disturbances is via the unsteady triple deck formulation since the limit $Re \to \infty$ is implicit in the boundary layer approximation itself. Bodonyi and Smith (1981) carry out a similar high Reynolds number expansion for the upper branch of disturbances and Gajjar and Cole (1989) extend this analysis to include the effects of a non-zero Mach number.

The lower branch is, in essence, unaffected by the compressibility effects, at least at subsonic speeds (see §4.2.2). A similar technique can be applied to TS waves in channel flow.

The two advantages of the structural approach to boundary layer stability theory and the asymptotic solution of the governing Navier-Stokes equations in an expansion in inverse powers of the Reynolds number are as follows. Firstly it is a "rational" procedure (in the sense of Van Dyke (1964)). This means that the importance of neglected effects, such as the non-parallelism of the basic boundary layer flow, can be gauged at any stage of the expansion and if necessary incorporated at higher orders in the expansion (Smith 1979a). It leads naturally to approximations that are consistent with the governing Navier-Stokes equations. Secondly it naturally leads to a nonlinear equation governing the flow close to the wall for a relatively small disturbance amplitude. In the case of lower branch disturbances in incompressible flow, a nonlinear equation results where the disturbance size is that of the basic velocity profile at the position of the critical layer, and this turns out to require a disturbance velocity of only $O(Re^{-1/8})$. Since transition is a nonlinear phenomenon, this is an important feature. This nonlinearity has been exploited to gain an understanding of many features of the transition process, e.g. the saturation and equilibrium amplitudes for lower branch disturbances close to the neutral point (Smith (1979b)) and the nonlinear development of relatively high frequency disturbances, leading to the equations governing large amplitude waves (Smith and Burgraff (1985), Smith (1986a&b), Smith and Stewart (1987)).

There are two main criticisms of the triple deck approach. Firstly there is the objection that it is only an asymptotic solution of the governing equations. This is often countered by the argument that the boundary layer approximation itself is also only valid for infinite Reynolds number. In addition the Reynolds number is often extremly large in practical situations. Furthermore it

often turns out that the predictions of the theory are in agreement with experiments or computations down to quite small values of the Reynolds number. The most convincing argument in its favour, however, is that it makes clear the physical processes at work in the fluid and eases an understanding of the interactions between them. The second objection is that the triple deck can only capture the lower branch of the disturbances. This is not quite true since the relatively high frequency limit of the triple deck equations, as used in chapters 5 & 6 of this thesis, captures all the mechanics of the upper branch disturbances except the crossover to stability at the neutral point and the possible effects of saturation of a disturbance due to nonlinear effects within the critical layer. In addition Smith and Burgraff (1985) argue that in natural transition it is the lower branch that is met first as the wave travels downstream and so it is the nonlinear development of the lower branch disturbances that is of importance, especially in the case of larger amplitude disturbances.

The development of lower branch disturbances is not the only cause of instability in boundary layers and not the only cause of transition. In a decelerating free stream the boundary layer vorticity profile develops a maximum which implies that it is subject to the inviscid Rayleigh instability which is typically more dangerous than the TS instability. On a concave plate the Görtler instability is important. In the presence of cross-flow in the boundary layer the net vorticity profile in some direction can contain a maximum triggering the Rayleigh instability. In compressible flows the inviscid Rayleigh instability is slightly modified and so-called higher modes of instability develop which are more unstable. Finally and most importantly there is the possibility of interaction between these modes of instability typified perhaps by the wave-vortex interaction. In these mechanisms a very small amplitude, oblique pair of TS or Rayleigh waves can interact wth a longitudinal vortex structure whose amplitude is the same as the basic

oncoming flow. This gives rise to the possibility of a small wave altering the basic flow by a significant amount. This leads to the generation of shear layers and inflexion points within the boundary layer profile and the triggering of the inviscid instabilities mentioned above. There follows a rapid cascade of instabilities and turbulent motion. This idea of wave-vortex interaction is a promising one for the description of a host of transition phenomena. See Hall and Smith (1989) and Smith and Walton (1990). However, this thesis does not consider this interaction.

There are many routes to turbulence starting from linear TS waves. Which one the flow takes depends on the amplitude and frequency spectrum of the initial disturbance. A description of the types seen experimentally and the theory describing them can be found in the introductions to chapters 5 and 6. The study of the nonlinear triple deck has been able to shed light on much of the physics of these routes. As mentioned above, Smith and Burgraff and Smith follow the development of a disturbance through increasing amplitudes to a stage where the disturbance is essentially inviscid and bursts of vorticity emanate from a viscous sublayer. As the amplitude increases still further the work of Smith, Doorly and Rothmeyer (1987) is important in the understanding of the structure of turbulent spots in boundary layers. Smith and Stewart (1987) use the triple deck as a starting point in the study of the resonant triad mechansim of mode interaction in transition (see Craik (1971), Craik (1985)). Stewart and Smith (1987) study the secondary instability of a two-dimensional wave to three-dimensional disturbances and the effects of the non-parallelism of the basic flow on the growth rate.

These theories originated in the study of incompressible, subsonic boundary layers on flat plates. With the increase in the speed of travel of aircraft has come a need to understand compressible, transonic or hypersonic flows and the elements of the triple deck theory are now being applied to different flow regimes and

to different geometries. Smith (1989) investigates lower branch disturbances in supersonic and hypersonic flows. Cowley and Hall (1990) look at waves in the presence of a leading edge shock in a hypersonic flow. Avis (1989) and Duck and Hall (1989a&b) look at axisymmetric flows. The work of the latter half of this thesis is an initial investigation into transonic flows.

The problem which we study originates in the boundary layer on an engine nacelle of a commercial airliner. The speed of the aircraft and the geometry of the nacelle means that, at certain operating conditions of the engine, the speed of the free stream at the point of transition is transonic, in the range $0.8 < M_\infty < 1.2$, with M_∞ the local Mach number. Associated with this transonic flow is a pocket of supersonic flow and a weak shock which, although not sufficiently strong to provoke separation and transition, may well have some influence on the transition process. The work of Smith (1989) identifies two different types of lower branch disturbance at transonic speeds. The first is the so-called major mode. This is an oblique wave directed at an O(1) angle to the direction of the free stream. The second type is the minor mode and is directed at a lesser, $O(|M_\infty^2-1|^{1/2})$, angle to the free stream. We study these minor modes. These modes are fast-moving compared with the major modes and are directed more strongly in the direction of the oncoming stream. There comes a stage, therefore, as the Mach number approaches unity, when the wave speed balances that of the slowest-travelling sound wave in the free stream. The regime where these two speeds are of the same order has $M_\infty^2-1 \sim (Re^{-1/9})$ and the wave speed also $O(Re^{-1/9})$. It leads to a triple deck structure for the lower branch disturbance with unsteadiness in both the boundary layer equation and the free stream equation.

In §4.2 we derive the scales for the motion and the nonlinear triple deck equations governing the disturbance. We then go on to discuss the solution of the linearised form of these equations in §4.3. It has long been realised (Rhyzhov and Zhuk (1980)) that two-dimensional linear

lower branch disturbances in supersonic flow are all stable. The transonic regime discussed here allows us to trace the development of the lower branch disturbances from subsonic speeds, where there is a range of frequencies that are amplified, through transonic speeds and to supersonic speeds. It is found that waves directed at an angle less than $O(|M_\infty^2-1|^{1/2})$ to the direction of the free stream, with $M_\infty > 1$, (within the wave-Mach cone) rapidly become affected by the non-parallel nature of the boundary layer as their growth rates are reduced. As the Mach number increases they become primarily neutral disturbances travelling downstream at the speed of the slowest-moving sound wave and the strength of the viscous-inviscid interaction and so the growth rate is very much reduced. We also discuss unsteady (upstream-travelling wave) modifications of the steady upstream influence solution to the supersonic triple deck problem (Stewartson and Williams (1969)) which arise in transonic flow.

The knowledge of the stability characteristics of the boundary layer to linear disturbances gained in this chapter is utilised in chapters 5 and 6 in formulating weakly nonlinear theories of the development of a wavepacket and of mode interaction. These lead on to the study of the boundary layer response to larger amplitude disturbances, effectively extending the work of Smith and Burgraff into the transonic regime. This yields some new features unique to transonic flow. Perhaps the most important of these is a weakly nonlinear description of a Benjamin-Feir secondary sideband instability of a primarily two-dimensional disturbance in the presence of a slight degree of spanwise warping. This has the effect of increasing the growth rate of the disturbance. The evidence is that this instability extends, to some degree, into the subsonic compressible regime.

Chapter 7 studies the interactive structure which arises at Mach numbers still closer to unity for relatively low frequency disturbances. It is of interest in that it captures an unsteady shock / boundary layer

interaction and presents a possibly powerful mechanism for bypass transition.

§4.2 Definitions And Scalings.

§4.2.1 Introductory comments.

We start with a summary of the Navier-Stokes equations, which govern the flow of the fluid. We introduce a reference length L_∞, and reference velocity U_∞. Since the fluid is compressible it is necessary to introduce reference values for the temperature, density, viscosity, heat conductivity, and coefficients of specific heat of the fluid at constant pressure and at constant volume. These are T_∞, ρ_∞, μ_∞, k_∞, $c_{p\infty}$, $c_{v\infty}$ respectively. We can now derive a typical value for the pressure, $\rho_\infty U_\infty^2$, and a representative time scale for the motion, L_∞/U_∞. Important non-dimensional quantities of the flow are the Reynolds number, $Re = U_\infty L_\infty \rho_\infty/\mu_\infty$, and the Mach number, $M_\infty = U_\infty/a_\infty$, where a_∞ is a typical speed for sound waves in the flow and is given by $a_\infty^2 = (\gamma-1)c_{p\infty}T_\infty$. Here γ is the ratio of specific heats of the gas, $c_{p\infty}/c_{v\infty}$. If we use the above quantities to non-dimensionalise the governing equations they reduce to

$$\frac{\partial \rho}{\partial t} + \underline{\nabla}.(\rho \underline{u}) = 0, \tag{4.2.1a}$$

$$\rho \frac{D\underline{u}}{Dt} = -\underline{\nabla}p + \frac{1}{Re}\underline{\nabla}\left((\mu'-2/3\mu)\underline{\nabla}.\underline{u}\right) + \frac{1}{Re}\left(\underline{\nabla}.(\mu\underline{\nabla}\,\underline{u}) + \underline{\nabla}(\mu\underline{\nabla}.\underline{u})\right), \tag{4.2.1b}$$

$$p = \rho T/\gamma M_\infty^2, \tag{4.2.1c}$$

$$\rho \frac{D(c_p T)}{Dt} = \frac{(\gamma-1)M_\infty^2}{Re}\Phi + (\gamma-1)M_\infty^2 \frac{Dp}{Dt} + \frac{1}{Re\sigma}\underline{\nabla}.(k\underline{\nabla}\,T). \tag{4.2.1d}$$

Here μ' is the bulk viscosity of the fluid

non-dimensionalised with μ_∞, $\underline{u}$ is the velocity vector (u,v,w), p the pressure, ρ the density, and T the temperature of the fluid at a point $\underline{r} = (x,y,z)$ at time t. The substantial derivative, D/Dt, is defined as $\partial/\partial t + \underline{u}.\underline{\nabla}$ and Φ is the dissipation function

$$\Phi = (1/4)\mu(\underline{\nabla}\,\underline{u} + (\underline{\nabla}\,\underline{u})^T):(\underline{\nabla}\,\underline{u} + (\underline{\nabla}\,\underline{u})^T) + (\mu'-2/3\mu)(\underline{\nabla}.\underline{u})^2. \qquad (4.2.1e)$$

The Prandtl number σ is defined as $\mu_\infty c_{p\infty}/k_\infty$ and is approximately 0.72 for air. We, however, make the approximation of a model fluid and assume $\sigma = 1$. The work of this thesis can be generalised for any value of σ, since the equations we later derive as governing the disturbance are independent of σ, whose only influence is on the basic flow and so on the normalisation of these governing equations. At transonic speeds it is also reasonable to assume that c_p and k do not vary with temperature and to set them equal to 1 in the above equations.

We now consider two limits of the Navier-Stokes equations as $Re \to \infty$. The first leads simply to the Euler equations

$$\frac{\partial \rho}{\partial t} + \underline{\nabla}.(\rho\underline{u}) = 0, \qquad (4.2.2a)$$

$$\rho \frac{D\underline{u}}{Dt} = -\underline{\nabla}\, p, \qquad (4.2.2b)$$

$$p = \rho T/\gamma M_\infty^2, \qquad (4.2.2c)$$

$$\rho \frac{DT}{Dt} = (\gamma-1)M_\infty^2 \frac{Dp}{Dt}. \qquad (4.2.2d)$$

If, in addition to being inviscid, the fluid motion is also irrotational then it will remain so and we can introduce a potential $\hat{\phi}$ such that $\underline{u} = \underline{\nabla}\hat{\phi}$. The potential can be shown to satisfy

$$\hat{\phi}_{xx}(a^2 - u^2) + \hat{\phi}_{yy}(a^2 - v^2) + \hat{\phi}_{zz}(a^2 - w^2) =$$
$$\hat{\phi}_{tt} + 2uv\hat{\phi}_{xy} + 2uw\hat{\phi}_{xz} + 2vw\hat{\phi}_{yz} + 2u\hat{\phi}_{xt} + 2v\hat{\phi}_{yt} + 2w\hat{\phi}_{zt}, \qquad (4.2.3a)$$

where a^2 is the speed of sound and varies with position. It is related to $\hat{\phi}$ by

$$a^2 - M_\infty^{-2} = -(\gamma-1)(\hat{\phi}_t + 1/2\ (\underline{\nabla}\hat{\phi})^2 - 1/2\ Q^2)), \qquad (4.2.3b)$$

where Q^2 is the magnitude of the velocity vector at the point at which the sound speed is equal to its reference value, M_∞^{-1}, assuming that the motion there is steady. The pressure and density at any point in the flow field can be calculated, if $\hat{\phi}$ is known, from the equations

$$a^2 = \gamma p/\rho, \qquad D/Dt\ (p\rho^{-\gamma}) = 0. \qquad (4.2.3c\text{-}d)$$

If we linearise (4.2.3) so that the flow is a small perturbation from a uniform flow in the x-direction, the equation governing the perturbation potential, $\tilde{\phi}$ is

$$\tilde{\phi}_{xx}(1-M_\infty^2) + \tilde{\phi}_{yy} + \tilde{\phi}_{zz} = M_\infty^2(\tilde{\phi}_{tt} + 2\tilde{\phi}_{xt}). \qquad (4.2.4)$$

Sound waves, which are responsible for the transfer of information throughout this inviscid, irrotational flow, satisfy this equation. Two-dimensional plane waves, i.e. those in which $\partial/\partial_y = \partial/\partial_z = 0$, have a streamwise velocity, c_s, given by

$$1 - M_\infty^2 = M_\infty^2(c_s^{\,2} - 2c_s),$$

i.e.

$$c_s = 1 - 1/M_\infty \quad \text{or} \quad c_s = 1 + 1/M_\infty. \qquad (4.2.5)$$

These expressions are simply the sum of the speed of the uniform flow and the speed of a sound wave which, without the uniform flow, would travel towards $x = -\infty$ or $+\infty$

respectively. As $M_\infty \to 0$ and the flow becomes subsonic these speeds become large and the free stream tends to react quasi-steadily to slower motions, such as boundary layer disturbances. Similarly, if $M_\infty \to \infty$, the free stream also reacts quasi-steadily to slow boundary layer disturbances but, since in this case both waves move downstream, its adjustment will be governed by a hyperbolic equation. On the other hand, if M_∞ is close to 1 the slower of the two speeds becomes close to zero. The wave moves upstream if $M_\infty < 1$ and downstream otherwise. This speed can be similar to that of the boundary layer instability waves and have an effect on their development. It is the magnitude of this velocity which is important in the stability of transonic boundary layers, especially in the case of two-dimensional disturbances.

The second limit of interest leads to the Prandtl boundary layer equations (see Stewartson (1964)). In this theory the steady Euler equations are assumed to be sufficient to determine the steady flow away from the surface of the body, where the effects of viscosity are presumed to be negligible. We impose inviscid boundary conditions on the Euler equations, which predict a slip velocity, $(u_e,0,w_e)$, at the surface. This is assumed to be reduced to zero in a thin region of thickness $O(Re^{-1/2})$ - the boundary layer. In this region we write $y = y_b Re^{-1/2}$, $\underline{u} = \underline{u}(x,y_b,z) = (U_0,Re^{-1/2}V_0,W_0)$, $\rho = R_0(x,y_b,z)$, and $T = T_0(x,y_b,z)$. On substitution into (4.2.1) and taking the limit $Re \to \infty$, this leads to

$$(R_0U_0)_x + (R_0V_0)_{y_b} + (R_0W_0)_z = 0, \qquad (4.2.6a)$$

$$R_0(U_0U_{0x} + V_0U_{0y_b} + W_0U_{0z}) = -p_x + C(x)(T_0U_{0y_b})_{y_b}, \qquad (4.2.6b)$$

$$R_0(U_0W_{0x} + V_0W_{0y_b} + W_0W_{0z}) = -p_z + C(x)(T_0W_{0y_b})_{y_b}, \qquad (4.2.6c)$$

$$p_{y_b} = 0, \tag{4.2.6d}$$

$$p = \rho T/\gamma M_\infty^2, \tag{4.2.6e}$$

$$R_0(U_0T_{0x} + V_0T_{0y_b} + W_0T_{0z}) = (\gamma-1)M_\infty^2(U_{0y_b}{}^2 + W_{0y_b}{}^2) + (\gamma-1)M_\infty^2(U_0p_x+W_0p_z) + C(x)(T_0T_{0y_b})_{y_b}, \tag{4.2.6f}$$

with boundary conditions $U_0 = V_0 = W_0 = 0$ at $y_b = 0$ and $U_0 \to u_e$, $W_0 \to w_e$ as $y_b \to \infty$. The driving pressure, p, is given by the solution of the Euler equations. We have used Chapman's law, $\mu = C(x)T_0$, to relate the viscosity to the tepmerature where $C(x) = \mu_w(x)/T_w(x)$. Here the subscript w indicates the value at the wall $y_b = 0$. This approximation is valid as long as the variations in the temperature are not too extreme, which will be the case at transonic speeds. This so-called classical boundary layer formulation, in which the external flow is calculated first and then a boundary layer fitted to it to ensure that the no-slip conditions are satisfied, is valid as long as the boundary layer does not separate and a solution for the boundary layer equations can be found over the whole body or in the region of interest.

§4.2.2 The scaling arguments and disturbance equations.

We presume that the steady flow over a surface and the associated boundary layer can be calculated, at least locally from a prescribed exterior flow, by using the above strategy and consider the stability of the boundary layer flow. Let us concentrate on a region in the vicinity of $(x_0,0,z_0)$ where there is no cross flow and so W_0 in equations (4.2.6) is zero, and the flow external to the boundary layer is parallel to the x-axis. Cross flow instability is itself a dangerous instability but we do not consider it here. We take the reference quantities used in deriving equations (4.2.1) to be those just outside the boundary layer at this point, and L_∞ to be a

representative streamwise length, say the chord length of an aerofoil. These reference values, the Chapman constant and the skin friction parameter $\hat{\lambda} = U_{0y_b}(0)/(U_\infty/L_\infty)$ vary with x_0 and z_0 and indeed the boundary layer profile itself develops on a length scale which is O(1) as $Re \to \infty$, and so in general the problem of the stability of the boundary layer is one in which this non-parallelism of the basic flow must be taken into account. We, however, concentrate on disturbances which are short relative to this development length and so reduce the base flow to be effectively parallel to leading order. We also presume that the body is flat to this order. The particular disturbances upon which we will concentrate are Tollmien-Schlichting waves which are, at the high Reynolds numbers required for the boundary layer approximation, viscous-inviscid phenomena (see §4.1). Since we are looking at disturbances in the transonic regime where M_∞ is close to unity and as a result the slowest-moving sound wave in the free stream is very slow compared with its speed in more supersonic or subsonic conditions, we look for disturbances in which this slow speed is important.

The boundary layer thickness at $(x_0,0,z_0)$ is of the order of $Re^{-1/2}C^{1/2}T_w$, from equation (4.2.6b,c&f), since in our non-dimensionalisation $\rho_w = T_w^{-1}$. We use, therefore, the O(1) variable $\tilde{y} = yRe^{1/2}C^{-1/2}T_w^{-1}$ to describe the main part of the boundary layer. Let the size of the streamwise velocities which make up the disturbance be ε and its streamwise length scale be L_x. If the spanwise scale is L_z we may introduce O(1) coordinates X and Z such that

$$[x - x_0,\ z - z_0] = [L_xX,\ L_zZ]. \qquad (4.2.7)$$

We write the streamwise velocity near the wall as $u = \varepsilon U$ where $U = O(1)$ as $Re \to \infty$. Near the wall we presume that the base flow, U_0, behaves like $U_0 \sim \lambda\tilde{y}$ as $\tilde{y} \to 0$, where λ is the local normalised skin friction. Therefore, if the disturbance is concentrated in a region where $\tilde{y} = \Delta Y$, where $Y = O(1)$ and $\Delta \ll 1$ as $Re \to \infty$, then the disturbance

size balances that of the base flow if

$$\varepsilon = \lambda\Delta. \tag{4.2.8}$$

A perturbation of this size is sufficient to provoke a nonlinear response in the boundary layer. The inertial effects associated with the perturbation are of a size $O(\rho_w\varepsilon^2/L_x)$ and so a typical pressure associated with the disturbance is of a size $O(\rho_w\varepsilon^2)$. Viscous effects close to the wall also balance these inertial terms if

$$\lambda\Delta^3/L_x = 1. \tag{4.2.9}$$

We concentrate on the so-called lower branch of the Tollmien-Schlichting disturbances in which the critical layer, i.e. that point in the boundary layer at which the speed of the disturbance matches that of the base flow, is close to the wall, where viscous effects are important. Thus, if the timescale associated with the motion is τ, we require the balance

$$L_x/\tau = \varepsilon \tag{4.2.10}$$

and we write $t = \tau T$, where T is $O(1)$ as $Re \to \infty$. Consider now the motion in the main part of the boundary layer where $\tilde{y}$ is $O(1)$. If the relative size of the streamwise disturbance velocity to the oncoming boundary layer velocity profile in this region is $\tilde{\varepsilon} << 1$, we expect the solution, for two-dimensional disturbances, to expand as follows.

$$u \sim U_0(\tilde{y}) + \tilde{\varepsilon}\,\tilde{U}(\tilde{y}) + \ldots, \tag{4.2.11a}$$

$$v \sim \tilde{\varepsilon}Re^{-1/2}(C^{1/2}T_w/L_x)\tilde{V}(\tilde{y}) + \ldots, \tag{4.2.11b}$$

$$\rho \sim R_0(\tilde{y}) + \tilde{\varepsilon}\,\tilde{R}(\tilde{y}) + \ldots, \tag{4.2.11c}$$

$$p \sim (\gamma M_\infty^2)^{-1} + \rho_w\varepsilon^2 P. \tag{4.2.11d}$$

We expect that $\varepsilon = O(\tilde{\varepsilon})$ as $Re \to \infty$. If we substitute the above into the Navier-Stokes equations and take the limit $Re \to \infty$ then

$$R_0\tilde{U}_X + U_0\tilde{R}_X + (R_0\tilde{V})_{\tilde{y}} = 0, \qquad (4.2.12a)$$

$$U_0\tilde{U}_X + \tilde{V}U_{0\tilde{y}} = 0, \qquad (4.2.12b)$$

$$U_0\tilde{R}_X + \tilde{V}U_{0\tilde{y}} = 0, \qquad (4.2.12c)$$

$$P_{\tilde{y}} = 0, \qquad (4.2.12d)$$

with solutions

$$\tilde{U} = A\,U_{0\tilde{y}}, \quad \tilde{V} = -A_X U_0, \quad \tilde{R} = AR_{0\tilde{y}}, \qquad (4.2.13a\text{-}c)$$

for some function $A(X,Z)$. Thus in the main part of the boundary layer the free stream is merely displaced upwards by an $O(\tilde{\varepsilon})$ amount, $-A$. As $\tilde{y} \to \infty$ this solution asymptotes

$$u \sim 1 + O(\tilde{\varepsilon}^2), \qquad (4.2.14a)$$

$$v \sim (-A_X)Re^{-1/2}C^{1/2}T_w/L_x, \qquad (4.2.14b)$$

$$\rho \sim 1 + O(\tilde{\varepsilon}^2), \qquad (4.2.14c)$$

and as $\tilde{y} \to 0$,

$$u \sim \lambda\tilde{y} + \tilde{\varepsilon}\lambda A = \varepsilon(Y + \tilde{\varepsilon}\lambda/\varepsilon\, A). \qquad (4.2.15)$$

Thus we see that the boundary condition on the velocity near the wall, U, as $Y \to \infty$, is $U \to Y + A$ and that $\tilde{\varepsilon} = \varepsilon/\lambda$. Consider now the effect that these motions in the boundary layer have on the free stream, where the motion is irrotational. There is a vertical velocity given by (4.2.14b) emerging from the boundary layer and if this decays over a vertical scale in which $y = H\bar{y}$, with $\bar{y} = O(1)$ as $Re \to \infty$, then the velocity can be described by a potential function

$$\hat{\phi} = x + S\phi(X,\bar{y},Z,T), \qquad (4.2.16)$$

where ϕ is O(1) as $Re \to \infty$ and

$$S = \varepsilon H Re^{-1/2} C^{1/2} T_w/(\lambda L_x). \qquad (4.2.17)$$

The pressure generated by this potential $\hat{\phi}$ is $(\gamma M_\infty^2)^{-1} - (S/L_x)\hat{\phi}_x$ from equations (4.2.3b-d) and this is $(\gamma M_\infty^2)^{-1} + (\rho_w \varepsilon^2)P$, and so of the same size as the pressure associated with the motions at the bottom of the boundary layer, provided that

$$L_x^2 \varepsilon / H Re^{-1/2} = C^{1/2} T_w^2/\lambda, \qquad (4.2.18a)$$

$$P = -\phi_x. \qquad (4.2.18b)$$

However from (4.2.8) and (4.2.9) we know that $\varepsilon = L_x^{1/3}\lambda^{2/3}$, and so

$$L_x^{7/3}/H Re^{-1/2} = C^{1/2} T_w^2/\lambda^{5/3}. \qquad (4.2.19)$$

Equation (4.2.19) contains the essence of the scalings which lead to a viscous-inviscid interaction.

We now need only to consider the relative sizes of the scales for the motion in the streamwise direction (L_x) and in the normal direction (H) in the free stream. It is a characteristic of transonic flows that, unlike in subsonic or supersonic flows (where $H = L_x$), typical normal length scales are much larger than streamwise distances. This is due essentially to the slower speed of travel of the information carried by the slower sound wave, in the streamwise direction, than in the normal or indeed in the spanwise directions. The latter speeds are unaffected by the oncoming streamwise speed which is close, in the case of transonic flow, to the speed of sound waves. If we write $(M_\infty^2 - 1) = md \ll 1$, where m is O(1) as $Re \to \infty$, then the equation governing the perturbation potential in the free stream (4.2.3a) is linear if $S/L_x \ll d$ and is

$$\phi_{yy} + \phi_{zz} = 2\phi_{xT} + m\phi_{xx}, \qquad (4.2.20)$$

if

$$H^2 = L_z^2 = \tau L_x = L_x^2/d. \qquad (4.2.21)$$

This balance is motivated by the desire to include unsteadiness in the equation governing the perturbation in the free stream, as well as in the wall layer equations. Thus the speed of travel of the Tollmien-Schlichting waves, $O(L_x/\tau)$, is of the same magnitude as the speed of travel of information in the free stream, $O(d/2)$.

The results (4.2.19&21) enable us to find all the scalings mentioned in the above analysis

$$L_x = Re^{-3/9}C^{1/3}T_w^{4/3}\lambda^{-4/3}, \qquad (4.2.22a)$$

$$L_z = Re^{-5/18}C^{5/18}T_w^{10/9}\lambda^{-13/9}, \qquad (4.2.22b)$$

$$H = Re^{-5/18}C^{5/18}T_w^{10/9}\lambda^{-13/9}, \qquad (4.2.22c)$$

$$d = Re^{-1/9}C^{1/9}T_w^{4/9}\lambda^{2/9}, \qquad (4.2.22d)$$

$$\tau = Re^{-2/9}C^{2/9}T_w^{8/9}\lambda^{-14/9}, \qquad (4.2.22e)$$

$$\varepsilon = Re^{-1/9}C^{1/9}T_w^{4/9}\lambda^{2/9}, \qquad (4.2.22f)$$

$$S = Re^{-5/9}C^{5/9}T_w^{11/9}\lambda^{-8/9}. \qquad (4.2.22g)$$

We now consider the magnitude of the spanwise velocity w and its effect on the above arguments. The spanwise variation of the motion in the free stream sets up a spanwise pressure gradient $(S/(L_zL_x))P_z$ and this forces a motion in the main part of the boundary layer. The results (4.2.13a-c), for the main body of the boundary layer, remain unaltered but are supplemented by

$$w = Re^{-5/18}C^{5/18}T_w^{1/9}\lambda^{5/9}\, B/(U_0R_0), \qquad (4.2.23)$$

where $B_x = -P_z$. As the region where $\tilde{y} = \varepsilon Y/\lambda$, with $Y = O(1)$, is approached the size of w increases so that

$$w = Re^{-3/18}C^{1/6}T_w^{-1/3}\lambda^{1/3}\, B/Y. \qquad (4.2.24)$$

This, however, is small compared with the magnitude of the streamwise velocity variations ε, and so the motion of the disturbance close to the wall is effectively two-dimensional, although the motion in the free stream is three-dimensional. This feature arises directly from the shortening of streamwise length scales in transonic flows. Thus A is a function of X and T only.

To summarise then, we expand the flow variables as follows as $Re \to \infty$. The streamwise and spanwise distances are as defined by (4.2.7) and (4.2.22). In the lower deck, i.e. the region close to the wall, we have

$$y \sim Re^{-11/18} C^{11/18} T_w^{13/9} \lambda^{-7/9} Y, \qquad (4.2.25a)$$

$$u \sim \varepsilon U, \qquad (4.2.25b)$$

$$v \sim Re^{-7/18} C^{7/18} T_w^{5/9} \lambda^{7/9} V, \qquad (4.2.25c)$$

$$w \sim 0, \qquad (4.2.25d)$$

$$\rho \sim T_w^{-1}, \qquad (4.2.25e)$$

$$p \sim (\gamma M_\infty^2)^{-1} + Re^{-2/9} C^{2/9} T_w^{-1/9} \lambda^{4/9} P. \qquad (4.2.25f)$$

In the main part of the boundary layer, the middle deck, we write

$$y \sim Re^{-1/2} C^{1/2} T_w \tilde{y}, \qquad (4.2.26a)$$

$$u \sim U_0 + \varepsilon/\lambda \; A(X) \; U_{0\tilde{y}}, \qquad (4.2.26b)$$

$$v \sim \varepsilon Re^{-1/2} C^{1/2} T_w/(L_x \lambda) \; (-A_X(X)) \; U_0(\tilde{y}), \qquad (4.2.26c)$$

$$w \sim Re^{-5/18} C^{5/18} T_w^{1/9} \lambda^{5/9} \; B/(U_0 R_0), \qquad (4.2.26d)$$

$$\rho \sim R_0(\tilde{y}) + \varepsilon/\lambda \; A(X) \; R_{0\tilde{y}}(\tilde{y}), \qquad (4.2.26e)$$

$$p \sim (\gamma M_\infty^2)^{-1} + Re^{-2/9} C^{2/9} T_w^{-1/9} \lambda^{4/9} P, \qquad (4.2.26f)$$

and in the free stream or upper deck we define a normal coordinate, $\bar{y}$ and a velocity potential ϕ,

$$y \sim H\bar{y}, \tag{4.2.27a}$$

$$\hat{\phi} \sim x + S\,\phi(X,\bar{y},Z), \tag{4.2.27b}$$

$$p \sim (\gamma M_\infty^2)^{-1} + Re^{-2/9}C^{2/9}T_w^{-1/9}\lambda^{4/9}\,\bar{P}, \tag{4.2.27c}$$

$$M_\infty^2 - 1 \sim dm. \tag{4.2.27d}$$

The density and the pressure in the upper deck can be found from the relations (4.2.3b-d) and in fact

$$\bar{P} = -\phi_X(X,\bar{y},Z). \tag{4.2.27e}$$

If we substitute these expansions into the Navier-Stokes equations we find that, as we expected, the disturbance is governed by the system

$$U_X + V_Y = 0, \tag{4.2.28a}$$

$$U_T + UU_X + VU_Y = -P_X + U_{YY}, \tag{4.2.28b}$$

$$U = V = 0 \text{ at } Y = 0 \text{ and } U \to Y + A \text{ as } Y \to \infty, \tag{4.2.28c-e}$$

$$\bar{P}_{yy} + \bar{P}_{ZZ} = 2\bar{P}_{XT} + m\bar{P}_{XX}, \tag{4.2.28f}$$

$$\bar{P} \to P \text{ and } \bar{P}_y \to A_{XX} \text{ as } \bar{y} \to 0.\ \bar{P} \to 0 \text{ as } X^2+\bar{y}^2+Z^2 \to \infty. \tag{4.2.28g-i}$$

See Figure (4.2.1).

If, at these Mach numbers, there are transverse velocities of a size $O(\varepsilon L_Z/L_X) = O(Re^{-1/18}C^{1/18}T_w^{2/9}\lambda^{1/9})$, they enter into the lower deck equations, which become

$$U_X + V_Y + W_Z = 0, \tag{4.2.29a}$$

$$U_T + UU_X + VU_Y + WU_Z = -P_X + U_{YY}, \tag{4.2.29b}$$

$$W_T + UW_X + VW_Y + WW_Z = W_{YY}, \tag{4.2.29c}$$

where W is the scaled spanwise velocity of the disturbance. The boundary conditions on U remain unaltered but that on W is $W \sim \bar{B}/Y$ as $Y \to \infty$ where $\bar{B}_X = 0$. Thus in the main part of the boundary layer this transverse flow is represented by

$$w = Re^{-3/18} C^{3/18} T_w^{-1/3} \lambda^{1/3} \bar{B}/(U_0 R_0), \qquad (4.2.30)$$

as opposed to (4.2.23). In this case, however, $\bar{B}_X = 0$ and w does not vary in the streamwise direction in the main deck. As a result the motions forced in the free stream are independent of X and, although described by a potential of $O(Re^{-4/9})$ rather than $O(Re^{-5/9})$ as in (4.2.22g), they cannot interact with the lower deck through equations (4.2.27e), even though the pressure contribution, associated with its time derivative, is $O(Re^{-2/9})$. Thus we see that three-dimensional motions are possible within the wall layer with these scalings. However in many flows we expect that w is of size $O(Re^{-5/18})$ near the wall as in (4.2.26d) and so the motion is governed by (4.2.28). It is upon this case that this thesis concentrates although equation (4.2.29) could be of interest in the study of wave-vortex interactions at transonic speeds.

§4.2.3 Further comments and discussion.

Another regime of interest should be mentioned here. If the disturbances in the wall layer are such that the length scales are similar in both the spanwise and streamwise directions, the above structure is not a valid description of the motion. Instead the appropriate structure is that of the so-called major transonic mode identified by Smith (1989). This has the unsteady three-dimensional boundary layer equations governing the motion in the lower deck, i.e. an additional $-P_z$ term on the right hand side of (4.2.29c), but the free stream equation is reduced to

$$\bar{P}_{yy} + \bar{P}_{ZZ} = 0. \qquad (4.2.31)$$

Here, instead of reducing the relative streamwise scale of the motion, the closeness of the Mach number to unity causes the free stream motions to be governed entirely by transverse effects. The wavelength of the disturbance is $O(Re^{-3/8})$ here, which is shorter than the wavelength in the motions described by (4.2.29), which are associated with the minor transonic mode of Smith (1989). The longer waves imply that any growth rate over the scale of the waves will be relatively less in the case of the minor modes. Hence the term "minor".

The regime leading to (4.2.28) is of relevance to nearly two-dimensional disturbances in the boundary layer which are at angles of at most $O(Re^{-1/18})$ away from the direction of the oncoming two-dimensional flow. These disturbances are such that, in a slightly supersonic free stream, they can be directed to lie close to or inside the wave-Mach cone, which lies about the x-axis with a semi-angle of $\tan^{-1}[(M_\infty^2-1)^{1/2}]$ which here is $O(m^{1/2}Re^{-1/18})$. All Tollmien-Schlichting waves, of length $O(Re^{-3/8})$ and directed within this cone, decay if $(M_\infty^2-1) = O(1)$, and is positive (Ryzhov and Zhuk (1980)). In this case the free stream reacts in a quasi-steady fashion. However, it is possible for disturbances which are sufficiently oblique as to be directed outside the cone to grow (the major mode of Smith (1989)). In a subsonic free stream there is the possibility of growing two-dimensional disturbances. The present structure can be used to study the change in the behaviour of the waves as the Mach number increases above unity or the direction of a 3D disturbance in a supersonic free stream approaches and passes into the wave-Mach cone. It is found that the Tollmien-Schlichting mode becomes subject to strong non-parallel effects as its rate of growth decreases.

§4.3.1 The dispersion relation.

As a first step in the analysis of equations (4.2.28), we assume that the disturbance size is small, so that they may be linearised about the undisturbed state, U = Y, and consider normal mode solutions. This approach has the advantage of making clear the structure of the solutions admitted by the equations and also acts as a starting point for the weakly nonlinear analysis pursued in later sections of this thesis. We therefore look for solutions in which

$$(U,V,A,P,\bar{P}) \sim (Y,0,0,0,0) + h[\, E(u,v,a,p,\bar{p}) + c.c \,] + \ldots$$

$$h \to 0, \tag{4.3.1}$$

where $E = \exp i(\alpha X + \beta Z - \Omega T)$, and c.c. represents the complex conjugate of the preceding expression. We first derive a dispersion relation for these linearised disturbances and then examine their behaviour in the limits of high frequency and increasing Mach number.

If we substitute (4.3.1) into (4.2.28) we find that

$$i\alpha u + v_Y = 0, \tag{4.3.2a}$$

$$-i\Omega u + i\alpha Y u_Y + v = -i\alpha p + u_{YY}, \tag{4.3.2b}$$

$$u \to a \text{ as } Y \to \infty, \quad u = v = 0 \text{ at } Y = 0, \tag{4.3.2c-e}$$

$$\bar{p}_{yy} - \gamma^2 \bar{p} = 0, \quad \gamma^2 = 2\Omega\alpha + \beta^2 - m\alpha^2, \tag{4.3.2f-g}$$

$$\bar{p} \to p, \ \bar{p}_y \to -\alpha^2 a \text{ as } \bar{y} \to 0 \text{ and } \bar{p} \to 0 \text{ as } \bar{y} \to \infty. \tag{4.3.2h-j}$$

Differentiation of (4.3.2b) and use of (4.3.2a) leads to an equation for u_Y with solution

$$u_Y = D\mathrm{Ai}(\xi), \quad \xi = (i\alpha)^{1/3} Y + \xi_0, \quad \xi_0 = -i^{1/3}\Omega/\alpha^{2/3}, \tag{4.3.3a-c}$$

where Ai is Airy's function and D is a constant. The boundary conditions applied to this solution lead to

$$p = (i\alpha)^{-2/3} D Ai'(\xi_0), \tag{4.3.4a}$$

$$a = (i\alpha)^{-1/3} D \int_{\xi_0}^{\infty} Ai(q)dq, \tag{4.3.4b}$$

$$-\pi/3 < \arg(i\alpha)^{1/3} < \pi/3. \tag{4.3.4c}$$

Thus,

$$\frac{p}{a} = (i\alpha)^{-1/3} \frac{Ai'(\xi_0)}{\int_{\xi_0}^{\infty} Ai(q)dq}. \tag{4.3.5}$$

In addition, the equation for $\bar{p}$ (4.3.2f-g,j) and the interaction conditions (4.3.2h-i) lead to

$$\bar{p} = p e^{-\gamma \bar{y}}, \qquad \text{Real}(\gamma) > 0, \tag{4.3.6a-b}$$

and so

$$\frac{p}{a} = \frac{\alpha^2}{\gamma}. \tag{4.3.7}$$

Thus, combining (4.3.7) and (4.3.5), we have the dispersion relation

$$(i\alpha)^{1/3} \frac{\alpha^2}{\gamma} = \frac{Ai'(\xi_0)}{\kappa}, \tag{4.3.8a}$$

$$\kappa = \int_{\xi_0}^{\infty} Ai(q)dq, \qquad \gamma^2 = (2\Omega\alpha + \beta^2 - m\alpha^2), \tag{4.3.8b-c}$$

$$-\pi/3 < \arg(i\alpha)^{1/3} < \pi/3, \quad \text{Real}(\gamma) > 0. \tag{4.3.8d-e}$$

We concentrate here on the problem of the spatial stability of the boundary layer, although we shall also

consider temporal instability when we look at the behaviour of the disturbances as $m \to \infty$ in §4.3.5. Therefore we presume Ω and β to be real and given, corresponding to a known frequency and wavenumber in the spanwise direction. With these assumptions (4.3.8) is solved for $\alpha = \alpha_r + i\alpha_i$ with α_r and α_i real. Then the wave number of the disturbance in the streamwise direction, which depends on its frequency and orientation, is α_r, whilst its spatial growth rate, $p^{-1}dp/dX$, is $(-\alpha_i)$.

We investigate this dispersion relation in the following sections. The first considers neutral downstream-travelling modes. Next we consider the upstream influence modes predicted by equation (4.3.8). In §4.3.5, we look at the effects of large m, which have, in certain cases, connections with relatively high frequency disturbances. We end with some comments on the linear theory of boundary layer stability in transonic flow.

§4.3.2 Neutral waves.

We first consider neutral disturbances, i.e. those with $\alpha_i = 0$, for which $\alpha = \alpha_N$ and $\Omega = \Omega_N$, say. The condition for Ai'/κ to be real is, from Drazin and Reid (1981),

$$\Omega_N = d_1 \alpha_N^{2/3}, \qquad (4.3.9)$$

and so

$$\alpha_N^{7/3} = d_2(2d_1\alpha_N^{5/3} + \beta^2 - m\alpha_N^2)^{1/2},$$

$$d_1 \approx 2.3, \quad d_2 \approx 1.0. \qquad (4.3.10a\text{-}c)$$

Since $\mathrm{Real}(\gamma) > 0$ we must also have

$$\beta^2/\alpha^2 > m - 2d_1/\alpha_N^{1/3} = m - 2\Omega_N/\alpha_N, \qquad (4.3.11a)$$

i.e.

$$\beta^{*2}/\alpha^{*2} > (M_\infty^2 - 1) - 2c^*, \qquad (4.3.11b)$$

where the superscript * indicates a quantity unscaled with the Reynolds number, and c^* is the speed of the wave. This is in contrast to the result (Smith (1989)) for the regime with $M_\infty^2-1 = O(1)$ and $c^* \sim O(Re^{-1/8})$ as $Re \to \infty$, which reads

$$\beta^{*2}/\alpha^{*2} > (M_\infty^2-1). \qquad (4.3.12)$$

This latter result implies that neutral waves must be directed outside the wave-Mach cone which subtends an angle of $\tan^{-1}((M_\infty^2-1)^{1/2})$ with the direction of the oncoming flow. On the other hand (4.3.11) shows that linear neutral Tollmien-Schlichting waves can be directed inside the cone, in the transonic regime, if they are travelling sufficiently fast. What is of importance is the relative speed of the wave to that of the slowest-moving sound wave in the free stream. Thus even if both the characteristic sound waves are being swept downstream by a supersonic free stream, a neutral wave, and by implication the neighbouring growing waves, can exist if they themselves travel more quickly downstream so that in their frame of reference there is a characteristic which moves upstream. The wave must be subsonic in the free stream according to the definition of Mack (1987).

It is worth noting, in order to extend the results of this work away from the transonic regime, that similar behaviour occurs as a more oblique, "major mode" wave approaches its cut-off angle, $\beta^{*2}/\alpha^{*2} \to (M_\infty^2-1)+$. We know from Smith (1989) that the dispersion relation for neutral modes in this case is

$$\alpha_N^{1/3}(\alpha_N^2 + \beta^2) = d_2[\beta^2 - (M_\infty^2-1)\alpha_N^2]^{1/2}, \qquad (4.3.13)$$

where $\partial_x = iRe^{3/8}\alpha_N$, $\partial_z = iRe^{3/8}\beta$ and $\partial_t = -iRe^{2/8}d_1\alpha_N^{2/3}$. On the approach to the cut-off, the neutral wavenumber can be shown to be

$$\alpha_N \sim \varepsilon^{3/11}\bar{\alpha}_N, \qquad \bar{\alpha}_N = 2^{3/11}[M_\infty^2-1]^{3/11}\left(\frac{d_2}{M_\infty^2}\right)^{6/11}\bar{\beta}^{3/11}, \tag{4.3.14a-b}$$

$$\beta \to (M_\infty^2-1)^{1/2}\alpha_N + (M_\infty^2-1)^{1/2}\varepsilon\bar{\beta}, \tag{4.3.14c}$$

where $\varepsilon << 1$ and $\bar{\beta} = O(1)$. Thus the speed of the wave increases to $d_1\varepsilon^{-1/11}\bar{\alpha}_N^{-1/3}Re^{-1/8}$. We have incurred a relative error of the order of

$$Re^{-1/8}2\Omega\alpha_N/[\beta^2-(M_\infty^2-1)\alpha_N^2] \sim O(Re^{-1/8}\varepsilon^{-9/11}),$$

in presuming that the free stream reacts quasi-steadily. This becomes $O(1)$ when $\varepsilon \sim Re^{-11/72}$ at which point, including the effects of free stream unsteadiness, the corrected expression for $\bar{\alpha}_N$ becomes

$$\bar{\alpha}_N = 2^{3/11}\left(\frac{d_2}{M_\infty^2}\right)^{6/11}[\bar{\beta}(M_\infty^2-1) + d_1\bar{\alpha}_N^{5/3}]^{3/11}. \tag{4.3.15}$$

Now we see that as $\bar{\beta}(M_\infty^2-1) \to 0$ the unsteady term in the free stream equation dominates the decay of the disturbance there and we have the result

$$\bar{\alpha}_N = d_2(2d_1)^{1/2}/\ M_\infty^2. \tag{4.3.16}$$

Here $\partial_x = iRe^{3/9}\bar{\alpha}_N$ and $\partial_z = iRe^{3/9}(M_\infty^2-1)^{1/2}\bar{\alpha}_N + iRe^{2/9}(M_\infty^2-1)^{1/2}\bar{\beta}$. The wave speed is $O(Re^{-1/9})$.

We have seen that, as a neutral wave approaches the cut-off of the wave-Mach cone, unsteadiness in the free stream takes over as the controlling influence there and enables waves to exist at least just inside the cone ($\bar{\beta} < 0$).

§4.3.3 Unstable / stable Tollmien-Schlichting waves.

We now turn to a consideration of the more general downstream-travelling waves. We first consider the limit $m \to -\infty$ which should match with the subsonic Tollmien-Schlichting wave dispersion relation of, say, Smith (1979a&b). We scale the variables according to

$$(\alpha,\Omega,\beta) \sim (\tilde{\alpha}|m|^{3/8},\tilde{\Omega}|m|^{2/8},\tilde{\beta}|m|^{7/8}), \qquad (4.3.17)$$

and find that (4.3.8) becomes

$$\left(\frac{Ai'(\xi_0)}{\kappa}\right)(2\tilde{\alpha}\tilde{\Omega}|m|^{-9/8} + \tilde{\beta}^2 + \tilde{\alpha}^2)^{1/2} = (i\tilde{\alpha})^{1/3}\tilde{\alpha}^2. \qquad (4.3.18)$$

When $|m|$ becomes $O(Re^{1/9})$, so that $(1-M_\infty^2)$ is $O(1)$ as $Re \to \infty$, this reduces to

$$\left(\frac{Ai'(\xi_0)}{\kappa}\right)(\tilde{\beta}^2 + \tilde{\alpha}^2)^{1/2} = (i\tilde{\alpha})^{1/3}\tilde{\alpha}^2, \qquad (4.3.19)$$

where $\partial_x = iRe^{3/8}\tilde{\alpha}$, $\partial_z = iRe^{3/8}\tilde{\beta}$ and $\partial_t = -iRe^{2/8}\tilde{\Omega}$. This is the subsonic dispersion relation if, as in (4.2.28a-e), transverse pressure gradients are neglected within the boundary layer. In subsonic interactive flow the free stream is governed by the equation $\bar{P}_{xx} + \bar{P}_{zz} + \bar{P}_{yy} = 0$, in these new scalings, whilst the boundary layer equations are as in (4.2.29a-b) but with $-|M_\infty^2-1|\ P_z$ added to the right hand side of (4.2.29b). To obtain these normalised equations in this form, where the Mach number dependence has been scaled out (except in the boundary layer) it is necessary to scale the spanwise lengthscale with $|M_\infty^2-1|^{-7/8}$ and the streamwise lengths with $|M_\infty^2-1|^{-3/8}$. Similarly the streamwise and transverse velocities must be scaled differently. To see this we can either consider the equations of Smith (1989) or carry out a similar analysis to that used in §4.2.2, only this time aiming for the above equation in the free stream rather than (4.2.28f). Therefore as $|M_\infty^2-1| \to 0$, and the subsonic flow approaches transonic speeds, the angle described by the ratio $\tilde{\beta}/\tilde{\alpha}$

decreases to $O((1-M_\infty^2)^{1/2})$ and the dispersion relation becomes that of the minor transonic mode described by Smith (1989), but in the case of a subsonic free stream. This result is identical with (4.3.19). Thus we see that the solutions of (4.3.8a-d) match back to the standard subsonic results as $m \to -\infty$, approaching the minor oblique transonic mode in the case of three-dimensional disturbances.

Figure 4.3.1 illustrates the growth rate for the normal mode disturbances for values of m of order unity. It can be seen that two-dimensional growing waves can survive in the just-supersonic regime, in contrast to the fully supersonic case where all modes decay.

The effects of large values of m, and the approach to a supersonic free stream are considered in §4.3.5.

§4.3.4 Upstream influence modes.

There are two distinct modes of wave satisfying the dispersion relation (4.3.8). Firstly, there are the downstream-travelling Tollmien-Schlichting waves covered in both the previous two sections and the next one and secondly, there are upstream-travelling, unsteady modifications of the upstream influence mode in supersonic flow. (See Stewartson and Williams (1969)). The eigenvalue corresponding to these upstream influence waves is illustrated in Figure 4.3.2.

For $\Omega = 0$ (4.3.8) reduces to

$$(i\alpha)^{1/3}\alpha^2 = -c_1(\beta^2 - m\alpha^2)^{1/2}, \qquad (4.3.20a)$$

$$c_1 = -3Ai'(0) = 0.7665, \qquad (4.3.20b)$$

together with the conditions (4.3.8d-e). Thus $\alpha = (-i)r$ where r is real and is the positive root of

$$r^{7/3} = c_1(\beta^2 + mr^2)^{1/2}, \qquad (4.3.21)$$

so that

$$r \sim c_1^{3/4} m^{3/8} \quad \text{as } \beta \to 0 \quad \text{and} \quad r \sim c_1^{3/7} \beta^{3/7} \text{ as } \beta \to \infty. \tag{4.3.22a-b}$$

The first of these results matches with the steady two-dimensional supersonic result of Stewartson and Williams. The second has no Mach number dependence and illustrates the approach to the more oblique major modes of Smith (1989). It also shows how the length scale of the upstream influence decreases as the mode becomes directed away from the downstream direction and, as a result, becomes less influenced by the fast-moving supersonic flow in the free stream.

Two-dimensional, unsteady upstream influence modes also exist. We first consider the case of small m. If $m\alpha^2 << 2\Omega\alpha$ and $\beta^2 << 2\Omega\alpha$ as $\Omega \to 0$ the appropriate asymptote for α is

$$\alpha \sim (2\Omega)^{3/11} c_1^{6/11} \exp(-5\pi i/11). \tag{4.3.23}$$

This result corresponds to relatively long wave motions in which a boundary layer reacts quasi-steadily to a free stream governed by the equation $\bar{P}_{yy} = 2\bar{P}_{XT}$. The relative errors in this result are those made in neglecting $m\bar{P}_{XX}$ and $\bar{P}_{ZZ}$ in the free stream equation and are $O(m\Omega^{-8/11})$ and $O(\beta^2\Omega^{-14/11})$ respectively. If we allow $m \sim O(\Omega^{8/11})$ and $\beta \sim O(\Omega^{7/11})$ as $\Omega \to 0$ this result matches with the upstream influence modes appropriate to the more transonic shock regime described in chapter 7. These are characterised by the time scale of the motion being determined by the slow motions in the free stream. The boundary layer can be expected to react instantaneously over these long time scales.

If Ω is large, then, for two-dimensional motions, the asymptote

$$\alpha \sim \Omega^{3/5} 2^{1/5} \exp(-4\pi i/5), \tag{4.3.24}$$

is appropriate. Here we have used (4.3.26). This solution

predicts $\gamma \sim 2^{3/5}\Omega^{4/5}\exp(-2\pi i/5)$ and $(i\alpha)^{1/3} \sim 2^{1/5}\Omega^{1/5}\exp(-\pi i/10)$, and so satisfies conditions (4.3.8d-e). The asymptote is also valid if the wave is oblique, provided that $\beta << O(\Omega^{4/5})$ as $\Omega \to \infty$. It also requires $m << O(\Omega^{2/5})$. At high frequencies these modes represent upstream-travelling and rapidly decaying waves. If the unsteadiness in the free stream is not strong enough to dominate the effects of the streamwise derivatives, i.e. $m = \Omega^{2/5}\bar{m}$, the argument of α in (4.3.24) varies from $-4\pi/5$ as $\bar{m} \to 0$ to $-3\pi/4$ as $\bar{m} \to \infty$, at which point the scaling for α becomes $\alpha \sim \Omega^{1/2}$. At large $\bar{m}$ the unsteadiness in the free stream is of secondary importance and the scalings match with those appropriate to high frequency, unsteady upstream influence in fully supersonic flow (see, for example, Duck (1985)).

If β is large ($\beta >> \Omega^{4/5}$), however, and $|m| << O(\Omega^{2/5})$ the high frequency asymptote is replaced by the oblique-wave asymptote

$$\alpha \sim \Omega^{1/3}\beta^{1/3}\exp(-2\pi i/3). \qquad (4.3.25)$$

The waves described by (4.3.24&25) are also possible if $\bar{m} < 0$ and the flow is subsonic, in both the two- and three-dimensional motions. The question therefore arises of what happens to these modes at smaller frequencies, since there are no acceptable exponential upstream influence modes in steady subsonic flow, rather the upstream influence is algebraic (Smith, Brighton, Jackson and Hunt (1981)). Figure 4.3.3 illustrates solutions of (4.3.8) for negative m. The crosses indicate a cut-off in the solutions, as the frequency decreases, which occurs when $\text{Real}(\gamma) = 0$. At this point the required decay of the disturbances in the free stream is lost. This cut-off is generally affected by viscous effects but we will illustrate it here by considering the case where cut-off occurs at large Ω, or when $|m|$ is great and the flow is very subsonic. In this case, using the result,

$$Ai'(\xi_0)/\kappa(\xi_0) \to -\xi_0 \quad \text{as } \xi_0 \to \pm\infty, \qquad (4.3.26)$$

the dispersion relation becomes

$$(2\Omega\alpha + \beta^2 + |m|\alpha^2)^{1/2} = \alpha^3/\Omega, \qquad (4.3.27)$$

where β, $|m|$ and Ω are all assumed to be real and $\beta^2 \sim O(|m|\alpha^2)$, $c \sim O(|m|)$, and $\Omega >> \alpha^{2/3}$ as $|m| \to \infty$. Cut-off occurs when $\text{Real}(\gamma) = 0$ and so

$$(2\Omega\alpha + \beta^2 + |m|\alpha^2)^{1/2} = -id, \qquad (4.3.28)$$

where d is real and positive. We have taken the root with negative imaginary part to ensure that the phase velocity of the wave at cut-off is directed outwards, away from the boundary layer. If α and Ω at cut-off are denoted by α_c and Ω_c, then we can show that

$$\Omega_c = (\sqrt{3}/2)^{3/2}|m|^{3/2}d^{1/2}, \qquad (4.3.29a)$$

$$\alpha_c = (\sqrt{3}/2)^{1/2}|m|^{1/2}d^{1/2}\exp(-5\pi i/6), \qquad (4.3.29b)$$

$$d = |m|^2\sqrt{3}(1 \pm \theta)/4, \quad \theta = (1 - 16\beta^2/3|m|^4)^{1/2}. \qquad (4.3.29c\text{-}d)$$

Therefore for two-dimensional disturbances ($\theta = 1$), in the limit of large frequency or large $|m|$, a cut-off occurs at

$$\Omega_c = 3|m|^{5/2}/4, \qquad \alpha_c = \sqrt{3}|m|^{3/2}\exp(-5\pi i/6)/2,$$

$$c_c = \Omega_c/\alpha_c = \sqrt{3}|m|\exp(5\pi i/6)/2, \qquad \text{Real}(c_c) = -3|m|/2. \qquad (4.3.30a\text{-}d)$$

This result requires $\Omega_c/\alpha_c^{2/3} \sim |m|^{3/2} >> 1$. For sufficiently oblique waves or smaller values of $|m|$, such that $\beta > \sqrt{3}|m|^2/4$, there is no cut-off since there is no suitable real d. Otherwise, if β is non-zero, there are two possible cut-off frequencies, implying a range of Ω between which these upstream influence modes are not possible. The cut-off (4.3.30) remains valid, neglecting $O(\beta^2/|m|^4)$ corrections , but there is an additional cut-off at the smaller frequency where

$$\Omega_c = \sqrt{3}|m|^{1/2}\beta/2, \quad \alpha_c = \beta\exp(-5\pi i/6)/|m|^{1/2}. \qquad (4.3.31a\text{-}b)$$

For this result to be valid, i.e. for the high frequency or large $|m|$ approximation to be correct, we require that $\Omega_c/\alpha_c^{2/3} \sim |m|^{5/6}\beta^{1/3} >> 1$, i.e. $\beta >> |m|^{-5/2}$ as $|m| \to \infty$. For smaller values of β the cut-off is affected by viscous effects and such simple analysis as that presented above is not possible.

We now turn to a consideration of the subsonic modes which have $\Omega = 0$ and $\xi_0 = 0$. These are steady, oblique upstream influence modes. Here $\alpha = -iq\beta^{3/7}c_1^{3/7}$ where $(1-q^2\mu) = q^{7/3}$ and $\mu = c_1^{6/7}|m|/(\beta^{8/7})$. This result is similar to (4.3.21) but with a crucial sign change. If μ is small, i.e. for a small value of $|m|$, or for a large value of β, then $q = 1$, agreeing with the result (4.3.22b). However, a large value of μ implies $q \sim \mu^{-1/2}$ and $\alpha \sim -i\beta/|m|^{1/2}$. This latter limit corresponds to the motion becoming primarily one with little interaction between the boundary layer and the free stream. We note, too, that the vertical decay scale of these motions, $[\text{Real}(\gamma)]^{-1}$, becomes very long as $|m| \to \infty$. Again, as in the similar limit with a supersonic free stream, the extent of the upstream influence decreases as the motion becomes more oblique. For all values of μ, $|\beta/\alpha| > |m|^{1/2}$ and so, in a sense, this influence is confined to be outside of a cone of semi-angle $|m|^{1/2}$ upstream of the disturbance. Similar behaviour to this can be seen in the inviscid wave dispersion relation (4.3.27) which holds for large β. If $|m| \sim O(\beta^{4/3}\Omega^{-2/3})$ as $\beta \to \infty$ then (4.3.27) implies

$$(\beta^2 + |m|\alpha^2)^{1/2} = \alpha^3/\Omega,$$

as opposed to the result (4.3.28). As $|m|$ increases still further, $\alpha \sim -i\beta/|m|^{1/2}$. This result implies that, as fully subsonic flow is approached and $|m|$ increases, oblique upstream-travelling disturbances become primarily governed by the free stream motion, with the dominant balance in the free stream being $|m|\bar{P}_{xx}+\bar{P}_{zz} = 0$. The

interaction with the boundary layer gives rise only to higher order effects. This is similar to the fate of downstream-travelling Tollmien-Schlichting waves as $m \to +\infty$, described in the next section.

The results of this section are summarised in Figure 4.3.4. This illustrates the various inviscid modes discussed (large Ω and large β) and how they vary as m decreases from $+\infty$ to $-\infty$.

§4.3.5 The limit of increasing Mach number.

To investigate the effect of a large positive value of m we first consider two-dimensional waves, as these are likely to be the most strongly affected. Neutral waves must, from (4.3.11a), travel at speeds, c, greater than m/2. Thus since ξ_0 scales like $c\alpha^{1/3}$, there are two possibilities. Firstly, if α remains O(1) as $m \to \infty$, then $\xi_0 \to \infty$, and we can make use of the large ξ_0 expansion (4.3.26) to simplify the dispersion relation. This corresponds to approaching the upper branch disturbances which, due to their faster speeds, are unaffected by the transonic nature of the flow, at least with these scalings of the Mach number with the Reynolds number. See the comments on the upper branch of Tollmien-Schlichting disturbances in §4.3.6. The second possibility has $\alpha \sim O(m^{-3})$ as $m \to \infty$. With this scaling ξ_0 remains O(1) and the disturbances are of the lower branch type. This possibility will be shown to correspond to a weakening of the interaction between the boundary layer and the free stream equations. As a result the problem of determining the growth rate of the lower branch disturbances becomes one in which the non-parallel nature of the boundary layer profile must be considered.

If $m \to \infty$ and we scale $\Omega = m^{5/2}\bar{\Omega}$, $\alpha = m^{3/2}\bar{\alpha}$, $\beta = m^2\bar{\beta}$, where $\bar{\Omega}$, $\bar{\alpha}$, and $\bar{\beta}$ are O(1), we find that

$$(2\bar{\Omega}\bar{\alpha} + \bar{\beta}^2 - \bar{\alpha}^2)^{1/2} = \frac{\bar{\alpha}^3}{\bar{\Omega}}\left(1 + \frac{(1+i)\bar{\alpha}}{\sqrt{2}\, m^{9/4}\bar{\Omega}^{3/2}}\right), \qquad (4.3.32)$$

and so, given $\bar{\Omega}$ and $\bar{\beta}$,

$$\bar{\alpha} = \bar{\alpha}_0\left(1 - \frac{(1+i)\bar{\alpha}_0\,(2\bar{\Omega}\bar{\alpha}_0 + \bar{\beta}^2 - \bar{\alpha}_0^{\,2})}{\sqrt{2}\,m^{9/4}\bar{\Omega}^{3/2}\,(5\bar{\Omega}\bar{\alpha} + 3\bar{\beta}^2 - 2\bar{\alpha}^{\,2})}\right), \qquad (4.3.33a)$$

$$(2\bar{\Omega}\bar{\alpha}_0 + \bar{\beta}^2 - \bar{\alpha}_0^{\,2})^{1/2} = \bar{\alpha}_0^{\,3}/\bar{\Omega}. \qquad (4.3.33b)$$

This approach can also be used to derive the high frequency limit of the dispersion relation, used in the weakly nonlinear analysis of chapters 5 and 6. If we look at the limit $\Omega \to \infty$ and, using the scalings above as a guide, scale $\alpha = \bar{\alpha}\Omega^{3/5}$, $\beta = \bar{\beta}\Omega^{4/5}$ and $m = \bar{m}\Omega^{2/5}$ we derive a similar result to (4.3.33) giving $\bar{\alpha}$ at relatively high frequency. If $\bar{m}$ is set equal to zero this latter expression corresponds to a high frequency, lower branch disturbance in transonic flow, where the free stream motions are determined primarily by the balance $\bar{P}_{yy} = 2\bar{P}_{xT}$. The limit above corresponds to a disturbance forced to be of high frequency due to the cut-off imposed by the requirement that the wave move downstream more rapidly than the sound waves in the free stream.

On the other hand, as mentioned above, it is possible for the disturbances to remain of the lower branch type as the flow becomes more supersonic. If, as $m \to \infty$, we write

$$\alpha = \hat{\alpha}m^{-3}, \quad \Omega = \hat{\Omega}m^{-2} \quad \beta = \hat{\beta}m^{-5/2}, \qquad (4.3.34)$$

where $\hat{\alpha}$, $\hat{\Omega}$, and $\hat{\beta}$ are O(1), the dispersion relation becomes

$$(2\hat{\Omega}\hat{\alpha} + \hat{\beta}^2 - \hat{\alpha}^2)^{1/2} = \frac{(i\hat{\alpha})^{1/3}\hat{\alpha}^2(\kappa/Ai')(\hat{\xi}_0)}{m^{9/2}}, \qquad (4.3.35a)$$

$$\hat{\xi}_0 = (-i)^{1/3}\hat{\Omega}/\hat{\alpha}^{2/3} = (-i)^{1/3}\Omega/\alpha^{2/3} = \xi_0. \qquad (4.3.35b)$$

Thus, for large m and to first order, the dispersion relation is simply that for plane sound waves, represented by (4.3.35a) with the right hand side set equal to zero. If we look for spatial instability, we must have

$$\hat{\alpha} = \hat{\alpha}_0 - am^{-9}, \qquad 2\hat{\Omega}\hat{\alpha}_0 + \hat{\beta}^2 - \hat{\alpha}_0^2 = 0, \qquad (4.3.36a\text{-}b)$$

$$(a)^{1/2} = \frac{(i\hat{\alpha})^{1/3}\hat{\alpha}^2(\kappa/Ai')(\hat{\xi}_0)}{(2\hat{\alpha}_0 - 2\hat{\Omega})^{1/2}}. \qquad (4.3.36c)$$

Since $\hat{\xi}_0$ is real to first order it is convenient to rewrite (4.3.36c) in terms of the Teitjens function, F (see, for example, Drazin and Reid (1981)).

$$(a)^{1/2} = \frac{\hat{\alpha}_0^3}{\hat{\Omega}} \frac{1}{(1 - F(\bar{Y}))} \frac{\hat{\alpha}_0^{1/2}}{(\hat{\alpha}_0^2 + \hat{\beta}^2)^{1/2}}, \qquad (4.3.37a)$$

$$\bar{Y} = \hat{\Omega}/\hat{\alpha}_0^{2/3}. \qquad (4.3.37b)$$

The relative error in assuming that the argument of the Teitjens function is real is that in assuming there is no interaction and so is, if $\hat{\beta} = 0$ so that $\hat{\Omega} \sim O(\hat{\alpha}_0)$, of size $O(\hat{\alpha}_0^2/(1-F)^2m^9)$. This becomes O(1) when $\hat{\Omega}$ is large, $O(m^{9/2})$, and so $\hat{\alpha}_0 \sim O(m^{9/2})$. This corresponds to $\Omega \sim m^{5/2}$, $\alpha \sim m^{3/2}$, and so it is the regime covered by equation (4.3.33). Oblique disturbances, as well as high frequencies, will reinstate the interaction to first order. If $\hat{\beta}$ is large then $\hat{\alpha}_0 \sim \hat{\beta}$. If in addition $\hat{\Omega} \sim \hat{\beta}^{2/3}$ then $\bar{Y}$ remains O(1) and the disturbances remain of the lower branch type. The interaction is reinstated when $\hat{\beta} = O(m^{27/8})$. This corresponds to $\partial_X \sim m^{3/8}$, $\partial_T \sim m^{2/8}$ and $\partial_Z \sim m^{7/8}$ and these scalings indicate a return to the $L_X \sim Re^{-3/8}$ scalings for oblique, minor mode Tollmien-Schlichting disturbances in supersonic flows, as the importance of the unsteadiness in the free stream equations decreases. Alternatively this result can be viewed in reverse, as an illustration of the fate of oblique disturbances as their direction approaches that of the wave-Mach cone.

Figures 4.3.5a&b show the real and imaginary parts of $(1-F)^{-1}$ and $-(1-F)^{-2}$ for real argument and illustrate that there is a cut-off in these disturbances, associated with Real(γ) (= Real($a^{1/2}$)) approaching zero as

$\bar{Y} = (\hat{\alpha}_0^2 - \hat{\beta}^2)/(2\hat{\alpha}_0^{5/3}) \rightarrow 0.85+$. This result is the equivalent, for non-neutral waves at large values of m, of (4.3.11). If $\bar{Y}$ is less than 0.85 (an approximate value) $a^{1/2}$ becomes negative. Thus, as m increases, the speed of the waves approaches m/2, the sonic speed, but only waves with a frequency greater than $\Omega_c = (.597)/m^2$, and with wavenumber greater than $2\Omega_c/m$, can exist in the two-dimensional case. Thus the effects of this cut-off become less wide-ranging as the Mach number increases. Another point to notice is that the speed of the waves is

$$\text{Real}\left(\frac{\Omega}{\alpha}\right) = \text{Real}\left(\frac{m}{2} \left\{1 + \frac{a\, m^{-7}}{2\Omega}\right\} \right), \qquad (4.3.37c)$$

which is less than the sound speed, m/2, if Real(a) < 0. This is the case for a range of values of $\bar{Y}$ just greater than the cut-off, $\bar{Y} \approx 0.85$. These modes are therefore supersonic in the sense of Mack (1987), in that their speed is less than $1-M_\infty^{-1}$. They are unstable for values of $\bar{Y}$ less than 2.3 and stable otherwise, although the growth rates are very small.

These lower branch modes in a supersonic free stream are long and develop slowly due to their weak interaction with the boundary layer. Their growth is thus likely to be affected by the non-parallel nature of the basic boundary layer flow. We have been able to neglect these effects in the above analysis due to the short length scales involved in the disturbances. A useful way to view these modes is to consider the temporal stability problem and consider the motion in a frame travelling downstream with the speed of the slowest-travelling sound wave, m/2. The free stream equation for two-dimensional disturbances becomes, with the scalings (4.3.34),

$$m^{-9}\bar{P}_{yy} = \bar{P}_{XX} + 2\bar{P}_{XT}. \qquad (4.3.38)$$

If we now make the transformation

$$\partial_T = -1/2\ \partial_X + m^{-9}\partial_{\hat{T}}, \qquad (4.3.39)$$

this becomes

$$\bar{P}_{yy} = 2\bar{P}_{x\hat{T}}. \qquad (4.3.40)$$

The nonlinear boundary layer equation (4.2.28b) becomes

$$-1/2\ U_X + UU_X + VU_Y + m^{-9}U_{\hat{T}} = -P_X + U_{YY},$$

and the interactive boundary conditions and continuity equation in (4.2.28) remain unaltered. If we linearise this system, in the limit of large m, we find a dispersion relation

$$(2\omega\hat{\alpha})^{1/2}Ai'(\bar{\xi}_0) = \hat{\alpha}^2(i\hat{\alpha})^{1/3}\kappa(\bar{\xi}_0), \quad \bar{\xi}_0 = -(i\hat{\alpha})^{1/3}/2. \qquad (4.3.41a\text{-}b)$$

In this formulation $\partial_{\hat{T}} = -i\omega$, $\partial_X = i\hat{\alpha}$ and (4.3.41) is an equation for ω, the second order contribution to the frequency, as a function of $\hat{\alpha}$. The first order expression for the frequency is simply the acoustic relation

$$\hat{\Omega} = \hat{\alpha}/2, \quad \Omega = \alpha m/2. \qquad (4.3.41c)$$

The above approach is used in Appendix 5A to investigate the largem properties of the weakly nonlinear solution of (4.2.28) found in chapter 5.

Alternatively, we can introduce a long spatial scale, rather than the slow temporal one, via the transformations

$$\partial_X \to \partial_X + m^{-9}\partial_{\hat{X}}, \quad \partial_T \to -1/2\ \partial_X. \qquad (4.3.42a\text{-}b)$$

The free stream equation then reads

$$\bar{P}_{yy} = 2\bar{P}_{x\hat{X}}, \qquad (4.3.43)$$

and the dispersion relation is, if $\partial_T = -i\hat{\Omega}$ and $\partial_{\hat{X}} = ia$,

$$(-2\hat{\Omega}a)^{1/2}Ai'(\bar{\xi}_0) = (2\hat{\Omega})^2(2i\hat{\Omega})^{1/3}\kappa(\bar{\xi}_0), \quad \bar{\xi}_0 = -(2\hat{\Omega}i)^{1/3}/2. \qquad (4.3.44a\text{-}b)$$

We now consider how three-dimensional effects alter these small growth rates. First, as mentioned above, if $\partial_z = i\hat{\beta}$ is as large as $O(m^{7/8})$ the interaction is reinstated at first order and equations (4.3.41&44) do not apply. We note, next, that (4.3.36b) can be rewritten as

$$2\frac{\hat{\Omega}}{\hat{\alpha}} = 2c = \left(1 - \frac{\hat{\beta}^2}{\hat{\alpha}^2}\right). \qquad (4.3.45)$$

Thus as $\hat{\beta} \to \infty$, $\hat{\alpha} \sim \hat{\beta}$ and $c \to 0$, agreeing with the first point. For $O(1)$ $\hat{\beta}$, however, we see that the oblique nature of a disturbance has the result of reducing the speed of the acoustic wave and therefore decreasing the long spatial scale over which growth occurs. This, in turn, increases the growth rate of the disturbance. Finally, if β is as small as $O(m^{-2})$ as $m \to \infty$ it will enter in the form of a $+\beta^2$ inside the square root in equations (4.3.41a) and (4.3.44a) and affect the growth rate directly.

In the derivation of the triple deck equations (4.2.28) we neglect terms associated with compressibility of relative order $\alpha^{1/3}Re^{-1/9}$, if the surface is cooled or heated (i.e. $R_y(0) \neq 0$), and of size $\alpha^{2/3}Re^{-2/9}$ if the surface is adiabatic ($R_y(0) = 0$). In addition in making the assumption that the local values of the skin friction, Chapman's constant, etc. are constant we incur an error of $O(\alpha Re^{1/3})$. The relatively weak interaction as $m \to \infty$ and the associated slow growth rates balance these errors when $m \sim Re^{1/90}$, $Re^{2/99}$, and $Re^{1/36}$ in turn, since $\alpha \sim m^{-3}$. This corresponds to $M_\infty^2 - 1 \sim Re^{-1/10}$, $Re^{-1/11}$, and $Re^{-1/12}$ respectively. The first two scalings of the Mach number give rise (in the case of linear disturbances) to modes primarily governed by a free stream interacting with a boundary layer satisfying

$$-1/2\ U_X = -P_X + U_{YY}, \qquad (4.3.46)$$

and the effects of compressibility enter at a higher order in the Reynolds number. However the third size of Mach number, $M_\infty = 1 + O(Re^{-1/12})$, leads to a wave structure

that moves an O(1) distance downstream in the time scale associated with the interaction and its growth or decay. Alternatively, in the spatial stability context, its growth is determined over an O(1) distance in x as $Re \to \infty$. Thus the normalisation used in deriving (4.2.28) varies over the length scale of the interaction and the question of growth or decay of the disturbance becomes fundamentally affected by the non-parallel nature of the boundary layer. If M_∞ is any larger it seems that the first mode wave becomes simply a neutral acoustic wave which is swept downstream instantaneously on the timescales upon which the boundary layer can react. Nonlinear solutions may well involve singularities in the boundary layer as this pressure wave travels past, since the boundary layer can react only relatively slowly. See Elliot, Smith and Cowley (1983).

§4.3.6 Further comments and discussion.

We now make some final points concerning the linear theory of boundary layer disturbances with a transonic free stream. The first concerns inviscid inflexional, or Rayleigh modes. These are the compressible counterpart of inviscid modes which are possible if the velocity profile contains an inflexion point. In incompressible flow the flat plate, Blasius profile contains no such inflexion point and so no Rayleigh modes are possible. In compressible flow, however, the inflexion point criterion is replaced by the generalised inflexion point condition - $D(\bar{R}D\bar{U}) = 0$ where D stands for $\partial/\partial y$ and $\bar{R}$ and $\bar{U}$ are the undisturbed density and velocity profiles respectively (Lees and Lin (1946), Lees and Reshotko (1962)). The eigenvalue problem for determining the wavenumber, given the frequency, for a two-dimensional disturbance is

$$p'' - \frac{2\bar{M}'}{\bar{M}} p' - \alpha^*(1 - \bar{M}^2)p = 0, \quad p'(0) = 0, \quad p(\infty) = 0,$$

$$\bar{M} = \bar{R}^{1/2}(\bar{U} - c^*)M_\infty .$$

Here, $\partial_x = iRe^{1/2}\alpha^*$, $\partial_t = iRe^{1/2}\Omega^*$ and $c^* = \Omega^*/\alpha^*$. The factoring out of the skin friction etc., carried out in the derivation of (4.2.28) has not been carried out here. This linear, inviscid equation can be analysed in the limit $M_\infty \to 1$, $c^* \to 0$ with the scalings $\alpha^* \sim O(\varepsilon^{3/2})$, $\Omega^* \sim O(\varepsilon^{5/2})$, $c^* \sim O(\varepsilon)$, and $M_\infty^2 - 1 \sim O(\varepsilon)$ where $\varepsilon << 1$. The result is the neutral inviscid version of the high frequency / large m result (4.3.32). The scalings of the two systems also match. This limit corresponds to approaching the long, neutral sonic wave of Lees and Lin in the transonic regime, where the speed of this wave is small. The growth rate of this mode, at transonic speeds, is determined by higher order matching, and the effect of the critical layer at the generalised inflexion point is determined in an intermediate viscous-inviscid regime. The analysis of this system is, of course, similar to the high Reynolds number upper branch analysis of Bodonyi and Smith (1981), for the incompressible Blasius profile, or that of Gajjar and Cole (1989) who consider the compressible case and the effect of the generalised inflexion point.

The effects of a transonic free stream, rather than a subsonic or supersonic free stream, as studied by Gajjar and Cole, would seem to be as follows. Firstly, since the speed of the modes is faster, a new balance will be set up when this speed is of the same order as the sound speed in the free stream, just as in the case of lower branch disturbances. The scales themselves will depend on the wall conditions which determine the position of the generalised inflexion point in the flow. For adiabatic walls we have the speed $c \sim \delta$, $L_x \sim \delta^7$ and $M_\infty^2 - 1 \sim \delta$. There is a lower region, including the critical layer, of thickness $Re^{-1/2}\delta$, a Stokes layer of thickness $Re^{-1/2}\delta^3$ and an unsteady region in the free stream of thickness $Re^{1/2}\delta^{21}$. Here δ is $Re^{-1/17}$. In the case of a cooled or heated wall, in contrast, $L_x \sim \delta^5$, and the thicknesses of the regions mentioned above become $Re^{-1/2}\delta$, $Re^{-1/2}\delta^2$, and $Re^{1/2}\delta^{18}$ with now $\delta = Re^{-1/13}$. These are slight modifications of the scales used by Gajjar and Cole, who find $\delta = Re^{-1/16}$ and $Re^{-1/12}$ in turn. In each case the

vertical velocity expands like $Re^{-1/3}L_x^{-1}\delta(v_0 + \delta v_1 + \delta^2 v_2 + \ldots)$ and the critical layer smooths out the logarithmic irregularity in v_2 in the case of the insulated wall and in v_1 otherwise. This provokes a phase shift of $-\pi$ for linear disturbances which balances, in magnitude, the phase shift from the Stokes layer which is responsible for the growth of lower branch disturbances. Nonlinear effects will come into play at low amplitudes within the critical layer. This structure will govern the disturbances as M_∞ increases above unity and, as the flow becomes still more supersonic, we can expect a development into non-parallel modes similar to that which occurs in the case of the lower branch, although due to their greater speeds the upper branch will survive, unaffected by non-parallelism at first order, until larger values of the Mach number.

The second comment regards the relative importance of these two-dimensional non-parallel supersonic first mode disturbances. They have slow growth rates both because of their length and due to the weakness of the interaction. The linear stability of the boundary layer is thus likely to be determined by the development of oblique first mode disturbances which are not forced to be non-parallel in the just-supersonic case but, instead, become non-parallel at large Mach numbers ($M_\infty \sim Re^{1/10}$) (see Smith (1989)). In addition, of course, there are the inviscid Rayleigh modes which are generally faster-moving and shorter and therefore more unstable than first mode disturbances. Their faster speeds allow them to last further into the supersonic regime before becoming primarily a neutral sound wave (the Lees and Lin sonic wave) as their speed approaches $1-1/M_\infty$. Finally we should consider waves which decay vertically within the boundary layer itself, such as those which arise from wall cooling. An analysis of the effects of wall cooling on the first mode disturbances and on the Rayleigh modes is presented in Seddoughi, Bowles and Smith (1990).

§4.4 SUMMARY.

Below we list the main results of this chapter.

1) We have derived the scalings for the minor mode of Tollmien-Schlichting disturbances as the Mach number of the flow nears unity. The scalings bring in an unsteadiness of motions in the free stream reflecting the finite speed of travel of information there on the time scales associated with the disturbance. The length scale in the streamwise direction of these disturbances is $O(Re^{1/3})$ as $Re \to \infty$. The transverse length scale is $O(Re^{-5/18})$ and the Mach number, M_∞, is such that $|M_\infty^2-1| = O(Re^{-1/9})$.

2) The free stream unsteadiness is also important in fully supersonic flows when Tollmien-Schlichting waves are directed close to the wave-Mach cone.

3) We have studied the unsteady modifications of the supersonic upstream influence mode which exist in transonic flow. These are upstream-travelling, decaying waves. These waves also exist in just-subsonic flow but are subject to a cut-off as the flow becomes fully subsonic.

4) As the Mach number increases from unity, Tollmien-Schlichting waves, directed within the wave-Mach cone, continue to exist, subject to a cut-off at low frequencies. Their growth rates become strongly diminished in supersonic flow and they develop into modes that are primarily acoustic in nature with a weak interaction between the boundary layer and the free stream giving rise to the small growth rate. The waves with frequencies just above the cut-off frequency have speeds greater than $1-M_\infty^{-1}$ and are supersonic. When $M_\infty = 1+O(Re^{-1/12})$ the growth occurs over a scale at which the boundary layer itself develops and the waves become affected by the associated non-parallel effects.

FIGURE CAPTIONS FOR CHAPTER 4.

Figure 4.2.1 A sketch showing the scales of motion for Tollmien-Schlichting disturbances in a boundary layer associated with a transonic free stream ($(M_\infty^2-1) = 1 + mRe^{-1/9}$). The streamwise length scale is $O(Re^{-3/9})$ and is much shorter than the spanwise or vertical scales (both $O(Re^{-5/18})$). The speed of the disturbance is $O(Re^{-1/9})$.

Figure 4.3.1 Plots of the growth rate ($-\alpha_i$) against frequency (Ω) for linear waves in a transonic boundary layer. The dispersion relation for these waves is equation (4.3.8). The Mach number of the free stream is $1 + mRe^{-1/9}/2$ and so is slightly supersonic in the cases where m is positive. Figure (a) shows waves for a range of values of m. Figure (b) shows waves with a subsonic free stream. Figure (c) illustrates waves with positive m and a small value of Ω. For some large positive values of m it proves difficult to find solutions for small values of Ω. It is possible that this has some connection with the cut-off at small Ω and large m described in §4.3.5.

Figure 4.3.2 Upstream influence modes in just supersonic flow. Figure (a) shows two-dimensional modes as the frequency, Ω, increases from zero for various values of $m = (M_\infty^2-1)Re^{1/9}$ (m = 1/20, 1/4, 1, 4, 8). Figure (b) presents oblique modes as Ω increases for m = 1 and various values of the spanwise wavenumber, β^2 = 1/2, 2, 6, 10.

Figure 4.3.3 Upstream influence modes in just-subsonic flow. A cross indicates the position at which a mode becomes subject to the cut-off described in §4.3.4. Figure (a) shows two-dimensional modes as Ω increases for m of -2, -1, -1/4, -1/100. Also shown is the position of the cut-off when it is governed by inviscid effects (valid for large $|m|$, see equation (4.3.30)). Figure (b) illustrates oblique subsonic modes with $|m| = 5$ and shows the position of the cut-off for $\beta^2 = 1, 4, 8, 24, 36$. Figure (c) is of similar modes but with $|m| = 1$ and $\beta^2 = 1/10, 1/4, 1, 4, 8$ and shows that at small enough $|m|$ sufficiently oblique waves can avoid the cut-off (equation (4.3.29)).

Figure 4.3.4 A sketch showing the variation of inviscid upstream-travelling modes with m and β. The value of m varies from $-\infty$ (subsonic flow) to ∞ (supersonic flow). The various asymptotes illustrated in this figure can be found in §4.3.4.

Figure 4.3.5 Figure (a) shows the real and imaginary parts of $(1-F(\bar{Y}))^{-1}$, where F is the Teitjens function and $\bar{Y}$ is real. The point marked (1) indicates the value at which $\text{Real}((1-F)^{-1}) = 0$, corresponding to the cut-off in the downstream-travelling waves in the limit of large m. See equation (4.3.37). Figure (b) illustrates $-(1-F)^{-2}$. Values of $\bar{Y}$ for which the imaginary part of this is positive correspond to unstable waves in (4.3.37). The points marked (1) and (3) are neutral points with (1) corresponding to the cut-off mentioned above. The point marked (2) corresponds to the minimum value of $\bar{Y}$ such that the waves described by (4.3.37) are subsonic, i.e. their speed is greater than $1-M_\infty^{-1}$.

Figure 4.2.1

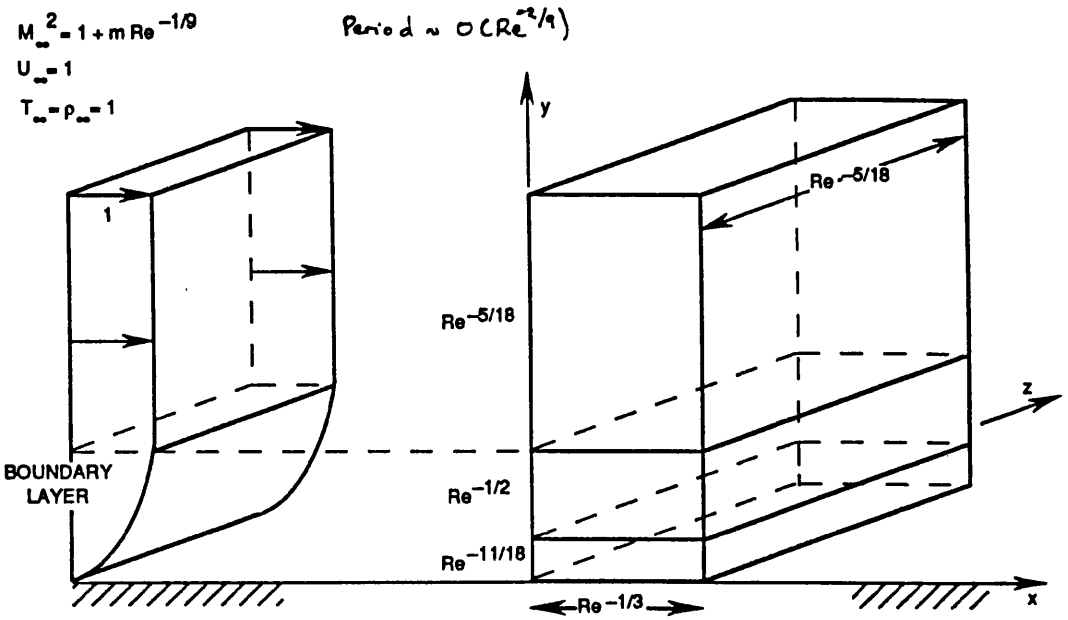

Figure 4.3.1

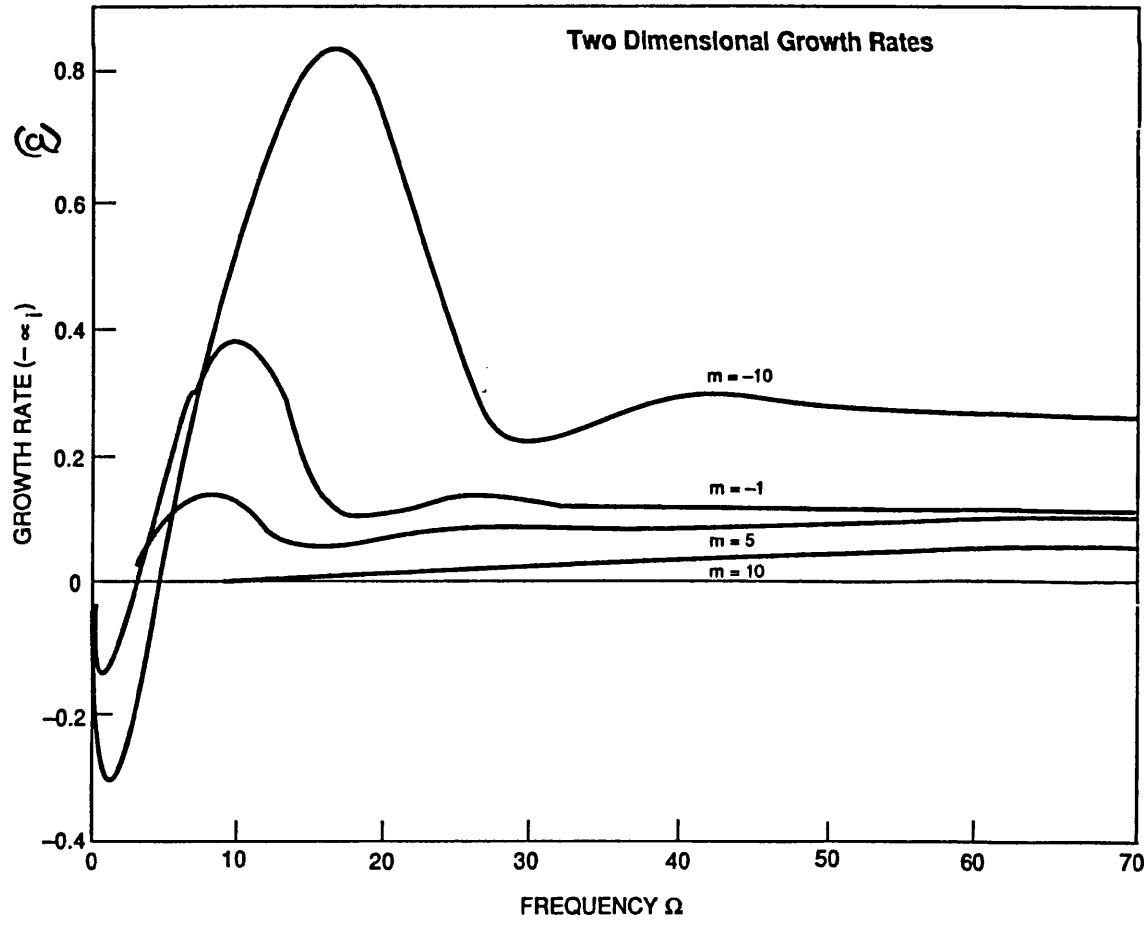

Figure 4.3.1

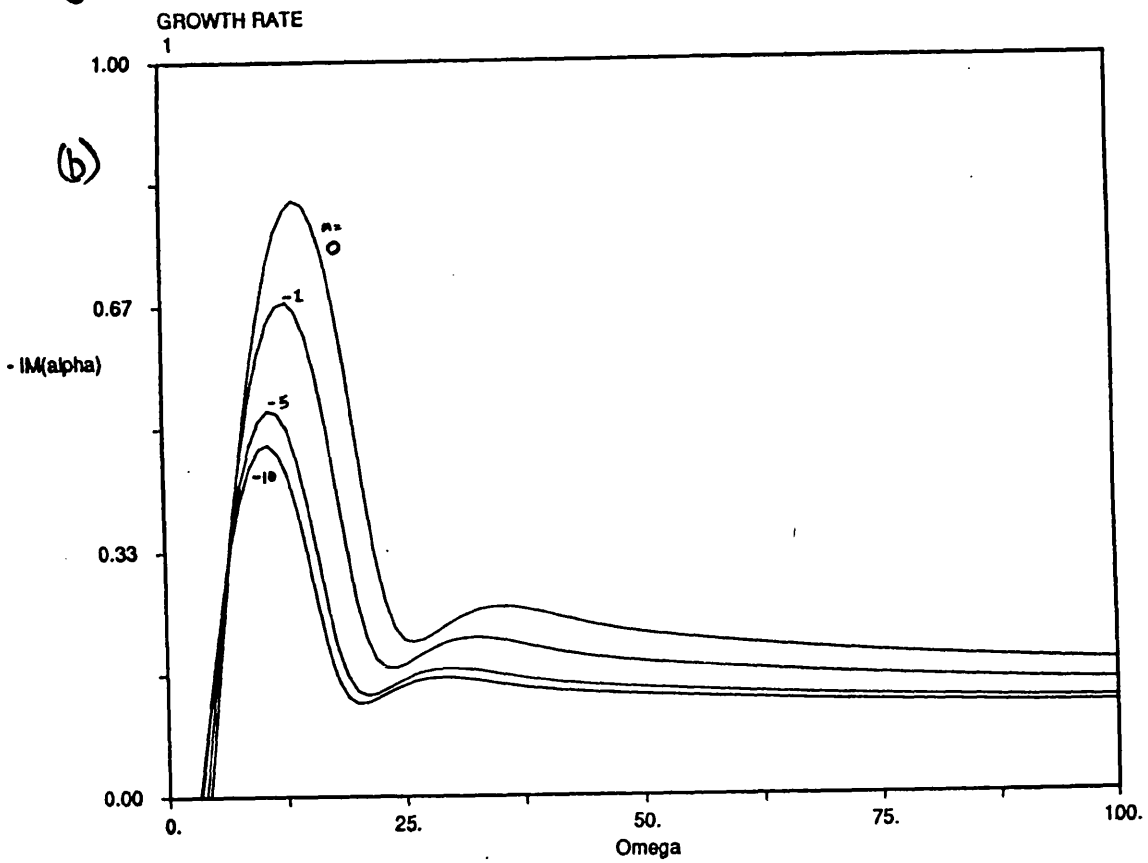
GROWTH RATE
1
1.00
(b)
m=0
-1
-5
-10
0.67
- IM(alpha)
0.33
0.00
0.
25.
50.
75.
100.
Omega

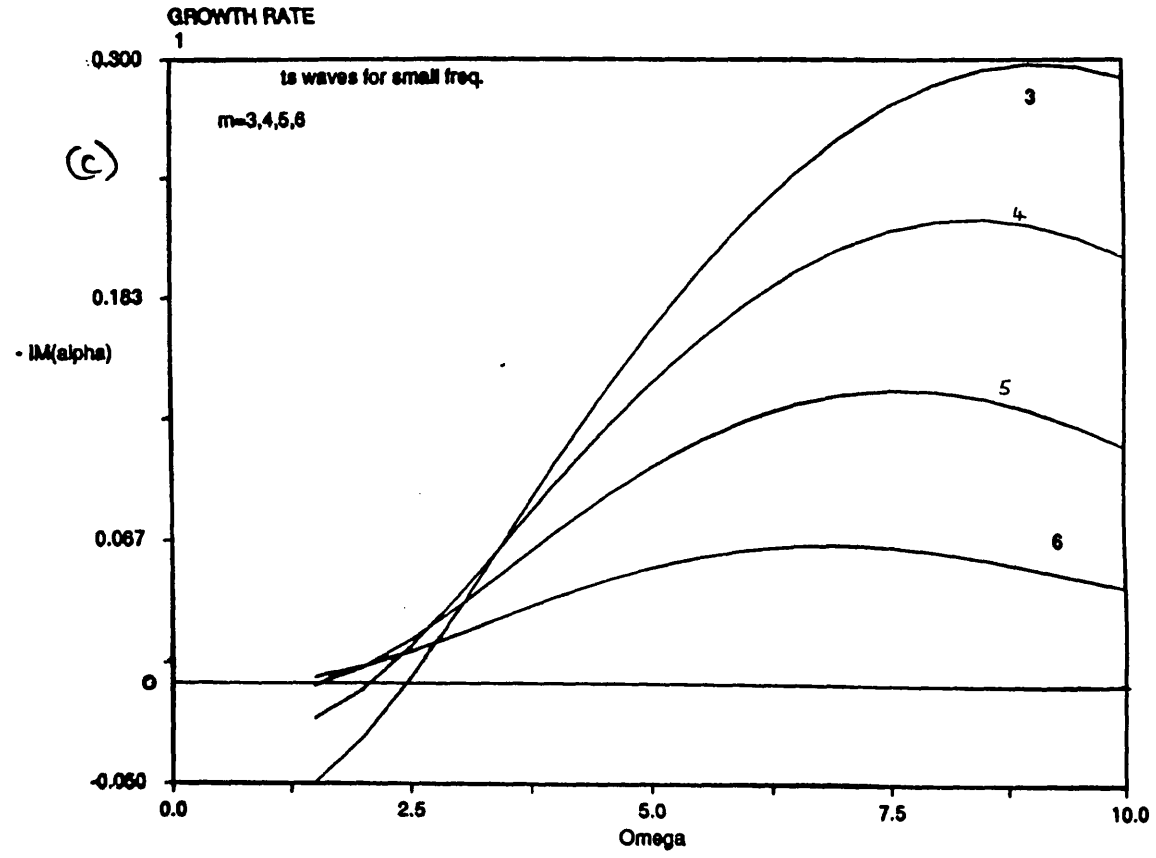
GROWTH RATE
1
0.300
ts waves for small freq.
m=3,4,5,6
(c)
3
4
5
6
0.183
- IM(alpha)
0.067
0
-0.050
0.0
2.5
5.0
7.5
10.0
Omega

Figure 4.3.2

Upstream Influence Mode

(a)

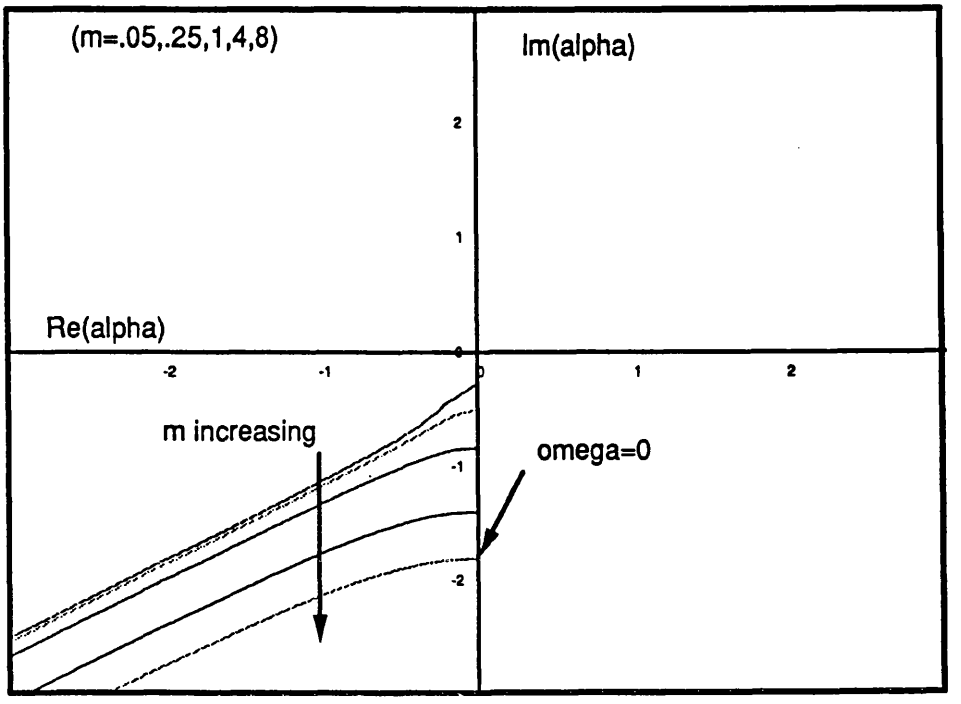

Oblique Upstream Influence Modes

(b)

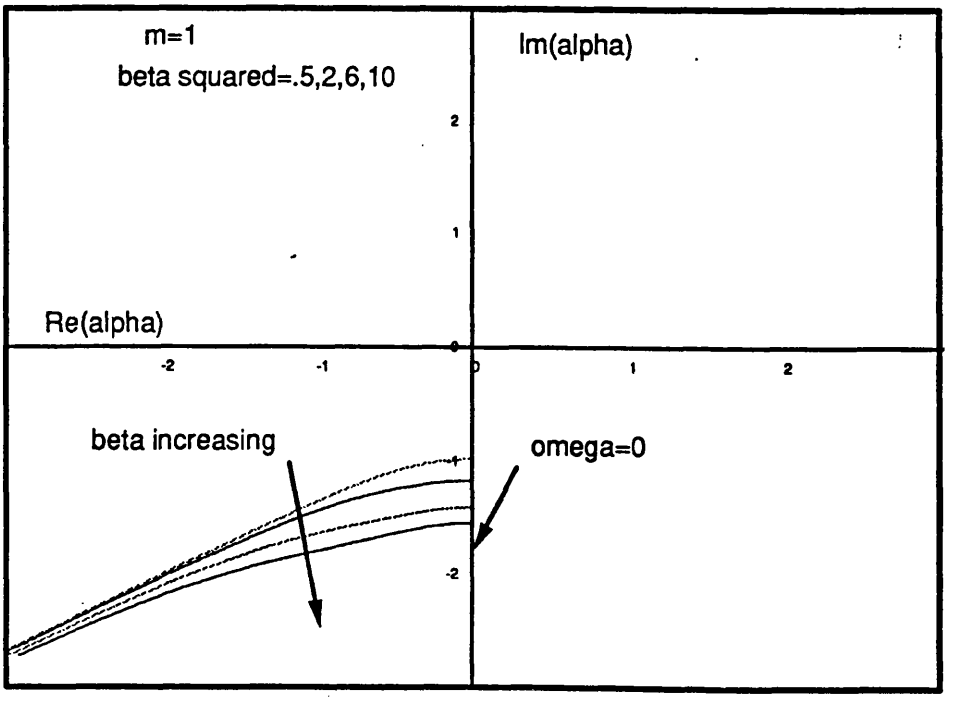

Figure 4.3.3

Upstream Influence Modes (2D Subsonic Flow)

(a)

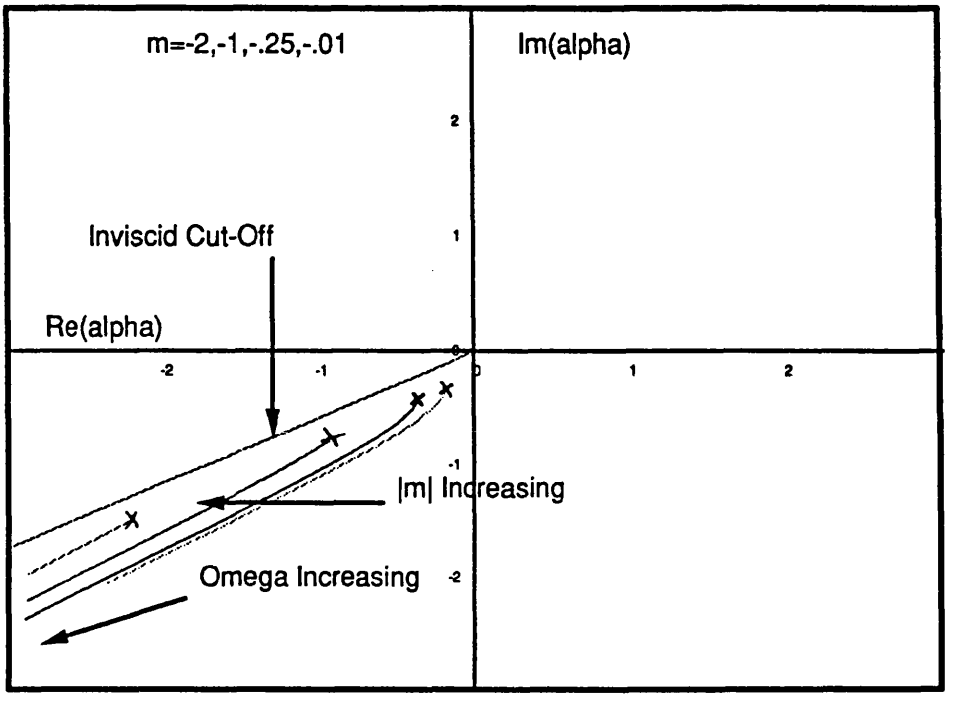

Oblique, Subsonic Upstream Influence Modes

(b)

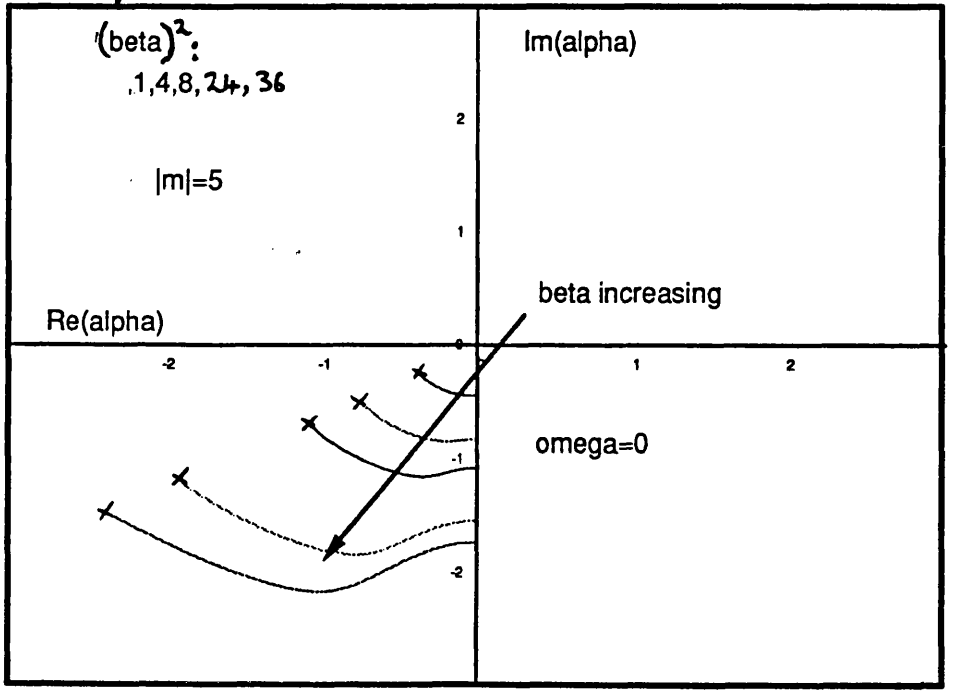

Figure 4.3.3

Oblique, Subsonic, Upstream Influence Modes.

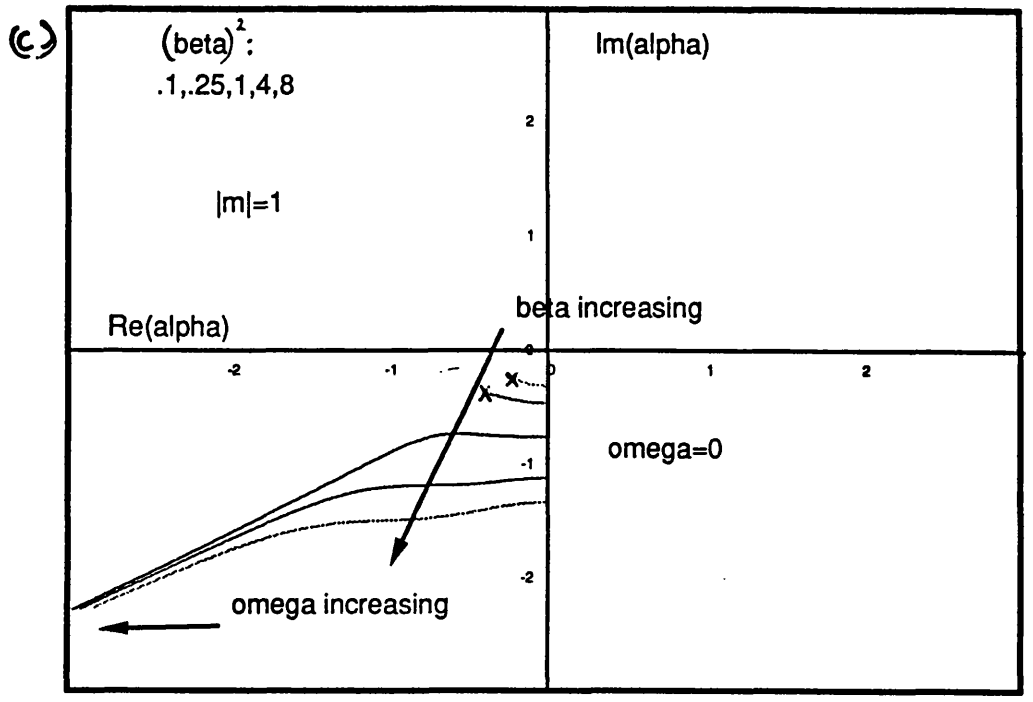

Figure 4.3.4

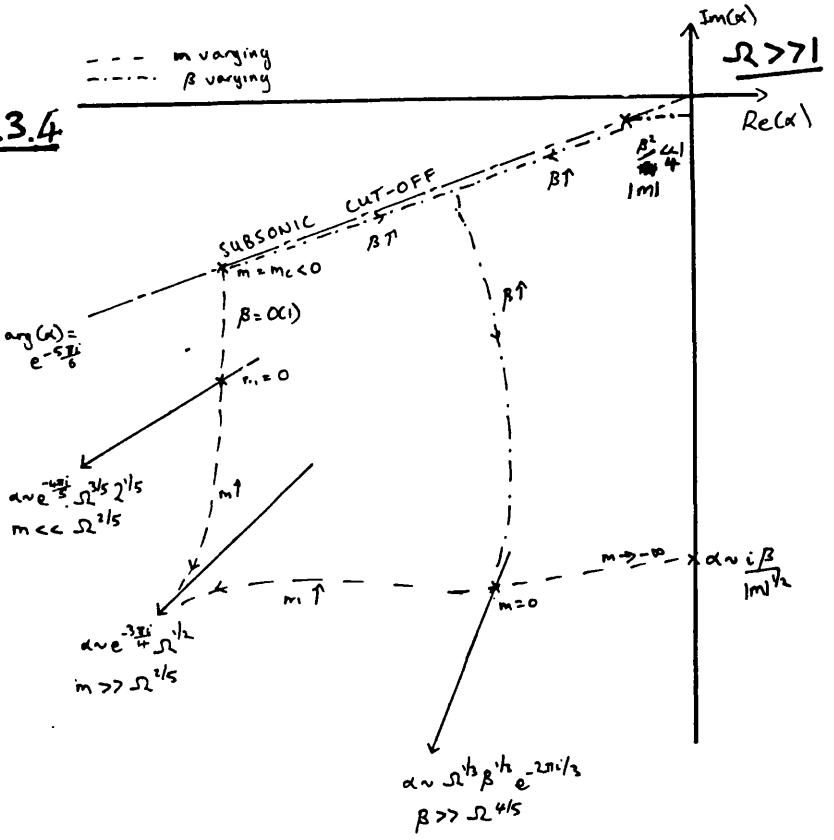

Figure 4.3.6

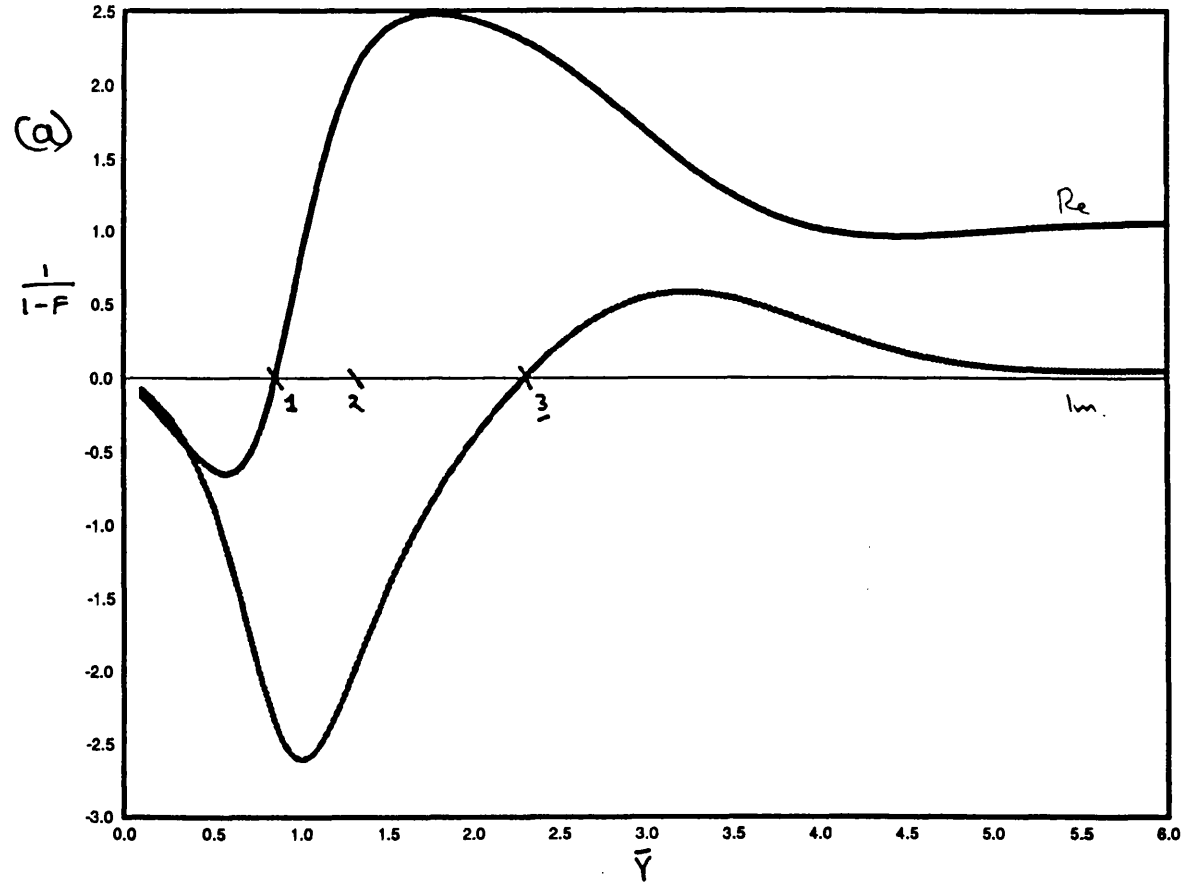

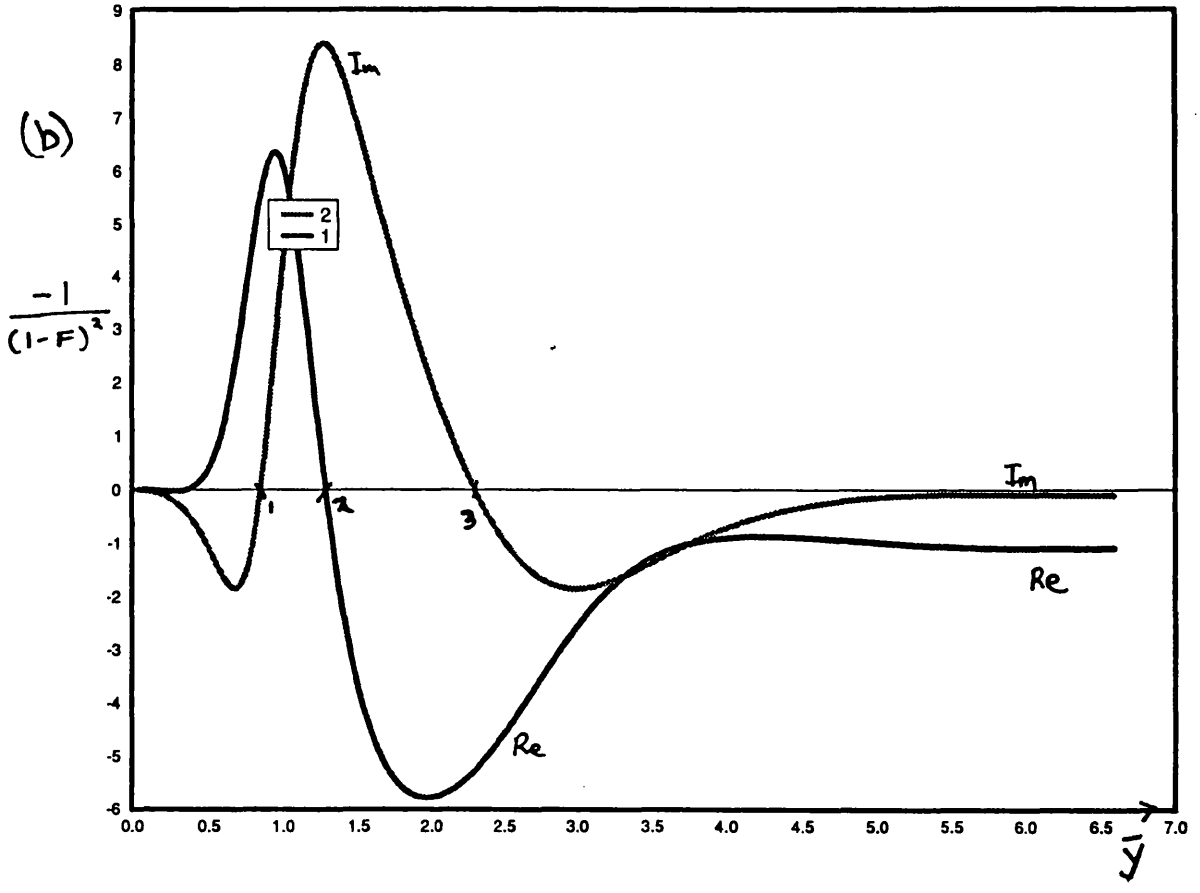

Chapter Five

THREE-DIMENSIONAL $(\text{AMPLITUDE})^3$ INTERACTIONS AND THE DEVELOPMENT OF NONLINEAR DISTURBANCES IN TRANSONIC BOUNDARY LAYERS.

§5.1 Introduction; Natural Transition For Large Disturbances.

The introduction to chapter 4 states that, even in natural transition, there are many routes from laminar to turbulent flow. These routes are characterised by the sequence of nonlinear interactions or secondary instabilities which the unsteady disturbance may experience as it travels downstream. Alhough the original experiments of Schubauer and Skramstad (1947) were the first to identify Tollmien-Schlichting (TS) waves with transition of the boundary layer on a flat plate, it has been only in more recent years that modern experimental techniques have been able to distinguish between the subsequent developments of these waves which characterise different transition mechanisms.

The work of this chapter can, to a degree, be identified as being appropriate to a type of transition seen in incompressible boundary layers, known as K-type transition. This notation, introduced by Herbert and Morkovin (1979), is prompted by the experimental work of Klebanoff, Tidstrom and Sargent (1962), which was the first to identify this route. This mechanism is associated with quite high disturbance amplitudes with r.m.s. velocities in the boundary layer of approximately 1-2% of the free stream velocity. The features of this type of transition are as follows. An initially two-dimensional wave becomes unstable to a three-dimensional perturbation which has the form of a spanwise variation in the intensity of the disturbance. These variations are known as peaks and valleys. Associated with this, as transition proceeds, is the presence of lines of hairpin vortices in the streamwise direction with a wavelength exactly that of the initial TS disturbance. In the latter stages of transition, bursts of high frequency oscillation, known as spikes, are seen. These develop into turbulent spots which eventually fill the boundary layer.

Although, as explained later in this section, the experimental results of Klebanoff et al. do not indicate

that it is an important feature in the development of the three-dimensional nature of the transition, in incompressible flow, the large amplitude of the initial disturbance involved suggests the study of an $(\text{amplitude})^3$ type of nonlinearity. In this type of weakly nonlinear theory the amplitude of the fundamental disturbance varies as a result of its nonlinear reproduction through the interaction of the fundamental with its second harmonic and mean flow terms, as well as through growth induced by viscous-inviscid interaction. This work was done, in the case of incompressible flow, by Smith and Burgraff (1985) and Smith (1986a&b). Here we extend this work to the transonic regime.

Section 5.2 considers disturbances in a Blasius boundary layer and leads, through a weakly nonlinear analysis, to a Schrödinger equation governing the downstream development of the amplitude of the wavepacket of the disturbance. The wavepacket is directed at an angle of $O(Re^{-1/18})$ to the free stream as $Re \to \infty$ when the Mach number, M_∞, is such that $|M_\infty^2-1| \sim O(Re^{-1/9})$. As a result the amplitude is governed by the nonlinear equation derived in chapter 4 (4.2.28) and its behaviour at infinitesimal amplitudes is described in §4.3. A multiple-scales analysis is used to determine the amplitude of the fundamental wave. This requires a separation of the scales of motion into that of the wavelength and that over which the growth occurs due to viscous effects. This step can be made rational, in an asymptotic expansion, for only two types of wave: those near the lower branch neutral point and those of relatively high frequency. In the latter case the wavelength shortens and the growth rate becomes small (see §4.3.5) and it is this case which we consider. These are waves that are nearing the upper branch of TS disturbances. The shortening of the wavelength of the disturbance in this limit also justifies the neglect of the non-parallel nature of the Blasius boundary layer (at least for Mach numbers that are not much greater than unity, see Appendix 5A). We use the separation of scales

to balance the weak growth with the weak effects of nonlinear regeneration at small disturbance amplitudes.

The solutions to the governing Schrödinger equation are considered in section §5.3 in two special cases (a) and (b). The case (a) is of a wavepacket travelling in the downstream direction and the equation governs its amplitude modulation in an oblique (ξ-) direction. This direction depends on the Mach number and the spanwise wavenumber of the wavepacket. It is this case that contains, as a sub-case, the development of a two-dimensional wavepacket with a weak spanwise amplitude modulation. Case (b) concerns the modulation in the streamwise direction of waves travelling in the ξ-direction.

The results lead to the conclusion that wavepackets directed at an angle less than some $O(Re^{-1/18})$ value (which is dependent on the Mach number) are subject to a sideband (Benjamin-Feir) instability which has the effect of increasing the growth rate to three times that of a more oblique wave, in scaled terms. It also introduces seemingly chaotic features to the flow and a rapid broadening of the spectral content of the disturbance. In the case of waves of type (a) this corresponds to an instability to spanwise modulations of a two-dimensional wavepacket, with the growth rate of these modulations being greatest for those of the longest spanwise wavelength. This is in contrast with the incompressible case, which has a similar increase in growth rate for waves more oblique than 54.7° (Smith (1986b)).

The nonlinearity in the problem is such that, as in the incompressible case, the Stuart-Landau coefficient of the Schrödinger equation is purely imaginary. This precludes the occurrence of the finite-time breakdown in the solution which occurs in similar work by Hocking, Stewartson and Stuart (1971). Instead the wavepacket grows exponentially in amplitude. Eventually the response of the fluid close to the wall, where the basic boundary layer flow is slowest (the Stokes layer) becomes nonlinear and the large-amplitude-inviscid stage or stage 2 of Smith and

Burgraff (1985) is reached. This stage is relevant to the latter stages of the K-type of transition. We study this stage in §5.4 and draw the conclusion that the transonic free stream has a stabilising influence in this regime, reducing the likelihood of vorticity bursts from the nonlinear wall layer which is governed by the classical non-interactive boundary layer equations.

Finally, in §5.5, we consider the Euler stage of transition in transonic flow.

We make two final comments here. Firstly, it has not been possible to find experimental results of the quality of those avaliable for incompressible boundary layer transition. K-type transition may or may not occur at transonic speeds. This makes it difficult to gauge the importance of the theoretical results described above, one of which predicts a mechanism for the onset of three-dimensionality in the disturbance which is unique to transonic flow. The second point concerns the relevance of this weakly nonlinear theory to the initial stages of K-type transition in flows with zero Mach number. The experiments of Klebanoff et al. indicate that the development of the three-dimensional perturbations, in incompressible flow, is due not to an $(\text{amplitude})^3$ response and the nonlinear generation of harmonics and mean flow terms, but to the existence of longitudinal vortex structures. The understanding of this particular route to transition is likely to be gained, therefore, through a study of the wave-vortex interaction mechanism mentioned in §4.1. This has the power to explain the significant alteration of the mean flow profile seen in the peaks and valleys and the resultant triggering of an intermittent Rayleigh instability which is likely to be responsible for the spikes seen in the experiments. It is thus important that the theory of this interaction be extended to cover the transonic regime.

§5.2 Derivation Of The Weakly Nonlinear Equation.

As mentioned in the introduction to this chapter, the relatively slow growth exhibited by linear disturbances of relatively high frequency on the lower branch scalings allows a weakly nonlinear analysis of the development of a wavepacket. In this section we present a derivation of the scalings used in deriving an (amplitude)^3 nonlinear effect and the analysis which leads to a nonlinear Schrödinger equation, which governs the temporal growth of a wavepacket in a frame moving with the group velocity of the disturbance.

The nonlinearity in the unsteady, transonic triple deck equations (4.2.28) is quadratic, of the form $U_T \sim UU_X \sim P_X$. As a result, a fundamental disturbance proportional to $\tilde{E}$ or $\tilde{E}^{-1}$, where $\tilde{E} = \exp i(\tilde{\alpha}X + \tilde{\beta}Z - \Omega T)$, and with a pressure of an amplitude of size h, say, will generate a velocity of size hT/X. The small nonlinear terms will act upon this velocity and generate velocities of size h^2T^3/X^3, varying as $\tilde{E}^0$ (a mean flow adjustment) and as $\tilde{E}^2$ and $\tilde{E}^{-2}$ (second harmonics). These small velocities will themselves interact with the original disturbance, through the nonlinearity, and reproduce the fundamental disturbance at a size of $O(h^3T^5/X^5)$. This occurs through products of the type $\tilde{E}^0\tilde{E}$ and $\tilde{E}^2\tilde{E}^{-1}$. Thus the fundamental pressure disturbance is reproduced at an amplitude $O(h^3T^4/X^4)$, a size of relative magnitude $O(h^2T^4/X^4)$ compared with the original amplitude. Consider now linear high frequency disturbances. These develop according to the dispersion relation (4.3.33) which is

$$\bar{\alpha} \sim \bar{\alpha}_0\left[\, 1 \;-\; \frac{1}{\Omega^{9/10}}\,\frac{(1+i)}{\sqrt{2}}\,\frac{\bar{\alpha}_0^7}{(2\bar{\alpha}_0^6 + \bar{\alpha}_0 + \bar{\beta}^2)}\,\right], \qquad (5.2.1a)$$

$$\bar{\alpha}_0^{\,3} = (2\bar{\alpha}_0 + \bar{\beta}^2 - \bar{m}\bar{\alpha}_0^{\,2})^{1/2}, \qquad (5.2.1b)$$

where

$$\tilde{\beta} = \Omega^{4/5}\bar{\beta}, \qquad m = \Omega^{2/5}\bar{m}, \qquad \tilde{\alpha} = \Omega^{3/5}\bar{\alpha},$$

and $\bar{\beta}$, $\bar{m}$, $\bar{\alpha} \sim O(1)$, as $\Omega \to \infty$. This implies that $T^4/X^4 \sim \Omega^{-8/5}$.

In a weakly nonlinear analysis of this type we aim to balance the reproduction of the fundamental wave, through nonlinear effects, with its slow growth over the relatively long scales implied by (5.2.1a,b). The relative size of the growth term is $O(\Omega^{-9/10})$ and so this balance leads to the result $\Omega^{-9/10} \sim h^2T^4/X^4 \sim h^2\Omega^{-8/5}$, i.e. $h \sim \Omega^{7/10}$. Therefore the size of the streamwise velocity perturbations due to the fundamental disturbance is $O(\Omega^{-1/20})$ and the relative decrease in amplitude between the fundamental wave and that of the mean flow and harmonic terms is $O(\Omega^{-9/20})$. Similar considerations lead to the following multiple-scale expansion of equations (4.2.28), where $\varepsilon = \Omega^{-1/20}$,

$$U \sim \varepsilon(u_0 + \varepsilon^9 u_1 + \varepsilon^{18} u_2 + \ldots), \qquad (5.2.2a)$$

$$V \sim \varepsilon^{-1}(v_0 + \varepsilon^9 v_1 + \varepsilon^{18} v_2 + \ldots), \qquad (5.2.2b)$$

$$P \sim \varepsilon^{-7}(P_0 + \varepsilon^9 P_1 + \varepsilon^{18} P_2 + \ldots), \qquad (5.2.2c)$$

$$\bar{P} \sim \varepsilon^{-7}(\bar{P}_0 + \varepsilon^9 \bar{P}_1 + \varepsilon^{18} \bar{P}_2 + \ldots), \qquad (5.2.2d)$$

$$A \sim \varepsilon(A_0 + \varepsilon^9 A_1 + \varepsilon^{18} A_2 + \ldots), \qquad (5.2.2e)$$

$$\partial_X \sim \varepsilon^{-12}(\partial_{x_0} + \varepsilon^9 \partial_{x_1} + \varepsilon^{18} \partial_{x_2} + \ldots), \qquad (5.2.2f)$$

$$\partial_T \sim \varepsilon^{-20}(\partial_{t_0} + \varepsilon^9 \partial_{t_1} + \varepsilon^{18} \partial_{t_2} + \ldots), \qquad (5.2.2g)$$

$$\partial_Z \sim \varepsilon^{-16}(\partial_{z_0} + \varepsilon^9 \partial_{z_1} + \varepsilon^{18} \partial_{z_2} + \ldots), \qquad (5.2.2h)$$

$$m = \varepsilon^{-8}\bar{m}, \quad \bar{y} = \varepsilon^{16} y^*, \quad Y = \varepsilon^{10} Y^*, \qquad \varepsilon \to 0. \qquad (5.2.3a\text{-}c)$$

In this expansion we assume that all the x_0, z_0 and t_0 dependence occurs in the exponential term which governs the wave-like behaviour on these relatively fast scales. The other space and time scales are slower and it is upon

these that either the mean flow and second harmonics are generated or, on the longest scale of all, the amplitude of the fundamental varies. The linear increase in U, $U \to Y$ as $Y \to \infty$, (equation (4.2.28e)) is incorporated into the boundary condition satisfied by the mean part of u_1 as $Y^* \to \infty$.

We write

$$u_0 = u_{01} E + u_{01}^{+} E^{+},$$

and use similar expressions for P_0, $\bar{P}_0$, A_0, v_0, where the superscript + indicates the complex conjugate, and $E = \exp i(\alpha x_0 + \beta z_0 - t_0)$. The expansion (5.2.2&3) is then substituted into the nonlinear equations (4.2.28). At first order we find that the disturbance is governed by the system

$$\bar{P}_{01y^*y^*} + \bar{P}_{01z_0z_0} = \bar{m}\, \bar{P}_{01x_0x_0} + 2\, \bar{P}_{01x_0t_0}, \qquad (5.2.4a)$$

$$\bar{P}_{01y^*} \to A_{01x_0x_0}, \quad y^* \to 0, \qquad (5.2.4b)$$

$$\bar{P}_{01} \to P_{01}, \quad y^* \to 0, \qquad (5.2.4c)$$

$$-i\, u_{01} = -i\alpha\, P_{01} + u_{01}'', \qquad (5.2.4d)$$

$$i\alpha\, u_{01} + v_{01Y^*} = 0, \qquad (5.2.4e)$$

$$u_{01} = v_{01} = 0 \text{ at } Y^* = 0, \quad u_{01} \to A_{01} \text{ as } Y^* \to \infty, \qquad (5.2.4f\text{-}h)$$

where $'$ indicates ∂_{Y^*}. These imply that

$$u_{01} = A_{01}(1 - e^{-\sigma Y^*}), \quad v_{01} = -i\alpha A_{01}\left(Y^* - \frac{1 - e^{-\sigma Y^*}}{\sigma}\right), \qquad (5.2.5a\text{-}b)$$

$$\bar{P}_{01} = \tilde{P}_{01} e^{-\gamma y^*}, \qquad (5.2.5c)$$

$$\bar{P}_{01} = \tilde{P}_{01}, \quad \gamma P_{01} = \alpha^2 A_{01}, \qquad (5.2.5d\text{-}e)$$

and, from (5.2.4d) and (5.2.5a),

$$A_{01} = \alpha P_{01}, \tag{5.2.5f}$$

where $\sigma^2 = -i$, $\text{Real}(\sigma) > 0$, $\gamma^2 = (2\Omega\alpha + \beta^2 - \bar{m}\alpha^2)$ and $\text{Real}(\gamma) > 0$.

Comparing (5.2.5e) and (5.2.5f) we find the dispersion relation at this order to be

$$\gamma = \alpha^3. \tag{5.2.6}$$

This is exactly the inviscid version of (5.2.1).

At second order the nonlinearity in (4.2.28b) balances terms such as u_{01t_1} and u_{01t_0}. This nonlinearity consists of the terms

$$E^2(i\alpha u_{01}^2 + v_{01}u_{01Y}^*) + E^{-2}(-i\alpha u_{01}^{+2} + v_{01}^+ u_{01Y}^{+*}) +$$
$$E^0(v_{01}u_{01Y}^{+*} + v_{01}^+ u_{01Y}^*),$$

which are

$$E^2[i\alpha^3 P_{01}^2(1 - e^{-\sigma Y^*} - \sigma Y^* e^{-\sigma Y^*})] + c.c +$$
$$E^0 i\alpha^3 |P_{01}|^2 \left(Y^*\sigma\, e^{-\sigma Y^*} - Y^*\sigma^+ e^{-\sigma^+ Y^*} + \left(\frac{\sigma}{\sigma^+} - \frac{\sigma^+}{\sigma}\right) e^{-(\sigma+\sigma^+)Y^*} \right.$$
$$\left. + \frac{\sigma^+}{\sigma} e^{-\sigma^+ Y^*} - \frac{\sigma}{\sigma^+} e^{-\sigma Y^*} \right),$$

or, defining H.T. and M.T. (harmonic and mean terms),

$$E^2(i\alpha^3 P_{01}^2)(\text{ H.T. }) + E^{-2}(-i\alpha^3 P_{01}^{+2})(\text{ H.T.}^+\text{ })$$
$$+ E^0(i\alpha^3 |P_{01}|^2)(\text{ M.T. }).$$

With forcing of this type in mind for u_1 we write it as

$$u_1 = E^0 u_{10} + E u_{11} + E^{-1} u_{11}^+ + E^2 u_{12} + E^{-2} u_{12}^+,$$

and express P_1, $\bar{P}_1$, A_1, and v_1 similarly.

We find that the second harmonic term is governed by the equations

$$\bar{P}_{12y^*y^*} = 4\gamma^2\bar{P}_{12}, \tag{5.2.7a}$$

$$\bar{P}_{12y^*} \to 4\alpha^2 A_{12} \text{ and } \bar{P}_{12} \to P_{12} \text{ as } y^* \to 0, \tag{5.2.7b-c}$$

$$-2iu_{12} + i\alpha^3 P_{01}{}^2(\text{ H.T.}) = -2i\alpha P_{12} + u_{12}'', \tag{5.2.7d}$$

$$2i\alpha u_{12} + v_{12Y^*} = 0, \tag{5.2.7e}$$

$$u_{12} = v_{12} = 0 \text{ at } Y^* = 0, \quad u_{12} \to A_{12} \text{ as } Y^* \to \infty. \tag{5.2.7f-h}$$

Solving these, we find from (5.2.7d) that

$$\alpha P_{12} + 3\alpha^3 P_{01}{}^2/2 + D = 0 \text{ for some } D,$$

$$A_{12} = \alpha P_{12} + \alpha^3 P_{01}{}^2/2.$$

However from (5.2.7a-c) and (5.2.6),

$$\bar{P}_{12} = 2A_{12}/\alpha, \quad \bar{P}_{12} = P_{12}.$$

As a result we can determine D and so

$$A_{12} = -\alpha^3 P_{01}{}^2/2 \quad \text{and} \quad P_{12} = -\alpha^2 P_{01}{}^2. \tag{5.2.8a-b}$$

Therefore,

$$u_{12} = \alpha^3 P_{01}{}^2[(1-\sigma Y^*)e^{-\sigma Y^*} - (1 + e^{-\sqrt{2}\sigma Y^*})/2\ ],$$

$$v_{12} = -2i\alpha^4 P_{01}{}^2[Y^* e^{-\sigma Y^*} - Y^*/2 - (1 - e^{-\sqrt{2}\sigma Y^*})/(2\sqrt{2}\sigma)].$$

(5.2.9a-b)

Now we consider the mean flow terms. These satisfy

$$u_{10}'' = i\alpha^3 |P_{01}|^2 (\text{M.T.}),$$

$$u_{10} = 0 \text{ at } Y^* = 0, \; u_{10} \to Y^* + A_{10} \text{ as } Y^* \to \infty,$$

and so

$$u_{10} = Y^* - 2\alpha^3 |P_{01}|^2 \, \mathrm{Im}\left[\frac{\sigma^+}{\sigma} \frac{(1-e^{-(\sigma+\sigma^+)Y^*})}{(\sigma+\sigma^+)^2} - \frac{(1-e^{-\sigma^+ Y^*})}{\sigma\sigma^+} + 2\frac{(1-e^{-\sigma^+ Y^*})}{\sigma^{+2}} - \frac{Y^* e^{-\sigma^+ Y^*}}{\sigma^+} \right]. \tag{5.2.10}$$

Thus

$$A_{10} = 3|P_{01}{}^2|\alpha^3, \quad v_{10} = 0. \tag{5.2.11a-b}$$

The mean pressure term P_{10} cannot be found in this analysis.

We now consider the behaviour of the extra fundamental term at second order, EP_{11}. This term does not suffer any forcing from nonlinear terms and u_{11} satisfies

$$-iu_{11} + u_{01t_1} = -i\alpha P_{11} - P_{01x_1} + u_{11}'', \tag{5.2.12a}$$

$$u_{11} = 0 \text{ at } Y^* = 0 \text{ and } u_{11} \to A_{11} \text{ as } Y^* \to \infty. \tag{5.2.12b-c}$$

Thus

$$u_{11} = (\alpha P_{11} - iP_{01x_1} - i\alpha P_{01t_1})(1 - e^{-\sigma Y^*}) + P_{01t_1} \frac{\alpha Y^* e^{-\sigma Y^*}}{2\sigma},$$

and applying the boundary conditions we find that

$$\alpha P_{11} - A_{11} = iP_{01x_1} + i\alpha P_{01t_1}. \qquad (5.2.13)$$

The disturbance in the upper deck satisfies the equations

$$\bar{P}_{11y^*y^*} - \gamma^2\bar{P}_{11} = 2i\alpha\bar{m}\bar{P}_{01x_1} - 2i\beta\bar{P}_{01z_1} + 2i\alpha\bar{P}_{01t_1} - 2i\bar{P}_{01x_1},$$

$$\bar{P}_{11} \to P_{11}, \qquad \bar{P}_{11y^*} \to 2i\alpha A_{01x_1} - \alpha^2 A_{11} \text{ as } y^* \to 0. \qquad (5.2.14a\text{-}c)$$

However, from (5.2.5c-d,f), $\bar{P}_{01} = P_{01}e^{-\gamma y^*}$ and $A_{01} = \alpha P_{01}$, so

$$\bar{P}_{11} = \tilde{P}_{11}e^{-\gamma y^*} - \frac{i}{\gamma}\left[(\alpha\bar{m}-1)P_{01x_1} - \beta P_{01z_1} + \alpha P_{01t_1}\right]y^*e^{-\gamma y^*}.$$

So, from the conditions (5.2.14), we find that $\tilde{P}_{11} = P_{11}$ and

$$\alpha P_{11} - A_{11} = \frac{i}{\gamma^2}\left[-(3\alpha+2\beta^2-\bar{m}\alpha^2)P_{01x_1} + \alpha\beta P_{01z_1} - \alpha^2 P_{01t_1}\right].$$

Combining this with (5.2.13) leads to

$$P_{01t_1} + \frac{1}{\alpha}\left[\frac{5\alpha + 3\beta^2 - 2\alpha^2\bar{m}}{3\alpha + \beta^2 - \alpha^2\bar{m}}\right]P_{01x_1} + \frac{1}{\beta}\left[\frac{-\beta^2}{3\alpha + \beta^2 - \alpha^2\bar{m}}\right]P_{01z_1}$$

$$= 0. \qquad (5.2.15)$$

Equation (5.2.15) corresponds to the disturbance being neutral over the x_1 scale in a frame moving with its group velocity. The velocity in the X-direction, cg_X, is positive and is $O(\Omega^{2/5})$, and that in the Z-direction, cg_Z, is $O(\Omega^{1/5})$ and is directed opposite to the phase velocity. The coefficient of P_{01x_1} in (5.2.15) is cg_X, whilst the coefficient of P_{01z_1} is cg_Z.

We now introduce a notation which is useful in the study of these high frequency limits. If we write

$$\bar{A} = 2/\alpha^5, \qquad \bar{B} = \beta^2/\alpha^6, \qquad \bar{C} = -\bar{m}/\alpha^4, \tag{5.2.16}$$

the linear neutral dispersion relation (5.2.6) becomes

$$\bar{A} + \bar{B} + \bar{C} = 1. \tag{5.2.17}$$

The term $\bar{A}$ measures the importance of unsteadiness in the free stream and is always positive. $\bar{B}$ is also positive and gauges three-dimensional effects, whilst $\bar{C}$ can be positive or negative depending only on the sign of $\bar{m}$. The right hand side of (5.2.17) represents the effect of the interaction of the free stream with the boundary layer. In this notation

$$cg_x = \frac{1}{\alpha}\left[\frac{6-\bar{A}-2\bar{C}}{2+\bar{A}}\right] = \frac{1}{\alpha}\left[\frac{4+\bar{A}+2\bar{B}}{2+\bar{A}}\right] = \frac{\bar{F}}{\alpha}, \tag{5.2.18a}$$

$$cg_z = \frac{1}{\beta}\left[\frac{-2\bar{B}}{2+\bar{A}}\right] = \frac{\bar{G}}{\beta}. \tag{5.2.18b}$$

Equations (5.2.18a-b) define $\bar{F}$ and $\bar{G}$.

We now turn to the third order of the expansion and in particular the term proportional to E. We identify these terms by the suffix 21. In the boundary layer u_{21} satisfies

$$\begin{aligned} &-iu_{21} + u_{11t_1} + u_{01t_2} + \\ &\quad (i\alpha u_{01}^{+}u_{12} + i\alpha u_{10}u_{01} + v_{12}u_{01Y}^{+*} + v_{01}u_{01Y}^{*} + v_{01}^{+}u_{12}) = \\ &\qquad\qquad -i\alpha P_{21} - P_{11x_1} - P_{01x_2} + u_{21}'', \end{aligned} \tag{5.2.19}$$

with boundary conditions $u_{21} = 0$ at $Y^* = 0$ and $u_{21} \to A_{21}$ as $Y^* \to \infty$. This equation governs the development of the fundamental term u_{21} within the boundary layer and its form is similar to (5.2.4d-h) which governs the term u_{01}.

We therefore expect that, together with the system governing the disturbance in the free stream and the matching conditions expanded to this order, this equation will yield a secularity equation governing the development of P_{01} over the longer scales x_2 and t_2. To determine this equation we simply evaluate equation (5.2.19) as $Y^* \to \infty$ where $u_{21} = A_{21}$. This gives

$$\alpha P_{21} - A_{21} = iA_{11t_1} + iA_{01t_2} + iP_{11x_1} + iP_{01x_2} - \frac{\alpha^2}{\sigma} P_{01} - \frac{5\alpha^5}{2} P_{01}|P_{01}|^2,$$

or, if we use (5.2.13) and (5.2.5f) to eliminate A_{01} and A_{11} in favour of P_{01} and P_{11} we find

$$\alpha P_{21} - A_{21} = i\left(\alpha P_{11t_1} + P_{11x_1}\right) + i\left(\alpha P_{01t_2} + P_{01x_2}\right) + \alpha P_{01t_1t_1} + P_{01x_1t_1} - \frac{\alpha^2}{\sigma} P_{01} - \frac{5\alpha^5}{2} P_{01}|P_{01}|^2. \qquad (5.2.20)$$

In evaluating the nonlinear terms we have used (5.2.5a-b,8,9a-b,10,11).

The third order fundamental terms in the free stream and the matching conditions are

$$\bar{P}_{21y^*y^*} - \gamma^2\bar{P}_{21} = 2i[(\alpha\bar{m}-1)\bar{P}_{01x_2} + \alpha\bar{P}_{01t_2} - \beta P_{01z_2}] + 2i[(\alpha\bar{m}-1)\bar{P}_{11x_1} + \alpha\bar{P}_{11t_1} - \beta P_{11z_1}] + \bar{m}\bar{P}_{01x_1x_1} - \bar{P}_{01z_1z_1} + 2\bar{P}_{01x_1t_1}, \qquad (5.2.21)$$

and

$$\bar{P}_{21y^*} \to 2i\alpha A_{01x_2} + 2i\alpha A_{11x_1} + A_{01x_1x_1} - \alpha^2 A_{21}$$

$$= 2i\alpha^2(P_{01x_2}+P_{11x_1}) + 3\alpha P_{01x_1x_1} + 2\alpha^2 P_{01x_1t_1} - \alpha^2 A_{21},$$

$$\bar{P}_{21} \to P_{21}, \qquad \text{as } y^* \to 0.$$

(5.2.22a-b)

Here we have used equations (4.2.28f-i), (5.2.5f), and (5.2.13). The right hand side of (5.2.21) can be written as

$$A^* e^{-\gamma y^*} + B^* y^* e^{-\gamma y^*},$$

where

$$A^* = 2i\alpha^5[-(\bar{C}+\bar{A}/2)(P_{01x_2} + P_{11x_1}) + (\alpha\bar{A}/2)(P_{01t_2} + P_{11t_1})$$
$$- (\alpha\bar{B}/\beta)(P_{01z_2} + P_{11z_1})]$$
$$+ \alpha^4[-\bar{C}P_{01x_1x_1} - (\alpha^2\bar{B}/\beta^2)P_{01z_1z_1} + (\alpha\bar{A})P_{01x_1t_1}],$$

and

$$B^* = 2\gamma\alpha^4[(\bar{C}+\bar{A}/2)^2 P_{01x_1x_1} + 2(\alpha\bar{B}/\beta)(\bar{C}+\bar{A}/2)P_{01x_1z_1}$$
$$- \bar{A}(\bar{C}+\bar{A}/2)\alpha P_{01x_1t_1} - (\alpha\bar{A})(\alpha\bar{B}/\beta)P_{01z_1t_1}$$
$$+ (\alpha\bar{B}/\beta)^2 P_{01z_1z_1} + (\alpha\bar{A}/2)^2 P_{01t_1t_1}].$$

Equations (5.2.21&22) imply that

$$\alpha P_{21} - A_{21} = -\frac{1}{2\alpha^5}\left[A^* + \frac{B^*}{2\gamma}\right] - 2i(P_{01x_2} + P_{11x_1})$$
$$- \frac{3}{\alpha}P_{01x_1x_1} - 2P_{01t_1x_1},$$

and comparing this result with (5.2.20) we find the relation

$$(1+\bar{A}/2)[(P_{01t_2}+P_{11t_1})+cg_x(P_{01x_2}+P_{11x_1})+cg_z(P_{01z_2}+P_{11z_1})]$$

$$-\frac{i}{2}\left[\left(\frac{6-\bar{C}+(\bar{C}+\bar{A}/2)^2}{\alpha^2}\right)P_{01x_1x_1}+\left(\frac{2\bar{B}(\bar{C}+\bar{A}/2)}{\alpha\beta}\right)P_{01x_1z_1}\right.$$

$$+\left(\frac{\bar{B}(\bar{B}-1)}{\beta^2}\right)P_{01z_1z_1}+\left(\frac{6+\bar{A}-\bar{A}(\bar{C}+\bar{A}/2)}{\alpha}\right)P_{01x_1t_1}$$

$$\left.+\left(\frac{-\bar{A}\bar{B}}{\beta}\right)P_{01z_1t_1}+(2+\bar{A}^2/4)P_{01t_1t_1}\right]$$

$$=\alpha\frac{(1-i)}{\sqrt{2}}P_{01}-\alpha^4\frac{5i}{2}P_{01}|P_{01}|^2.$$

Without loss of generality we can assume that P_{11} depends on $(x_1-cg_xt_1)$ and $(z_1-cg_zt_1)$ only and so satisfies an equation similar to (5.2.15). Using this result and (5.2.15) to rewrite the time derivative, ∂_{t_1}, in terms of spatial derivatives, allows us to obtain the following result, which is valid in a reference frame moving with the group velocity,

$$(1+\bar{A}/2)\frac{\partial P_{01}}{\partial t_2}-i\left\{\frac{\hat{A}}{\alpha^2}\frac{\partial^2P_{01}}{\partial x_1^2}+\frac{\hat{B}}{\alpha\beta}\frac{\partial^2P_{01}}{\partial x_1\partial z_1}+\frac{\hat{C}}{\beta^2}\frac{\partial^2P_{01}}{\partial z_1^2}\right\}$$

$$=\alpha\frac{(1-i)}{\sqrt{2}}P_{01}-\alpha^4\frac{5i}{2}P_{01}|P_{01}|^2, \qquad (5.2.23)$$

where

$$\hat{A}=-(1/2)[\bar{C}-15+(1+2\bar{A})\bar{F}^2+(3\bar{A}+4\bar{C})\bar{F}], \qquad (5.2.24a)$$

$$\hat{B}=-(1/2)[2(1+2\bar{A})\bar{F}\bar{G}+(3\bar{A}+4\bar{C})\bar{G}+4\bar{B}\bar{F}], \qquad (5.2.24b)$$

$$\hat{C}=-(1/2)[\bar{B}+(1+2\bar{A})\bar{G}^2+4\bar{B}\bar{G}]. \qquad (5.2.24c)$$

As a final step in this analysis we can eliminate the cross-derivative terms by using the spatial coordinates X_1

and ξ_1 where $X_1 = x_1$ and $\xi_1 = x_1 - (2\beta\hat{A}/\alpha\hat{B})z_1$ and normalise the equations by introducing the quantities

$$\hat{P} = P_{01}/\lambda_1,\ \xi = \xi_1/\lambda_2,\ X = X_1/\lambda_3,\ T = t_2/\lambda_4, \tag{5.2.25}$$

$$\lambda_1 = (\sqrt{2}/5\alpha^3)^{1/2},\ \lambda_2 = |\hat{A}\hat{H}\sqrt{2}/\alpha^3|^{1/2},\ \lambda_3 = |\hat{A}\sqrt{2}/\alpha^3|^{1/2}, \tag{5.2.26a-c}$$

$$\lambda_4 = \sqrt{2}(1+\bar{A}/2)/\alpha, \tag{5.2.26d}$$

$$\hat{H} = (4\hat{A}\hat{C} - \hat{B}^2)/\hat{B}^2. \tag{5.2.26e}$$

This leads to

$$\hat{P}_T - i\ \mathrm{sgn}\hat{A}\ (\hat{P}_{XX} + \mathrm{sgn}\hat{H}\ \hat{P}_{\xi\xi}) = (1-i)\hat{P} - i\ \hat{P}|\hat{P}|^2. \tag{5.2.27}$$

The line ξ_1 = constant corresponds to

$$z_1 = (\alpha\hat{B}/2\beta\hat{A})(X_1 - \xi_1). \tag{5.2.28}$$

The solutions of equation (5.2.27), a nonlinear Schrödinger equation, correspond to the development of a relatively high frequency wavepacket, of spanwise wavenumber β and streamwise wavenumber given by equation (5.2.6), which travels downstream with the group velocity, which has a negative Z-component. Within this travelling frame, lower order dispersion effects and viscous growth interact with the nonlinearity over a relatively long timescale and govern the development of the disturbance amplitude. The change of variables to X and ξ corresponds to picking out suitable coordinates for describing the effects of dispersion within this moving frame, and the coefficients λ_2 and λ_3 determine the scales over which these dispersive effects act, the scales being short if the corresponding coefficients are small.

We note here that we can rewrite (5.2.23) in slightly more general form than (5.2.27) if we use the variables $\bar{\xi}$ and $\bar{\zeta}$ where

$$x_1 = \frac{\hat{B}}{2\alpha}\frac{1}{\mu_1-\mu_2}\left\{\frac{\bar{\xi}\,M_1\sqrt{(M_2^2-1)}}{|\mu_1|^{1/2}} - \frac{\bar{\zeta}\,M_2\sqrt{(M_1^2-1)}}{|\mu_2|^{1/2}}\right\}, \quad (5.2.29a)$$

$$z_1 = -\frac{1}{\beta}\frac{1}{\mu_1-\mu_2}\left\{\frac{\bar{\xi}\,M_1}{|\mu|_1^{1/2}} - \frac{\bar{\zeta}\,M_2}{|\mu|_2^{1/2}}\right\}, \quad (5.2.29b)$$

$$\mu_{1,2} = \{\hat{A} + \hat{C} \pm \sqrt{((\hat{A}+\hat{C})^2-4\Delta)}\}, \quad \Delta = \hat{A}\hat{C}-\hat{B}^2/4, \quad (5.2.29c\text{-}d)$$

$$M_{1,2} = \sqrt{(1 + 2(\hat{A} - \mu_{1,2})/\hat{B})}. \quad (5.2.29e)$$

Equation (5.2.23) is then

$$\hat{P}_T - i\,(\mathrm{sgn}(\mu_1)\hat{P}_{\bar{\xi}\bar{\xi}\bar{\xi}} + \mathrm{sgn}(\mu_2)\hat{P}_{\bar{\zeta}\bar{\zeta}\bar{\zeta}}) = (1-i)\hat{P} - i\,\hat{P}|\hat{P}|^2. \quad (5.2.30)$$

If the eigenvalues μ_1 and μ_2 are different in sign, equation (5.2.23) is hyperbolic and we can expect solutions different from those in the case where they are of the same sign and the equation is elliptic. Figures 5.2.1a&b show the two eigenvalues plotted against $\bar{m}$ and β. It seems that μ_1 is always positive but that μ_2 changes sign as β increases, becoming negative for the least oblique disturbances. The resulting change in the qualitative nature of the solution is discussed in the next section.

§5.3 Solutions Of The Equation.

§5.3.1 The special cases (a) and (b).

The various coefficients used in the derivation of equation (5.2.27) are presented in Figures 5.3.1a-i. The important points to notice are the regions of the $(\bar{m},\beta)$ plane where $\hat{A}$ or $\hat{A}\hat{H}$ (or equivalently $\hat{A}\hat{H}\hat{B}^2$) are different in sign, since the solutions of (5.2.23) are different according to the sign of the dispersive term on the right hand side of (5.2.27). For example, consider the special

cases (a) and (b).

a) $$\hat{P} = Q^a(\xi,T)\exp(-iT + inX - in^2T\,\mathrm{sgn}\hat{A}),$$

$$Q^a_T - i\,s^a Q^a_{\xi\xi} = Q^a - i\,Q^a|Q^a|^2, \qquad s^a = \mathrm{sgn}(\hat{A}\hat{H}),$$

(5.3.1a)

b) $$\hat{P} = Q^b(X,T)\exp(-iT + in\xi - in^2T\,\mathrm{sgn}\hat{A}\,\mathrm{sgn}\hat{H}),$$

$$Q^b_T - i\,s^b Q^b_{XX} = Q^b - i\,Q^b|Q^b|^2, \qquad s^b = \mathrm{sgn}(\hat{A}).$$

(5.3.1b)

If s^a and s^b are positive, the large-time behaviour of the solutions to equations (5.3.1a-b) is of a wavepacket which spreads in X or ξ like exp(2T/3) and which has an amplitude growing like exp(2T/3). The phase of Q varies like exp(4T/3). See Smith (1986a). On the other hand, if the coefficient of the dispersive term is positive (s^a or $s^b < 0$), it acts as a focussing influence and the growing wavepacket is itself subject to a rapidly growing Benjamin-Feir type of sideband instability, see Benjamin and Feir (1967). This consists of localised, short, O(exp(-2T)) width spikes of large amplitude, O(exp(2T). The phase of the disturbance varies within these spikes like exp(4T). These spikes can occur seemingly at random upon the basic solution, due to their small width and rapid growth rate, and the downstream form has many randomly positioned, thinning spikes, of large amplitude, and a corresponding significant broadening of the frequency spectrum of the disturbance. See Smith (1986b). This change in behaviour of the solution is associated with the change in type of the equation and so a change in sign of one of the eigenvalues in equation (5.2.29c). The focussing is associated with the hyperbolic form of the equation. A numerical solution of the full system (5.2.30) would be of interest but here we investigate only the special cases of the plane waves (5.3.1a-b). The relevance

of equations (a) and (b) and the implications of their solutions are discussed separately below. Also discussed is the two-dimensional version of equation (5.2.23), the limit of which, at large $\bar{m}$, is covered in Appendix 5A.

§5.3.2 Solutions in case (a) and two-dimensional disturbances.

It can be seen from Figure 5.3.1(i) that sgn($\hat{A}\hat{H}$) is negative, corresponding to the more rapid growth, in a region of the ($\bar{m}$,β) plane which borders the line $\beta = 0$. This region extends for negative $\bar{m}$, a point discussed later in this section, but as $\bar{m}$ increases it is confined to smaller values of β. A limit typical of this regime is $\beta \to 0$ and in this case

$$\bar{A} + \bar{C} = 1-\bar{B}, \ \bar{B} << 1, \tag{5.3.2a}$$

$$\bar{F} \sim (4+\bar{A})/(2+\bar{A}) \sim O(1), \ \bar{G} \sim -2\bar{B}/(2+\bar{A}) \sim O(\beta^2), \tag{5.3.2b-c}$$

$$\hat{A} \sim (3\bar{A}^2+4\bar{A}+8)/2(2+\bar{A})^2 \sim O(1), \tag{5.3.2d}$$

$$\hat{B} \sim \bar{A}\bar{B}(\bar{A}+8)/(2+\bar{A})^2 \sim O(\beta^2), \tag{5.3.2e}$$

$$\hat{C} \sim -\bar{B}/2 \sim O(\beta^2), \tag{5.3.2f}$$

$$\hat{H} \sim (-1/\bar{B})[(3\bar{A}^2+4\bar{A}+8)(2+\bar{A})^2/(\bar{A}+8)^2] \sim O(\beta^{-2}), \text{ and is -ve,} \tag{5.3.2g}$$

$$\hat{A}\hat{H} \sim (-1/2\bar{B})[(3\bar{A}^2+4\bar{A}+8)/(\bar{A}+8)]^2 \sim O(\beta^{-2}), \text{ and is -ve,} \tag{5.3.2h}$$

$$2\beta\bar{A}/\alpha\bar{B} \sim (\beta/\alpha)[(3\bar{A}^2+4\bar{A}+8)/(\bar{A}+8)](1/\bar{A}\bar{B}) \sim O(\beta^{-1}). \tag{5.3.2i}$$

For the above to hold for large values of $\bar{A}$ and $\bar{C}$, $\bar{B}$ must be smaller than O(1) as $\bar{A}$ and $\bar{C} \to \infty$. This limit, of large $\bar{A}$ and $\bar{C}$, is relevant for large $\bar{m}$. On the other hand, if $\bar{B} = b$, say, is O(1) the appropriate expansion for large $\bar{A}$ and $\bar{C}$ is

$$\bar{F} \sim 1-2(b+1)/\bar{C}, \quad \bar{G} \sim 2b/\bar{C}, \tag{5.3.3a-b}$$

$$\hat{A} \sim (3-b)/2, \quad \hat{B} \sim b, \quad \hat{C} \sim -b/2, \tag{5.3.3c-e}$$

$$\hat{H} \sim -3/b, \quad \hat{A}\hat{H} \sim 3(b-3)/2b, \tag{5.3.3f-g}$$

where $\bar{C} \to -\infty$ and $\bar{A} = -\bar{C} + (1-b)$. Thus, for large $\bar{m}$, $\hat{A}$ changes sign where $b = 3$. We consider this feature further in §5.3.3. We note that $\hat{H}\hat{B}^2 = 4\Delta$, where Δ is defined in (5.2.29d), and that $\hat{H}$ does not change sign in this limit. As a result the type of the equation and so the qualitative nature of the solution do not alter as $\hat{A}$ changes sign. Expansions (5.3.2) and (5.3.3) agree as $\bar{A} \to \infty$.

From the results (5.3.2) we can see that, as $\beta \to 0$, λ_2 becomes large and $\xi \sim z_1$. (See (5.2.26b,28)). The coefficients $\lambda_{1,3,4}$ remain O(1). This corresponds to a two-dimensional wave with a slight degree of warping in the Z-(spanwise-) direction. This warping allows a secondary instability of the two-dimensional wavepacket to occur, governed by (5.3.1a). This has the form of focussing in the Z-direction and the appearance of spikes of large disturbance amplitude.

As a check on this result, the analysis of §5.2 can be repeated with ∂_Z scaling with Ω like $\Omega^{4/5}\Omega^{-9/20} \sim \Omega^{7/20}$, instead of $\Omega^{4/5}$. This restricts the three-dimensional influence to the (amplitude)^3 level of the expansion. If $\partial_Z = \Omega^{7/20}\partial_{z_1}$, the result is

$$(1+\bar{A}/2)\frac{\partial P_{01}}{\partial t_2} - \frac{i}{\alpha^2}\left[\left(\frac{3\bar{A}^2+4\bar{A}+8}{2(2+\bar{A})^2}\right)\frac{\partial^2 P_{01}}{\partial x_1^2} - \frac{\bar{A}}{4}\alpha\frac{\partial^2 P_{01}}{\partial z_1^2}\right]$$
$$= \alpha\frac{(1-i)}{\sqrt{2}}P_{01} - \frac{5i}{2}\alpha^4|P_{01}|^2P_{01}, \tag{5.3.4a}$$

in a frame moving in the positive X-direction with a speed implied by

$$\frac{\partial P_{01}}{\partial t_1} + \frac{1}{\alpha}\frac{(4+\bar{A})}{(2+\bar{A})}\frac{\partial P_{01}}{\partial x_1} = 0. \tag{5.3.4b}$$

We can normalise equation (5.3.4a) using the new variables $\hat{P}$, X and T and the normalising factors $\lambda_{1,3,4}$ introduced in (5.2.26), with the understanding that the limit as $\beta \to 0$ has been taken. The new variables required are $\bar{z}$ and $\bar{\lambda}_2$, where

$$z_1 = \bar{\lambda}_2 \bar{z} \qquad \text{and} \qquad \bar{\lambda}_2 = |\sqrt{2}/\alpha^7|^{1/2}. \tag{5.3.5a-b}$$

We then find

$$\hat{P}_T - i\,(\hat{P}_{XX} - \hat{P}_{\bar{z}\bar{z}}) = (1-i)\hat{P} - i\,\hat{P}|\hat{P}|^2. \tag{5.3.6}$$

Therefore a wave of the type $\hat{P} = Q(\bar{z},T)\exp(-iT+inX-in^2T)$ is governed by

$$Q_T + i\,Q_{\bar{z}\bar{z}} = Q - i\,Q|Q|^2, \tag{5.3.7}$$

and so is subject to focussing in the spanwise direction and the resulting destabilisation.

Without the $\partial^2_{z_1 z_1}$ term equations (5.3.4a-b) govern the development of a two-dimensional disturbance and exhibit only spreading behaviour, in contrast to the solution when small warping is present. They are considered further in the limit $\bar{m} \to \infty$ in Appendix 5A.

It is worth considering what happens to the type of solution described by (5.3.1a) and (5.3.2a-i) as $\bar{m} \to \pm\infty$. For large positive $\bar{m}$ we have seen from Figure 5.3.1(i) that the value of β at which s^a changes decreases. This is due primarily to the relation, $\alpha \sim 2/\bar{m}$, valid for small β and large $\bar{m}$, see (4.3.34&36b). Since $\bar{B} = \beta^2/\alpha^6$, we see that $\bar{B} \sim \beta^2\bar{m}^6/2^6$ and so for $\bar{B}$ to be small, and hence for this behaviour to occur, β must be smaller than $O(\bar{m}^{-3})$, which decreases rapidly. We know from (5.3.3c) that the crossover from type (a) to type (b) occurs where b = 3 and so $\beta = 8\sqrt{3}/\bar{m}^3$ as $\bar{m} \to \infty$. The behaviour in the case of O(1) values of β for large $\bar{m}$ is related to equation (b) and is discussed in subsection §5.3.3, although the distinction between solutions of type (a) and (b) is somewhat

artificial, since $\hat{A} = 0$ simply corresponds to the direction associated with the focussing effects being coincident with the X-direction.

As $\bar{m} \to -\infty$ we approach the subsonic minor modes (See §4.3.3). If we now consider larger values of β than in the previous paragraph, with $\alpha \sim |\bar{m}|^{1/4}\alpha^*$ and $\beta \sim |\bar{m}|^{3/4}\beta^*$, then as $\bar{A} \to 0$ the dispersion relation becomes $\bar{B} + \bar{C} = 1$, where, for the purposes of these results, $\bar{B} = \beta^{*2}/\alpha^{*6}$ and $\bar{C} = 1/\alpha^{*4}$. The coefficients become

$$\bar{C} \sim 1-\bar{B}, \tag{5.3.8a}$$

$$\bar{F} \sim 2(1+\bar{B}/2), \qquad \bar{G} \sim -\bar{B} \tag{5.3.8b-c}$$

$$\hat{A} \sim (1/2)(3\bar{B}^2+\bar{B}+2), \quad \hat{B} \sim -3\bar{B}^2, \quad \hat{C} \sim (1/2)(3\bar{B}^2-\bar{B}), \tag{5.3.8d-f}$$

$$\hat{H} \sim (5\bar{B}-2)/9\bar{B}^4. \tag{5.3.8g}$$

Thus $\hat{A}\hat{H} < 0$ if $\bar{B} < 2/5$ and so focussing occurs if

$$\beta^*/\alpha^* < (2/5)^{1/2}\alpha^{*2}. \tag{5.3.9}$$

We note that $\alpha^{*2} \sim |\bar{m}|^{1/2}$ as $\bar{m} \to -\infty$. The result (5.3.9) implies that there must be disturbance angles, bordering zero, which suffer this focussing and the induced increased growth rate in subsonic, compressible flow, although Smith (1986a) indicates that this is not the case for purely two-dimensional motion. The limit of this crossover angle as $\bar{m} \to -\infty$ has $\beta^*/\alpha^* = (2/3)^{1/2}$. Smith (1986b) shows that in incompressible flow ($M_\infty = 0$) waves at angles <u>greater</u> than 54.7° are subject to a similar secondary instability. Similarly, Bowles and Smith (1989) state that major mode transonic waves <u>more</u> oblique than 68.53° are also destabilised. The appearance of enhanced instability in the less oblique minor modes due to nonlinear effects, as the Mach number increases from zero towards unity would seem to be a feature worthy of further study, especially since on linear grounds it is the more

oblique modes that are the most unstable. It seems likely that the single incompressible crossover angle will connect to both the major mode crossover and the minor mode crossover angles as M_∞ increases. The former angle remains O(1) as $M_\infty \to 1-$ whilst the latter becomes $O([1-M_\infty^2]^{1/2})$ and matches with equation (5.3.9).

§5.3.3 Solutions in case (b).

The solutions of equation (b) become subject to a sideband instability and the associated increased growth rate when $\hat{A}$ is negative. Equation (5.3.3c) implies that $\hat{A}$ changes sign, at least for large $\bar{m}$, when $\beta = 8\sqrt{3}/\bar{m}^3$, or, since the scaling $\bar{A} \sim \bar{C}$ predicts $\alpha \sim 2/\bar{m}$, when $\beta/\alpha = 4\sqrt{3}/\bar{m}^2$. It is at this point too that $\hat{A}\hat{H}$ changes sign and λ_2 becomes zero. Thus at this point the solutions of equation (a) merge with those of (b). Asymptotic results for $\bar{C} \to -\infty$ reveal that $\hat{A}$ remains negative and $|\hat{A}|$ grows to be $O(|\bar{C}|)$ as β increases from these $O(\bar{m}^{-3})$ values through sizes of $O(\bar{m}^{-1/2})$. Also $|\hat{A}|$ remains large until $\beta \sim O(\bar{m}^{1/3})$. If $\beta \sim O(\bar{m}^{-1/2})$ then $\alpha \sim O(\bar{m}^{-1})$ and so $\bar{A} \sim \bar{B} \sim \bar{C} \sim O(\bar{m}^5)$ and the dispersion relation becomes

$$\bar{A} + \bar{B} + \bar{C} = 0.$$

Here the interaction between the boundary layer and the free stream is weak and this is reflected in the large values of $\bar{A}$, $\bar{B}$ and $\bar{C}$. As β increases further to a size of $O(\bar{m}^{1/3})$ a regime is reached where $\bar{A} \sim O(|\bar{C}|^{1/2})$ and $B \sim O(|\bar{C}|)$. Thus $\alpha \sim O(\bar{m}^{-1/6})$ and $|\bar{C}| \sim O(\bar{m}^{5/3})$. With the expansions

$$\bar{A} \sim \sigma|\bar{C}|^{1/2} + a \ , \ \bar{B} \sim |\bar{C}| - \sigma|\bar{C}|^{1/2} + (1-a),$$

where $\sigma = O(1)$, $|\bar{C}| \to \infty$ ($\sigma \approx 2\bar{m}/\beta^3$), we find that

$$\hat{A} \sim \bar{C}/2(1 - 12/\sigma^2), \quad \hat{H} \sim - |\bar{C}|^{-1}(3-20/\sigma^2)/(1-12/\sigma^2)^2. \qquad (5.3.10a\text{-}b)$$

Therefore $\hat{A}$ again takes positive values if $\sigma < \sqrt{12}$. This implies that the asymptote for the curve $\hat{A} = 0$, as $\bar{m} \to \infty$, is

$$\beta \sim (1/3)^{1/6}\, \bar{m}^{1/3}, \qquad \beta/\alpha \sim \bar{m}^{1/2}\left(1 - \frac{3^{1/6}}{\bar{m}^{5/6}}\right). \qquad (5.3.11a\text{-}b)$$

More important is the position at which $\hat{H} = 0$ since it is this curve which determines whether or not the solution enjoys the increased growth rate associated with the focussing in one direction. This has the asymptote

$$\beta \sim (3/5)^{1/6}\, \bar{m}^{1/3}, \quad \beta/\alpha \sim \bar{m}^{1/2}\left(1 - \frac{5^{1/6}}{3^{1/6}\bar{m}^{5/6}}\right). \qquad (5.3.12a\text{-}b)$$

The behaviour of the coefficients $\hat{A}$ and $\hat{A}\hat{H}$ as β increases from zero towards these $O(\bar{m}^{1/3})$ values, is summarised in Figure 5.3.2. This change in sign of the coefficients takes place for waves directed, to first order, along the boundary of the wave-Mach cone discussed in §4.2.3. Although these are asymptotic results for large $|\bar{C}|^{1/2}$ and in the Figures 5.3.1 this regime attains a $|\bar{C}|$ of only around 5, we can expect the structure described above to emerge as $\bar{m}$ increases in the vicinity of $\beta \sim O(\bar{m}^{1/3})$. Indeed, numerical evaluation of the coefficients for values of $\bar{m}$ around 8 confirms this trend. In addition more careful numerical investigation of the coefficients shows that this order of events, as β increases, is also seen at smaller values of $\bar{m}$, although the critical values of β become very close in the range $4 < \bar{m} < 4.5$.

On linear grounds, the waves directed inside the wave-Mach cone suffer from a strongly reduced growth rate as the interaction weakens - this is reflected, too, in the increase in λ_1 and so in the timescale upon which this nonlinear development takes place, as $\bar{m}$ increases. The nonlinear focussing gives rise to an increase in the growth rate, but this is unlikely to compensate for any but the smallest value of $\bar{m}$.

§5.4.1 The development of a two-dimensional wavepacket.

The weakly nonlinear analysis for a high frequency, dispersive wavepacket described in §§5.2&3 leads, for the special cases considered, to a prediction of a disturbance which grows in time and so, as the packet moves downstream, in space. It also either spreads or breaks up into shortening, large amplitude peaks, depending on whether it is more or less oblique than an $O(Re^{-1/9})$ angle which depends on the Mach number. We now follow the work of Smith and Burgraff (1985) and investigate the implications for the next stage in the development of this nonlinear disturbance as it travels downstream in a transonic flow. Alternatively the structure derived below will govern the response of the boundary layer to a more sudden, sufficiently high frequency and large disturbance, such as may be encountered in bypass transition.

We concentrate first on a further examination of the difference between a two-dimensional disturbance and the slightly three-dimensional wavepacket (warped two-dimensional wave, equation (5.3.4a-b)). This section considers two-dimensional disturbances while the next section considers the warped case.

The Stokes layer at the wall in which $Y \sim O(\Omega^{-1/2})$, is assumed linear in §5.2 and leads to equation (5.2.4d). However it becomes nonlinear as the disturbance size increases. The nonlinearity becomes important when the disturbance has grown to such a size that

$$\varepsilon^9 u_{01} u_{01x_0} \sim P_{01x_0}, \tag{5.4.1}$$

using the notation of §5.2. This implies, since $\alpha P_{01} \sim u_{01}$, that $P_{01} \sim \varepsilon^{-9}/\alpha^2$. However we know from §5.3.2 that, for two-dimensional disturbances, since they suffer no sideband instability,

$$P_{01} \sim \lambda_1 \exp(2t_2/3\lambda_4), \tag{5.4.2}$$

and so we can expect the expansion to fail due to a fully nonlinear reaction near to the wall when

$$t_2 \sim O(3\lambda_4 \ln\{\Omega^{9/20}/(\alpha^2\lambda_1)\}/2). \qquad (5.4.3)$$

At this point the disturbance amplitude has risen to a level given by

$$P \sim \Omega^{7/20} P_{01} \sim O(\Omega^{4/5}/\alpha^2). \qquad (5.4.4)$$

If α is O(1), i.e. we do not consider the limits $\bar{m} \to \pm\infty$ (although the results agree with Smith and Burgraff (1985) as $\bar{m} \to -\infty$ and with Appendix 5A for large positive $\bar{m}$), these results suggest the scalings

$$[U, V, P, \bar{P}, A] = [\Omega^{2/5}U^*, \Omega^{1/2}V^*, \Omega^{4/5}P^*, \Omega^{4/5}\bar{P}^*, \Omega^{2/5}A^*],$$

$$[\partial_X, \partial_T, \partial_Y, \partial_{\bar{y}}] = [\Omega^{3/5}\partial_{X^*}, \Omega\partial_{T^*}, \Omega^{1/2}\partial_{Y^*}, \Omega^{4/5}\partial_{\bar{y}^*}], \qquad (5.4.5a\text{-}b)$$

as $\Omega \to \infty$, with again, $m = \Omega^{2/5}\bar{m}$.

The length scale of the waves is therefore just as in §5.2, where the pressure-amplitude is only $O(\Omega^{7/20})$, although in the context of a natural transition the position of the wavepacket is

$$O(\lambda_4 c g_x \Omega^{3/10} 3\ln\{\Omega^{9/20}/(\alpha^2\lambda_1)\}/2), \qquad (5.4.6)$$

further downstream, on the original triple deck length scale. The wavepacket has spread to be of an extent of $O(\lambda_3\Omega^{3/10}/(\alpha^2\lambda_1))$, also on these scales. The group velocity, cg_x, is defined in (5.2.18a), with $\bar{B} = 0$. The distance (5.4.6) exhibits a strong dependence on the Mach number, varying as $|\bar{m}|^{-1/2}$, for large negative $\bar{m}$, and like $\bar{m}^7$ as $\bar{m} \to +\infty$. Thus we see again the increased stability of the flow to two-dimensional disturbances as it becomes more supersonic.

On substitution of the scalings (5.4.5) into the triple deck equations (4.2.28), the governing equations are found to be

$$U^*_{T^*} + U^*U^*_{X^*} + V^*U^*_{Y^*} = -P^*_{X^*} + U^*_{Y^*Y^*}, \qquad (5.4.7a)$$

$$U^*_{X^*} + V^*_{Y^*} = 0, \qquad (5.4.7b)$$

$$U^* = V^* = 0 \text{ at } Y^* = 0, \qquad (5.4.7c\text{-}d)$$

$$U^* \to A^* \text{ as } Y^* \to \infty, \qquad (5.4.7e)$$

$$\bar{P}^*_{\bar{y}^*\bar{y}^*} = \bar{m}\bar{P}^*_{X^*X^*} + 2\bar{P}^*_{X^*T^*}, \qquad (5.4.7f)$$

$$\bar{P}^* \to P^*, \ \bar{P}^*_{\bar{y}} \to A^*_{X^*X^*} \text{ as } \bar{y}^* \to 0 \text{ and } \bar{P}^* \to 0 \text{ at } \infty. \qquad (5.4.7g\text{-}i)$$

The only difference between these and the full triple deck equations is the boundary condition (5.4.7e) which reflects the large size of the disturbance. This allows us to simplify (5.4.7) by neglecting, for the moment, the boundary conditions at the wall. Thus we write

$$U^* = A^*, \qquad (5.4.8a)$$

and so

$$A^*_{T^*} + A^*A^*_{X^*} = -P^*_{X^*}, \qquad (5.4.8b)$$

together with (5.4.7f-i).

In order to impose the boundary conditions at the wall it is necessary to use the classical boundary layer equations there. These are (5.4.7a-e) where $P^*_{X^*} = A^*A^*_{X^*}$ and A^* is prescribed by the solution of (5.4.8b). These are subject to a finite time singularity (see, for example, van Dommelen and Shen (1980), van Dommelen and Cowley (1990)) and so we must accept that equations (5.4.8b, 5.4.7f-i) govern the development of the disturbance for only as long as the classical boundary

layer at the wall has a solution. The failure of this structure is associated with the bursting of vorticity from the sublayer near the wall into the main part of the boundary layer where the disturbance is governed by inviscid mechanics. These bursts serve to broaden the frequency spectrum of the disturbance, as smaller scales come into play and are the subject of much current work (see, for example, van Dommelen and Cowley (1990), Elliot and Smith (1987)). This theoretical result has much in common with experimental and computational studies of transitional boundary layers, for example the computations of Laurien and Kleiser (1989) and Zang and Krist (1989).

§5.4.2 The development of a slightly warped, two-dimensional wavepacket.

We now consider the similar development of the slightly warped, two-dimensional waves. Here, due to the sideband instability, the growth of the disturbance is three times as fast (in normalised terms) and is accompanied by a rapid decrease in the spanwise length scale of the disturbance and an increase in its three-dimensional nature (although the boundary layer is still governed by the two-dimensional equations). The spanwise length scale is of a size

$$\Omega^{-4/5}\Omega^{9/20}\bar{\lambda}_2 \exp(-2t_2/\lambda_4),$$

where $\bar{\lambda}_2$ is $|\sqrt{2}/\alpha^7|$. See (5.3.5). The Stokes layer becomes nonlinear three times as quickly as in the pure two-dimensional case (5.4.3) and therefore this occurs at a downstream distance a third of that given in (5.4.6). At this point the z_1-scale becomes

$$O(\Omega^{-4/5}\bar{\lambda}_2\alpha^2\lambda_1) \sim O(\Omega^{-4/5}/\alpha^3).$$

For $\bar{m}$ of O(1), this scale is short enough to enter at first order into the equation governing the free stream response. Thus with the scalings (5.4.5a-b) together with $\partial_z = \Omega^{4/5}\partial_{z^*}$, we find that the disturbance is governed by

(5.4.8b, 5.4.7g-i) but with (5.4.7f) replaced by

$$\bar{P}^{*}_{y^{*}y^{*}} + \bar{P}^{*}_{z^{*}z^{*}} = \bar{m}\bar{P}^{*}_{x^{*}x^{*}} + 2\bar{P}^{*}_{x^{*}T^{*}}. \qquad (5.4.9)$$

As in the two-dimensional case we have the possibility of bursts of vorticity from the wall layer, but the slight degree of warping has decreased the time at which this bursting becomes possible by a factor of three.

§5.4.3 More general disturbances.

We now turn to a consideration of the more general cases of disturbances satisfying equations (a) and (b) of §5.3.1. As above, the expansion used in §5.2 fails when the boundary layer becomes fully nonlinear and this occurs at exactly the same point that the slow (x_1, z_1) and fast (x_0, z_0) spatial scales become comparable. Here, however, the focussing occurs in the ξ-direction and so affects both the x_1 and z_1 scales. We see therefore that the increase in amplitude has the same effect as is described above in §§5.4.1 & 5.4.2. The disturbance, initially governed by equation (5.2.23) develops and becomes governed by equations (5.4.8b, 5.4.7g-i, 5.4.9) in small areas of relatively large amplitude, whilst (5.2.23) continues to hold in regions unaffected by the spikes of rapidly increasing amplitude.

More specifically, if we compare the two Z-scales of the motion we find that they coincide first for disturbances for which the scale of ξ_1 is initially closest to the short length scale of the wave. This corresponds to a small value of λ_2 and a small value of $\hat{H}$. Therefore the regions of large amplitude and the possibility of sublayer bursting are likely to appear first for disturbances directed in the direction of the critical angle which separates the spreading and the focussing solutions. We have the asymptotes (5.3.12) and (5.3.9) for this angle as $\bar{m} \to \pm\infty$. This angle is of size $O(Re^{-1/18})$ and coincides with the edge of the wave-Mach cone for large $\bar{m}$.

§5.4.4 Some solutions of the equation governing two-dimensional disturbances.

Here we discuss possible solutions of the two-dimensional equations (5.4.7), leaving aside the possibility of vorticity bursts from the classical sublayer at the wall. Equations (5.4.8b) and (5.4.7f-i) can be combined to give, dropping the *'s now,

$$A_T + AA_X = -\frac{1}{2^{3/2}\pi}\int_{-\infty}^{T}\int_{-\infty}^{\bar{X}}\frac{A_{pp}(p,q)}{(T-q)^{1/2}(\bar{X}-p)^{3/2}}\,dp\,dq, \qquad (5.4.10a)$$

$$\bar{X} = X - \bar{m}(T-q)/2. \qquad (5.4.10b)$$

This equation is a transonic counterpart of the Benjamin-Ono and Burger equations which govern the development of corresponding disturbances in the subsonic and supersonic regimes respectively (Smith and Burgraff (1985), Benjamin (1967)). These equations can be derived from the above as $\bar{m} \to -\infty$ or $+\infty$ respectively if $X = O(|\bar{m}|^{3/8})$, $T = O(|\bar{m}|^{1/4})$, $A = O(|\bar{m}|^{1/8})$ in both cases. This integral form of the free stream response makes clear the importance of the speed at which the disturbance travels relative to the sound speed ($\bar{m}/2$). In addition, if $\bar{m}$ is finite and negative, the resulting effect of a finite range of upstream influence at a given time is made explicit. This is caused by the finite speed of sound on these scalings.

Simple travelling wave solutions, depending only on X-cT, exist. These are governed either by the Benjamin-Ono form,

$$(A-c)A_X = -\frac{(2c-\bar{m})^{-1/2}}{\pi}\int_{-\infty}^{\infty}\frac{A_{ss}(s)}{(X-s)}\,ds, \qquad (5.4.11)$$

in relative subsonic flow ($c > \bar{m}/2$), or by the Burger form

$$(A-c)A_X = |2c-\bar{m}|^{-1/2}A_{XX}, \qquad (5.4.12)$$

in relative supersonic flow ($c < \bar{m}/2$). The solutions to (5.4.11) and (5.4.12) are always smooth. Nonlinear-wave and soliton solutions exist for the Benjamin-Ono equation, whilst the Burger equation exhibits only decaying solutions if A is zero at infinity.

The necessity that c be greater than $\bar{m}/2$ for the travelling wave to be governed by the Benjamin-Ono form has implications for the maximum wave amplitude and steepness that can be obtained in a just-supersonic flow. For example, Smith and Burgraff identify nonlinear waves which match back to the sinusoidal form of §§5.2&3 as their amplitude decreases but which become slower and steeper as they become larger. The above lower bound, of $\bar{m}/2$, on their speed, prevents these steeper waves, which are more likely to provoke sublayer bursting and its associated effect of the introduction of shorter scales. Instead as c decreases to $\bar{m}/2$ the length scale of the waves increases like $c^{-1}|2c-\bar{m}|^{-1/2}$ whilst their amplitude remains $O(\bar{m}/2)$. Upstream-travelling wave solutions of the Benjamin-Ono equation are also prohibited. In the case of the Burger equation, Smith and Burgraff show that the form of the solution is essentially invariant under a transformation of the type $X \rightarrow X-cT$ so that any solution can be translated with uniform speed with no important changes in its properties. More specifically, if $c < \bar{m}/2$, a change in the speed of the wave does not increase its steepness, which would make bursting more likely. As a result a decrease of the wave speed in just-supersonic flow causes a change in the governing equation from (5.4.11) to (5.4.12). Thus a limit is imposed on the steepness of the wave, at least for the travelling waves discussed by Smith and Burgraff. Therefore we can gauge the effect of a given supersonic Mach number in prohibiting, to some degree, the likelihood of sublayer bursting, at least in two-dimensional flows.

As mentioned previously, the Benjamin-Ono and Burger equations are not subject to a finite time singularity. We do not know whether this is also the case in the transonic form and although the numerical work necessary to confirm

or deny this possibility has not been carried out it is worth describing the form of a possible breakdown since it would be an important mechanism, unique to transonic flow, for introducing short spatial scales. To investigate this possibility we first scale the factor $\bar{m}/2$ from the governing equations by making use of the following scalings

$$[X,T,P,\bar{P},A,\bar{y}] \sim [\tau^{3/2},\tau^{5/2},\tau^{-2},\tau^{-2},\tau^{-1},\tau^{2}], \quad \tau = (2/\bar{m}). \tag{5.4.13}$$

The governing equations are still (5.4.10a-b) but with $\bar{m}/2$ replaced by unity. Once this is done, and if we write B for $2A/\bar{m}$, we can consider the effect of moving in a frame with the sonic speed $\bar{m}/2$ and introduce $\bar{X} = X-T$, in coordinates scaled as in (5.4.13). Then integrating the equation once in $\bar{X}$ and assuming that $B \to 0$ at $-\infty$ we find that

$$\int_{-\infty}^{\bar{X}} B_T \, ds + \frac{(B-1)^2}{2} = \frac{1}{2} + \frac{1}{2^{1/2}\pi}\int_{-\infty}^{T}\int_{-\infty}^{\bar{X}} \frac{B_{pp}(p,q)}{(T-q)^{1/2}(\bar{X}-p)^{1/2}}\, dpdq.$$

This equation is equivalent to (5.4.10a-b). We now search for a similarity solution of this equation as $T \to 0-$, of the form

$$\hat{B}(\bar{X},T) = \hat{B}(\bar{X}/|T|^{3/5})/|T|^{2/5}, \qquad |T| \to 0.$$

In this limit the speed of the motions in the boundary layer relative to $\bar{m}/2$ is becoming so large that the effects of the moving frame become negligible and the governing equations are exactly those which apply with $\bar{m} = 0$. The similarity form, $\hat{B}$, satisfies

$$\frac{1}{2}\hat{B}^2 + \frac{3}{5}\hat{x}\hat{B} - \frac{1}{5}\int_{-\infty}^{\hat{x}} \hat{B}dp = \frac{1}{2^{1/2}\pi}\int_{1}^{\infty}\int_{-\infty}^{\hat{x}} \frac{B''(p/q^{3/5})\, dpdq}{(T-q)^{1/2}(\hat{x}-p)^{1/2}q^{8/5}},$$

where $\hat{x} = \bar{X}/|T|^{3/5}$ and $\hat{B} \to 0$ as $\hat{x} \to \pm\infty$. A solution to this equation has not been found, if indeed there is one, which is not the case in the corresponding equations for the Burger and Benjamin-Ono systems. It corresponds to the coupled system

$$(2/5)\hat{B} + (3/5)\hat{x}\hat{B}_{\hat{x}} = -\Pi_{\hat{x}}, \qquad \hat{B} \to 0 \text{ as } \hat{x} \to \pm\infty,$$

$$5\bar{\Pi}_{\hat{y}\hat{y}} = 2[7\bar{\Pi}_{\hat{x}} + 3\hat{x}\bar{\Pi}_{\hat{x}\hat{x}} + 4\hat{y}\bar{\Pi}_{\hat{x}\hat{y}}], \qquad \bar{\Pi} \to 0 \text{ at } \infty,$$

$$\bar{\Pi} \to \Pi \text{ and } \bar{\Pi}_{\hat{y}} \to \hat{B}_{\hat{x}\hat{x}} \text{ as } \hat{y} \to 0.$$

The free-stream equation is of mixed type, being elliptic if $\hat{y}^2 < -(15/8)\hat{x}$ and hyperbolic otherwise.

§5.5 The Euler Stage Of Transition In Transonic Boundary Layers.

We have seen (equation (5.4.13)) that the Mach number scales out of the fully nonlinear, inviscid equations of §5.4. The length and time scales for the motion vary like $|\bar{m}|^{-3/2}$ and $|\bar{m}|^{-5/2}$ respectively. As $|\bar{m}|$ increases, therefore, and the free stream speed moves away from transonic, there comes a stage where the length scale of the disturbance shortens to become comparable with the boundary layer thickness itself. This occurs when $\bar{m} = O(Re^{1/9}\Omega^{-2/5})$ i.e. at the point at which $|M_\infty^2 - 1|$ becomes O(1), since then

$$L_x \sim Re^{-3/9}\Omega^{-3/5}(Re^{1/9}\Omega^{-2/5})^{-3/2} \sim O(Re^{-1/2}).$$

Simultaneously the time scale becomes $O(Re^{-1/2})$ and the typical amplitude scale of the disturbance reaches O(1), whilst the upper deck reduces in thickness to merge with the boundary layer. More importantly, the speed of the disturbance increases to be O(1) and so the position of the critical layer, where the speed of the basic flow is the same as that of the disturbance, must be situated in

the main part of the boundary layer. Since this speed must be greater than $1-1/M_\infty$ in supersonic flow, we see that any two-dimensional disturbance in supersonic flow must be governed by this system. The governing equations are the two-dimensional Euler equations

$$\rho_t + (\rho u)_x + (\rho v)_y = 0, \tag{5.5.1a}$$

$$\rho(u_t + uu_x + vu_y) = -p_x, \tag{5.5.1b}$$

$$\rho(v_t + uv_x + vv_y) = -p_y, \tag{5.5.1c}$$

$$\rho(p_t + up_x + vp_y) = \gamma p(\rho_t + u\rho_x + v\rho_y), \tag{5.5.1d}$$

$$(u,v,\rho,p) \to (1,0,1,\gamma^{-1}M_\infty^{-2}) \text{ as } y \to \infty, \tag{5.5.1e}$$

$$v = 0 \text{ at } y = 0. \tag{5.5.1f}$$

Here ρ is the density of the fluid and γ is the ratio of specific heats (see §4.2.1). Three-dimensional disturbances are governed by the three-dimensional Euler equations (4.2.2) but it must be remembered that sufficiently oblique waves need not be governed by this system since they are not affected by the wave-Mach cone and they may have speeds low enough that viscous effects are important. Associated with these inviscid equations is a viscous sublayer at the wall in which the classical boundary layer equations are satisfied. Just as in §5.4, this is subject to a finite time singularity which can be interpreted as vorticity erupting from the fluid near the wall and into the main part of the boundary layer.

If equations (5.5.1) are linearised about the basic boundary layer flow the resulting equations are the compressible Rayleigh equations studied by many authors (for example, Lees and Lin (1946), Mack (1974), (1984), (1987)). See also the comments of §4.3.6. These equations exhibit a multitude of solutions, which depend strongly on the Mach number and the basic boundary layer profile. There is much current analytical research in the area

(Smith and Brown (1989), Gajjar and Cole (1989), Cowley and Hall (1990), Sedougghi, Bowles and Smith (1990)). Gajjar and Cole extend the analyis into the weakly nonlinear regime. Equations (5.5.1) govern the fully nonlinear development of these modes.

We can view parts of the work both in this section, and the preceding sections of this chapter, as following a two-dimensional, relatively high frequency, Tollmien-Schlichting disturbance as the local Mach number of the flow increases through the transonic regime. We see that as the critical layer of any surviving disturbance must be an O(1) distance from the wall, the disturbance is forced to become governed by the Euler equations. Other, slower, modes become non-parallel in the way described in §4.3.5. Alternatively the Euler scales are achieved for $\bar{m}$ of O(1) if the scaled frequency of the disturbance, Ω, is raised to $O(Re^{5/18})$. In this case the flow remains transonic and the flow in the upper part of the boundary layer, where we can linearise about the near-uniform profile, is governed by (4.2.2) with $M_\infty = 1$.

The Euler equations match to the equations governing the disturbances we study in §5.4 as the speed of the disturbance decreases and its length scale increases. If M_∞-1 is O(1) and positive they link with the Burger equation, whilst if it is negative a match with the Benjamin-Ono equation is achieved. If, instead, as the speed decreases the value of $|M_\infty^2-1|$ is also scaled to be small then equation (5.4.10a-b) is obtained. This latter result can be seen as follows. If $\bar{\varepsilon} \ll 1$ we scale the variables according to

$$(\partial_x,\ \partial_t,\ M_\infty^2-1) \sim (\bar{\varepsilon}^{3/2}\partial_X,\ \bar{\varepsilon}^{5/2}\partial_T,\ \bar{m}\bar{\varepsilon}), \qquad (5.5.2)$$

then, where y is O(1), i.e. in the main body of the boundary layer, we expand thus

$$[u,v,p,\rho] = [U_B + \bar{\varepsilon}u_1,\ \bar{\varepsilon}^{5/2}v_1,\ \gamma^{-1}(1-\bar{m}\bar{\varepsilon}) + \bar{\varepsilon}^2 p_1,\ R_B + \bar{\varepsilon}\rho_1], \qquad (5.5.3)$$

where U_B and R_B are the velocity and density profiles of the basic boundary layer. Substitution of these into (5.5.1) yields equations with the solution

$$u_1 = A(X)U_{By},\quad v_1 = -A_X U_B,\quad \rho_1 = AR_{By}. \tag{5.5.4a-c}$$

In the region where $y = \bar{\varepsilon}^{-2}\bar{y}$ and $\bar{y} = O(1)$, i.e. in the free stream, the solution expands as

$$[u,v,p,\rho] = [1 + \bar{\varepsilon}^2\hat{u}_2 + \bar{\varepsilon}^3\hat{u}_3,\quad \bar{\varepsilon}^{5/2}\hat{v}_2 + \bar{\varepsilon}^{7/2}\hat{v}_3,$$
$$\gamma^{-1}(1-m\bar{\varepsilon}) + \bar{\varepsilon}^2\hat{p}_1 + \bar{\varepsilon}^3 p_2,\quad 1 + \bar{\varepsilon}^2\hat{\rho}_2 + \bar{\varepsilon}^3\rho_3], \tag{5.5.5}$$

and is governed by the equations

$$\left.\begin{aligned} \hat{\rho}_{2X} + \hat{u}_{2X} &= 0 \\ \hat{\rho}_{2T} + \hat{\rho}_{3X} + \hat{u}_{3X} + \hat{v}_{2\bar{y}} &= 0 \end{aligned}\right\} \text{ from (5.5.1a),}$$

$$\left.\begin{aligned} \hat{u}_{2X} &= -\hat{p}_{1X} \\ \hat{u}_{2T} + \hat{u}_{3X} &= -\hat{p}_{2X} \end{aligned}\right\} \text{ from (5.5.1b),}$$

$$\left.\begin{aligned} \hat{v}_{2X} &= -\hat{p}_{1\bar{y}} \\ \hat{v}_{2T} + \hat{v}_{3X} &= -\hat{p}_{2\bar{y}} \end{aligned}\right\} \text{ from (5.5.1c),}$$

$$\left.\begin{aligned} \hat{\rho}_{1X} &= \hat{\rho}_{2X} \\ \hat{p}_{1T} + \hat{p}_{2X} &= \hat{\rho}_{2T} + \hat{\rho}_{3X} - \bar{m}\hat{\rho}_{2X} \end{aligned}\right\} \text{ from (5.5.1d).}$$

These can be manipulated, together with (5.5.4a-c), to yield

$$\hat{p}_{1\bar{y}\bar{y}} = \bar{m}\hat{p}_{1XX} + 2\hat{p}_{1XT} \quad \text{and} \quad \hat{p}_{1\bar{y}} \to A_{XX} \text{ as } \bar{y} \to 0. \tag{5.5.6}$$

Finally, close to the wall, if $y = \bar{\varepsilon}^2 Y$ and $Y = O(1)$, and the wall is held at a constant temperature, we let

$$[u,v,p,\rho] = [\bar{\varepsilon}\bar{u},\ \bar{\varepsilon}^{7/2}\bar{v},\ \bar{\varepsilon}^2\hat{p}_1,\ R_B(0)], \tag{5.5.7}$$

and find

$$\bar{u}_X + \bar{v}_y = 0, \tag{5.5.8a}$$

$$R_B(0)(\bar{u}_T + \bar{u}\bar{u}_X + \bar{v}\bar{u}_Y) = -\hat{p}_{1X}, \tag{5.5.8b}$$

and, in order to match with (5.5.4a-c),

$$\bar{u} \sim \lambda(Y + A) \text{ and } \bar{v} \sim -\lambda A_X Y \text{ as } Y \to \infty, \tag{5.5.9a-b}$$

where λ is $U_{By}(0)$. Therefore, evaluating (5.5.8b) as $Y \to \infty$, we find

$$R_B(0)\lambda\ (A_T + \lambda A A_X) = -\hat{p}_{1X}. \tag{5.5.10}$$

With the scaling-out of the factors $R_B(0)$ and λ from (5.5.10), equations (5.5.6&10) are exactly (5.4.7f-i, 5.4.8).

§5.6 SUMMARY.

Below we list the main results of this chapter.

1) We have derived a weakly nonlinear equation which governs the development of a wavepacket of the so-called minor mode Tollmien-Schlichting disturbances in a transonic boundary layer. These modes are directed at angles of $O(Re^{-1/18})$ to the oncoming flow at a Mach number M_∞ such that $|M_\infty^2-1| = O(Re^{-1/9})$. It is found that wavepackets directed at angles less than some value are subject to a sideband instability. This instability increases the growth rate of the disturbance and broadens its frequency spectrum.

2) Purely two-dimensional wavepackets do not suffer from such an instability but the result above implies that they are unstable if they have a slight degree of spanwise variation.

3) As the flow becomes more subsonic this enhanced instability persists. This is in contrast with the result of Smith (1986b) who shows that in incompressible flow it is only sufficiently oblique modes which suffer from this sideband instability. More work in this area is required therefore to trace the development of the instability as the Mach number decreases towards zero.

4) For supersonic Mach numbers the sideband instability is possible for all disturbances directed within the wave-Mach cone (except purely two-dimensional disturbances). However the increased growth rate due to this nonlinear effect is unlikely to compensate for the dramatic stabilising influence of increasing Mach number which is discussed in §4.3.5.

5) For disturbances with a normalised pressure-amplitude of $O(\Omega^{4/5})$ as Ω, the scaled and normalised frequency of the disturbance (see equation (4.2.22)), becomes large, a transonic boundary layer responds in a nonlinear inviscid fashioin. This response corresponds to similar responses in incompressible and supersonic boundary layers described by Smith and Burgraff (1985) and matches with their results in the appropriate limits. The inviscid mechanics of this disturbance are complemented by the possibility of bursts of vorticity from a viscous sublayer at the wall.

6) Nonlinear travelling wave solutions to these large amplitude disturbance equations have a limit imposed on their steepness in just-supersonic flow. This arises from the restriction that they have speeds greater than $1-M_{\infty}^{-1}$. This limit on the wave steepness reduces the likelihood of vorticity bursting from the wall layer.

7) We have identified the scalings for the so-called Euler stage of transition in transonic boundary layers.

APPENDIX 5A THE LIMIT OF INCREASING MACH NUMBER FOR TWO-DIMENSIONAL DISTURBANCES.

The simplicity of the two-dimensional version of the Schrödinger equation (5.2.23) allows an analysis of the variation of the nonlinear balances involved as the flow becomes more supersonic in the limit $\bar{m} \to \infty$. From the study of two-dimensional linear waves in this limit (§4.3.5) we know that the interaction between the boundary layer and the free stream weakens and the dispersion relation becomes essentially that for a plane sound wave. The growth or decay due to the interaction becomes a second order effect. More specifically, as $\bar{m} \to \infty$, equation (5.2.1b) with $\beta = 0$ yields the result $\alpha \sim 2\bar{m}^{-1} + O(\bar{m}^{-6})$. Therefore the relative error in taking $\alpha = 2/\bar{m}$ is $O(\bar{m}^{-5})$. Using the notation of §5.2, the size of x_0, i.e. the length of the wave, and x_1, the scale over which the mean flow terms are generated, are $\bar{m}$ and $\varepsilon^{-9}\bar{m}^{3/2}$ respectively, as $\bar{m}$ increases. The latter scaling results from the expression for λ_3 (5.2.26c) and the fact that $\hat{A} \sim O(1)$ as $\bar{m} \to \infty$. Therefore x_1 is of a size $\varepsilon^{-9}\bar{m}^{1/2}x_0$. The relative sizes of these two lengths balances the $O(\bar{m}^{-5})$ error mentioned above when $\bar{m} \sim \varepsilon^{-2}$, or $m \sim O(\Omega^{1/2})$. We write $m = \Omega^{1/2}m_1$ where m_1 is $O(1)$ as $\Omega \to \infty$. With these scalings the amplitude of the pressure disturbance required in order that the nonlinear regeneration of the fundamental over the scale of the viscous growth is $O(\Omega^{1/2})$. In detail the scalings are

$$[U, V, P, A] = O([1, 1, \Omega^{1/2}, 1]), \tag{5A.1a}$$

$$[X, Y, T, \bar{y}] = O([\Omega^{-1/2}, \Omega^{-1/2}, \Omega^{-1}, \Omega^{1/2}]). \tag{5A.1b}$$

From the work on linear modes in §4.3.5, we know that a useful technique, when the interaction is weak, is to consider the motion in a frame moving with the acoustic speed m/2. We make the transformation

$$\partial_T = -m/2\ \partial_X + \partial_t. \tag{5A.2}$$

This yields the equation for the free stream disturbances

$$\bar{P}_{yy} = 2\bar{P}_{Xt}, \tag{5A.3a}$$

and, in the boundary layer, (4.2.28b) becomes

$$-m/2\ U_X + U_t + UU_X + VU_Y = -P_X + U_{YY}. \tag{5A.3b}$$

With the scalings (5A.1), U_t in the boundary layer is of the same order as the nonlinear terms as $\Omega \to \infty$. A multiple scales expansion is used just as in §5.2. Here, however

$$\partial_t \sim \Omega^{-1/2}(\partial_{t_0} + \Omega^{-1/2}\partial_{t_1} + \Omega^{-1}\partial_{t_2}), \tag{5A.4a}$$

$$\partial_X \sim \Omega^{-1/2}(\partial_{X_0} + \Omega^{-1/2}\partial_{X_1} + \Omega^{-1}\partial_{X_2}). \tag{5A.4b}$$

If the variation on the short scales in the travelling frame is confined to the exponential term $\hat{E} = \exp i(\alpha X_0 - \omega t_0)$ where ω is the frequency of the motion within the travelling frame, then $\alpha = 2/m_1$ from (5A.2) and (5A.4a). At first order in the expansion we find the high frequency, inviscid dispersion relation

$$\omega = 16m_1^{-5}, \tag{5A.5}$$

as expected from the linear theory. At second order we find that a mean flow correction and harmonics are generated. The terms proportional to the fundamental $\hat{E}$ yield

$$P_{01t_1} + c_g\ P_{01X_1} = i\alpha^{10}P_{01}/2, \tag{5A.6}$$

where $c_g = 3\omega/\alpha = 24/m_1^4$. Thus the amplitude of P_{01} does not vary within this frame. Its phase does vary, however.

At third order we derive the pressure-amplitude equation

$$\alpha^{-5}P_{01t_2} - 3i/2\alpha^2 P_{01X_1X_1} - 5\alpha^4/2\ P_{01X_1} =$$

$$\alpha(1-i)/\sqrt{2}\ P_{01} - 7i\alpha^{10}/8 - 5i\alpha^4/2\ P_{01}|P_{01}|^2. \qquad (5A.7)$$

However, a moving frame transformation applied to (5A.7) shows that there is no qualitative change in the nonlinear behaviour of the disturbance amplitude at these larger values of m.

This result is true at still larger m. When $m \sim \Omega^{5/8}$ and $P \sim \Omega^{11/16}$, the relative error in neglecting the interaction in the dispersion relation balances the relative difference between the scales x_0 and x_2. Again a moving frame can be employed to simplify the analysis and it is found that there is no difference in the qualitative behaviour. The correction to the result $\alpha = 2/m_1$ enters only in the amplitude equation, derived at second order, but, as in the $m \sim \Omega^{1/2}$ case above, it affects only the phase of the disturbance. We note, however, that although the length scales associated with the amplitude equation vary only a little from the case of smaller m, the timescale associated with the growth increases dramatically. For still larger m the error in neglecting the interaction in the first order dispersion relation has no effect on the growth over the scales on which the amplitude equation holds. Here the governing equation is

$$\alpha^{-5}P_{01t_2} - 3i/2\alpha^2 P_{01X_1X_1} = \alpha(1-i)/\sqrt{2}\ P_{01} - 5i\alpha^4/2\ P_{01}|P_{01}|^2, \qquad (5A.8)$$

in place of (5A.7) where the variables are suitably scaled with Ω. Again $\alpha = 2/m$. This result is exactly that which would be obtained by letting $\bar{m} \to \infty$ in the formulae for the two-dimensional coefficients (5.2.24a&c). There are no significant differences from the $\bar{m} = O(1)$ case except that

the timescale over which the growth to occurs is greatly increased. This leads to an increase in the streamwise distance that the wavepacket must travel before it is significantly affected by the growth described by (5A.8). This in turn leads to the possibility of the growth rate being affected by the non-parallel nature of the basic boundary layer flow, just as is the case for the linear waves, discussed in §4.3.5.

In contrast to the above, there are differences as m increases in the fully nonlinear, inviscid stage covered in §5.4, if the size of the disturbance is not scaled to increase with m. The boundary layer is governed by

$$-m/2\ A_X + AA_X = -P_X, \tag{5A.9}$$

within a frame moving downstream with a speed m/2, and the free stream has the controlling equation

$$\bar{P}_{yy} = 2\bar{P}_{XT^*}, \tag{5A.10}$$

where T^* describes the long timescale over which the interaction has an effect. Together with the interaction conditions equations (5A.9&10) lead to an integral equation, valid in the moving frame, for an initial value problem,

$$(B-1)^2 = 1 + \int_{-\infty}^{T^*}\int_{-\infty}^{\bar{X}} \frac{\partial^2 B(p,q)/\partial p^2}{(T^*-q)^{1/2}(\bar{X}-p)^{1/2}}\,dp\,dq. \tag{5A.11}$$

Here $B = 2m^{-1}A$ and X and T^* have been normalised. The boundary conditions are $B \to 0$ as $|\bar{X}| \to \infty$. The cases $B = -1$ and $B = 0$ correspond to stationary and sonic travel respectively in the laboratory frame. The classical viscous sublayer, required to ensure that the no-slip boundary condition is satisfied at the wall, reacts quasi-steadily due to the slow timescale of the motion in the free stream and so is subject, not to the van Dommelen singularity, but to the singular forms described by

Elliot, Smith and Cowley (1983). These are appropriate to the steady classical boundary layer on an upstream-moving surface. In contrast to the finite time Van Dommelen singularity these are of a finite X form and so the question arises of whether or not a self-consistent solution of the form outlined above, and including the effects of the sublayer, can exist for all $\bar{X}$ at a given time. A similar question arises in §7.4.

FIGURE CAPTIONS FOR CHAPTER 5.

Figure 5.2.1 This shows contour plots of the eigenvalues, μ_1 and μ_2, (see equation (5.2.29c)), derived from the quadratic form of the dispersive terms in (5.2.23), for various $\bar{m}$ and β. Here β is the scaled spanwise wavenumber and $\bar{m}$ is the scaled value of $(M_\infty^2-1)Re^{1/9}$. Equation (5.2.23) is hyperbolic where μ_2 is negative and elliptic otherwise. It seems that μ_1 is always positive.

Figure 5.3.1 (a-i) This shows contour plots of various coefficients of interest in the high frequency analysis and normalisation leading to the nonlinear Schrödinger equation (5.2.27). The coefficients are plotted against $\bar{m}$ and β.

(a) The streamwise wavenumber, α, given by the high frequency dispersion relation (5.2.6). We note that α decreases as $\bar{m}$ increases.

(b) The (scaled) angle β/α which the wave makes with the direction of the oncoming stream.

(c) The group velocity in the x-direction of a disturbance, given by equation (5.2.18a).

(d) The group velocity in the z-direction of a disturbance, given by equation (5.2.18b). We note that this is negative.

(e) The ratio of the group velocities, cg_z/cg_x. This gives the (scaled) angle between the direction of motion of the frame in which the Schrödinger equation (5.2.23) is valid and the oncoming free stream. It can be seen to have a maximum for the oblique, primarily acoustic disturbances which occur for large values of $\bar{m}$. See §5.3.3.

(f) The coefficient $\hat{A}$ in equation (5.2.23). A change in the sign of $\hat{A}$ from positive to negative indicates a change from the possibility of sideband instability (and the associated increased growth) occurring in disturbances of type (a) to the possibility of it occurring in those of type (b).

Here (a) and (b) refer to the equations of §5.3.1. The value $\hat{A} = 0$ corresponds to the primary direction along which focussing occurs coinciding with the streamwise (X-) direction.

(g) The coefficient $\hat{B}$ in equation (5.2.23). The value $\hat{B} = 0$ corresponds to the focussing being primarily in the spanwise (Z-) direction. The warped wave case of equation (5.3.4) is of relevance to the region about $\beta = 0$.

(h) The coefficient $\hat{H}\hat{B}^2$. A change in the sign of this coefficient from negative to positive corresponds to a change in type of equation (5.2.23) from hyperbolic to elliptic and the suppression of the sideband instability which can give rise to increased growth rates and spectrum broadening.

(i) The coefficient $\hat{A}\hat{H}\hat{B}^2$. The sign of this coefficient is the sign of s^a in equation (5.3.1a). If it is negative there is the possibility of an increased growth rate of the disturbances governed by this equation, due to the sideband instability.

Figure 5.3.2 This is a sketch showing the variation of $\hat{A}$ and $\hat{H}$ with β at large values of $\bar{m}$. See §5.3.3.

Figure 5.2.1

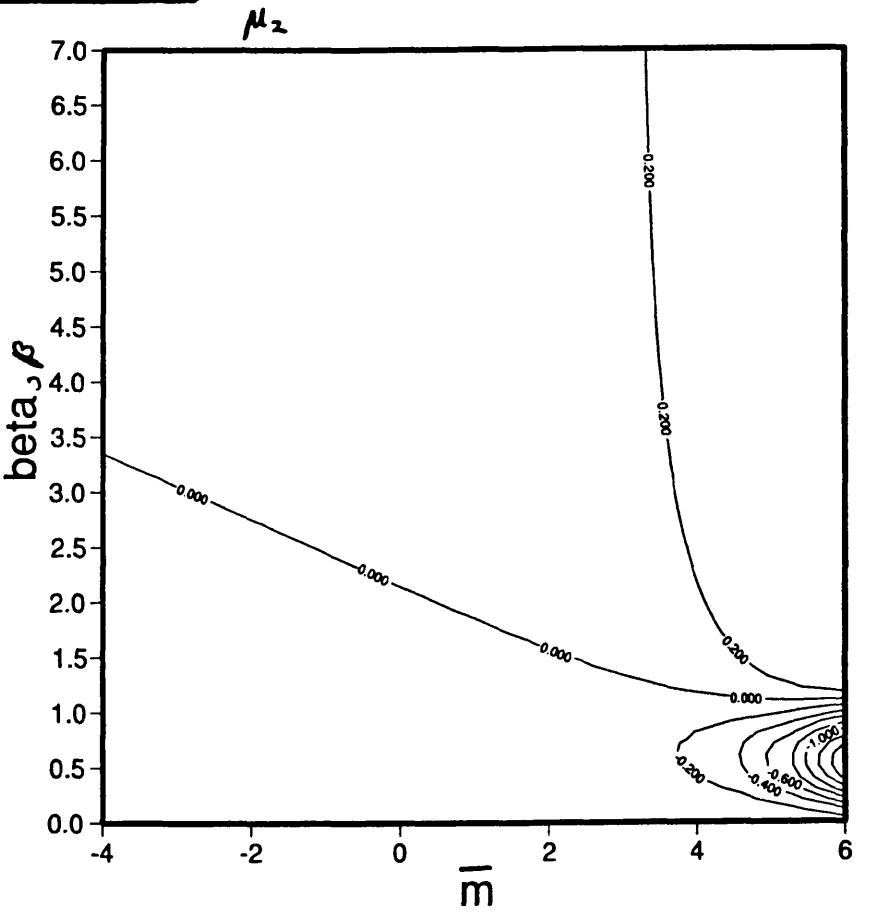
μ_2
beta, β
$\bar{m}$
0.200
0.000
-0.200
-0.400
-0.600
-1.000

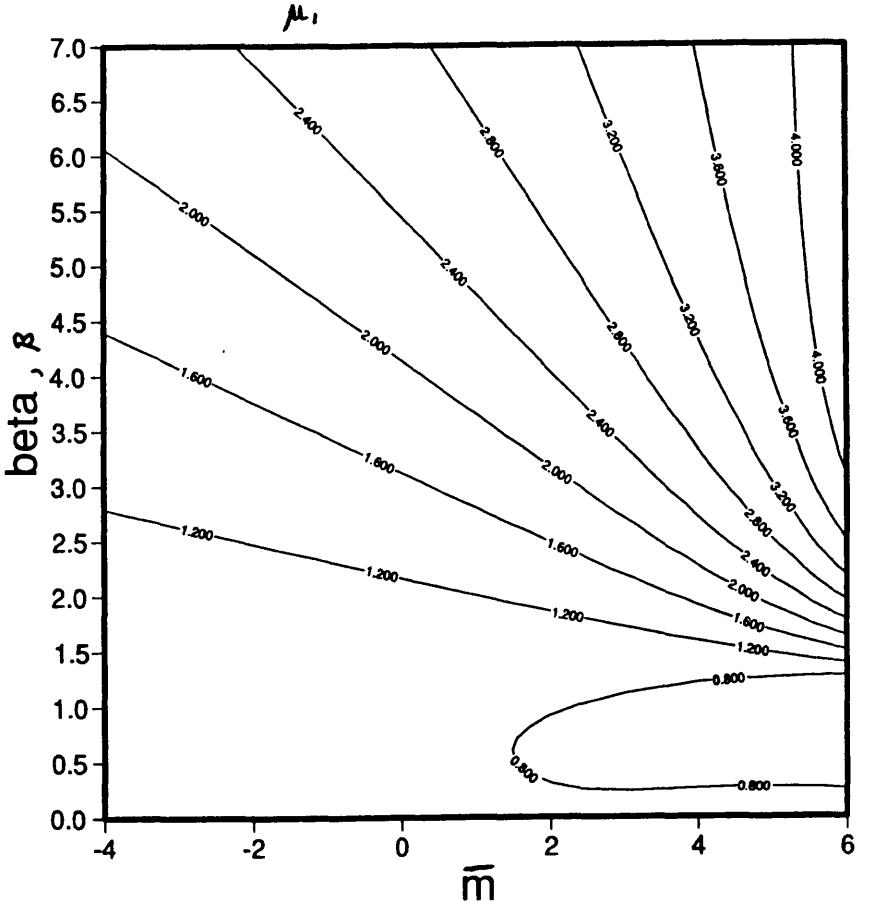
μ_1
beta, β
$\bar{m}$
2.400
2.000
1.600
1.200
2.800
3.200
3.600
4.000
0.800

Figure 5.3.1

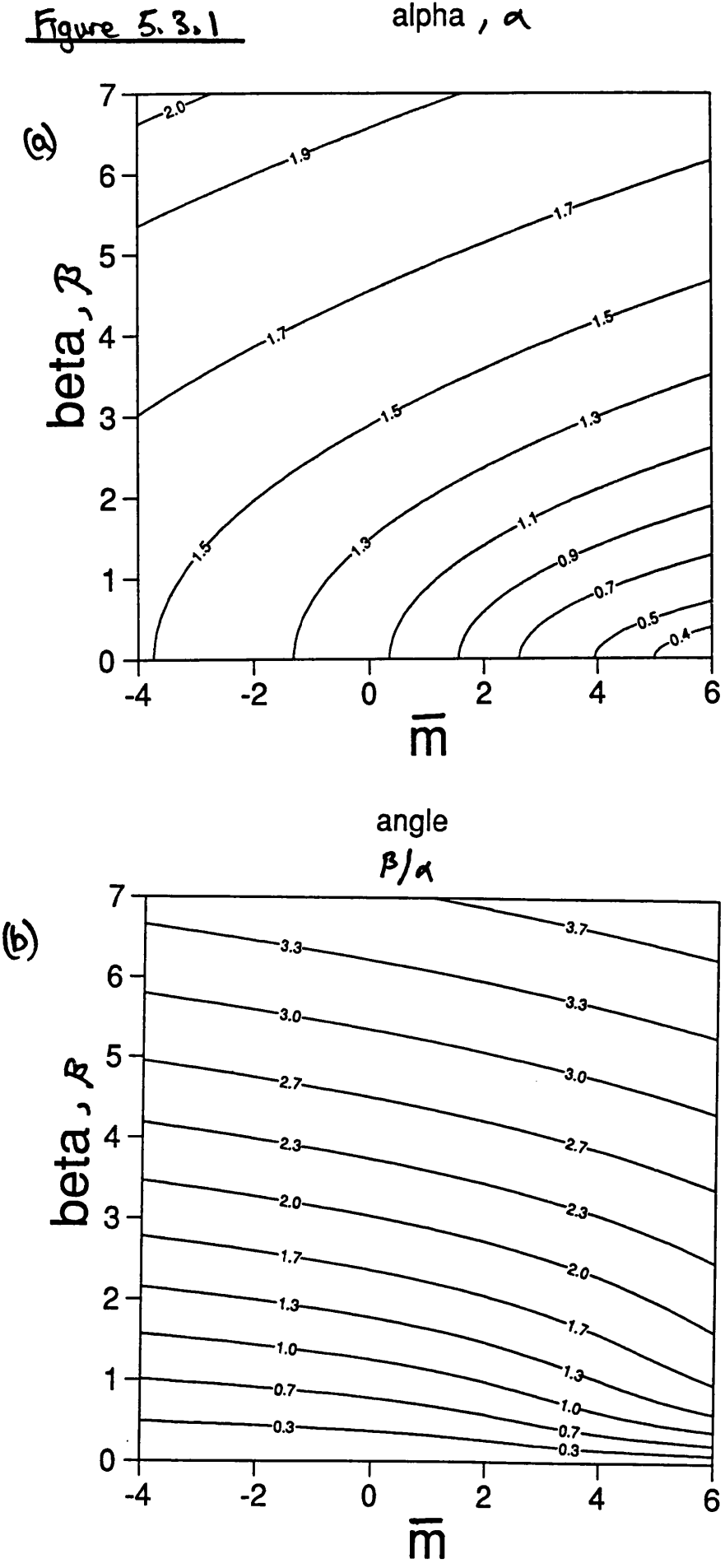
alpha , α
(a)
beta, β
m̄
2.0
1.9
1.7
1.7
1.5
1.5
1.3
1.3
1.1
0.9
0.7
0.5
0.4
angle
β/α
(b)
beta, β
m̄
3.7
3.3
3.3
3.0
3.0
2.7
2.7
2.3
2.3
2.0
2.0
1.7
1.7
1.3
1.3
1.0
1.0
0.7
0.7
0.3
0.3

Figure 5.3.1 the x group velocity, cg_x

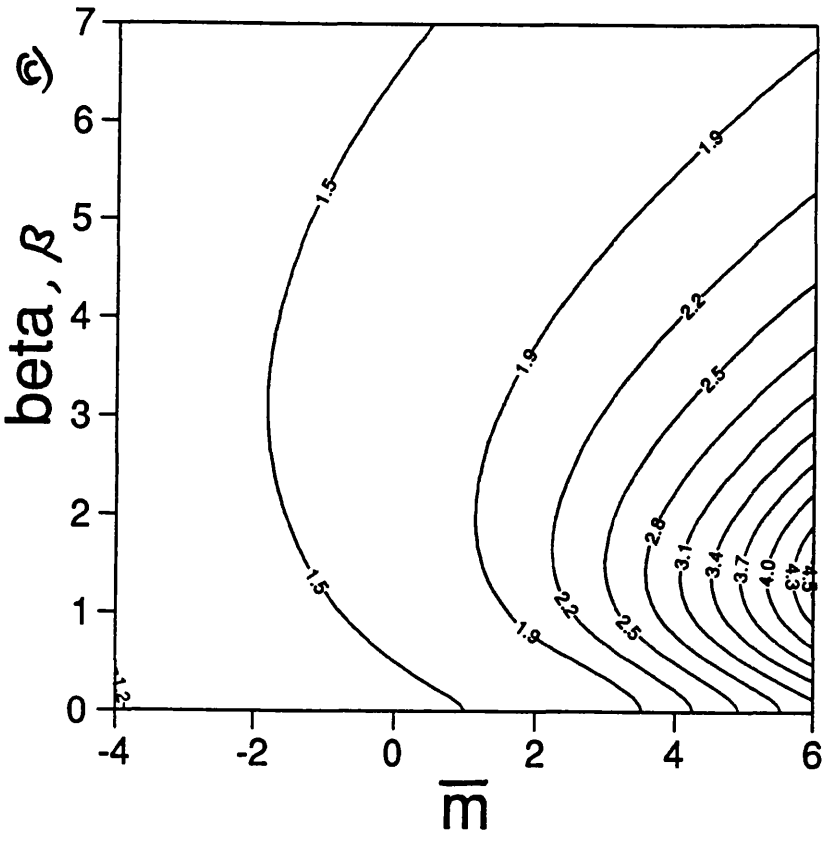

the z group velocity, cg_z

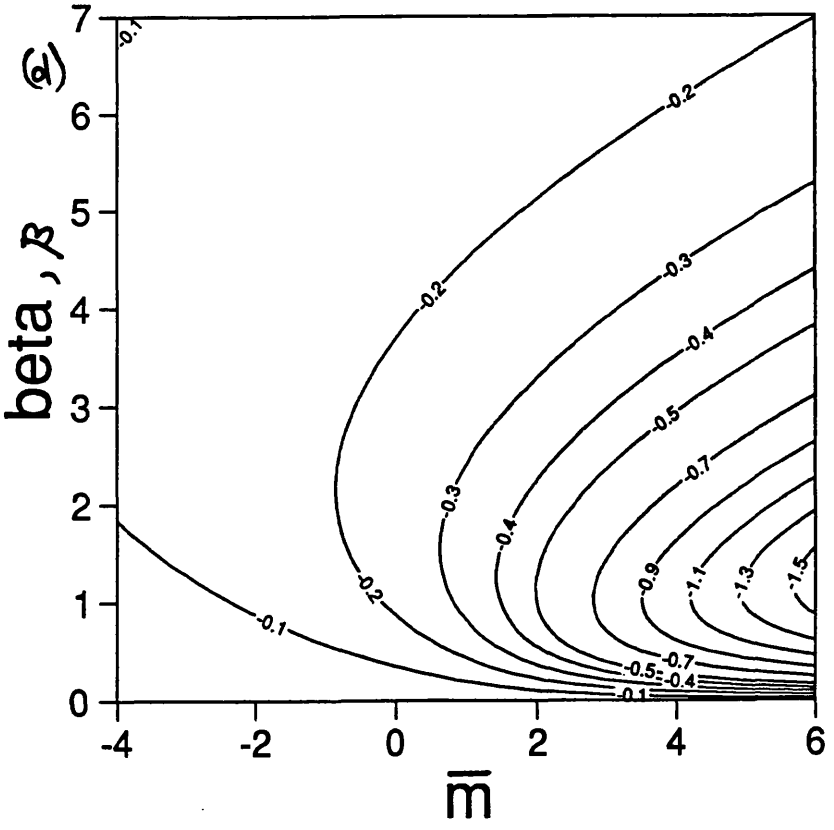

Figure 5.3.1

cgz / cgx

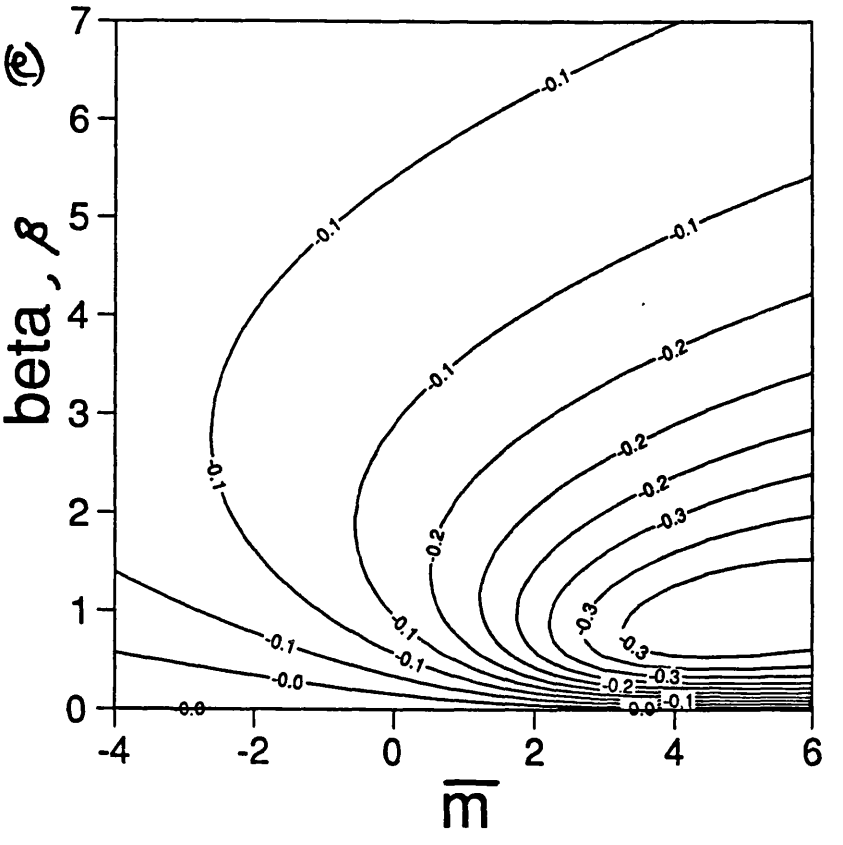

the coefficient $\hat{A}$

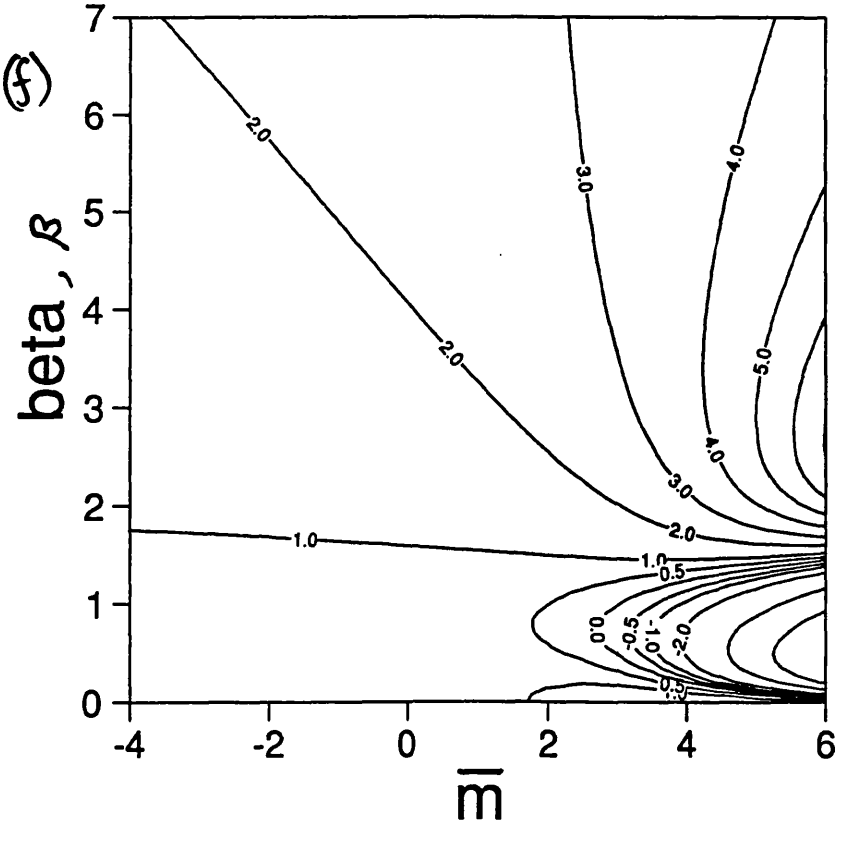

Figure 5.3.1 the coefficient $\ddot{B}$

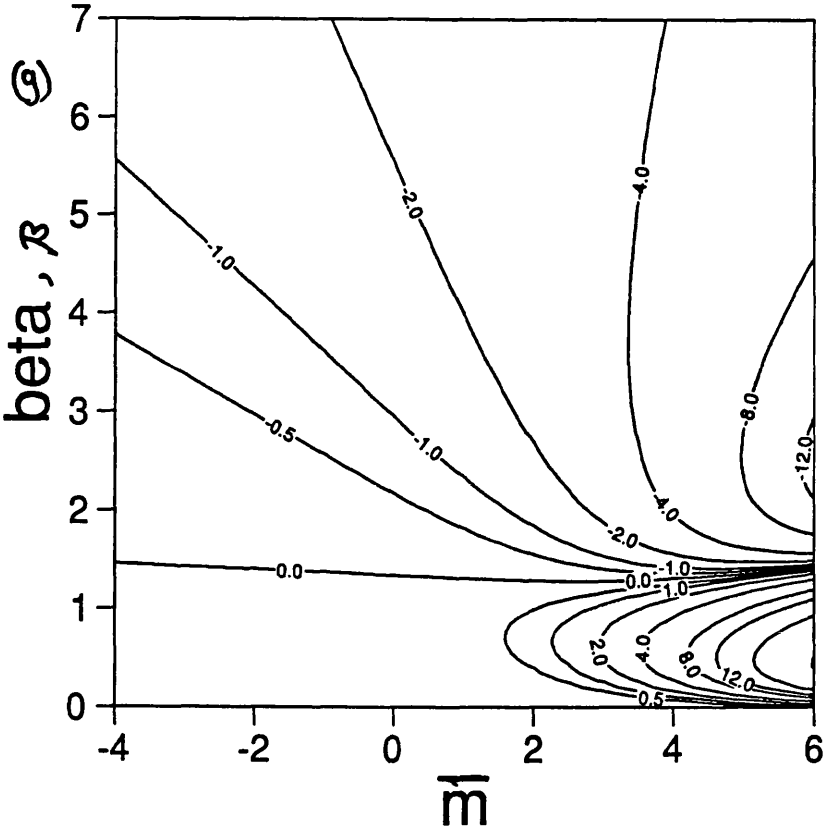

the coefficient $\hat{H}\hat{B}^2$

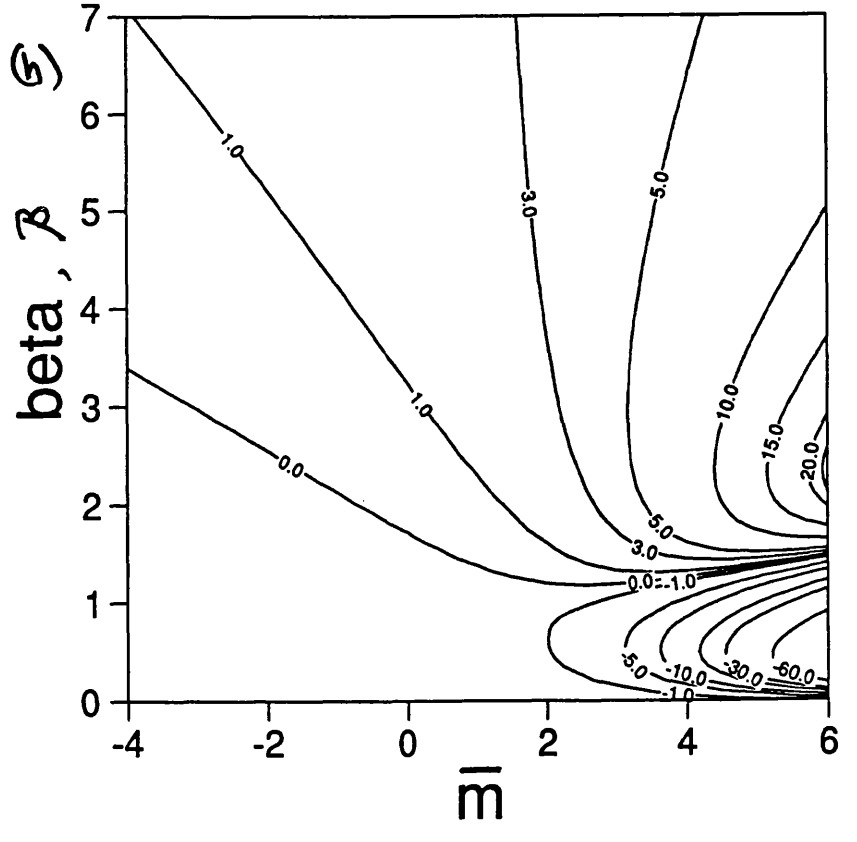

Figure 5.3.1 the coefficient $\hat{A}\hat{H}\hat{B}^2$

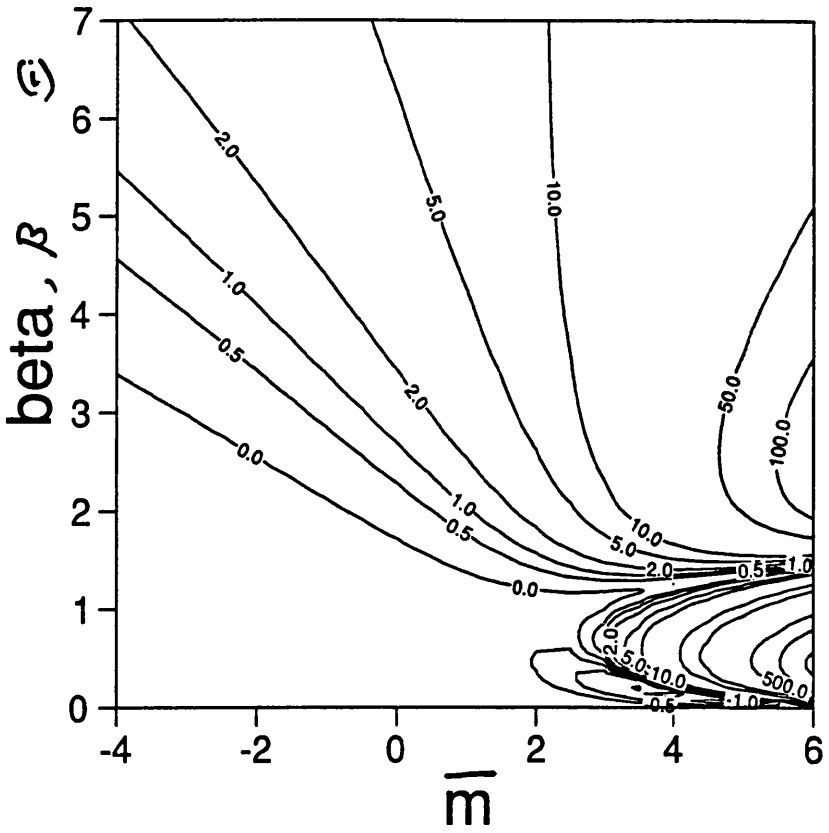

Figure 5.3.2

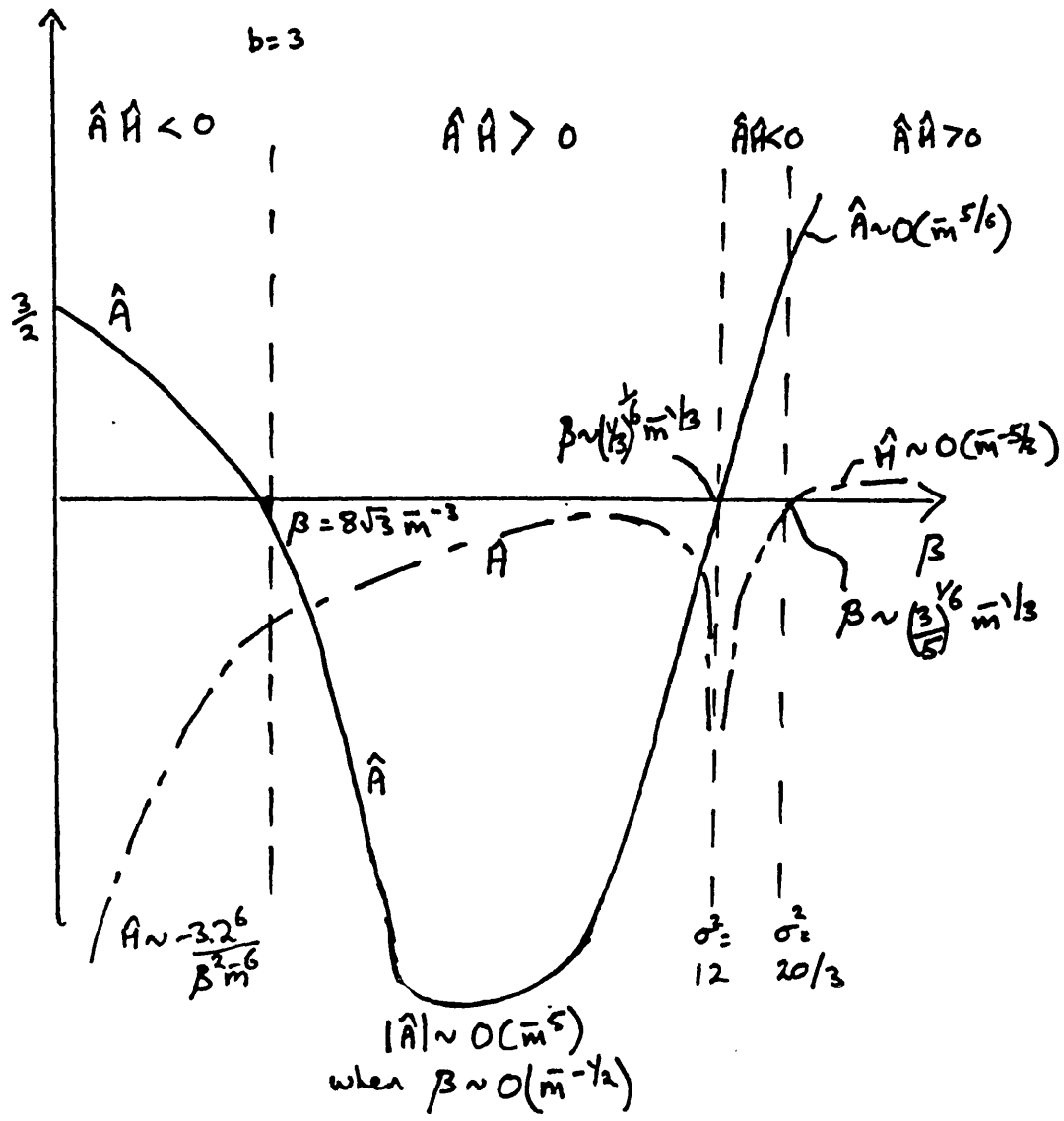

$b\propto\frac{\beta^2\bar{m}^6}{2^6}$

$\sigma\approx\frac{2\bar{m}}{\beta^3}$

Chapter Six

RESONANT TRIADS AND (AMPLITUDE)^2 INTERACTIONS IN TRANSONIC BOUNDARY LAYERS.

§6.1 Introduction; Natural Transition For Small Disturbances.

Chapter 5 considers weakly nonlinear interactions of Tollmien-Schlichting waves which occur at an $(\text{amplitude})^3$ level and leads to an equation governing the development of a relatively high frequency, three-dimensional wavepacket as it moves downstream. Nonlinear interactions can also take place between triads of waves at the $(\text{amplitude})^2$ level and it is interactions of this type that are the subject of this chapter.

The study of so-called resonant triads is relevant to a transition mechanism other than the route described in §5.1. This new type occurs at smaller initial disturbance amplitudes (the r.m.s. velocity fluctuations of the disturbance are approximately 0.1% of the free stream velocity) and involves the gradual filling of the energy spectrum through nonlinear wave interactions. In incompressible flow the first such interaction involves the fundamental wave, with frequency f say, interacting with a subharmonic of frequency f/2. This subharmonic is an oblique wave and in incompressible flow its direction is at 60° to that of the oncoming free stream. As transition progresses, staggered arrays of hairpin vortices are generated with their streamwise wavelength twice that of the original fundamental wave (Saric and Thomas (1984)).

This onset of three-dimensionality and the importance of the subharmonic can be explained by the resonant triad mechanism, suggested by Craik (1971), in which a suitable pair of oblique waves are selectively amplified by a nonlinear interaction with a two-dimensional wave. This type of transition is called subharmonic transition or (after Herbert and Morkovin (1979)) C-type.

Experiments by Kachanov, Koslov and Levchenko (1978) and Kachanov and Levchenko (1984) confirm the presence of this interaction in transitional incompressible boundary layers and Smith and Stewart (1987) use triple deck theory to give a rational description of the nonlinear

development of the three interacting modes. They show that, as confirmed by experiments, the three-wave system eventually gains the growth rate of a single two-dimensional mode. This is in excess, for incompressible flow, of that of a single linear oblique mode.

This nonlinear theoretical work has been extended by Avis (1989) to axisymmetric flows and, importantly, to an investigation of the effects of detuning. The triad proposed by Craik predicts the amplification of a single oblique mode, whilst the experiments of Kachanov and Levchenko detect the amplification of a broad band of disturbances centred, in the frequency spectrum, about the subharmonic. Avis finds that the effect of such detuning is to delay the onset of the phase locking that occurs with resonance. This has the effect of slightly reducing the growth rate but does not destroy the triad mechanism.

We should also mention here the so-called Herbert or H-type transition mechanism (Herbert, Bertolotti and Santos (1987)). This is similar to the C-type mechanism and is also subharmonic. However the spanwise wavelength of the three-dimensional perturbation is different, in general, and indeed can take a range of values. The resonance is between a Tollmien-Schlichting mode and a Squire vorticity mode (Squire (1933)). Using the shape assumption, i.e. choosing the (finite) amplitude of the initial (linear) two-dimensional mode, good agreement in the initial linear growth rate against spanwise wavenumber for a given three-dimensional disturbance with experimental measurements can be obtained. See, for example, Corke and Mangano (1989). It is of interest to note that the H-type mechanism reduces to the C-type when the amplitude of the Tollmien-Schlichting wave is allowed to become small. In any situation other than this the shape assumption is not a "rational" step (in the sense of van Dyke (1964)).

In this chapter we extend the work of Smith and Stewart to transonic boundary layers. We take as our starting point the triple deck equations, derived in §4.2,

which describe the nonlinear development of Tollmien-Schlichting waves which are either two-dimensional or at an angle of at most $O(Re^{-1/18})$ to the streamwise direction. In this chapter the Mach number of the flow, M_∞^2, is such that $|M_\infty^2-1| = O(Re^{-1/9})$. Using the high frequency limit of the dispersion relation for linear waves, as in §5.2, we set up a multiple-scales expansion of the unsteady triple deck equations (4.2.28). This expansion leads to a triad of linked nonlinear equations governing the amplitude of a two-dimensional wave and a pair of oblique waves.

A major difference between incompressible flow and transonic flow is that in the latter it is the most oblique high frequency waves which are most unstable on linear grounds (see equation (5.2.1) in the limit $\bar{\beta} \to \infty$), whilst in the former these are the least unstable (see, for example, Smith and Stewart). Of particular interest in transonic flow, therefore, is the possibility, especially in the case of just-supersonic flow where two-dimensional modes suffer from an extremely low growth rate, of nonlinear effects transferring energy from three-dimensional waves to two-dimensional waves, increasing their growth rate.

The oblique modes, in the triad, turn out not to be symmetric, but to lie to one side of the fundamental. Their frequency is also not equal to half that of the fundamental. This is unlike Craik's symmetric triad mechanism. The modes still interact, but it is not clear whether they become phase locked and resonate in the same way. In §§6.3-4 we consider the limits of large and small spanwise wavenumber. In these limits the linear growth rates of two of the waves become identical and are widely separated from that of the third.

§6.2 The Scalings And Derivation Of The Triad Equations.

The triple deck equations appropriate to nearly two-dimensional transonic flow are

$$U_X + V_Y = 0, \tag{6.2.1a}$$

$$U_T + UU_X + VU_Y = -P_X + U_{YY}, \tag{6.2.1b}$$

$$U = V = 0 \text{ at } Y = 0 \text{ and } U \to Y + A \text{ as } Y \to \infty\ , \tag{6.2.1c-e}$$

$$\bar{P}_{yy} + \bar{P}_{zz} = 2\bar{P}_{xT} + m\bar{P}_{xx}, \tag{6.2.1f}$$

$$\bar{P} \to P \text{ and } \bar{P}_{\bar{y}} \to A_{xx} \text{ as } \bar{y} \to 0,\ \bar{P} \to 0 \text{ as } X^2+\bar{y}^2+Z^2 \to \infty, \tag{6.2.1g-i}$$

$$M_\infty^2 - 1 = dm, \tag{6.2.1j}$$

where d is defined in (4.2.22d) and is $O(Re^{-1/9})$ as $Re \to \infty$. We know (equation (5.2.1)) that, at high frequencies, linear, two-dimensional solutions of this system have a length scale, L, of $O(\Omega^{-3/5})$ where Ω is the (large) disturbance frequency. Viscous growth occurs over the much longer $O(\Omega^{3/10})$ scale. If we suppose that the amplitude of the pressure in the disturbance is O(h) then the velocity provoked is, from (6.2.1b), of a size $O(h/L\Omega) \sim O(h\Omega^{-2/5})$. The nonlinear inertial effects are therefore of a size $O(UU_X) \sim O(h^2\Omega^{-1/5})$. For the relative error in neglecting these nonlinear effects ($O(h\Omega^{-4/5})$) to balance the small growth (of relative size $O(\Omega^{-9/10})$) we must have $h \sim \Omega^{-1/10}$. A pressure of this size will provoke a possible $(\text{amplitude})^2$ interaction over the length scales associated with the viscous growth of the wave.

The triad interaction rests on there being a system of three waves each of which satisfies the linear dispersion relation and such that the product of any two of them yields the third (or its complex conjugate). Any such system of three waves of amplitude h will give an interacting triad system. To fix matters here, however, we

insist that one of them (mode 2) be a two-dimensional wave, proportional to $E_2 = \exp i(\tilde{A}x_0 - t_0)$, where x_0 and t_0 are the scaled, fast, space and time variables. At high frequencies, the neutral dispersion relation, on these rapid scales, is

$$(2\Omega\alpha + \beta^2 - \bar{m}\alpha^2)^{1/2} = \alpha^3/\Omega, \qquad (6.2.2a)$$

where $m = \bar{m}\Omega^{2/5}$, and β is the spanwise wavenumber of the disturbance. This can be rewritten as

$$\alpha^6 + \bar{m}\alpha^2\Omega^2 - 2\alpha\Omega^3 - \beta^2\Omega^2 = 0, \qquad (6.2.2b)$$

if we take care to choose only roots such that $\mathrm{Re}(\alpha^3/\Omega)$ is positive. We consider two oblique waves proportional to

$$E_1 = \exp i\{(1+s)\tilde{A}x_0 + \beta z_0 - (1+\mu)t_0\}, \qquad (6.2.3a)$$

$$E_3 = \exp i\{s\tilde{A}x_0 + \beta z_0 - \mu t_0\}, \qquad (6.2.3b)$$

where s and μ are to be found. These modes interact with each other and with the two-dimensional mode E_2 according to the relations

$$E_1 = E_2E_3, \quad E_2 = E_1E_3^+, \quad E_3 = E_1E_2^+, \qquad (6.2.4a\text{-}c)$$

where the superscript + denotes the complex conjugate. Equations (6.2.2b) and (6.2.4) require that

$$R(1+\mu,\beta) = R(1,0) + R(\mu,\beta), \qquad (6.2.5a)$$

$$R(1,0) = \tilde{A}, \quad s = R(\mu,\beta)/\tilde{A}, \qquad (6.2.5b\text{-}c)$$

where $R(q,\beta)$ is the unique positive root of

$$\phi^6 + \bar{m}q^2\phi^2 - 2q^3\phi - \beta^2q^2 = 0. \qquad (6.2.5d)$$

Therefore, given $\bar{m}$ and β, (6.2.5) gives $\tilde{A}$, μ, and s which

describe the triad system. Numerical investigations show that triads exist for all β and all $\bar{m}$. This result is complemented by the consideration of the limiting cases of small and large β in later sections of this chapter. Figure 6.2.1 illustrates the value of μ for the triads for a range of β and $\bar{m}$. The values of s and μ are always positive. The oblique modes found by this method are at an angle of $O(Re^{-1/18})$ to the streamwise direction due to the scalings inherent in (6.2.1). We note too that both the oblique modes are directed towards the same side of the two-dimensional mode. This is unlike the incompressible case where the system is symmetric. The mode proportional to E_3 (mode 3) is more oblique than that proportional to E_1 (mode 1).

The expansion used to find solutions of equations (6.2.1) proceeds as follows, using the scales derived above for guidance,

$$\varepsilon = \Omega^{-1/10}, \quad Y = \varepsilon^5 Y^*, \quad \bar{y} = \varepsilon^8 y^*, \quad m = \varepsilon^{-4}\bar{m}, \tag{6.2.6a-d}$$

$$P \sim \varepsilon(P_0 + \varepsilon^9 P_1 + \ldots), \tag{6.2.6e}$$

$$U \sim \varepsilon^5(Y^* + U_0 + \varepsilon^9 U_1 + \ldots), \tag{6.2.6f}$$

$$V \sim \varepsilon^4(V_0 + \varepsilon^9 V_1 + \ldots), \tag{6.2.6g}$$

$$\bar{P} \sim \varepsilon(\bar{P}_0 + \varepsilon^9 \bar{P}_1 + \ldots), \tag{6.2.6h}$$

$$A \sim \varepsilon^5(A_0 + \varepsilon^9 A_1 + \ldots), \tag{6.2.6i}$$

$$\partial_X \sim \varepsilon^{-6}(\partial_{x_0} + \varepsilon^9 \partial_{x_1} + \ldots), \tag{6.2.6j}$$

$$\partial_Z \sim \varepsilon^{-8}(\partial_{z_0} + \varepsilon^9 \partial_{z_1} + \ldots), \tag{6.2.6k}$$

$$\partial_T \sim \varepsilon^{-10}(\delta_{t_0} + \varepsilon^9 \partial_{t_1} + \ldots). \tag{6.2.6l}$$

Here x_0, z_0 and t_0 represent the fast scales associated

with the wavelength and frequency of the neutral wave. All the dependence on these scales is presumed to be restricted to the exponential factors E_1, E_2, and E_3.

We write P_0 and P_1 as

$$P_0 = P_{01}E_1 + P_{02}E_2 + P_{03}E_3 + (\text{ complex conjugates }), \tag{6.2.7a}$$

$$P_1 = P_{11}E_1 + P_{12}E_2 + P_{13}E_3 + (\text{ complex conjugates }) + (\text{ terms in } E_j^2 \text{ and } E_j^0,\ j = 1,2,3\ ), \tag{6.2.7b}$$

and use similar expressions for the other variables.

In the following analysis we use the notation

$$g_j = (-i)(E_{jx_0}/E_j), \quad h_j = (i)(E_{jt_0}/E_j), \quad f_j = g_j/h_j, \tag{6.2.8a-c}$$

so that

$$g_j = [(1+s)\tilde{A},\ \tilde{A},\ s\tilde{A}], \qquad h_j = [(1+\mu),\ 1,\ \mu],$$

$$f_j = [(1+s)\tilde{A}/(1+\mu),\ \tilde{A},\ s\tilde{A}/\mu], \qquad j = [1,\ 2,\ 3]. \tag{6.2.9a-c}$$

Substitution of (6.2.6) and (6.2.7a) into equations (6.2.1) leads, in a similar fashion to the work of §5.2, to the first order equations

$$-ih_jU_{0j} = -ig_jP_{0j} + U_{0j}'', \tag{6.2.10a}$$

$$ig_jU_{0j} + V_{0j}' = 0, \tag{6.2.10b}$$

$$V_{0j} = U_{0j} = 0 \text{ at } Y^* = 0 \text{ and } U_{0j} \to A_{0j} \text{ as } Y^* \to \infty. \tag{6.2.10c-e}$$

Here $'$ represents ∂_{Y^*}. These lead to the results

$$U_{0j} = f_j P_{0j}(1 - e^{\sigma_j Y^*}), \tag{6.2.11a}$$

$$V_{0j} = -ig_j f_j P_{0j}(Y^* - (e^{\sigma_j Y^*} - 1)/\sigma_j), \tag{6.2.11b}$$

$$A_{0j} = f_j P_{0j}, \tag{6.2.11c}$$

$$\sigma_j = h_j^{1/2} \exp(3\pi i/4). \tag{6.2.11d}$$

The free stream equations at first order lead to the results

$$\bar{P}_{0jy^*} = A_{0j}(-g_j^2), \quad P_{0j} = \bar{P}_{0j}|_{y^* = 0}, \tag{6.2.12a-b}$$

from (6.2.1g-h), and from (6.2.1f-i) we find

$$\bar{P}_{0jy^*y^*} - \gamma_j^2 \bar{P}_{0j} = 0, \tag{6.2.13a}$$

$$\gamma_j^2 = (2g_j h_j + \beta^2 - \bar{m}g_j^2), \; j = 1,3, \quad \gamma_2^2 = (2g_2 h_2 - \bar{m}g_2^2). \tag{6.2.13b-c}$$

Combining (6.2.12&13) and (6.2.11c) gives

$$\gamma_j = g_j^2 f_j, \; j = 1,2,3. \tag{6.2.14}$$

These are the high frequency dispersion relations for the individual waves of the triad.

At second order the nonlinear terms on the left hand side of (6.2.1b), evaluated at $Y^* = \infty$, give a contribution

$$i\Big[\{Y^* + \sum_j f_j(P_{0j}E_j + P_{0j}^+E_j^+)\}\{\sum_j f_j g_j(P_{0j}E_j - P_{0j}^+E_j^+)\} -$$

$$\sum_j f_j g_j(P_{0j}E_j - P_{0j}^+E_j^+)Y^* + \sum_j f_j g_j(\sigma_j^{-1}P_{0j}E_j - (\sigma_j^+)^{-1}P_{0j}^+E_j^+)\Big]$$

$$= i\Big[\, NL_jE_j - VG_jE_j \,\Big], \tag{6.2.15a}$$

say, where

$$NL_jE_j = \sum_j f_j(P_{oj}E_j + P_{oj}^+E_j^+) \sum_j f_jg_j(P_{oj}E_j - P_{oj}^+E_j^+),$$

(6.2.15b)

$$VG_jE_j = \sum_j f_jg_j(\sigma_j^{-1}P_{oj}E_j - (\sigma_j^+)^{-1}P_{oj}^+E_j^+), \qquad (6.2.15c)$$

and we consider only the parts of the right hand sides of (6.2.15b-c) which are proportional to E_j.

In a way similar to that in §5.2, we find that the second order contributions in the boundary layer equation yield

$$i(g_jP_{1j} - h_jA_{1j}) = -i(NL_j - VG_j) - P_{ojx_1} - f_jP_{ojt_1}.$$

(6.2.16)

Turning again to the free stream equations and the interaction conditions, we can show that

$$(\gamma_jP_{1j} - g_j^2A_j) = -\mathfrak{L}_j(P_{oj}/2\gamma_j) - 2ig_jf_jP_{ojx_1}, \qquad (6.2.17a)$$

where $\mathfrak{L}_j$ is the linear operator

$$\mathfrak{L}_j = i(2\bar{m}g_j - 2h_j)\partial_{x_1} + i2g_j\partial_{t_1} - i2\beta_j\partial_{z_1}, \qquad (6.2.17b)$$

with $\beta_2 = 0$ and $\beta_{1,3} = \beta$.

Combining (6.2.16) and (6.2.17) leads to the triad equations

$$(1 + \bar{A}_j/2)\left\{\frac{1}{h_j}\frac{\partial P_{oj}}{\partial t_1} + \frac{\bar{F}_j}{g_j}\frac{\partial P_{oj}}{\partial x_1} + \frac{\bar{G}_j}{\beta_j}\frac{\partial P_{oj}}{\partial z_1}\right\} = i(VG_j - NL_j)/g_j,$$

(6.2.18)

where, extending the notation introduced in §5.2, $\bar{A}_j = 2h_j^3/g_j^5$, $\bar{B}_j = \beta_j^2/g_j^6$ $j = 1$ & 3, $\bar{B}_2 = 0$, $\bar{F}_j = (4+2\bar{B}_j+\bar{A}_j)/(2+\bar{A}_j)$ and $\bar{G}_j = -2\bar{B}_j/(2+\bar{A}_j)$.

The right hand side of (6.2.18) can be evaluated using (6.2.15b-c) ,(6.2.4) and (6.2.5a) to give

$$(1 + \bar{A}_j/2)\left\{\frac{1}{h_j}\frac{\partial P_{0j}}{\partial t_1} + \frac{\bar{F}_j}{g_j}\frac{\partial P_{0j}}{\partial x_1} + \frac{\bar{G}_j}{\beta_j}\frac{\partial P_{0j}}{\partial z_1}\right\} = \frac{f_j}{h_j^{1/2}}\frac{1-i}{\sqrt{2}}P_{01} - i\,V_j, \tag{6.2.19a}$$

$$V_j = f_2 f_3 P_{02} P_{03},\ f_1 f_3 P_{01} P_{03}^{+},\ f_1 f_2 P_{01} P_{02}^{+},\quad j = 1,2,3. \tag{6.2.19b}$$

Equation (6.2.19) governs the development of the three interacting waves. The right hand side contains terms giving the linear growth, due to viscous effects, and terms describing the nonlinear linkage between the modes. The left hand side corresponds to movement within a frame travelling downstream with the group velocity of the individual waves. The group velocity is, of course, different for each mode, as is the linear growth rate.

A solution of the full partial differential system would be of interest (Avis (1989) solves a similar system for the case of symmetric, incompressible, triads in an axisymmetric boundary layer). Here, however, we concentrate on the special case of motion which is dependent only on time, suppressing the dependence on the slow spatial variables, x_1 and z_1. This gives a set of ordinary differential equations. Similar equations are investigated by Smith and Stewart, but with the important difference that, due to the symmetry of their oblique waves, the equations governing their oblique modes are identical.

We now narrow down our field of interest still further and, as an initial stage in the study of (6.2.19), consider the limits of large and small β.

§6.3 The Limit Of Large Spanwise Wavenumber.

If β, the transverse wavenumber of the oblique modes, is large the positive root of equation (6.2.5d) asymptotes $\beta^{1/3}q^{1/3}$, and so (6.2.5a) implies

$$\tilde{A} = \beta^{1/3}(1 + \mu)^{1/3} - \beta^{1/3}\mu^{1/3}. \qquad (6.3.1a)$$

Thus we find

$$\mu \sim \beta^{1/2}/(3\tilde{A})^{3/2}, \qquad s \sim 3\beta^{1/2}/(3\tilde{A})^{3/2}, \qquad (6.3.1b\text{-}c)$$

where $\tilde{A}$ can be found, given $\bar{m}$, from (6.2.5b&d).

To first order, the oblique waves in this case have the dispersion relation, $\bar{B}_j = 1$. They are, therefore, more oblique than those that match, as $\bar{m} \to -\infty$, to the transonic minor modes, i.e. $\beta >> |\bar{m}|^{3/4}$. The contribution to relation (6.3.1) from the oblique waves is independent of the Mach number. For large positive $\bar{m}$ we need the restriction $\beta >> \bar{m}^2$, and, since the streamwise wavenumber of the oblique modes, α, is $s\tilde{A} \sim \beta^{1/2}/(3\tilde{A})^{1/2}$ and $\tilde{A} \sim O(1/\bar{m})$ as $\bar{m} \to \infty$, this implies that the oblique waves lie outside the region of the wave-Mach cone which has $\beta/\alpha \sim \bar{m}^{1/2}$. In fact the oblique waves are directed at an angle $(3\tilde{A}\beta)^{1/2}$ to the streamwise direction.

In this limit we find

$$h_j \sim (\beta^{1/2}/(3\tilde{A})^{3/2},\ 1,\ \beta^{1/2}/(3\tilde{A})^{3/2}), \qquad (6.3.2a)$$

$$g_j \sim (\beta^{1/2}/(3\tilde{A})^{1/2},\ \tilde{A},\ \beta^{1/2}/(3\tilde{A})^{1/2}), \qquad (6.3.2b)$$

$$f_j \sim (3\tilde{A},\ \tilde{A},\ 3\tilde{A}). \qquad (6.3.2c)$$

The two oblique waves, which have a much more rapid linear growth rate than does the two-dimensional wave, become identical to first order. If we use as our timescale the relatively rapid scale associated with the oblique modes we can make the transformations

$$t_1 = t/(3\tilde{A}\beta)^{1/4}, \qquad P_{01}^2 = 3P_1^2(1 + \tilde{A}^{-5})/(3\tilde{A})^2, \qquad (6.3.3a\text{-}b)$$

$$P_{02}^2 = 9P_2^2/(3\tilde{A}\beta)^{1/2}, \quad P_{03}^2 = 3P_3^2(1 + \tilde{A}^{-5})/(3\tilde{A})^2, \qquad (6.3.3c\text{-}d)$$

and rewrite (6.2.19), with the spatial derivatives suppressed, as

$$P_{1t} = (1-i)P_1/\sqrt{2} - iP_2P_3, \qquad (6.3.4a)$$

$$P_{2t} = \qquad\qquad - iP_1P_3^+, \qquad (6.3.4b)$$

$$P_{3t} = (1-i)P_3/\sqrt{2} - iP_1P_2^+, \qquad (6.3.4c)$$

to first order as $\beta \to \infty$.

We note that, although the oblique waves represent the same mode to this order, there are no non-trivial solutions to (6.3.4) with $P_1 = P_3$. The system represents two rapidly growing three-dimensional modes interacting through a triad mechanism with a two-dimensional mode. These two-dimensional motions therefore gain energy at a rate greater than one would expect on linear grounds. If $\bar{m} > 0$ this mode will be within the wave-Mach cone. A preliminary numerical solution of (6.3.4), using a simple predictor-corrector scheme, is shown in Figure 6.3.1. Whether or not this nonlinear system has a solution in which the three waves lock together and grow at a common, exponential growth rate, as in the system studied by Smith and Stewart, is a matter for further research. The numerical work does not point to such behaviour, however. Instead there seems to be an interchange of energy between modes 1 and 2 at a rate determined by the amplitude of mode 3, which itself seems to grow exponentially.

§6.4 The Limit Of Small Spanwise Wavenumber.

If, as opposed to the case of large β, we look at the limit of small β, we find that two of the waves become almost identical two-dimensional modes whilst the third becomes a very oblique wave. This can be seen as follows.

For small β we scale μ such that $\beta = b\mu^{1/5}$, where b is an O(1) constant to be found. Provided that

$$\bar{m}\mu^{2/5}b^{-4/3} << 1, \qquad 2\mu b^{-5/3} << 1, \tag{6.4.1a-b}$$

R(q,b) becomes, as in §6.3, the root of

$$\phi^6 = \beta^2\mu^2 = b^2\mu^{12/5}, \tag{6.4.2}$$

i.e.

$$R(\mu,\beta) \sim b^{1/3}\mu^{2/5}. \tag{6.4.3}$$

Since β and μ are small we expect that

$$R(1+\mu,\beta) = R(1,0) + \tilde{A}K\mu^{2/5}, \tag{6.4.4}$$

where K is to be found and $R(1,0) = \tilde{A}$. If the restrictions (6.4.1a&b) are satisfied one can show, by substitution of (6.4.4) into (6.2.5d), that

$$\tilde{A}K(1 + 2\tilde{A}^5) = b^2/2. \tag{6.4.5}$$

Equations (6.4.4) and (6.2.5a) imply that $\tilde{A}K\mu^{2/5} = R(\mu,\beta)$, which is $b^{1/3}\mu^{2/5}$, from (6.4.3). Thus we determine K and b,

$$K = b^{1/3}/\tilde{A}, \qquad b = [2(1+2\tilde{A}^5)]^{3/5}. \tag{6.4.6a-b}$$

Therefore

$$\mu \sim \beta^5\lambda^3, \qquad s \sim \frac{\beta^2\lambda}{\tilde{A}}, \qquad \lambda = [2(1+\tilde{A}^5)]^{-1}. \tag{6.4.7a-c}$$

As $\bar{m} \to \infty$ we know that $\tilde{A} \sim O(1/\bar{m})$ and so $b \sim O(1)$. Also, as $\bar{m} \to -\infty$, $\tilde{A} \sim O(|\bar{m}|^{1/4})$ and $b \sim O(|\bar{m}|^{3/2})$. Therefore, the conditions (6.4.1a&b) can be shown to require only $\beta << \bar{m}^{-1/2}$, as $\bar{m} \to \infty$. This is the only additional condition on β, other than that it be small, that (6.4.1a-b) imposes as $\bar{m} \to \pm\infty$. It implies that the

three-dimensional wave is less oblique than the oblique acoustic modes identified in §5.3.3.

In the limit $\beta \to 0$, therefore, the coefficients g_j, h_j and f_j become

$$g_j \sim (\tilde{A},\ \tilde{A},\ \beta^2\lambda\ ),\quad h_j \sim (1,\ 1,\ \beta^5\lambda^3), \tag{6.4.8a-b}$$

$$f_j \sim (\tilde{A},\ \tilde{A},\ \beta^{-3}\lambda^{-2}). \tag{6.4.8c}$$

The oblique wave, proportional to E_3, is at an angle of $O((\lambda\beta\tilde{A})^{-1})$, and is relatively long and of low frequency when compared with the nearly identical two-dimensional modes, proportional to E_1 and E_2. Thus, as β decreases, we may expect the relatively high frequency approximation to fail in describing the oblique mode, and equations (6.2.19) to be no longer appropriate.

If we choose new variables

$$t_1 = [\beta^{1/2}\ \lambda^{1/2}\ ]\ t, \tag{6.4.9a}$$

$$P_{01} = [\beta^{-3/2}(1+\tilde{A}^{-5})^{1/2}/(\tilde{A}\lambda^{3/2})]\ P_1, \tag{6.4.9b}$$

$$P_{02} = [\beta^{-3/2}(1+\tilde{A}^{-5})^{1/2}/(\tilde{A}\lambda^{3/2})]\ P_2, \tag{6.4.9c}$$

$$P_{03} = [\beta^{5/2}(1+\tilde{A}^{-5})\lambda^{3/2}/\tilde{A}]\ P_3, \tag{6.4.9d}$$

then (6.2.19) becomes, with the spatial variations suppressed,

$$P_{1t} = \quad -iP_2P_3, \tag{6.4.10a}$$

$$P_{2t} = \quad -iP_1P_3^+, \tag{6.4.10b}$$

$$P_{3t} = (1-i)/\sqrt{2}\ P_3\ \ -iP_1P_2^+. \tag{6.4.10c}$$

This system represents the nonlinear interaction of a relatively slow and long three-dimensional wave of small amplitude but of large growth rate due to its obliqueness, with two, larger amplitude, almost identical and much

shorter two-dimensional waves. It has not yet been investigated, either analytically or numerically.

§6.5 Discussion.

This chapter shows that an (amplitude)^2 type of nonlinear interaction can occur between waves in a transonic boundary layer. It seems that, at any Mach number in the transonic range, a relatively high frequency lower branch Tollmien-Schlichting disturbance, in an otherwise undisturbed boundary layer, can interact with many pairs of oblique high frequency modes. We go on to derive the weakly nonlinear governing equations for this mode interaction and make a start at investigating their properties.

A question arises as to which of the many possible pairs of oblique modes, for a given Mach number, is the most suitable to consider when modelling the process of transition. A partial answer to this problem lies, of course, in the range of disturbances initially present in the boundary layer at the start of the transition process. In addition it seems likely that if, for example, a range of disturbance frequencies are seeded at a sufficiently low amplitude that the nonlinear terms in (6.2.19) are unimportant, at least at the start of the process, it is the most oblique modes which will grow most rapidly and first activate the nonlinear terms.

Another question is that of how these transonic triads fit into a complete picture of (amplitude)^2 interactions at general Mach number. Craik's triad system, studied in the high frequency limit used here by Smith and Stewart, is symmetric, whilst the system considered here is not, in general. It can, however, be easily extended to a symmetric system, by the addition of two modes proportional to $\tilde{E}_1$ and $\tilde{E}_3$ where $\tilde{E}_1$ and $\tilde{E}_3$ are identical with E_1 and E_3 except that β is replaced by $-\beta$. These two waves will also interact with the two-dimensional mode 2. and so give a symmetric system of five interacting waves.

This is of interest in conjunction with the limit $\bar{m} \to -\infty$. If β is scaled with the Mach number so that the modes become minor transonic waves, it may be possible to extend these waves into the subsonic regime and to match them with Craik's incompressible triad in some fashion. The further work required to investigate these ideas, and also to learn more about the transonic triads themselves, is underway.

Figure Captions for Chapter 6.

Figure 6.2.1 This shows values of μ for triad formation for a range of values of β, the (scaled) spanwise wavenumber, and $\bar{m}$, the scaled value of M_∞^2-1. The wavenumber and frequency of a pair of waves which interact with a two-dimensional mode can be calculated from μ via equations (6.2.3&5).

Figure 6.3.1 This presents a preliminary solution of the triad equations (6.3.4) appropriate to large values of β. This shows an interchange of energy between modes 1 and 2. Mode 3 seems to grow exponentially. The latter stages of the interaction are unlikely to have been captured correctly due to the increasingly small time scales involved.

Figure 6.2.1

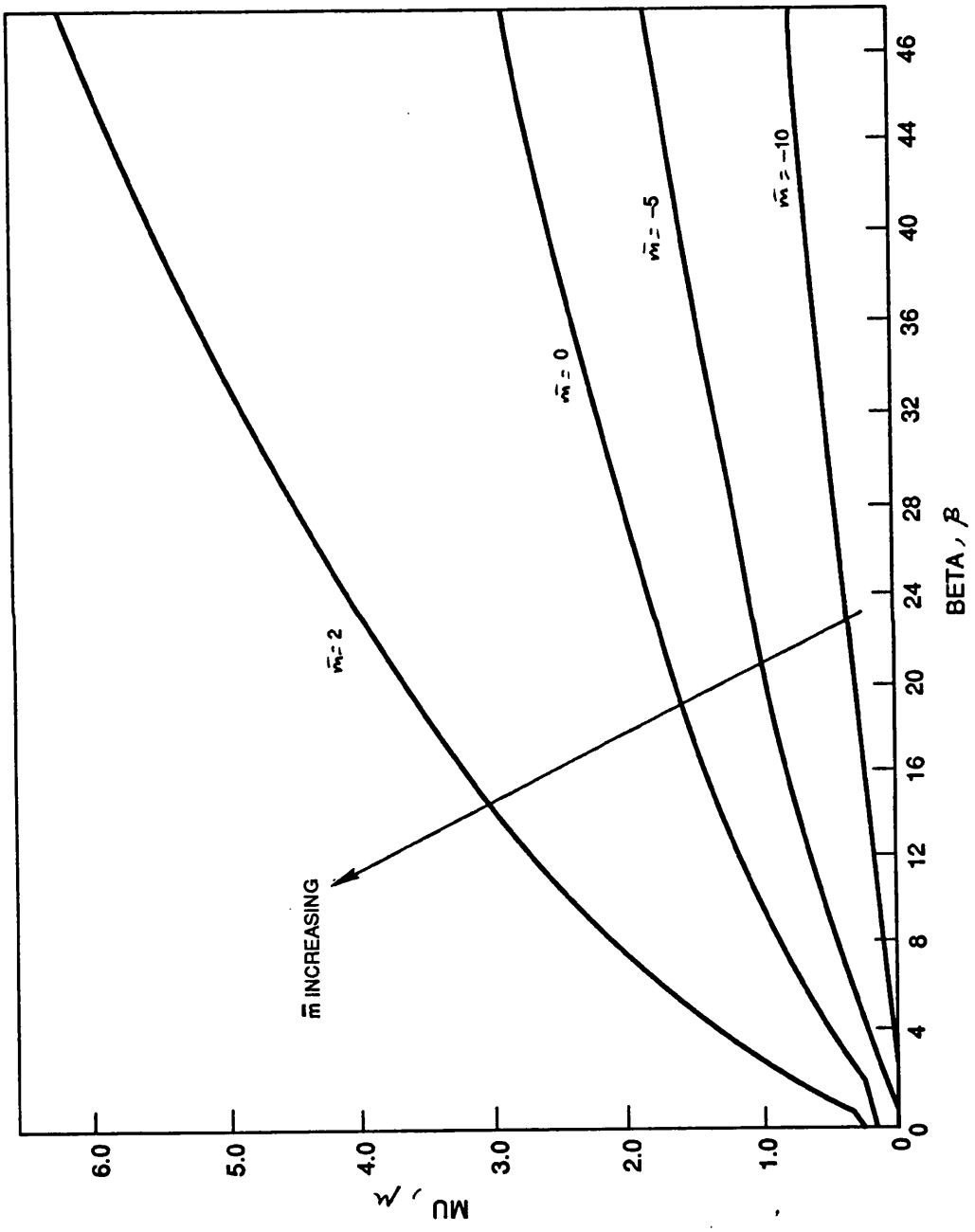
MU, μ
BETA, β
0
4
8
12
16
20
24
28
32
36
40
44
46
1.0
2.0
3.0
4.0
5.0
6.0
m̄ = 2
m̄ = 0
m̄ = -5
m̄ = -10
m̄ INCREASING

Figure 6.3.1

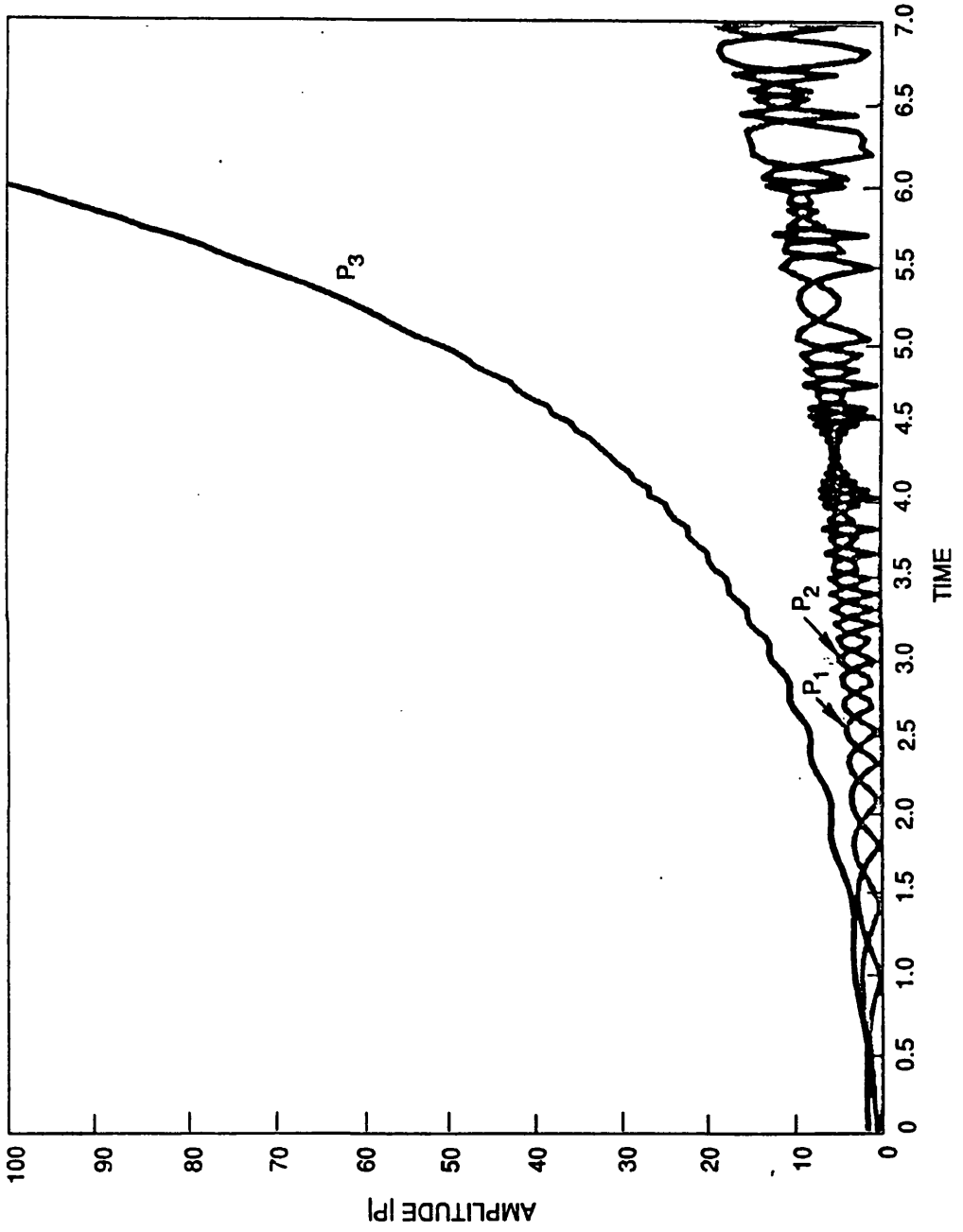
AMPLITUDE |P|
100
90
80
70
60
50
40
30
20
10
0
TIME
0
0.5
1.0
1.5
2.0
2.5
3.0
3.5
4.0
4.5
5.0
5.5
6.0
6.5
7.0
P3
P2
P1

Chapter Seven

UNSTEADY SHOCK / BOUNDARY LAYER INTERACTION IN TRANSONIC FLOW.

§7.1 Introduction And The Governing Equations.

This chapter investigates the behaviour of an interactive boundary layer, at transonic speeds, in the case where the Mach number is so close to unity that relatively small motions close to the wall are able to provoke a nonlinear response and therefore shocks in the free stream. This regime is of interest since, as we show, this feature gives rise to the possibility of a self-sustaining shock / boundary layer oscillation which could provide a means for a bypass rather than a natural transition to turbulence. This oscillation is similar in origin to the shock flutter or large scale shock buffetting seen on transonic aerofoils. See the work, experiments and calculations of Tijdeman and Seebas (1980), Bogar (1986), Howlett (1987) Howlett and Bland (1987), and Gibb (1989). It also, perhaps, has some relevance to the perceived unsteady nature of the shock / boundary-layer interaction at more supersonic speeds, studied by, for example, Dolling and Brusniak (1987), Muck, Andreopoulos, and Dussauge (1986) and Dolling (1989).

The range of Mach numbers, M_∞, for which a shock is possible in the free stream, i.e. for which the equations governing the flow there are nonlinear is given by $|M_\infty^2-1| \sim O(Re^{-1/5})$, as the Reynolds number, Re, becomes large. The steady flow in this regime has been studied by many authors. See Brilliant and Adamson (1974), Bodonyi and Kluwick (1977), (1982), Bodonyi (1979), Adamson and Messiter (1980), and Bodonyi and Smith (1986). The scales for the motion are well-known, although much of the work until now has been concerned with shockless flows or flows with oblique supersonic-to-supersonic shocks so the free stream equations are not of mixed type. In extending the work to cover unsteady flows it is found that the governing time scale (i.e. the slowest scale) is that governing the adjustment of the free stream and is $O(Re^{-1/10})$. On this scale the boundary layer reacts instantaneously and so the lower deck equations in the

governing triple deck formulation are quasi-steady. This feature has also been noted by Rizetta (1982).

We can derive the scales for the motion either by studying the work of previous authors (Brilliant and Adamson or Bodonyi and Smith), or from first principles, using arguments similar to those used in §4.2.2 in obtaining (4.2.28). Using the notation of §4.2.2, and aiming for a nonlinear reaction in the free stream provoked by the boundary layer displacement, we find that, instead of (4.2.20&21), we have

$$\phi_{\bar{y}\bar{y}} + \phi_{zz} = (K + (\gamma+1)\phi_x)\ \phi_{xx} + 2\phi_{xT}, \tag{7.1.1}$$

if

$$(M_\infty^2-1) = Kd,\ K = O(1) \text{ and } d << 1 \text{ as } Re \to \infty, \tag{7.1.2}$$

and

$$\tau L_x = H^2 = L_z^2 = L_x^3/S, \tag{7.1.3}$$

where γ is the ratio of specific heats of the gas. These results, together with others presented in §4.2.2, lead to the scalings

$$L_x = Re^{-3/10}C^{3/10}T_w^{\ 3/2}\lambda^{-7/5}, \tag{7.1.4a}$$

$$L_z = Re^{-1/5}C^{1/5}T_w^{\ 3/2}\lambda^{-8/5}, \tag{7.1.4b}$$

$$H = Re^{-1/5}C^{1/5}T_w^{\ 3/2}\lambda^{-8/5}, \tag{7.1.4c}$$

$$d = Re^{-1/5}C^{1/5}\lambda^{2/5}, \tag{7.1.4d}$$

$$\tau = Re^{-1/10}C^{1/10}T_w^{\ 3/2}\lambda^{-9/5}, \tag{7.1.4e}$$

$$\varepsilon = Re^{-1/10}C^{1/10}T_w^{\ 1/2}\lambda^{1/5}, \tag{7.1.4f}$$

$$S = Re^{-1/2}C^{1/2}T_w^{\ 3/2}\lambda^{-1}. \tag{7.1.4g}$$

The timescale for the viscous adjustment of the boundary layer over these length scales is $O(Re^{-1/5})$ and so is much shorter than τ, the timescale of the motion in the free stream. The expansions of the flow variables

proceed along similar lines to those presented in (4.2.25,26,27) but here we use the scalings suggested by (7.1.4). Three-dimensional effects enter near the wall in a similar fashion to that in the regime covered in §4.2.2. The governing equations are

$$U_X + V_Y + W_Z = 0, \tag{7.1.5a}$$

$$UU_X + VU_Y + WU_Z = -P_X + U_{YY}, \tag{7.1.5b}$$

$$UW_X + VW_Y + WW_Z = \quad W_{YY}, \tag{7.1.5c}$$

$$U = V = W = 0 \text{ on } Y = 0, \qquad U \to Y + A, \; W \to 0, \text{ as } Y \to \infty, \tag{7.1.5d-h}$$

$$\bar{P}_{yy} + \bar{P}_{ZZ} = [(K + (\gamma+1)\bar{P})\bar{P}_X]_X + 2\bar{P}_{XT}, \tag{7.1.5i}$$

$$\bar{P} \to P, \qquad \bar{P}_y \to A_{XX}, \text{ as } \bar{y} \to 0, \tag{7.1.5j-k}$$

where

$$\bar{P} = -\phi_X. \tag{7.1.5l}$$

The flow structure is illustrated in Figure 7.1.1.

The free stream equation (7.1.5i) has been written in conservation form. The far field boundary conditions are problem-dependent. However they will be typically either an increase in pressure between $X \to -\infty$ and $X \to +\infty$ which supports a shock in the free stream or, alternatively, if K is negative, zero pressure at both extremes of X, with a shock appearing close to the wall in response to some localised forcing from the boundary layer. See Figure 7.1.2. We note that the assumption of potential flow is valid even though shocks are present. This is due to the relative weakness of the shock. The error incurred in assuming potential flow is proportional to the cube of the velocity jump across the shock (von Mises (1958)) and so is at most $O((S/L_X)^3) \sim O(Re^{-3/5})$.

There are two sources of nonlinearity in the problem

- the unsteady shock and the quasi-steady lower deck equations.

As in the work of chapters 4 to 6 we concentrate on disturbances in which W is identically zero in (7.1.5). The length scales involved in this unsteady shock / boundary layer interaction are longer than those in the problems studied in chapters 4 to 6 which are longer still than those governing Tollmien-Schlichting waves in incompressible flow. The length scale is exactly that governing steady transonic flow, indeed equation (7.1.5i) is an unsteady version of the transonic small perturbation equation which is a well-known approximation to the Euler equations in the transonic regime. As a result of this and the quasi-steady nature of the boundary layer equation, two-dimensional travelling wave solutions to (7.1.5), with a speed c say, can be found simply since the unsteady problem reduces to the steady problem but with the reduced Mach number altered from K to K-2c. The quasi-steady response of the boundary layer also implies that, in an otherwise undisturbed boundary layer, the only possible solutions of the linearised form of (7.1.5) are upstream influence solutions and there exist no neutral or growing waves. These upstream influence solutions are investigated in §7.2. Sections 7.3 and 7.4 investigate, in a tentative fashion, the possibilities arising from a shock oscillation resonating with a neutral wave which may be possible in a grossly disturbed boundary layer (following, for example, a separation in the lee of a shock or downstream of a wedged trailing edge). Finally §7.5 considers some further points and suggests possibilities for some further research needed on this, potentially very powerful, nonlinear interaction.

§7.2 Small Disturbance Properties (Unseparated Flow).

The linearisation of (7.1.5) about a basic, undisturbed, attached flow (U - Y and P both small) leads, in a similar fashion to that of §4.3.1, to the dispersion

relation

$$\alpha^2(i\alpha)^{1/3} = 3Ai'(0)(2\Omega\alpha + \beta^2 - K\alpha^2)^{1/2}, \qquad (7.2.1a)$$

$$\text{Real}((2\Omega\alpha + \beta^2 - K\alpha^2)^{1/2}) > 0, \quad |\arg((i\alpha)^{1/3})| \le \pi/3, \qquad (7.2.1b\text{-}c)$$

for normal mode disturbances, proportional to $\exp(i(\alpha X+\beta Z-\Omega T)$. This equation can be obtained in the limit of small frequency and m, from the dispersion relation for the case $M_\infty^2-1 \sim mRe^{-1/9}$. See §4.3.4. It produces only stable, upstream-travelling waves, akin to the upstream influence modes studied in §4.3.4.

We write

$$\alpha = (|K|^{3/8}/d^{3/4})s^3, \qquad (7.2.2a)$$

$$\beta = (|K|^{7/8}/d^{3/4})\bar{\beta}, \qquad (7.2.2b)$$

$$\Omega = (|K|^{11/8}/2d^{3/4})\bar{\Omega}, \qquad (7.2.2c)$$

where d is $|3Ai'(0)|$, allowing (7.2.1a) to be written as

$$i^{2/3}s^{14} \pm s^6 - \bar{\Omega}s^3 - \bar{\beta}^2 = 0, \qquad (7.2.3a)$$

if K is positive or negative respectively. The results (7.2.1b-c) reduce to

$$-5\pi/21 \le \arg(s) < -2\pi/21, \qquad (7.2.3b)$$

$$-\pi/2 < \arg(s) < \pi/6, \qquad (7.2.3c)$$

with the equality in (7.2.3b) corresponding to a disturbance which does not decay in the free stream but which has an outward-going phase velocity.

We consider first the supersonic range, K > 0, in steady flow, $\bar{\Omega} = 0$. If

$$s = r\exp(-\pi i/6), \qquad (7.2.4a)$$

with r real, then

$$r^{14} - r^6 = \bar{\beta}^2. \qquad (7.2.4b)$$

Therefore $r \sim \bar{\beta}^{1/7}$ as $\bar{\beta} \to \infty$ and $r \to 1$ as $\bar{\beta} \to 0$. These results lead to the asymptotes

$$\alpha \sim (-i)K^{3/8}d^{-3/4}, \text{ as } \beta \to 0 \text{ or } K \to \infty, \qquad (7.2.5)$$

$$\alpha \sim (-i)\beta^{3/7}d^{-3/7}, \text{ as } \beta \to \infty \text{ or } K \to 0. \qquad (7.2.6)$$

The first of these results is the well-known steady two-dimensional, upstream influence eigenvalue, in supersonic flow (Stewartson and Williams (1969)). The second is independent of Mach number. This feature can be traced to the modes being very oblique on these scalings and, as in §4.3.4, becoming associated more with the transonic major modes.

If a supersonic flow is unsteady, the eigenvalue, α, moves off the negative imaginary axis and represents a decaying, upstream-travelling wave. In the limit of large Ω or, more precisely, large $\bar{\Omega}$, where the relative importance of the unsteadiness depends on the Mach number, we have the asymptote

$$\alpha \sim \exp(-7\pi i/11)\ (4/d)^{3/22}\ \Omega^{3/11}. \qquad (7.2.7)$$

This result is true whatever the value of $\bar{\beta}$, provided it is finite. It represents short wavelength disturbances, travelling upstream and decaying rapidly.

If the flow is subsonic ($K < 0$), the large $\bar{\Omega}$ and large $\bar{\beta}$, zero-frequency results above remain unaltered. For O(1) values of $\bar{\beta}$ however the zero-frequency case has $|K|$ replacing K in (7.2.4a) and r satisfying

$$r^{14} + r^6 = \bar{\beta}^2, \qquad (7.2.8)$$

rather than (7.2.4b). Here, as $\bar{\beta} \to 0$, $r \sim \bar{\beta}^{1/3}$ and so

$$\alpha \sim (-i)|K|^{-1/2}\beta. \qquad (7.2.9)$$

This implies that such "steady upstream influence" modes in steady subsonic motion are confined to angles more oblique than $|K|^{1/2}$ (c.f. the downstream-facing wave-Mach cone in supersonic flow). Furthermore, in the unsteady case of non-zero $\bar{\Omega}$, these subsonic modes are subject to a cut-off at such values of $\bar{\beta}$ or $\bar{\Omega}$ that the disturbance decay in the free stream is lost and (7.2.1b) is violated. This occurs when $\arg(\alpha) = -5\pi/7$. Similar behaviour is seen in the upstream influence modes studied in §4.3.4. We can show that if the value of $[\Omega d^{3/4}/|K|^{11/8}\cos(2\pi/7)]^{1/3}$ lies between the positive roots of $r^{14} - r^6 + d^{3/2}|K|^{-7/4}\beta^2 = 0$ then no waves exist. Outside this range of frequencies the waves that are possible are again upstream-travelling, decaying disturbances. There is no such cut-off if $d^{3/2}|K|^{-7/4}\beta^2 > (5/14)^{3/4} - (5/14)^{7/4} \approx 0.297$. As a result, as the flow becomes locally more subsonic, corresponding to an increase in $|K|$, a wider range of modes becomes subject to a cut-off and very oblique waves are the only solutions to (7.2.1).

The behaviour of the roots of equation (7.2.1a-c) as $\bar{\beta}$ and $\bar{\Omega}$ are varied is summarised in Figure 7.2.1.

§7.3 Shock Oscillation.

We now consider the possibility of shock oscillation or flutter in two-dimensional flows. A tentative suggestion is to model an overall pressure rise in the free stream, from P_1 to P_2 say, as simply

$$P = P_1, \; X < 0, \quad P = P_2, \; X > 0, \tag{7.3.1a-b}$$

$$P_2 > P_1, \tag{7.3.1c}$$

over a relatively long scale. We therefore presume that there is a shock-like discontinuity at $X = 0$. The jump conditions satisfied across this shock can be found either by an expansion of the Rankine-Hugoniot conditions by using an expansion suggested by the scalings of (7.1.4),

or by an analysis of equation (7.1.5i) together with an assumption of irrotational flow, both written in conservation form. Both approaches lead to the results

$$\phi_1 = \phi_2, \tag{7.3.2a}$$

$$K + \tfrac{1}{2}(\gamma+1)(\phi_{1X} + \phi_{2X}) = G_{\bar{y}}^{-2} + 2G_T , \tag{7.3.2b}$$

at a shock given by $X = G(\bar{y},T)$. The subscripts 1, 2 refer respectively to values immediately upstream and immediately downstream of the unsteady shock. Alternatively, if the shock shape is written as $\bar{y} = F(X,T)$, (7.3.2b) becomes

$$KF_X^2 + 2F_XF_T = 1 - \tfrac{1}{2}(\gamma+1)\, F_X^2(\phi_{1X} + \phi_{2X}). \tag{7.3.2c}$$

If we now look for small oscillations about the steady state $G = 0$ (a normal shock) and (7.3.1), the governing equations reduce to a linearised version of (7.1.5i) and the linearised shock conditions

$$\phi_{1\bar{y}\bar{y}} = (K-(\gamma+1)P_1)\phi_{1XX} + 2\phi_{1XT} , \tag{7.3.3a}$$

$$\phi_{2\bar{y}\bar{y}} = (K-(\gamma+1)P_2)\phi_{2XX} + 2\phi_{2XT} , \tag{7.3.3b}$$

$$\phi_1 - P_1G = \phi_2 - P_2G, \tag{7.3.3c}$$

$$G_T = \tfrac{1}{4}(\gamma+1)(\phi_{1X} + \phi_{2X}). \tag{7.3.3d}$$

Oscillatory behaviour of the shock position, proportional to $\exp i(\alpha X-\Omega T)$, gives the jump condition, on elimination of G,

$$\phi_2 = \phi_1\left\{\frac{c - (P_2-P_1)(\gamma+1)/4}{c + (P_2-P_1)(\gamma+1)/4}\right\}, \quad c = \Omega/\alpha . \tag{7.3.4}$$

We note here that resonance will be possible if the speed of oscillation of ϕ_2 on the downstream side of the shock

is

$$c = -(P_2-P_1)(\gamma+1)/4, \qquad (7.3.5)$$

which is negative. The actual value of the speed will be determined by a consideration of the interaction of the free stream with the boundary layer. On the upstream side of the shock the interaction gives rise to the upstream influence modes studied in §7.2. These help to fix ϕ_1 as a single wave. Equation (7.3.4) transfers this solution across the shock discontinuity from which the downstream solution can be found either by the use of characteristics if the flow there is still supersonic, which is possible if the shock is oblique, or by spatial transforms if the flow is subsonic. On the downstream side, however, §7.2 also shows that, in the case of an undisturbed boundary layer, there are no neutral waves possible in either subsonic or supersonic flow. The next section goes on to consider waves which may be possible in various types of disturbed boundary layer.

§7.4 The Stability Of A Disturbed Boundary Layer.

An incident shock may well cause separation and if the separation is sufficiently strong we may model the flow using the inviscid, high wavenumber "UPSA" formulation of Smith (1986c&d), (1987). This is an extension, to the case of separated flow, of the type of approximation used in §5.4. In the present case of a quasi-steady boundary layer, however, the steady, classical, viscous sublayer at the wall associated with the large amplitude, inviscid response in the main part of the boundary layer may well have no solution, even at T = 0+. This is due to the possible (and indeed likely) presence of a finite distance Goldstein singularity (Goldstein (1948)), which arises when the steady boundary layer equations are driven by a prescribed adverse pressure gradient. The presence of such a singularity,

which is in general not removable (Stewartson (1970)), will imply here that the "UPSA" approximation is not valid, even for a finite time. However we will use the approximation since it may be of relevance in the case where the shock occurs in the vicinity of a wedged trailing edge of an aerofoil. In this case there is no need for such a viscous sublayer. In fact experiments indicate that shock flutter and aerofoil buffetting seem most likely to occur when separation occurs near to a wedged trailing edge (Gibb (1989)). In the "UPSA" formulation the governing equations become

$$UU_X = -P_X, \qquad (SU)_X = 0, \tag{7.4.1a-b}$$

$$(S+A)(S+A)_X = -P_X \ , \tag{7.4.1c}$$

together with the pressure-displacement law due to the interaction with the free stream (7.1.5i-k). Here U, P, S, A are functions of X and T and are, respectively, the velocity of the fluid beneath the separated shear layer, the pressure, the height of the shear layer above the wall and the (negative) displacement of the boundary layer. The scalings leading to this regime (and also the alternative simplification of a linearised boundary layer and a nonlinear free stream) are presented in Appendix 7A. A small disturbance of a basic flow described by these equations leads to the boundary layer response

$$[1 + S_0(S_0 + A_0)/U_0^2]\ P = -(S_0 + A_0)A, \tag{7.4.2}$$

where the subscript 0 represents the basic flow. This, coupled with the linearised transonic small perturbation equation, gives the dispersion relation

$$\alpha = (-A_0)(2c - K)^{1/2}, \tag{7.4.3}$$

in the further specialised case of strongly disturbed but unseparated motion. This is also relevant to the case of flow downstream of a wedged trailing edge, where (see

Smith and Merkin (1982)) $A \to -\theta X$ as $X \to \infty$ where θ is the semi-angle of the wedge, so that sufficiently far downstream the "UPSA" formulation is valid.

In the case of larger scale separated flow near to a trailing edge we can use the Sadovskii (1971) or Smith (1986d) model for a relatively long and thin eddy flow. See also Brown, Cheng and Smith (1988). This leads to the nonlinear equation governing the boundary layer response

$$P = d(T) - 1/8\ \zeta^2 \bar{S}^2, \tag{7.4.4}$$

where $\bar{S}$ is the eddy height (identified with -A here), ζ is the (uniform) vorticity within the eddy and d is an undetermined function of time. Linearisation leads to the law

$$P = 1/4\ \zeta^2 S_0 A, \tag{7.4.5}$$

and so to

$$\alpha = 1/4\ \zeta^2 S_0\ (2c - K)^{1/2}. \tag{7.4.6}$$

This result is similar to (7.4.3). Both imply that neutral waves can travel upstream with $-|K|/2 < c < 0$ or downstream, in subcritical motion, and downstream only in the supercritical case. It is the upstream-travelling waves that are of particular interest to us since it is these which may lead to a resonant reaction with the shock-flutter motion described by (7.3.4&5). This needs subsonic flow downstream of the shock, necessitating a study of (7.1.5) with mixed type flow in the free stream.

We therefore deduce that there is a possibility of resonance phenomena between the shock and the boundary layer motions giving rise, perhaps, to a strong means of bypass transition. The analysis above has some deficiencies, except in the important case of flow near to a trailing edge, in relying on a singularity-free solution to the steady, classical boundary layer equations. It is hoped, however, that numerical solutions of the problem,

currently being attempted, will show some similar behaviour.

§7.5 Further Comments.

This short chapter studies the unsteady interaction between a boundary layer and a free stream where shocks are either present or are likely to form. The slow time scale of these motions means that the boundary layer reacts quasi-steadily to the free stream disturbances. As a result Tollmien-Schlichting waves are not possible. There are, however, decaying, upstream-travelling modes.

We identify a condition for resonance to occur between shock motion and a wave within the boundary layer (equation (7.3.5)). These waves are likely to be present in separated flow near to a wedged trailing edge. Here the problems associated with Goldstein's singularity discussed in §7.4 do not arise.

It is hoped that numerical work, now in progress, will shed more light on this important interaction.

A second, more strongly nonlinear mechanism for shock / boundary layer interaction, is suggested by equations (7.1.5) and has its origin in the reversed flow singularity suffered by an interactive boundary layer as the size of the reversed region attains some (finite) limit (Smith (1988)). An upstream-moving shock can provoke separation and reversed flow locally. Within this reversed flow the singularity mentioned above can occur at some finite time, as the strength of the shock and so the size of the separated region attains some finite value. This may well lead to a collapse of the separated flow and to transition as shorter scales than those captured by (7.1.5) come into play. This is likely to reduce the downstream pressure and so the strength of the shock. This process may repeat giving a self-sustaining, and strongly nonlinear, oscillation.

APPENDIX 7A SOME LIMITS OF INTEREST.

We first present the scalings which lead to the inviscid, large amplitude, boundary layer formulation, similar to that used in equations (7.4.1). It is very similar to the approximation used in §5.4. If the size of the boundary layer disturbance has $U = O(h)$, where $h >> 1$, we use the scalings

$$[U, V, P] \sim [h, h^2, h], \tag{7A.1}$$

$$[Y, \bar{y}, T, X, K] \sim [1, h^{-3}, h^{-4}, h^{-2}, h^2]. \tag{7A.2}$$

The governing equation for the boundary layer, with an unsteady (on the timescale of the free stream motion) forcing by, for example, an obstacle given by $hf(X,T)$ at the wall is

$$P_X = -(A + f)(A + f)_X. \tag{7A.3}$$

The free stream responds through equation (7.1.5i-k) in these new, scaled variables. Associated with these equations are the classically-driven, steady, boundary layer equations governing the motion in a viscous region close to the wall. As mentioned in §7.4 it is unlikely that these will have a solution in general, thus invalidating the above approximation in certain cases.

As a second point, we investigate the equations in the case of a small disturbance size, but with K sufficiently small that the free stream response is still nonlinear. This is the limit investigated by Brilliant and Adamson (1974) in the case of steady flow. The scalings in this limit are, if $\varepsilon << 1$,

$$Y = \varepsilon^{-1/3}Y^*, \quad X = \varepsilon^{-1}X^*, \quad T = \varepsilon^{-3}T^*, \quad \bar{y} = \varepsilon^{-1}\bar{y}^*,$$

$$U = Y^* + \varepsilon u, \quad P = \varepsilon P^*, \quad V = \varepsilon^{5/3}v, \quad A = \varepsilon A^*.$$

The free stream equations remain as in (7.1.5i-k), but

written in these new variables. However the boundary layer equations may be linearised and solved to give the pressure-displacement response

$$P^* = \frac{(-3c\sqrt{3}\ \Gamma(2/3))}{2\pi}\int_{-\infty}^{X} \frac{A^*(\xi)}{(X-\xi)^{2/3}}\, d\xi, \qquad (7A.4)$$

where $c = |Ai'(0)|$, and Ai is Airy's function.

FIGURE CAPTIONS FOR CHAPTER 7.

Figure 7.1.1 The nonlinear disturbance structure for unsteady shock / boundary layer interaction at transonic speeds. An oncoming two-dimensional flow, with Mach number such that $|M_\infty^2-1| = O(Re^{-1/5})$ as $Re \to \infty$, is subject to a three-dimensional disturbance at a small, $O(Re^{-1/10})$, angle to the streamwise direction. The shock surface is effective only within the free stream.

Figure 7.1.2 Two different types of problem governed by equations (7.1.5). Figure (a) illustrates the possibility of the interaction leading to a self-sustaining oscillation of the boundary layer motion and the shock due to a locally decelerating external flow. Figure (b) shows the formation of shocks in an otherwise uniform free stream due to unsteadiness within the boundary layer.

Figure 7.2.1 A sketch summarising the behaviour of the upstream influence modes of the transonic regime with $|M_\infty^2-1| = O(Re^{-1/5})$ as $Re \to \infty$, as the spanwise wavenumber ($\bar{\beta}$), frequency ($\bar{\Omega}$), and scaled Mach number (K) are varied.

Figure 7.1.1

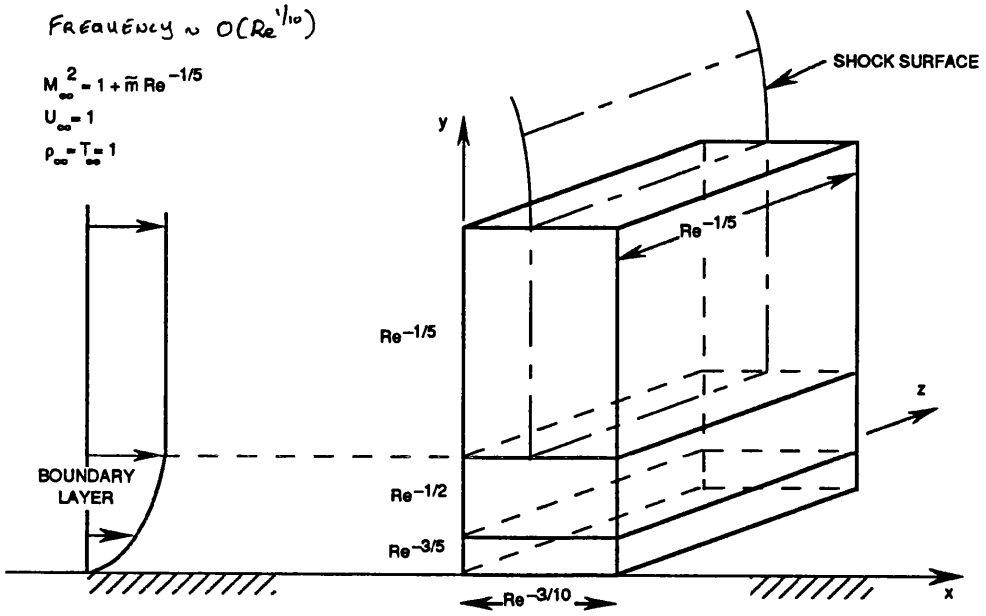

Figure 7.1.2

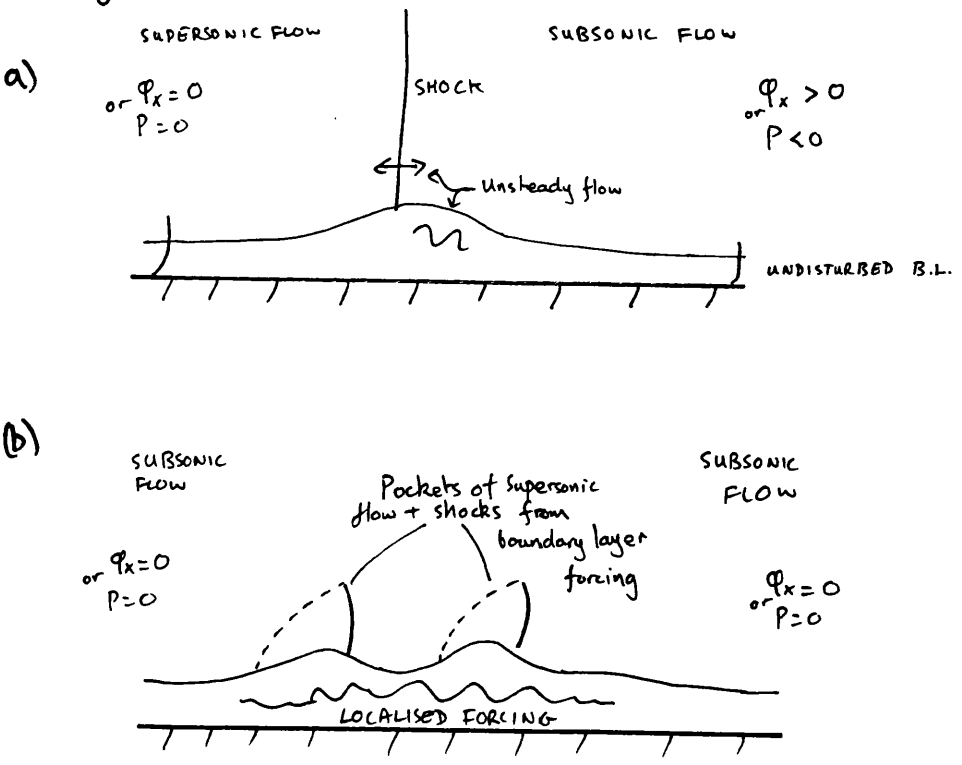

Figure 7.2.1

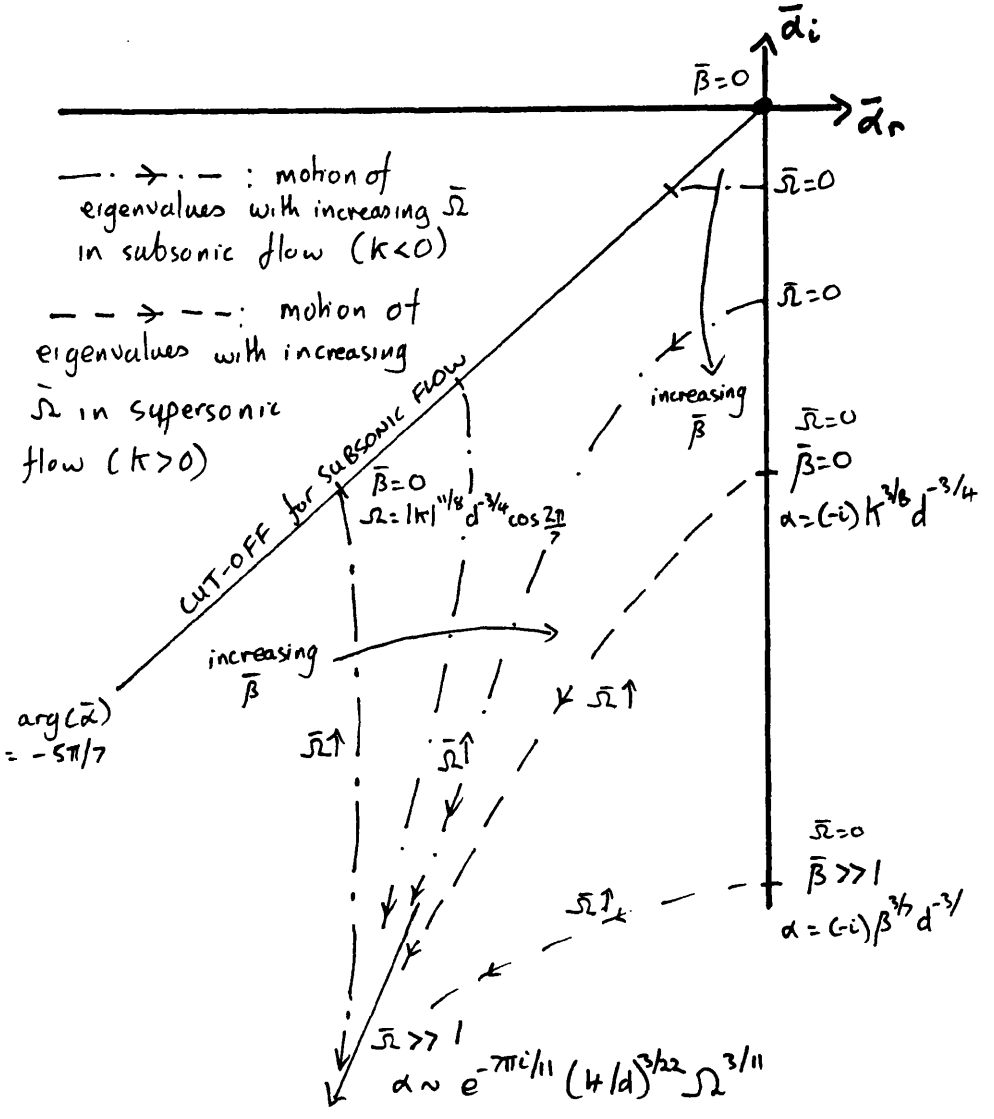

$$\alpha = \bar{\alpha}\,|\kappa|^{3/8} d^{-3/4} \qquad \Omega = \bar{\Omega}\,|\kappa|^{11/8} 2^{-1} d^{-3/4}$$

$$\beta = \bar{\beta}\,|\kappa|^{7/8} d^{-3/4}$$

REFERENCES.

Abramowitz, M. & Stegun, I.A. (Eds.) 1964 "Handbook of Mathematical Functions." Dover, New York.

Adamson, T.C. & Messiter, A.F. 1980 Analysis of two-dimensional interactions between shock waves and boundary layers. Ann. Rev. Fluid 12, 103.

Avis, R.G.H. 1989 Aspects of high Reynolds number flows past axisymmetric bodies. Ph.D. thesis, University of London.

Benjamin, T.B. 1967 Internal waves of permanent form on fluids of great depth. J. Fluid Mech. 29, 559.

Benjamin, T.B. & Lighthill, M.J. 1954 On cnoidal waves and bores. Proc. Roy. Soc. A224, 448.

Benjamin, T.B. & Feir, J.E. 1967 The disintegration of wavetrains in deep water. J. Fluid Mech. 27, 417.

Bodonyi, R.J. 1979 Transonic laminar boundary layer flow near convex corners. Q.J. Mech. & Appl. Math. 32, Part 1, 63.

Bodonyi, R.J. & Kluwick, A. 1977 Freely interacting transonic boundary layers. Phys. Fluids 20, 1432.

Bodonyi, R.J. & Smith, F.T. 1981 The upper branch stability of a Blasius boundary layer including non-parallel flow effects. Proc. R. Soc. Lond. A375, 65.

Bodonyi, R.J. & Kluwick, A. 1982 Supercritical transonic trailing edge flow. Q.J. Mech. & Appl. Math. 35, Part 2, 265.

Bodonyi, R.J. & Smith, F.T. 1986 Shock-wave laminar boundary layer interaction in supercritical transonic flow. Computers & Fluids 14, No. 2, 97.

Bogar, T.J. 1986 Structure of self-excited oscillations in transonic diffuser flows. AIAA Journal, 24, 54.

Bowles, R.I. & Smith, F.T. 1989 On boundary layer transition in transonic flow. UTRC Rept. No. 89-26.

Brilliant, H.M. & Adamson, T.C. 1974 Shockwave-boundary layer interactions in laminar transonic flow. AIAA Journal 12, No. 3.

Brotherton-Ratcliffe, R.V. 1986 Boundary layer effects in liquid layer flows. Ph.D. thesis, University of London.

Brown, S.N., Stewartson, K. & Williams, P.G. 1975 On expansive free interactions in boundary layers. Proc. Roy. Soc. Edinburgh 74A, 21.

Brown, S.N., Cheng, H.K. & Smith, F.T. 1988 Nonlinear instability and breakup of separated flow. J. Fluid Mech. 193, 191.

Carter, J.E. 1979 A new boundary layer inviscid iteration technique for separated flows. AIAA Paper No. 79-1450 (presented July 1979, Williamsburg, Virginia).

Chester, W. 1966 A model of the undular bore on a viscous fluid. J. Fluid Mech. 24, 367.

Christodoulou, K.N. & Scriven, L.E. 1989 The fluid mechanics of slide coating. J. Fluid Mech. 208, 321.

Corke, T.C. & Mangano, R.A. 1989 Resonant growth of three-dimensional modes in transitioning Blasius boundary layers. J. Fluid Mech. 209, 93.

Cowley, S.J. & Hall, P. 1990 On the instability of hypersonic flow past a wedge. To appear in J. Fluid Mech.

Craik, A.D.D. 1971 Nonlinear resonant instability in boundary layers. J. Fluid Mech 50, 393.

Craik, A.D.D. 1985 "Wave interactions in fluid flows." Cambridge Univ. Press.

Craik, A.D.D., Latham, R.C., Fawkes, M.J. & Gribbon, P.W.F. 1981 The circular hydraulic jump. J. Fluid Mech. 112, 347.

Davis, R.T. 1984 A procedure for solving the compressible interactive boundary layer equations for subsonic and supersonic flows. AIAA Paper No. 84-1614 (presented June 1984, Snowmass, Colorado).

Dolling, D.S. 1989 Review of separation shock-wave dynamics in supersonic interactive flows. Proc. Roy. Aero. Soc. Mtg. Prediction & Exploitation of Separated Flows, April 1989, London.

Dolling, D.S. & Brusniak, L. 1987 Separation shock motion in fin, cylinder and compression ramp induced turbulent interactions. AIAA Paper 87-1368.

Drazin, P.G. & Reid, W.H. 1981 "Hydrodynamic stability" Cambridge Univ. Press.

Duck, P.W. 1985 Laminar flow over unsteady humps: the formation of waves. J. Fluid Mech. 160, 465.

Duck, P.W. & Hall, P. 1989a Tollmien-Schlichting waves in axisymmetric supersonic flows. Q. J. Mech. & Appl. Math. 42 115.

Duck, P.M. & Hall, P. 1989b Submitted to J. Fluid Mech.

Eagles, P.M. 1988 Jeffrey-Hamel boundary layer flows over curved beds. J. Fluid Mech. 186, 583.

Eagles, P.M. & Daniels, P.G. 1986 Free surface boundary layer flow on a curved bed. I.M.A.J. Appl. Maths. 36, 101.

Edwards, D.E. & Carter, J.E. 1985 Analysis of three-dimensional separated flow with the boundary layer equations. AIAA Paper No. 85-1499.

Elliot, J.W., Smith, F.T. & Cowley, S.J. 1983 Breakdown of boundary layers: (i) on moving surfaces; (ii) in semi-similar unsteady flow; (iii) in fully unsteady flow. Geophys. Astrophys. Fluid Dynamics 25, 77.

Elliot, J.W. & Smith F.T. 1987 Dynamic stall due to unsteady marginal separation. J. Fluid Mech. 179, 489.

Fraenkel, L.E. 1962 Laminar flow in symmetric channels with slightly curved walls, I. On the Jeffrey-Hamel solutions for flow between plane walls. Proc. R. Soc. Lond. A267, 119.

Gajjar, J.S.B. 1983 On some viscous interaction problems in incompressible fluid flow. Ph.D. thesis, University of London.

Gajjar, J.S.B. & Smith, F.T. 1983 On hypersonic self-induced separation, hydraulic jumps and boundary layers with algebraic growth. Mathematika 30, 77.

Gajjar, J.S.B. & Cole, J.W. 1989 The upper branch stability of compressible boundary layer flows. Theor. and Comp. Fluid Dynamics 1, 105.

Gibb, J. 1989 The cause and cure of periodic flows at transonic speeds. Seminar at Royal Aero. Soc., London, Jan 5th 1989.

Goldstein, S. 1948 On laminar boundary layer flow near a point of separation. Q.J. Mech. & Appl. Math. 1, 43.

Hall, P. & Smith, F.T. 1986 The nonlinear interaction of Tollmien-Schlichting waves and Taylor Görtler vortices in curved channel flows. Proc. R. Soc. Lond. A417, 255.

Hall, P. & Smith, F.T. 1989 On strongly nonlinear vortex/wave interactions in boundary layer transition. ICASE report (in preparation).

Hamel, G. 1916 Spiralförmige Bewegungen zäher Flüssigkeiten. Jahrb. deutsch. Math.

Herbert, Th. & Morkovin, M.V. 1979 Dialogue on bridging some gaps in stability and transition research. In "Laminar and Turbulent Transition" edited by R. Eppler & H. Fasel (proceedings of IUTAM symposium Stuttgart 1979.)

Herbert, Th., Bertolotti, F.P. & Santos, G.R. 1987 Floquet analysis of secondary instability in shear flows in "Stability of time-dependent and spatially-varying flows" p. 43. Eds. D.L. Dwoyer and M.Y. Hussaini. Springer-Verlag.

Higgins, B.G. & Scriven, L.E. 1979 Interfacial shape and evolution equations for liquid films and other visco-capillary flows. Ind. Engng. Chem. Fundam. 18, 208.

Hocking, L.M., Stewartson, K. & Stuart, J.T. 1971 A nonlinear instability burst in plane parallel flow. J. Fluid Mech. 51 705.

Howlett, J. 1987 Efficient self-consistent viscous inviscid solutions for unsteady transonic flow. J. of Aircraft. 24, No 11, 737.

Howlett, J. & Bland, S. 1987 Calculation of viscous effects on transonic flow for oscillating airfoils and comparisons with experiment. NASA Technical paper 2731.

Ishigai, S., Nakanishi, S., Mizumo, M. & Imamura, T. 1977 Bull. J.S.M.E. 20, 85.

Jeffrey, G.B. 1915 The two-dimensional steady motion of a viscous fluid. Phil. Mag. 29, 445.

Kachanov, Yu.S., Kozlov, V.V. & Levchenko V.Ya. 1978 Nonlinear development of a wave in a boundary layer. Fluid Dynamics 12, 383.

Kachanov, Yu.S. & Levchenko, V.Ya. 1984 The resonant interaction of disturbances at laminar-turbulent transition in a boundary layer. J. Fluid Mech. 138, 209.

Klebanoff, P.S., Tidstrom, K.D. & Sargent, L.M. 1962 The three-dimensional nature of boundary layer instability. J. Fluid Mech. 12, 1.

Lamb, H. 1932 "Hydrodynamics." Cambridge Univ. Press.

Laurien, E. & Kleiser, L. 1989 Numerical simulation of boundary layer transition and transition control. J. Fluid Mech. 199, 403.

Lees, L. & Lin, C.C. 1946 NACA Tech. Note No 1115.

Lees, L. & Reshotko, E. 1962 Stability of the compressible laminar boundary layer. J. Fluid. Mech. 12, 555.

Lighthill, M.J. 1953 On boundary layers and upstream influence, (II). Supersonic flows without separation. Proc. Roy. Soc. London A217, 478.

Lighthill, M.J. 1963 Boundary layer theory. Chapter 2 of "Laminar Boundary layers." edited by L. Rosenhead. Oxford Univ. Press.

Lighthill, M.J. 1978 "Waves in Fluids." Cambridge Univ. Press.

Lin, C.C. 1955 "The theory of hydrodynamic stability." Cambridge Univ. Press.

Mack, L.M. 1974 On the application of linear stability theory to the problem of supersonic boundary layer transition. AIAA Paper No. 74-134.

Mack, L.M. 1984 Boundary layer stability theory. AGARD course on Stability & Transition, March 26-30 1984. Von Karman Institute of Fluid Dynamics, Belgium. AGARD Rept. No. 709.

Mack, L.M. 1987 Review of linear compressible stability theory. In "Stability of time dependent and spatially varying flows.", pp 164-187. Eds. D.L. Dwoyer & M.Y. Hussaini. Springer-Verlag.

Messiter, A.F. 1970 Boundary layer flow near the trailing edge of a flat plate. SIAM J. Appl. Math. 18, 241.

Muck, K.C., Andreopoulos, J. & Dussauge J-P. 1988 Unsteady nature of shock wave / turbulent boundary layer interaction. AIAA Journal 26 No. 2.

Neiland, V.Ya. 1969 Towards a theory of separation of the laminar boundary layer in a supersonic stream. Izv. Akad. Nauk. SSSR. Mech. Zhid. Gaza. 4.

Reyner, T.A. & Flügge-Lotz, I. 1968 Int. J. Fluid Mech. 89, 535.

Reynolds, O. 1883 An experimental investigation of the circumstances which determine whether the motion of water shall be direct or sinuous and of the law of resistance in parallel channels. Phil. Trans. R. Soc. Lond. 174, 935.

Rizetta, D.P. 1982 Procedures for the computation of unsteady transonic flows including viscous effects. NASA Contractor Report 166249, January 1982.

Rosenhead, L. 1940 The steady two-dimensional flow of a viscous fluid between two inclined plane walls. Proc. Roy. Soc. A175, 436.

Ryzhov, O.S. & Zhuk, V.I. 1980 Supersonic planar flows. Dokl. Akad. Nauk. SSSR. 253, 1326.

Sadovskii, V.S. 1971 Vortex regions in a potential stream with a jump of Bernoulli's constant at the boundary. Prikl. Mat. Mekh. Vol 35, 773.

Saric, W.S. & Thomas, A.S.W. 1984 Experiments on the subharmonic route to turbulence in boundary layers. In "Turbulence and Chaotic phenomena in Fluids." Proc. IUTAM Symp. Kyoto, Japan. Sept 5-12 1984.

Schlichting, H. 1933 Zur Entstehung der Turbulenz bei der Plattenströmung. Nachr. Ges. Wiss. Götingen, Math. Phys. Klasse, 181 (also ZAMM, 13 171).

Schubauer, G.B. & Skramstad, A.J. 1947 Laminar boundary layer oscillations and stability of laminar flow. J. Aeronaut. Sci. 14 69.

Sedougghi, S., Bowles, R.I. & Smith, F.T. 1990 Surface cooling effects on compressible boundary layer inviscid modes and viscous modes. ICASE report (in preparation).

Smith, F.T. 1974 Boundary layer flow near a discontinuity in wall conditions. J. Inst. Maths. Applics. 13, 127.

Smith, F.T. 1976 Flow through constricted and dilated channels, Parts 1 and 2. Q. J. Mech. & Appl. Math. 29,343.

Smith, F.T. 1979a On the non-parallel flow stability of the Blasius boundary layer. Proc. R. Soc. Lond. A366, 91.

Smith, F.T. 1979b Nonlinear stability of boundary layers for disturbances of various sizes. Proc. R. Soc. Lond. A368, 573.

Smith, F.T. 1982 On the high Reynolds number theory of laminar flows. I.M.A.J. Appl. Math. 28, 207.

Smith, F.T. 1986a Two-dimensional disturbance travel, growth & spreading in boundary layers. J. Fluid Mech. 169, 353.

Smith, F.T. 1986b The strongly nonlinear growth of three-dimensional disturbances in boundary layers. UTRC Rept. No. 86-10.

Smith, F.T. 1986c Separating flow: small scale, large scale and nonlinear unsteady effects. In "Boundary layer separation." Eds. F.T. Smith & S.N. Brown (Proceedings of the I.U.T.A.M. Symposium, London,1986).

Smith, F.T. 1986d Modelling of separating flow and its stability. J. Th. & Appl. Mech. Special Edition 1986, 47.

Smith, F.T. 1986e Concerning inviscid solutions for large scale separated flow. J. Eng. Maths. 20, 271.

Smith, F.T. 1987 Breakup in unsteady separation. A.S.M.E. Cincinnati.

Smith, F.T. 1988 A reversed flow singularity in interacting boundary layers. Proc. Roy. Soc. A420, 21.

Smith, F.T. 1989 On the first mode instability in subsonic, supersonic or hypersonic boundary layers. J. Fluid Mech. 198, 127.

Smith, F.T. & Duck, P.W. 1977 Separation of jets and thermal boundary layers from a wall. Q. J. Mech. & Appl. Math. 30, 143.

Smith, F.T., Brighton, P.W.M., Jackson, P.S. & Hunt, J.C.R. 1981 On boundary layer flow past two-dimensional obstacles. J. Fluid Mech. 113, 123.

Smith, F.T. & Merkin J.H. 1982 Triple deck solutions for subsonic flow past humps, steps, concave or convex corners & wedged trailing edges. Computers & Fluids 10, 7.

Smith, F.T. & Burgraff, O.R. 1985 On the development of large-sized, short-scaled disturbances in boundary layers. Proc R. Soc. Lond A399, 25.

Smith, F.T. & Stewart, P.A. 1987 The resonant-triad nonlinear interaction in boundary layer transition. J. Fluid Mech. 179, 227.

Smith, F.T., Doorly, D.J. & Rothmeyer, A.P. 1987 On boundary layer thickening in transition and vorticity slugs in internal flows. UTRC Rept. 87-43.

Smith, F.T. & Brown, S.N. 1989 The inviscid stability of a Blasius boundary layer at large values of the Mach number. Submitted to J. Fluid Mech.

Smith, F.T. & Walton, A.G. 1990 Nonlinear interaction of near planar Tollmien-Schlichting waves and longitudinal vortices in boundary layer transition. Mathematika 36.

Squire, H.B. 1933 On the stability of three-dimensional disturbances of viscous fluid flow between parallel walls. Proc. R. Soc. Lond. A142, 621.

Stewart, P.A. 1990 Ph.D. thesis, University. of London. In preparation.

Stewart, P.A. & Smith, F.T. 1987 Three-dimensional instabilities in steady and unsteady non-parallel boundary layers, including effects of Tollmien-Schlichting disturbances and cross flow. Proc. R. Soc. Lond. A409, 229.

Stewartson, K. 1964 "The theory of boundary layers in compressible fluids." Oxford Univ. Press.

Stewartson, K. 1970 Is the singularity at separation removable ? J. Fluid Mech. 44, 347.

Stewartson, K. 1974 Multistructured boundary layers on flat plates and related bodies. Adv. Appl. Mech. 14, 145.

Stewartson, K. & Williams, P.G. 1969 Self-induced separation. Proc. Roy. Soc. A312, 181.

Stuart, J.T. 1963 Hydrodynamic stability. Chapter 9 of "Laminar boundary layers." edited by L. Rosenhead. Oxford Univ. Press.

Tijdeman, H. & Seebas, R. 1980 Transonic flow past oscillating airfoils. Ann. Rev. Fluid Mech. 12 ,181.

Tollmien, W. 1929 Über die Entstehung der Turbulenz I. Nachr. Ges. Wiss. Götingen, Math. Phys. Klasse, 22, 44. (Translation: The production of turbulence. NACA TM 609, 1931.)

Townsend, A.A. 1956 "The structure of turbulent shear flow." Cambridge Univ. Press.

van Dommelen, L.L. & Shen, S.F. 1980 The spontaneous generation of the singularity in a separating boundary layer. J. Comput. Phys. 38, 125.

van Dommelen, L.L. & Cowley, S.J. 1990 On the Lagrangian description of unsteady boundary layer separation, Pt.1. General theory. J. Fluid Mech. 210, 593.

van Dyke, M. 1964 "Perturbation methods in fluid mechanics." Academic Press.

Veldman, A.E.P. 1983 A numerical view on strong viscous-inviscid interactions. NLRMP 83048U.

von Mises, R. 1958 "Mathematical theory of compressible flow." Academic Press, New York.

Watson, E.J. 1964 The radial spread of a liquid jet over a horizontal plane. J. Fluid Mech. 20, 481.

Wilson, S.D.R. & Jones, A.F. 1983 The entry of a falling film into a pool and the air-entrainment problem. J. Fluid Mech. 128, 219.

Zang, T.A. & Krist, S.E. 1989 Numerical experiments on stability & transition in plane channel flow. Theor. & Comput. Fluid Dynamics 1, 41.